



HAL
open science

Theoretical studies of optical non-linear effects in ultracold Rydberg gases

Andrey Grankin

► **To cite this version:**

Andrey Grankin. Theoretical studies of optical non-linear effects in ultracold Rydberg gases. Optics [physics.optics]. Université Paris Saclay (COMUE), 2016. English. NNT : 2016SACLO006 . tel-01367711

HAL Id: tel-01367711

<https://pastel.hal.science/tel-01367711>

Submitted on 16 Sep 2016

HAL is a multi-disciplinary open access archive for the deposit and dissemination of scientific research documents, whether they are published or not. The documents may come from teaching and research institutions in France or abroad, or from public or private research centers.

L'archive ouverte pluridisciplinaire **HAL**, est destinée au dépôt et à la diffusion de documents scientifiques de niveau recherche, publiés ou non, émanant des établissements d'enseignement et de recherche français ou étrangers, des laboratoires publics ou privés.

NNT : 2016SACLO006

THESE DE DOCTORAT
DE L'UNIVERSITE PARIS-SACLAY

préparée à
L'INSTITUT D'OPTIQUE GRADUATE SCHOOL

ÉCOLE DOCTORALE N°572
Ondes et Matière (EDOM)

Spécialité de doctorat : Physique

par

Andrey Grankin

Theoretical studies of optical non-linear effects in ultracold
Rydberg gases

Thèse présentée et soutenue à Palaiseau, le 21 Juin 2016

Composition du jury :

Prof. Jean-Michel Raimond	Président	Université Paris 6
Prof. Klaus Moelmer	Rapporteur	Université d'Aarhus
Prof. Michael Fleischhauer	Rapporteur	Université de Kaiserslautern
Prof. Igor Lesanovsky	Examineur	Université de Nottingham
Prof. Pierre Pillet	Examineur	Laboratoire Aimé Cotton, Université d'Orsay
Dr. Etienne Brion	Examineur	Laboratoire Aimé Cotton, Université d'Orsay
Prof. Philippe Grangier	Directeur de thèse	Institut d'Optique Graduate School



Résumé

Les photons apparaissent comme des vecteurs d'information fiables, car peu sensibles à leur environnement. Mais ils interagissent si faiblement entre eux que la réalisation directe de portes logiques optiques à deux qubits photoniques est impossible. On peut toutefois engendrer indirectement des interactions photon-photon substantielles, via la propagation dans un milieu optiquement non-linéaire. L'utilisation du phénomène de transparence électromagnétiquement induite permet, en particulier, d'induire une forte non-linéarité résonante, sur l'une des transitions d'un système à trois niveaux -- néanmoins pas encore détectable dans le domaine quantique. Pour augmenter les effets non-linéaires obtenus il a été récemment proposé de combiner cette approche au blocage d'excitation induit par les fortes interactions dipôle-dipôle entre atomes de Rydberg. On accroît encore les effets non-linéaires sur la lumière transmise en plaçant le milieu en cavité. L'étude théorique et expérimentale de ce dispositif a été menée dans le régime dispersif et pour une non-linéarité faible, dans le cas d'un faible champ sonde incident classique. Dans ce mémoire, nous nous intéressons aux effets optiques non-linéaires induits par un milieu Rydberg sur un champ quantique.

Dans le chapitre 1, nous présentons les équations dynamiques générales de notre système et rappelons les principales propriétés de la fonction de corrélation d'intensité que nous utiliserons pour caractériser les effets du milieu atomique sur la statistique quantique du champ incident. Dans le chapitre 2, nous considérons notre système dans le régime dispersif, i.e. lorsque l'état atomique intermédiaire est excité hors résonance et peut être éliminé adiabatiquement. Dans l'approximation des bulles Rydberg nous réduisons effectivement le milieu à un ensemble de « superatomes » à deux niveaux, couplés au mode de la cavité selon le modèle de Tavis-Cummings forcé. Nous calculons analytiquement et numériquement la fonction de corrélation d'intensité pour la lumière transmise, qui, selon les paramètres de la cavité, peut être “groupée” ou “dégrouper”. Dans le chapitre 3, nous présentons un traitement perturbatif du système, restreint à l'ordre le plus bas non nul en le champ sonde incident, valable, notamment, dans le régime résonant. Nous dérivons la fonction de corrélation d'intensité pour la lumière transmise et réfléchi, grâce à la factorisation des moyennes de produits d'opérateurs. Dans le régime résonant, nous identifions des conditions d'adaptation d'impédance de la cavité différentes selon les composantes du champ, qui suggèrent l'utilisation du dispositif en tant que filtre. Nous proposons enfin un modèle effectif non-linéaire à

trois bosons pour le système couplé atomes-cavité. Dans le chapitre 4, nous dépassons l'ordre le plus bas de la théorie de perturbation, en utilisant le formalisme de Schwinger-Keldysh. Par cette méthode, nous retrouvons les résultats du chapitre 3, sous une forme analytique, que nous étendons à l'ordre supérieur. Nous dérivons notamment des expressions analytiques pour les composantes élastique et inélastique du spectre de la lumière transmise par la cavité. Nous identifions ainsi une structure de résonance polaritonique, jusque-là inconnue, que nous interprétons physiquement. Dans le dernier chapitre, nous décrivons un protocole de porte logique photonique de haute fidélité, fondé sur le blocage Rydberg dans un ensemble atomique placé dans une cavité optique. Ce protocole peut être réalisé avec des cavités de finesse modérée et permet, en principe, un traitement efficace de l'information quantique codée dans des qubits photoniques. L'appendice A présente une application de nos méthodes aux résultats expérimentaux obtenus au laboratoire. Les appendices B-G reprennent différents points techniques du mémoire. L'appendice H reproduit un article relatif au chapitre 5.

Introduction

Photons appear as reliable information carriers since they interact very weakly with their environment. For the same reason, they hardly interact with each other which forbids the direct implementation of optical two-qubit gates. Such an interaction can actually be effectively emulated via the propagation through atomic nonlinear media.

In this chapter, we first review conventional nonlinear media and show that they fail to induce effects beyond the classical regime. Then we present Rydberg atoms, their physical properties and uses on quantum information purposes, and show that the strong dipole-dipole interactions between Rydberg atoms are expected to allow for optical nonlinearities strong enough to be noticeable at the single-photon level. Finally, we sketch the outline of the present dissertation.

Nonlinear optics

When propagating through an atomic medium, light interacts with the (valence) electrons, polarizes each atom which acquires a dipole $\langle d \rangle$. The average dipole moment per unit volume is $P = n_{at} \langle d \rangle$, where n_{at} is the atomic density (Boyd, 2003).

In an atomic medium, the polarization can be related to the electric field via:

$$P = \epsilon_0 \chi E \tag{1}$$

where χ is the susceptibility of the medium¹. Induced dipoles are not necessarily proportional to the electric field they are induced by, and the susceptibility χ can be expanded in powers of E (Boyd, 2003):

$$\chi = \chi^{(1)} + \chi^{(2)} E + \chi^{(3)} E^2 + \dots \tag{2}$$

In materials which have the spatial inversion symmetry, the $\chi^{(2)}$ term in Eq. (2) vanishes (Boyd, 2003), and therefore $\chi^{(3)}$ characterizes the nonlinear response of the sample at the lowest order. In general, the susceptibility Eq. (2) is a complex number. Its real and imaginary parts stand for the phase shift and absorption of the total field, respectively. In particular, the nonlinear shift accumulated by a monochromatic field

¹Assuming an isotropic medium with local response.

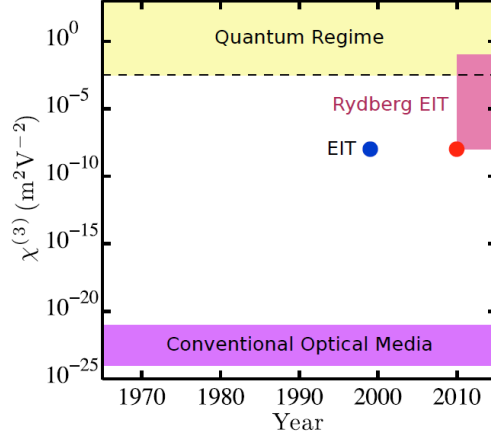


Figure 1: Schematic showing advances in the optical Kerr non-linear coefficient, $\chi^{(3)}$. Conventional optical materials have resonances in the ultra-violet leading to a small non-linearity in the visible and infra-red. Enormous enhancements of the non-linearity are possible by using resonant media but at the expense of loss. The loss can be reduced using the technique of electromagnetically induced transparency (EIT). The giant EIT non-linearity can be further enhanced using a Rydberg medium with strong dipole-dipole interaction. With Rydberg EIT it is possible to exceed the threshold for single photon non-linearities (dashed line) where a quantum description is required. Picture is taken from (Pritchard et al., 2013).

along the propagation in a medium of length L is given by

$$\phi_{nl} = \text{Re} [\chi^{(3)}] \frac{\omega}{2c} \mathcal{E}^2 L$$

Pushing the formula above beyond its applicability limit, *i.e.* out of the classical regime, we can roughly estimate the order of magnitude of the $\chi^{(3)}$ coefficient for ϕ_{nl} to be noticeable in the quantum regime by requiring $\phi_{nl} \approx \pi$ for a single-photon input ($\mathcal{E} \approx \mathcal{E}_{1ph}$). Denoting the bandwidth of the tightly-focused photon wavepacket by $\Delta\omega$, and assuming that the transverse waist w_0 and propagation length L are related via $L = \frac{\pi w_0^2}{\lambda}$, we get:

$$\begin{aligned} \phi_{nl} &\approx \text{Re} [\chi^{(3)}] \frac{k}{2} \chi^{(3)} \frac{\hbar\omega}{\epsilon_0 V} L \\ &\approx \frac{\pi^2}{\lambda} \text{Re} [\chi^{(3)}] \frac{\hbar\omega\Delta\omega}{\epsilon_0 \pi \lambda^2 c 2\pi} \lambda \\ &\approx \text{Re} [\chi^{(3)}] \frac{\pi \hbar \omega^3 \Delta\omega}{\epsilon_0 (2\pi)^3 c^3} \end{aligned} \quad (3)$$

Setting $\phi_{nl} \approx \pi$ and assuming $\Delta\omega \approx 2\pi \times 10^6 \text{ rad} \cdot \text{s}^{-1}$ and $\omega = 2\pi \times 10^{15} \text{ rad} \cdot \text{s}^{-1}$ we get $\text{Re} [\chi^{(3)}] \propto 10^{-3} \times \text{V}^{-2} \text{m}^2$.

Conventional off-resonant materials provide values of $\chi^{(3)}$ that are many orders of magnitude smaller. For example for air and for water they can be found to be $1.7 \times 10^{-25} \text{V}^{-2} \text{m}^2$ and $\sim 2.5 \times 10^{-22} \text{V}^{-2} \text{m}^2$, respectively (Pritchard et al., 2013). When the incident beam becomes resonant with a transition of the medium, the nonlinearity increases by many orders of magnitude but at the cost of stronger losses. A compromise may be sought for between (desired) dispersion and (unwanted) absorption, which however fails in achieving strong enough nonlinear effects to be noticeable at the single-photon level.

The coupling to an additional level, in a so-called electromagnetically induced transparency (EIT) configuration, allows one to still benefit from enhanced susceptibility while avoiding the spurious absorption mentioned above (Harris et al., 1990; Boller et al., 1991). In addition to the transparency window around the two-photon resonance, one observes the strong reduction of the group velocity of light (Budker et al., 1999; Hau et al., 1999). The reported non-linear susceptibility in such a medium is $\chi^{(3)} \sim 7 \times 10^{-8} \times \text{V}^{-2} \text{m}^2$, still insufficient to implement photonic interactions.

Much stronger nonlinearities can be achieved in high finesse cavity QED setups (Haroche and Raimond, 2006) with a single trapped atom in the strong coupling conditions. The latter are met when the coupling strength g between the atom and the mode is much bigger than atomic (γ_e) and cavity (γ_c) decay rates, (*i.e.* $g^2 \gg 2\gamma_c\gamma_e$). In this case, the Rabi splitting of the multiply-excited states, predicted by the Jaynes-Cummings model, is much bigger than the linewidths of the corresponding multiphoton transitions, giving rise to the few-photon nonlinearities observed, for instance, in (Birnbbaum et al., 2005; Schuster et al., 2008).

Another approach to reach strong non-linear susceptibilities consists in the collective enhancement of the response of the sample. This can be performed via long-range dipole-dipole interactions between one of the atomic levels used in the scheme. One of the most promising approaches is to use high-lying atomic levels, known as Rydberg states (Gallagher, 2005).

In the next sections, we present the main physical properties of Rydberg atoms as well as their main uses in quantum information protocols, before proceeding to the description of Rydberg-induced photon-photon interactions.

Rydberg atoms and their interactions

Rydberg atoms exhibit exaggerated properties which make them particularly appealing and useful for quantum information processing. Here, we make a brief summary of their relevant features.

The Rydberg states have relatively long radiative lifetimes that scale proportionally to the cube of the principal quantum number n^3 (for example Na(10d) the radiative lifetime is $\approx 1\mu\text{s}$) (Gallagher, 2005). The corresponding reduction of the decoherence

favors their use in various schemes of quantum information processing (Saffman et al., 2010).

The orbital radius of a Rydberg atom, and therefore, its dipole moment scales as the square of the principal quantum number n^2 (example Na(10d) the dipole moment is $\approx 143ea_0$). Moreover, the energy levels can be approximated by (Gallagher, 2005):

$$E_{nlj} = \frac{\text{Ry}}{(n - \delta_{lj}(n))^2}$$

where l and j are the orbital and the total angular momenta, Ry is the Rydberg constant and the quantum defect $\delta_{lj}(n)$ is a slowly varying function of principal quantum number. Small energy spacings (\sim MHz) and large dipole moments lead to enhanced dipole-dipole interactions between Rydberg atoms (Pritchard et al., 2013). The Hamiltonian of the electrostatic interaction of two Rydberg atoms A and B whose relative position is $\vec{R} = \vec{R}_B - \vec{R}_A$ (assuming that $R \gg n^2 a_0$ where a_0 is the Bohr radius) is given by $\hat{V}_{dd} = \frac{e^2}{R^3} \left(\hat{\vec{a}} \cdot \hat{\vec{b}} - 3 \left(\hat{\vec{a}} \cdot \vec{R} \right) \left(\vec{R} \cdot \hat{\vec{b}} \right) \right)$ where $\hat{\vec{a}}$ and $\hat{\vec{b}}$ are the position vector operators of the outer electrons of the corresponding atoms with respect to their nuclei. This Hamiltonian mainly mixes a given doubly Rydberg-excited two-atom state with the closest Rydberg manifolds. The corresponding perturbed eigenstate and eigenenergy can be computed by direct diagonalization of the full Hamiltonian. In the so-called Van der Waals regime, which corresponds to a detuned regime of the dipole-dipole interaction, the resulting energy shift takes the form $V(R) = -C_6/R^6$, where the coefficient C_6 scales as n^{11} (Saffman et al., 2010). In general C_6 has an angular dependence relative to the mutual arrangement of atoms (Saffman et al., 2010).

The dipole-dipole induced shifts $V(R)$ are so strong that they may compete with the Rabi frequency of an exciting laser and even forbid the transition towards a Rydberg state. This phenomenon theoretically predicted in (Lukin et al., 2001) and experimentally demonstrated in (Vogt et al., 2006; Urban et al., 2009), is called “dipole” or “Rydberg blockade”. Below, we review several examples of simple atomic configurations and protocols which, despite their simplicity, give an insight in the physics of the dipole blockade and reveal themselves very useful from the quantum information point of view.

Rydberg blockade: atomic quantum information processing and many-body physical features

We first consider a system of two atoms, referred to as “control” and “target”, respectively, and separated by the distance R . The target atom (T) is assumed to be initially prepared in a ground state, while the control (C) may be in a ground or a Rydberg level. When (T) is submitted to a laser beam of Rabi frequency Ω resonantly coupled to a transition towards a Rydberg state, its dynamics depends on (C): if (C) is in a ground state, (C) and (T) do not interact significantly, therefore (T) experiences unperturbed

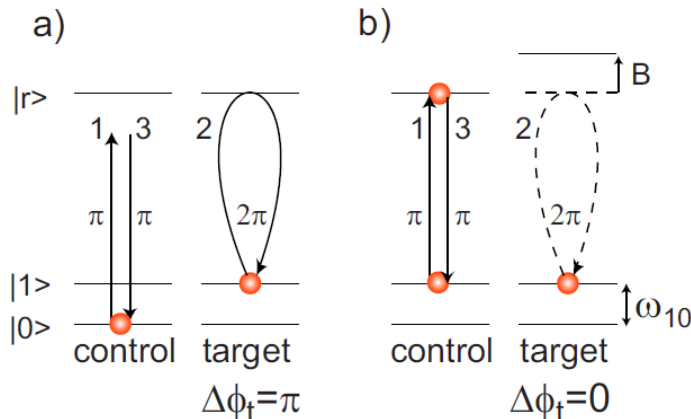


Figure 2: Rydberg blockade controlled phase gate operating on input states (a) $|01\rangle$ and (b) $|11\rangle$. Quantum information is stored in the basis states $|0\rangle$, $|1\rangle$ and state $|1\rangle$ is coupled to a Rydberg level $|r\rangle$ with excitation Rabi frequency Ω . The controlled phase gate is implemented with a three pulse sequence: (1) π pulse on control atom $|1\rangle \rightarrow |r\rangle$, (2) 2π pulse on target atom $|1\rangle \rightarrow |r\rangle \rightarrow |1\rangle$, and (3) π pulse on control atom $|r\rangle \rightarrow |1\rangle$. (a) The case where the control atom starts in $|0\rangle$ and is not Rydberg excited so there is no blockade. (b) The case where the control atom is in $|1\rangle$ which is Rydberg excited leading to blockade $B = V(R)$ of the target atom excitation. The picture is taken from (Saffman et al., 2010).

Rabi oscillations between the ground and Rydberg levels; by contrast, if (C) is in a Rydberg state, it effectively “shifts” the Rydberg state of (T) out of resonance with the laser of the quantity $V(R)$. Since the energy shift depends of R , the space can be effectively divided into two regions where $V(R) \gg \Omega$ and $V(R) \ll \Omega$ respectively. The boundary length R_b between these regions is defined by $V(R_b) \approx \Omega$, or equivalently $R_b \approx \sqrt[6]{\frac{C_6}{\Omega}}$.

In the first region where $R \ll R_b$ (which is called blockade volume), (T) cannot be excited to the Rydberg state if (C) itself is excited, as the laser is strongly off-resonant with the transition to the Rydberg state. Applying a 2π pulse ($\int ds \Omega(s) = 2\pi$) on the target, one therefore imposes an overall π phase factor on the two-atom wavefunction conditionally to (C) not being initially excited. Elaborating on this configuration, one can implement a phase gate on two qubits encoded in a pair of ground states of (C) and (T), as first proposed in (Jaksch et al., 2000) (see Fig. 2).

In the region $R \gg R_b$, the second atom can be excited to the Rydberg state but still experiences an energy shift which can be used to induce a phase on the system’s wavefunction.

To be more explicit, in this configuration the gate operation can be performed through applying two subsequent π pulses to both atoms (therefore exciting them both to the Rydberg state) separated by the waiting time $\frac{\pi}{V(R)}$ which imprints the π phase

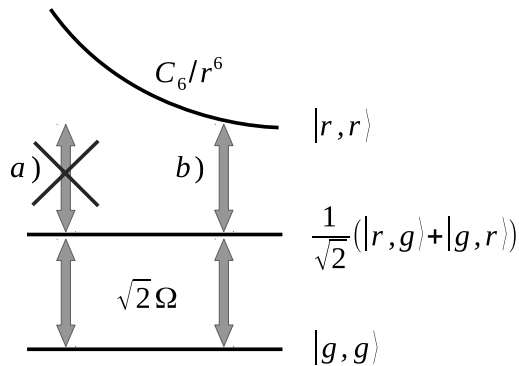


Figure 3: Energy level structure of the two-atom system being resonantly excited in a) complete blockade configuration, b) no blockade configuration.

on the wavefunction (Jaksch et al., 2000). As similar idea was proposed in (Protsenko et al., 2002) where authors assumed that the excitation lasers are detuned from the Rydberg state are brought back on resonance only in the presence of the dipole-dipole interactions. In (Brion et al., 2007c), the authors propose a scheme of implementation of the atomic phase gate, which avoids populating the Rydberg state.

Instead of individually addressing the atoms, one may also try to excite them collectively from the ground state $|gg\rangle$ with a resonant laser of Rabi frequency Ω (see Fig. 3). As above, if the atoms are located closer than R_b , the doubly excited state $|r, r\rangle$ is inaccessible by the laser (Fig. 3 (a)) The system therefore performs Rabi oscillations in the subspace within the subspace $|g, g\rangle$ and $\frac{1}{\sqrt{2}}\{|g, r\rangle + |r, g\rangle\}$ with the Rabi frequency enhanced by a $\sqrt{2}$ factor. This configuration can be used in order to create entanglement between atoms. In (Gaëtan et al., 2009) it was shown, for two Rb atoms located in traps separated by $\sim 3.5\mu m$ and simultaneously laser-excited on the transition towards the state $58d_{3/2}$, that the probability for both atoms to be in Rydberg state is strongly suppressed compared to the non-interacting configuration. In a subsequent experiment (Wilk et al., 2010) long-living entanglement was demonstrated by mapping the Rydberg state onto a different hyperfine (ground) state. Using a similar configuration a CNOT gate was demonstrated with two trapped Rb atoms separated by $10\mu m$ (Isenhower et al., 2010).

Due to the long-range character of dipole-dipole interactions, the blockade mechanism applies not only to few-atom systems but can be generalized to bigger ensembles. An extension of the original proposal (Jaksch et al., 2000) to mesoscopic-ensemble qubits was proposed in (Lukin et al., 2001). Similarly to the two-atom configuration, the many-atom system state space, can be restricted to the collective ground $|g_1 \dots g_N\rangle$ and singly excited $\frac{1}{\sqrt{N}} \sum_i |g_1 \dots r_i \dots g_N\rangle$ states, provided that multiply Rydberg-excited states are

strongly out of resonance. It can therefore be used in an analogous way to implement the two-qubit gate. Authors also propose to transfer the collective spin degrees of freedom to the photons, hence creating nonclassical states of light. Another collective approach is presented in (Brion et al., 2007a; 2008) where authors propose to use the internal atomic level structure to encode several quantum bits. In (Paredes-Barato and Adams, 2014) the authors propose an implementation scheme of the CZ gate, using the storage of photons in different Rydberg levels, which minimizes the distortion of photons, as it does not involve the propagation of excitations.

The field of quantum information and communication is very active and many proposals based on Rydberg blockaded atomic ensembles were recently put forward. Among many others, let us cite the implementation of quantum repeaters (Zhao et al., 2010; Brion et al., 2012) and quantum simulators (Weimer et al., 2010; Labuhn et al., 2015).

In general, the physics of dipole-dipole-interacting ensembles cannot be described only by means of the two-body interactions. In (Mourachko et al., 1998) authors study many-body effects in a dense atomic cloud and introduced the so-called “frozen Rydberg gas” model, which states that the motion of atoms on the timescales of the experiment is much smaller than the typical interatomic distance and therefore can be neglected. The complexity of the collective dynamics, generated by the Hamiltonian of dipole-dipole interactions in an atomic ensemble generates a lot of phenomena, more common in the field of condensed matter physics, e.g. thermalization, *etc.* The theoretical treatment of strongly correlated many-body problems is usually difficult, as many interesting effects can not be treated perturbatively. In (Lesanovsky et al., 2010) authors demonstrate that a coherently-driven two-level atomic ensemble thermalizes with respect to observables of the classical lattice gas for strong dipole-dipole interactions. The analogy with the second-order phase transition is pointed out in (Weimer et al., 2008) where authors derive the corresponding critical theory and demonstrate that in the saturated regime it describes the properties of the driven Rydberg two-level system. Extending these ideas, authors discuss the emergent universal scaling in (Löw et al., 2009). A similar many-body phenomenon is observed in (Schauß et al., 2012), where the competition between exciting laser and dipole-dipole interaction-induced shift leads to the formation of spatially ordered excitation patterns in a two-dimensional geometry.

Quantum nonlinear optics with Rydberg atoms

In this section we focus on the main subject of this dissertation, namely the effective interactions between photons, mediated by Rydberg-Rydberg interactions.

As soon as it was discovered, the dipole blockade appeared as a way to create non-classical states of light, using the storage of excitations in the form of Rydberg polaritons, as first introduced in (Lukin et al., 2001): due to blockade, a small atomic sample can only accommodate for and therefore store one photon. In (Dudin and

Kuzmich, 2012), the authors demonstrate a single-photon source based on the strong suppression of the two-excitation component in the spinwave stored in the Rydberg-blockaded ensemble and characterize it by measuring the intensity correlation function of the retrieved light. However, as will be shown in this section, the storage is not absolutely necessary and many interesting quantum phenomena can be observed with propagating photons.

The strong dipole-dipole interactions between Rydberg atoms can be converted into effective interactions between photons. An optical nonlinearity, arising from the dipole-dipole interactions of high-lying atomic levels was first observed in (Pritchard et al., 2010). The $\chi^{(3)}$ susceptibility, estimated in (Pritchard et al., 2013), though insufficient to implement interaction between photons, suggested that its higher density extrapolation should enter the “quantum realm”. The underlying idea consists in coupling optical photons to Rydberg atomic excitations, using a three-level ladder excitation scheme - the Rydberg blockade therefore effectively translates into a photon blockade.

The physical mechanism behind such effective photon-photon interactions can be seen as follows. Due to the dipole-dipole induced energy shift of doubly Rydberg excited ensemble states, a photon propagating through the medium as a dark-state polariton (Fleischhauer and Lukin, 2000) modifies the optical response of the ensemble in its neighborhood. Depending on the parameters, this may either change the group velocity or cause the scattering of a subsequent photon – emulating therefore an effective photon-photon interaction.

In (Friedler et al., 2005), the authors propose to combine the EIT ladder scheme with strong dipole-dipole interactions of one of the upper levels. According to their proposal, two photons of different polarizations are converted into two different polaritons when entering the medium. This requires an atomic medium with a double-ladder structure as shown in Fig. 4, the lower transitions $|g\rangle \rightarrow |e_{1,2}\rangle$ being driven by the photons while the upper transitions $|e_{1,2}\rangle \rightarrow |d_{1,2}\rangle$ are coupled to two classical fields of Rabi frequencies $\Omega_{1,2}$. It is well known that the speed of EIT dark-state polaritons can be tuned by changing the control field Rabi intensity: in particular, if the Rydberg polaritons are slowed down or almost stopped (then they essentially have an atomic character) in the vicinity of each other, they strongly interact via dipole-dipole interaction and may acquire a π phase factor (Friedler et al., 2005).

In the subsequent proposals based on Rydberg EIT polaritons, two physically different regimes were investigated. In the so-called *absorptive* case, the intermediate state of the ladder scheme is resonant with the probe field: in that case the first propagating photon increases the absorption for the second one by shifting the Rydberg state out of resonance, effectively transforming the atoms within the blockade volume into resonant two-level systems. By contrast, in the so-called *dispersive* regime, *i.e.* when the intermediate level is detuned, Rydberg spheres are essentially composed of non-resonant two-level atoms: absorption is negligible but dispersion is high and therefore the group velocity of a second incoming photon is substantially changed.

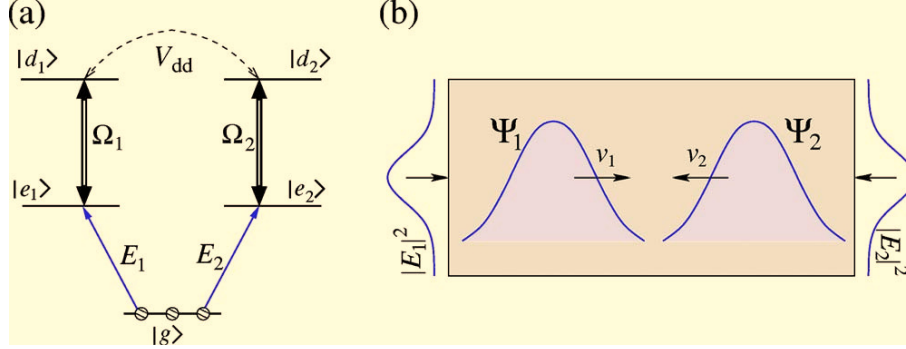


Figure 4: (a) Level scheme of atoms interacting with weak (quantum) fields $E_{1,2}$ on the transitions $|g\rangle \rightarrow |e_{1,2}\rangle$ and strong driving fields of Rabi frequencies $\Omega_{1,2}$ on the transitions $|e_{1,2}\rangle \rightarrow |d_{1,2}\rangle$. V_{dd} denotes the dipole-dipole interaction between pairs of atoms in Rydberg states $|d\rangle$. (b) Upon entering the medium, each field having Gaussian transverse intensity profile is converted into the corresponding polariton $\Psi_{1,2}$ representing a coupled excitation of the field and atomic coherence. These polaritons propagate in the opposite directions with slow group velocities $v_{1,2}$ and interact via the dipole-dipole interaction. Taken from (Friedler et al., 2005).

The original idea of photon-photon interactions via dipole blockade was further developed in (Gorshkov et al., 2011), and extended to co-propagating and stored photons, revealing, in particular, the strong correlations between photons in the co-propagating case. In (Gorshkov et al., 2013) authors considered the absorptive configuration of the EIT ladder, bringing the intermediate state to resonance which allows the system to transmit only the single photon component, while scattering the rest. In (Bienias et al., 2014), the authors used the scattering theory formalism to calculate the 1D scattering length and showed that, depending on the control field Rabi frequency, the effective interaction potential can be either attractive or repulsive. Moreover, in (Maghrebi et al., 2015) the authors predicted the existence of Coulomb bound states of photons. The complexity of the system makes authors resort to numerical and analytical techniques taken from the many-body physics (Negele and Orland, 1988; Giamarchi et al., 2004): in (Otterbach et al., 2013) authors used DMRG to numerically fit the parameters of Luttinger model to effectively describe the Wigner crystallization of photons in a Rydberg EIT medium; in (Moos et al., 2015) the authors developed an effective description of the Rydberg polariton propagation and dissipative coupling to bright-state polaritons, based on perturbation theory.

The experimental implementation of the *absorptive* regime, in a cloud with and optical depth per blockade sphere $OD_b \approx 5$ was reported in (Peyronel et al., 2012). The photon statistics of the light transmitted through the cloud was shown to be strongly antibunched due to the scattering of the multiphoton components in the incident light. By contrast, in the *dispersive* regime photons were experimentally shown to propagate as massive, mutually attracting particles, therefore leading to photon

bunching (Firstenberg et al., 2013). In addition, a conditional phase shift, resulting in polarization-entangled photon pairs was demonstrated.

In (Baur et al., 2014) the authors demonstrated the first Rydberg-based photon switch, which forbids the transmission of the “target” photon conditionally to the presence of a “gate” photon, stored in the ensemble as a Rydberg collective spinwave. The idea is again to take advantage of Rydberg EIT in the absorptive regime: if the cloud contains no excitation initially, then it is transparent to the target photon; by contrast, the latter is scattered by one of the effective resonant two-level atoms in the blockade sphere of an initially stored Rydberg spinwave. The coherence of the stored gate spinwave is affected by the presence of the target photon. As theoretically investigated in (Li and Lesanovsky, 2015), this effect can be reduced by stronger dipole-dipole interactions.

The single-photon transistor is very similar a single photon switch: in the former the single target photon is however replaced by a stronger input beam. The performance of such a transistor can be quantified by the “gain” which is given by the number of scattered photons of the target beam. In (Gorniaczyk et al., 2014; Tiarks et al., 2014) authors reported single photon transistors with gains $G > 10$.

Outline of this dissertation

To effectively enhance medium-induced optical nonlinear effects, it is natural to resort to a resonator (cavity) which allows for light multiple passes through the active medium. Such a system was studied both theoretically and experimentally in the dispersive regime for a relatively weak nonlinearity, so that the field could still be treated classically (Parigi et al., 2012; Stanojevic et al., 2013). In particular, in (Parigi et al., 2012) the authors demonstrated the intensity-dependent shift of the cavity resonance.

In this dissertation, we investigate the optical nonlinear effects induced by a Rydberg medium in the quantum regime.

In the *first* chapter we present the system we shall consider throughout the whole dissertation. We first provide equations governing the system’s dynamics in Schrödinger and Heisenberg pictures. In order to characterize the action of nonlinearity on the photonic field, we define the intensity correlation function $g^{(2)}$ and recall its basic properties.

In the *second* chapter we consider the so-called dispersive regime, *i.e.* when the intermediate state is far detuned, $\Delta_e \gg \gamma_e$, and can be eliminated. We moreover employ the bubble picture approximation in which the system effectively consists in an ensemble of two-level superatoms coupled to the cavity mode, described by the driven-dissipative Tavis-Cummings model. We evaluate numerically and analytically the $g^{(2)}$ function of the transmitted light, which, depending on the cavity parameters, is shown to be either bunched or antibunched.

In the *third* chapter we present an alternative treatment of the system, which allows us to investigate the resonant regime that was unexplored so far. Restricting ourselves to low feeding, we analytically derive the correlation function $g^{(2)}(\tau)$ for the transmitted and reflected lights, based on the factorization of the lowest perturbative order of operator product averages. We then propose an effective non-linear three-boson model for the coupled atom-cavity system: this Ansatz allows us to obtain the same results as the (more cumbersome) exhaustive treatment and gives a more intuitive physical picture of our system and its dynamical behavior. Finally, we investigate the resonant regime of the system ($\Delta_e \approx 0$) and our treatment reveals novel features of the pair correlation function $g^{(2)}$ due to the interplay of the impedance matching and dipole-dipole interactions.

In the *fourth* chapter we analyze the system in the so-called Schwinger-Keldysh contour formalism. Using Wick's theorem, we perturbatively expand correlation functions with respect to both feeding and dipole-dipole interactions Hamiltonians. We perform a complete resummation with respect to the latter, for each correlation function that we encounter in this chapter. Using this method we re-derive results of Chap. 3 in an analytic form. We also go beyond and derive analytic expressions for the elastic and inelastic components of the cavity transmission spectrum. We identify a polaritonic resonance structure in this spectrum, to our knowledge unreported so far, that we physically interpret.

In the *fifth* chapter we present a novel scheme for a high-fidelity photonic controlled-phase gate, based on the Rydberg blockade in an atomic ensemble loaded in an optical cavity. In our scenario, the π phase factor is induced by the reflection of the target photonic qubit on the cavity, conditioned by the presence of an intracavity stored polariton, associated to the control qubit. The resulting gate can be implemented with cavities of moderate finesse allowing for highly efficient and robust processing of quantum information encoded in photons.

Finally, App. A presents an application of our methods to an experimental measuring of nonlinear transmission of an optical cavity containing Rydberg atoms. Apps. B-G discuss various technical issues, and App. H is a preprint of an article related to Chap. 5 of this thesis.

Contents

1	Description of the system	21
1.1	Presentation of the system	22
1.1.1	General equations	24
1.1.2	Master equation	26
1.1.3	Heisenberg-Langevin equations	26
1.2	Quantum statistics of light	27
1.2.1	Measurement of the $g^{(2)}$ function.	28
1.2.2	Photon statistics	29
2	Rydberg-induced quantum optical nonlinearities in the dispersive regime	35
2.1	Effective two-level model	36
2.2	Rydberg bubble approximation	38
2.3	Tavis-Cummings Hamiltonian	40
2.4	Calculation of the $g^{(2)}$ function	42
2.5	Numerical results and discussion	44
2.6	Conclusion	47
3	Perturbative treatment at lowest-order	49
3.1	$g^{(2)}$ function in the perturbative regime	50
3.1.1	Factorization property	50
3.1.2	First order mean values	51
3.1.3	Second order mean values	51
3.1.4	Two-time correlation functions	53
3.2	Application to an experimental case.	53
3.2.1	Dispersive regime.	53
3.2.2	Resonant case	55
3.3	Effective non-linear three-boson model	57
3.3.1	Dispersive regime	60
3.3.2	Resonant case	60
3.4	Conclusion	60

CONTENTS

4	Schwinger-Keldysh contour formalism.	63
4.1	Introduction	64
4.1.1	Bosonic representation of the Hamiltonian	64
4.1.2	Contour-ordered representation of correlation functions	65
4.2	Wick's theorem and Green's functions	70
4.2.1	Wick's theorem	70
4.2.2	Green's functions	71
4.3	First order quantities	75
4.4	Factorization of averages in the lowest order	77
4.5	Intensity correlation function	79
4.5.1	$g^{(2)}$ function	79
4.5.2	T matrix	85
4.5.3	Relation to the decoupled case	86
4.5.4	Numerical results	88
4.6	$G^{(1)}$ correlation function	91
4.6.1	Elastic contribution	93
4.6.2	Inelastic contribution to $G_{out}^{(1)}$	96
4.6.3	Transmission spectrum	98
4.7	Conclusions	99
5	Photonic phase gate	103
5.1	Presentation of the protocol	104
5.2	Photon scattering on the cavity	107
5.2.1	Dynamical equations	107
5.2.2	Reference situation	108
5.2.3	Cavity with non-interacting two-level atoms	109
5.3	Gate operation	111
5.3.1	Evolution of $ 00\rangle, 10\rangle$	111
5.3.2	Evolution of $ 01\rangle$	111
5.3.3	Evolution of $ 11\rangle$	112
5.4	Numerical results	115
5.4.1	Choi-Jamiolkowsky fidelity	115
5.4.2	Dual rail encoding	117
5.5	Conclusions	118
6	Outlook	119
A	Transmission of an intracavity Rydberg medium: experimental results vs theoretical methods	121
A.1	S-Rydberg state	121
A.1.1	Presentation of the model	121

A.1.2 Comparison with the experimental data	123
A.2 D-Rydberg state	123
A.2.1 Presentation of the model	123
A.2.2 Experimental results vs theoretical methods	126
B Bosonic representation	129
B.1 Bosonic representation	129
B.2 Spinwave basis	131
C The second-order correlation function $g^{(2)}$ of the reflected/transmitted light	135
D Factorization of correlation functions.	137
E Calculation of $\langle aa \rangle^{(2)}$	139
F Factorization in the presence of extra dephasing	143
G Computation of integrals	147
H C-PHASE gate	149

CONTENTS

Chapter 1

Description of the system

Contents

1.1	Presentation of the system	22
1.1.1	General equations	24
1.1.2	Master equation	26
1.1.3	Heisenberg-Langevin equations	26
1.2	Quantum statistics of light	27
1.2.1	Measurement of the $g^{(2)}$ function.	28
1.2.2	Photon statistics	29

1. Description of the system

In this chapter we present the system we shall consider throughout the whole dissertation. It comprises an ensemble of ladder-type three-level atoms loaded in an optical cavity and excited in EIT conditions: the cavity mode drives the lower atomic transition while the upper transition to the Rydberg state is driven by a strong control field. In order to describe the behavior of the system we provide equations governing its dynamics in Schrödinger and Heisenberg pictures (Sec. 1.1). Due to the strong dipole-dipole interactions between Rydberg atoms, the system exhibits non-linear behavior, potentially noticeable at the single photon level: in order to characterize this nonlinearity we define the intensity correlation function $g^{(2)}$ (Sec. 1.2). The following chapters are devoted to its determination in various regimes. Here, we only recall its basic properties and give classical bounds on values it can take. We provide examples of states of light that violate these bounds, testifying therefore the quantum nature of light.

1.1 Presentation of the system

The system we consider is schematically shown on Fig. 1.1 : it comprises N atoms which present a three-level ladder structure with a ground $|g\rangle$, intermediate $|e\rangle$ and Rydberg states $|r\rangle$. The energy of the atomic level $|k = g, e, r\rangle$ is denoted by $\hbar\omega_k$ (by convention $\omega_g = 0$) and the coherence decay rates are γ_e (intermediate state) and γ_r (Rydberg state). The transitions $|g\rangle \leftrightarrow |e\rangle$ and $|e\rangle \leftrightarrow |r\rangle$ are respectively driven by a weak probe field of frequency ω_p and a strong control field of frequency ω_{cf} . Both fields can *a priori* be resonant or not with atomic transitions, the respective detunings being defined by $\Delta_e \equiv (\omega_p - \omega_e)$ and $\Delta_r \equiv (\omega_p + \omega_{cf} - \omega_r)$. Moreover, the atoms are placed in an optical cavity: we shall denote by $\gamma_c^{(L,R)}$ the respective decay rates through the left and right mirrors (see Fig. 1.1), with $\gamma_c \equiv \gamma_c^{(L)} + \gamma_c^{(R)}$. The transition $|g\rangle \leftrightarrow |e\rangle$ is supposed in the neighborhood of a cavity resonance. The frequency and annihilation operator of the corresponding mode are denoted by ω_c and a , respectively ; the detuning of this mode with the probe laser is defined by $\Delta_c \equiv (\omega_p - \omega_c)$ and α denotes the feeding rate of the cavity related to the incoming photon flux via $I_{in} = \frac{\alpha^2}{2\gamma_c^{(R,L)}}$. Finally, we introduce g (that we assume to be the same for all atoms) which is the single-atom coupling constant of the transition $|g\rangle \leftrightarrow |e\rangle$ with the cavity mode, and Ω_{cf} the Rabi frequency of the control field on the transition $|e\rangle \leftrightarrow |r\rangle$. In order to characterize the collective coupling of the atomic ensemble to the cavity mode we also define the cooperativity of the sample $C \equiv \frac{g^2 N}{2\gamma_e \gamma_c}$.

In order to be more specific, we provide the following set of experimentally feasible parameters. We assume that the atomic ensemble is composed of ^{87}Rb atoms. We use the following atomic levels as ground, intermediate and Rydberg states: $|g\rangle = |5s_{\frac{1}{2}}; F = 2\rangle$, $|e\rangle = |5p_{\frac{3}{2}}; F = 3\rangle$ and $|r\rangle = |nd_{\frac{5}{2}}; F = 4\rangle$, where the principal quantum number n will typically be chosen around 100. The decay rate of the intermediate level

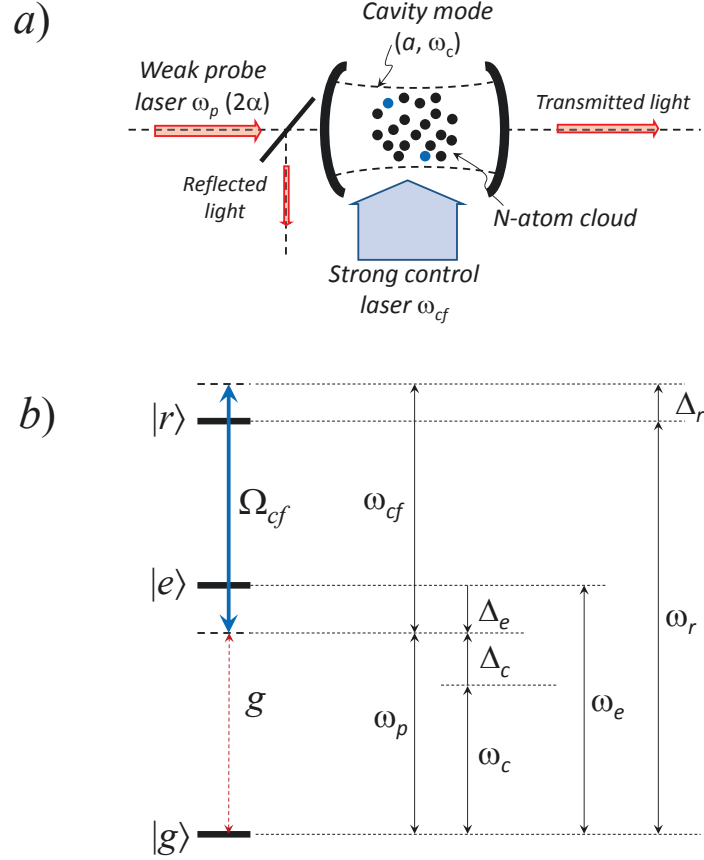


Figure 1.1: a) The setup consists of N cold atoms placed in an optical cavity which is fed by a weak (classical) laser beam of frequency ω_p and a strong control laser field of frequency ω_{cf} . b) The atoms present a three-level ladder structure $\{|g\rangle, |e\rangle, |r\rangle\}$. The transitions $|g\rangle \leftrightarrow |e\rangle$ and $|e\rangle \leftrightarrow |r\rangle$ are driven by the injected probe and control laser fields, respectively, with the respective coupling strength and Rabi frequency g and Ω_{cf} (see the text for the definitions of the different detunings represented here).

is given by $\gamma_e = 2\pi \times 3$ MHz. It is convenient to express all energy parameters in units of γ_e . In order to be consistent with the experimental work at IOGS for the cavity decay rate we take $\gamma_c = 0.3\gamma_e$. Since several physical effects of different natures shall be addressed in this dissertation, the parameters that are optimal may vary depending on our purpose: we shall therefore provide the complete set of parameters in each case specifically. We also notice that the principal quantum number of the Rydberg state n plays a double role as on one hand it increases the interatomic interaction coefficient $C_6 \approx 15000\gamma_e \left(\frac{n}{56}\right)^{11}$, but on the other it decreases the control field Rabi frequency $\Omega_{cf} \sim n^{-3/2}$ thus effectively decreasing the coupling to the Rydberg state.

Nonlinearity is generated in the system not only by the dipole-dipole interactions between Rydberg atoms but also by the EIT ladder scheme itself. The contribution of the latter is, however, negligible in the regime of parameters we use.

1. Description of the system

If the nonlinearity is relatively weak, the non-linear response can be estimated in the semiclassical regime in which the cavity mode is treated classically, *i.e.* $a \rightarrow \langle a \rangle$, while atoms remain quantum. This approach will be considered in both dispersive (Parigi et al., 2012; Stanojevic et al., 2013; Sevinçli et al., 2011) and resonant regimes (Boddeda et al., 2016).

When the nonlinearity becomes significant at the single-photon level, this approach, however, is no longer relevant and one has to consider the cavity mode field to be quantum. The non-linearity of the sample can then be characterized by its action on the quantum statistics of light transmitted through or reflected from the cavity. As one may expect, strong nonlinearities modify the response of the sample for a single photon and for pairs of photons in a different way. This effect is well addressed by means of the intensity correlation function $g^{(2)}$ that we explain in more details in Sec. 1.2.

In the sections below we give details on the mathematical framework that we use in order to describe the dynamics of the system.

1.1.1 General equations

The dynamics of an any *closed* quantum system can be generally described in three ways: Schrödinger, Heisenberg and interaction pictures. In this section we consider only the first two, leaving the description of the interaction picture to Chap. 4. In the Heisenberg picture all operators are time-dependent and the averaging is performed over the initial state of the system. On the other hand in Schrödinger picture the state of the system evolves in time while operators are taken at initial time.

We may apply both approaches to the system described above. For the sake of consistency one has to take into account the modes of the environment, so that the system {cavity + atoms+ baths} can be approximately considered closed. Below, we give the expression of the corresponding Hamiltonian of the *full* system in the frame rotating at the frequency ω_p for the intermediate state $|e\rangle$, the cavity baths and the electromagnetic field modes coupled to the transition $e \leftrightarrow g$, and the frequency $(\omega_p + \omega_{cf})$ for the Rydberg state $|r\rangle$ and the electromagnetic field modes coupled to the transition $r \leftrightarrow g$. In the RWA, the Hamiltonian takes the form

$$H = H_{at} + H_{cav} + V_{at-cav} + H_f + H_{bath} + V_{at-bath} + V_{cav-bath} \quad (1.1)$$

with

$$H_{at} = \sum_{n=1}^N \left\{ -\Delta_e \sigma_{ee}^{(n)} - \Delta_r \sigma_{rr}^{(n)} + \frac{\Omega_{cf}}{2} (\sigma_{re}^{(n)} + \sigma_{er}^{(n)}) \right\} + \frac{1}{2} \sum_{m,n}^N \kappa_{mn} \sigma_{rr}^{(m)} \sigma_{rr}^{(n)} \quad (1.2)$$

$$H_{cav} = -\Delta_c a^\dagger a \quad (1.3)$$

$$V_{at-c} = \sum_{n=1}^N g (a \sigma_{eg}^{(n)} + a^\dagger \sigma_{ge}^{(n)}) \quad (1.4)$$

$$H_f = \alpha (a + a^\dagger) \quad (1.5)$$

$$H_{bath} = \sum_{\lambda=L,R} \int d\omega \omega B_{\lambda,\omega}^\dagger B_{\lambda,\omega} + \int d\omega \omega \sum_{n=1}^N (D_{n,\omega}^\dagger D_{n,\omega} + C_{n,\omega}^\dagger C_{n,\omega}) \quad (1.6)$$

$$V_{at-bath} \approx \sum_{n=1}^N \int d\omega [g_c(\omega) C_{n,\omega} \sigma_{eg}^{(n)} + g_d(\omega) D_{n,\omega} \sigma_{rg}^{(n)} + \text{H.c.}] \quad (1.7)$$

$$V_{cav-bath} = \sum_{\lambda=L,R} \int d\omega g_\lambda(\omega) [B_{\lambda,\omega} a^\dagger + B_{\lambda,\omega}^\dagger a] \quad (1.8)$$

where $\sigma_{\mu,\eta}^{(n)} \equiv \mathbb{I}^{(1)} \otimes \dots \otimes \mathbb{I}^{(n-1)} \otimes |\mu\rangle \langle \eta| \otimes \mathbb{I}^{(n+1)} \otimes \dots \otimes \mathbb{I}^{(N)}$, ω_μ is the energy of the atomic level $|\mu\rangle$ for $\mu = e, r$ (with the convention $\omega_g = 0$), and $\kappa_{mn} \equiv \frac{C_6}{\|\vec{r}_m - \vec{r}_n\|^6}$ denotes the van der Waals interaction between atoms in the Rydberg level – when atoms are in the ground or intermediate states, their interactions are neglected. By $\Delta_c \equiv (\omega_p - \omega_c)$, $\Delta_e \equiv (\omega_p - \omega_e)$, and $\Delta_r \equiv (\omega_p + \omega_{cf} - \omega_r)$ we denote the cavity, intermediate and Rydberg state detunings, respectively. The operators $B_{\lambda=L,R}(\omega)$ denote the left ($\lambda = L$)/right ($\lambda = R$) handside bath operators coupled to the two-sided cavity mode with the respective coupling strengths $g_{\lambda=L,R}(\omega)$, whereas $\{C_n(\omega)\}$ and $\{D_n(\omega)\}$, are bath operators coupled to the atomic operators with the respective coupling strengths $g_c(\omega)$ and $g_d(\omega)$. Note that, here, we implicitly assumed that atoms are coupled to different baths, though with the same coupling constants. α denotes the cavity feeding rate which can be related to the incoming photon flux via $\frac{\alpha^2}{2\frac{g_{b,L}^2}{2\pi}}$, assuming that feeding is performed through the left mirror of the cavity.

In Schrödinger picture, the master equation for the full density matrix of the system ρ_f is given by

$$\frac{d}{dt} \rho_f = -i [H, \rho_f] \quad (1.9)$$

In the Heisenberg picture for any time-dependent operator \hat{X} of the system we have:

$$\frac{d}{dt} \hat{X} = i [H, \hat{X}]$$

Given the structure of the baths in the Hamiltonian Eqs. (1.2-1.8) we moreover

1. Description of the system

assume that the coupling coefficients of bath modes are frequency independent *i.e.* $g_{\lambda,c,d}(\omega) \approx g_{\lambda,c,d}$. This constitutes Markov approximation, under which the system {cavity+atoms} is effectively decoupled from the bath modes. As will be addressed in the following subsections, in Markov approximation, the interaction with baths is accounted for by merely introducing extra terms in the dynamical equations.

1.1.2 Master equation

Assuming that the subsystem {atoms,cavity} is initially disentangled from the baths, it will remain so under the conditions of Markov approximation and therefore the total density matrix of the system factorizes at all times $\rho_f(t) \approx \rho(t) \otimes \rho_{bath}(t)$. In this approximation, one deduces the Master equation for the reduced density matrix of the system $\rho(t)$ (Breuer and Petruccione, 2002):

$$\frac{d}{dt}\rho = -i[H_{sys}, \rho] + \mathcal{D}[\rho] \quad (1.10)$$

where H_{sys} is the Hamiltonian of the reduced system {cavity+atoms} Eqs. (1.2-1.5). We note that the master equation Eq. (1.10) contains extra terms compared to Eq. (1.9) that are denoted by $\mathcal{D}[\rho]$. This operator contains the so-called Lindblad decay superoperators that correspond to decays of Rydberg ($|r\rangle$) and intermediate ($|e\rangle$) states of each atom along with the decay of the cavity mode:

$$\begin{aligned} \mathcal{D}[\rho] &= (\gamma_c^R + \gamma_c^L) (2a\rho a^\dagger - a^\dagger a \rho - \rho a^\dagger a) \\ &+ \gamma_e \sum_{n=1}^N (2\sigma_{ge}^{(n)} \rho \sigma_{eg}^{(n)} - \sigma_{ee}^{(n)} \rho - \rho \sigma_{ee}^{(n)}) \\ &+ \gamma_r \sum_{n=1}^N (2\sigma_{gr}^{(n)} \rho \sigma_{rg}^{(n)} - \sigma_{rr}^{(n)} \rho - \rho \sigma_{rr}^{(n)}) \end{aligned} \quad (1.11)$$

1.1.3 Heisenberg-Langevin equations

Implementing Markov approximation in the Heisenberg picture leads to a modified set of dynamical equations. We note that due to the interaction with baths the Heisenberg equations for the {cavity+atoms} reduced system's operators (Walls and Milburn, 2007) writes

$$\frac{d}{dt}\hat{X} = i[H_{sys}, \hat{X}] - \gamma_x \hat{X} + F_x$$

where γ_x and F_x denote the decay rate and Langevin noise operator, associated to the operator X , respectively. Taking this into account we now write the set of Heisenberg-Langevin equations for all degrees of freedom of the reduced system:

$$\frac{d}{dt} a = (i\Delta_c - \gamma_c) a - i\alpha - ig \sum_i^N \sigma_{ge}^{(i)} + \sqrt{2\gamma_c^{(L)}} a_{in}^{(L)} + \sqrt{2\gamma_c^{(R)}} a_{in}^{(R)} \quad (1.12)$$

$$\frac{d}{dt} \sigma_{ge}^{(i)} = (i\Delta_e - \gamma_e) \sigma_{ge}^{(i)} - i\frac{\Omega_{cf}}{2} \sigma_{gr}^{(i)} + iga (\sigma_{ee}^{(i)} - \sigma_{gg}^{(i)}) + F_{ge}^{(i)} \quad (1.13)$$

$$\frac{d}{dt} \sigma_{gr}^{(i)} = (i\Delta_r - \gamma_r) \sigma_{gr}^{(i)} - i\frac{\Omega_{cf}}{2} \sigma_{ge}^{(i)} + iga \sigma_{er}^{(i)} - i\sigma_{gr}^{(i)} \sum_{j \neq i}^N \kappa_{ij} \sigma_{rr}^{(j)} + F_{gr}^{(i)} \quad (1.14)$$

$$\frac{d}{dt} \sigma_{er}^{(i)} = iD_{er} \sigma_{er}^{(i)} + i\frac{\Omega_{cf}}{2} (\sigma_{rr}^{(i)} - \sigma_{ee}^{(i)}) + iga^\dagger \sigma_{gr}^{(i)} - i\sigma_{er}^{(i)} \sum_{j \neq i}^N \kappa_{ij} \sigma_{rr}^{(j)} + F_{er}^{(i)} \quad (1.15)$$

where $a_{in}^{(L)}$, $a_{in}^{(R)}$ and $F_{\alpha\beta}^{(i)}$ denote the Langevin forces associated to the incoming fields from the left and right sides of the cavity and to the atomic operator $\sigma_{\alpha\beta}^{(i)}$, respectively. We also introduced the complex effective detunings $D_k \equiv (\Delta_k + i\gamma_k)$ for $k = c, e, r$ and $D_{er} \equiv (\Delta_r - \Delta_e) + i(\gamma_r + \gamma_e)$. Note that we chose to make the feeding factor α appear explicitly in Eq. (1.12): in technical terms, it corresponds to displacing the incoming field from the coherent state $|\alpha\rangle$ to the vacuum $|0\rangle$; to be consistent with this choice, from now on, we must set $\langle a_{in} \rangle = 0$.¹

In conclusion we emphasize that both pictures lead to the same equations for correlation functions and are thus equivalent. In this dissertation, we will use both methods to determine the intensity correlation function of light $g^{(2)}$ but in slightly different contexts (see Chaps. 2 and 3).

In the next section we define the $g^{(2)}$ function, recall its basic properties and give details about the physical information it provides.

1.2 Quantum statistics of light

The quantum statistics of light can be characterized by the distribution of pairs inside the corresponding quantized mode. To this end we consider the normalized probability to detect a pair of photons at two subsequent times t_1 and t_2 . Mathematically the $g^{(2)}(t_1, t_2)$ intensity correlation function of the light is defined as (Loudon, 2000):

$$g^{(2)}(t_1, t_2) \equiv \frac{\langle a^\dagger(t_1) a^\dagger(t_2) a(t_2) a(t_1) \rangle}{\langle a^\dagger(t_1) a(t_1) \rangle \langle a^\dagger(t_2) a(t_2) \rangle} \quad (1.16)$$

¹The set of Heisenberg-Langevin equations (1.12-1.15) allows us to recover the standard full linear spectral response of the intracavity EIT. Indeed, assuming $\alpha = \alpha(t)$ we get in the temporal Fourier space:

$$\langle a(\omega) \rangle = \frac{\alpha(\omega)}{\omega + D_c - \frac{g^2 N}{\omega + D_e - \frac{\Omega_{cf}^2}{4(\omega + D_r)}}$$

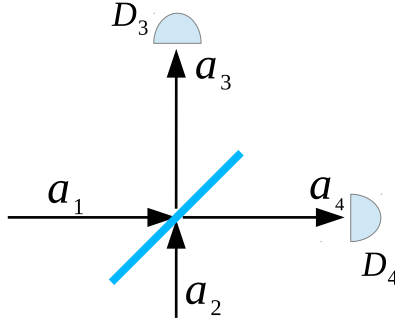


Figure 1.2: The scheme of the Hanbury Brown and Twiss experiment.

where $a(t) \equiv \frac{1}{\sqrt{2\pi}} \int d\omega a_\omega e^{-i\omega t}$ is the Heisenberg operator of the quantized field at the position of detector (assumed to be $z = 0$), while a_ω is the annihilation operator of the ω -frequency mode. The averaging in Eq. (1.16) is performed over the initial state of the system ρ_0 , *i.e.* $\langle \dots \rangle \equiv \text{Tr}[\dots \rho_0]$. We may notice that for a stationary field the expression Eq. (1.16) can be simplified to

$$g^{(2)}(\tau) \equiv \frac{\langle a^\dagger(0) a^\dagger(\tau) a(\tau) a(0) \rangle}{\langle a^\dagger(0) a(0) \rangle^2}$$

where we assumed the time-translational invariance of expressions:

$$\begin{aligned} \langle a^\dagger(t) a^\dagger(t+\tau) a(t+\tau) a(t) \rangle &= \langle a^\dagger(0) a^\dagger(\tau) a(\tau) a(0) \rangle \\ \langle a^\dagger(t) a(t) \rangle &= \langle a^\dagger(0) a(0) \rangle \end{aligned}$$

In the remainder of this section we shall show how to experimentally determine the $g^{(2)}$ function and more precisely relate its behavior to the quantum statistical properties of light.

1.2.1 Measurement of the $g^{(2)}$ function.

In this section we describe the method which is frequently used to experimentally determine the $g^{(2)}$ function. It is based on the intensity cross correlation measurement using the Hanbury-Twiss interferometer shown on Fig. 1.2². We denote by a_1, a_2 the annihilation operators of the two input modes of the interferometer and by a_3, a_4 those of the two output modes. We assume that the signal that we want to characterize has the density matrix ρ_1 and is sent on the first arm of the interferometer. The second arm is assumed in its vacuum state $|0\rangle$. The full density matrix of the system consisting of

²This setup allows to perform the measurement of the correlation function $g^{(2)}(\tau)$ for any delay time τ , contrary to the single-detector setup where the resolution is limited by the bandwidth of the detector.

two arms is thus given by $\rho = \rho_1 \otimes |0\rangle_2 \langle 0|_2$. According to the standard beam-splitter input-output relation, for two output channels (Scully and Zubairy, 1997) we have:

$$\begin{aligned} a_3(t) &= \frac{1}{\sqrt{2}} (a_1(t) + a_2(t)) \\ a_4(t) &= \frac{1}{\sqrt{2}} (a_1(t) - a_2(t)) \end{aligned}$$

Consider now photon fluxes on each detector separately:

$$\begin{aligned} \langle a_{3,4}^\dagger(t) a_{3,4}(t) \rangle &= \frac{1}{2} \langle (a_1^\dagger(t) \pm a_2^\dagger(t)) (a_1(t) \pm a_2(t)) \rangle \\ &= \frac{1}{2} \langle a_1^\dagger(t) a_1(t) \rangle \end{aligned}$$

where the plus and minus signs correspond to the third and fourth modes respectively. For the correlation of fluxes on the detectors D_1 at time t_1 and D_2 at time t_2 , we get respectively:

$$\langle a_3^\dagger(t_1) a_4^\dagger(t_2) a_4(t_2) a_3(t_1) \rangle = \frac{1}{4} \langle a_1^\dagger(t_1) a_1^\dagger(t_2) a_1(t_2) a_1(t_1) \rangle$$

we therefore conclude that $g^{(2)}(t_1, t_2)$ is given by the cross-correlation of intensities in two different output arms of the interferometer.

$$g^{(2)}(t_1, t_2) = \frac{\langle a_3^\dagger(t_1) a_4^\dagger(t_2) a_4(t_2) a_3(t_1) \rangle}{\langle a_3^\dagger(t_1) a_3(t_1) \rangle \langle a_4^\dagger(t_2) a_4(t_2) \rangle}$$

1.2.2 Photon statistics

In this subsection³ we show what information on the quantum statistics of light is contained in the $g^{(2)}(\tau)$ function. In both cases $\tau \neq 0$ and $\tau = 0$, we determine the classical bounds on the correlation functions and show when they can be violated due to the quantum nature of light. In the former case ($\tau \neq 0$) the violation of the classical inequality is associated to the effect known as antibunching while in the latter case ($\tau = 0$), it reveals the sub-Poissonian photon statistics. We stress that as shown in (Zou and Mandel, 1990) these effects do not necessarily occur together.

³This subsection essentially follows (Scully and Zubairy, 1997)

1. Description of the system

Bunching/antibunching

Let us first consider the photon flux $I(t) \equiv a^\dagger(t) a(t)$ treating it as a classical quantity, and introduce the joint probability density distribution $p_{cl}(t, I, t', I')$ for the field to have photon fluxes at times t and t' to be equal to I and I' , respectively. We have for the correlation function:

$$\langle I(t) I(t + \tau) \rangle_{cl} = \int dI dI' \times I \times I' \times p_{cl}(t, I, t + \tau, I') \quad (1.17)$$

Let us now apply the Cauchy-Schwarz inequality to Eq. (1.17):

$$\langle I(t) I(t + \tau) \rangle_{cl} \leq \left\{ \int dI \times I^2 \times p_{cl}(t, I) \right\}^{\frac{1}{2}} \left\{ \int dI \times I^2 \times p_{cl}(t + \tau, I) \right\}^{\frac{1}{2}}$$

where $p_{cl}(t, I) \equiv \int dI' p_{cl}(t, I, t + \tau, I')$. Consider now the limit $t \rightarrow \infty$, assuming the process is stationary ($\text{Lim}_{t \rightarrow \infty} [p_{cl}(t, I)] = \text{Lim}_{t \rightarrow \infty} [p_{cl}(t + \tau, I)]$) we have therefore:

$$\langle I(t) I(t + \tau) \rangle_{cl} \leq \langle I(t) I(t) \rangle$$

or, equivalently, the classical intensity correlation function $g_{cl}^{(2)}(\tau) \equiv \frac{\langle I(t+\tau)I(t) \rangle_{cl}}{\langle I(t) \rangle^2}$ obeys the inequality:

$$g_{cl}^{(2)}(\tau) \leq g_{cl}^{(2)}(0) \quad (1.18)$$

Now considering the quantized field, Eq. (1.16) can be put under the form:

$$g^{(2)}(\tau) \equiv \frac{\langle : I(t + \tau) I(t) : \rangle}{\langle : I(t) : \rangle^2}$$

In the quantum case the $g^{(2)}$ function obeys the inequality Eq. (1.18) for certain states. For example for the coherent state $|\alpha\rangle$, defined in the stationary case as $a(t)|\alpha\rangle = \alpha|\alpha\rangle$, we have $g_{cl}^{(2)}(\tau) = g_{cl}^{(2)}(0)$. The light for which the inequality (1.18) becomes strict at least for some τ : $g_{cl}^{(2)}(\tau) < g_{cl}^{(2)}(0)$ is called called *bunched*. In this case photons tend to come in groups. As soon as the inequality (1.18) is violated the corresponding state of light can not be explained by means of the classical probability density distribution p_{cl} . The effect that accompanies the inequality violation is called *antibunching*: for antibunched light, photons tend to come one by one, as schematically shown on Fig. 1.3. The well known example of an antibunched light is given by the resonant fluorescence from an atom. An example of a bunched is given by a chaotic light (Loudon, 2000).

We now use the Cauchy-Schwarz inequality once more for the same-time intensity correlation function:

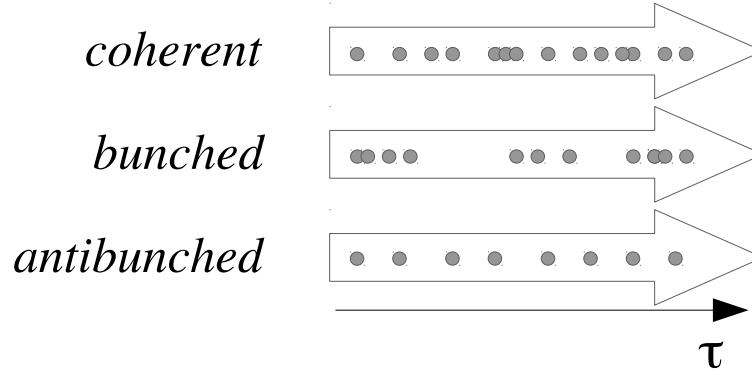


Figure 1.3: Schematic representation of different light statistics.

$$\begin{aligned}
 \langle I(t) I(t) \rangle_{cl} &\equiv \int dI \times I^2 \times p_{cl}(t, I) \\
 &\geq \left| \int dI \times I \times p_{cl}(t, I) \right|^2 \\
 &= \langle I(t) \rangle^2
 \end{aligned}$$

and consequently $g_{cl}^{(2)}(0) \geq 1$. We therefore conclude that any violation of this inequality would testify a quantum nature of light. In the quantum case the exact equality holds for coherent light, which follows Poissonian statistics, as will be shown below.

Single-mode coherent state Consider a single-mode coherent state defined as:

$$\begin{aligned}
 |\alpha\rangle &\equiv e^{\alpha a^\dagger + \alpha^* a} |0\rangle \\
 &= e^{\alpha a^\dagger - \frac{|\alpha|^2}{2}} |0\rangle
 \end{aligned}$$

The probability of detecting n photons is obviously given

$$\begin{aligned}
 P_n &= |\langle n | \alpha \rangle|^2 \\
 &= \left| \left\langle n \left| e^{\alpha a^\dagger - \frac{|\alpha|^2}{2}} \right| 0 \right\rangle \right|^2 \\
 &= e^{-|\alpha|^2} \frac{|\alpha|^{2n}}{n!}
 \end{aligned} \tag{1.19}$$

we therefore infer that the probability distribution is given by the Poissonian distribution with an average photon number given by $|\alpha|^2$. An important property of the

1. Description of the system

Poissonian statistics is that the variance of the photon number is equal to the square of its mean value. According to Eq. (1.19) we indeed have:

$$\langle n^2 \rangle - \langle n \rangle^2 = \langle n \rangle$$

Throughout the dissertation we will rather be interested in multimode coherent fields, whose main properties are, as shown below, akin to those of single-mode coherent fields.

Multimode coherent state Consider the multimode coherent state (Loudon, 2000) defined by:

$$\begin{aligned} |\alpha\rangle &\equiv e^{\sqrt{\langle n \rangle}(a_\alpha^\dagger - a_\alpha)} |0\rangle \\ a_\alpha(t) |\alpha\rangle &= \alpha(t) |\alpha\rangle \end{aligned}$$

where $a_\alpha^\dagger(t) \equiv \frac{1}{\sqrt{\langle n \rangle}} \int d\omega \alpha(\omega) a_\omega^\dagger e^{i\omega t}$ is the mode creation operator, $\alpha(t) = \frac{1}{\sqrt{2\pi}} \int d\omega \alpha(\omega) e^{-i\omega t}$ and $\langle n \rangle = \int |\alpha(t)|^2 dt$. First, it is easy to check $\langle \alpha | \alpha \rangle = 1$.

We now expand the coherent state $|\alpha\rangle$ in the following way:

$$\begin{aligned} e^{\sqrt{\langle n \rangle} a_\alpha^\dagger - \frac{1}{2} \langle n \rangle} |0\rangle &= e^{-\frac{1}{2} \langle n \rangle} \sum_n \langle n \rangle^{\frac{n}{2}} \frac{(a_\alpha^\dagger)^n}{n!} |0\rangle \\ &= e^{-\frac{1}{2} \langle n \rangle} \sum_n \frac{\langle n \rangle^{\frac{n}{2}}}{\sqrt{n!}} |n\rangle \end{aligned}$$

where we introduced the Fock state $|n\rangle \equiv \frac{(a_\alpha^\dagger)^n}{\sqrt{n!}} |0\rangle$, $\langle n | m \rangle = \delta_{n,m}$. We thus get that the total photon distribution in the coherent mode is given by a Poissonian distribution:

$$P_n = e^{-\langle n \rangle} \frac{\langle n \rangle^n}{n!} \quad (1.20)$$

Consider now the photon flux $I(t) \equiv a^\dagger(t) a(t)$ through a certain surface. One may demonstrate that the probability to detect m photons within the time interval $[t, t + \delta t]$ is given by:

$$P_m(\delta t) = \frac{(|\alpha(t)|^2 \delta t)^m}{m!} e^{-|\alpha(t)|^2 \delta t}$$

hence obeying a Poissonian statistics. Indeed, due to the superposition principle, the state of the field in each small time slice δt is also coherent, with the average photon number $|\alpha(t)|^2 \delta t$. Therefore, as in the single-mode case, we have for the intensity correlation function of the coherent light: $g^{(2)}(0) = \frac{(|\alpha(t)|^2 \delta t)^2}{(|\alpha(t)|^2 \delta t)^2} = 1$.

As soon as the variance of the photon number is superior or inferior to that of the coherent light for the same average flux the light field is called super or sub-Poissonian,

respectively (Scully and Zubairy, 1997). The simplest example of a sub-Poissonian light is given by the Fock state containing n photons:

$$\begin{aligned}
 |n\rangle &\equiv \frac{(a^\dagger_\alpha)^n}{\sqrt{n!}} |0\rangle \\
 \Rightarrow g^{(2)}(0) &= \frac{\langle n | a^\dagger(t) a^\dagger(t) a(t) a(t) | n \rangle}{|\langle n | a^\dagger(t) a(t) | n \rangle|^2} \\
 &= 1 - \frac{1}{n}
 \end{aligned} \tag{1.21}$$

The simplest example of super-Poissonian light is given by the thermal light for which $g^{(2)}(0) = 2$ (Loudon, 2000). According to Eq. (1.21) the $g^{(2)}(0)$ function for a single-photon state vanishes (this is also called “anticorrelation”), testifying the particle nature of light (Grangier et al., 1986).

In conclusion we note that the $g^{(2)}$ function contains an important information on the photon distribution in the light field. An effective interaction between photons can affect the statistics, redistributing them inside the initially coherent light.

1. Description of the system

Chapter 2

Rydberg-induced quantum optical nonlinearities in the dispersive regime

Contents

2.1	Effective two-level model	36
2.2	Rydberg bubble approximation	38
2.3	Tavis-Cummings Hamiltonian	40
2.4	Calculation of the $g^{(2)}$ function	42
2.5	Numerical results and discussion	44
2.6	Conclusion	47

2. Rydberg-induced quantum optical nonlinearities in the dispersive regime

In this chapter ¹, we consider the so-called dispersive regime of the system described in Chap. 1, *i.e.* when the intermediate state is excited far from resonance. Under this condition, dipole-dipole interactions induce only non-linear dispersive effects for the cavity mode, without generating extra losses in the system. Besides, due to the presence of the cavity the dispersive effects are enhanced.

As the intermediate state is far detuned, it remains mostly unpopulated during the evolution and its coherence can be eliminated from the dynamical equations (Brion et al., 2007b): as shown in (Guerlin et al., 2010) the system effectively behaves as an ensemble of two-level atoms coupled to the cavity mode (Sec. 2.1). In addition, we assume that the two-photon transition is also slightly detuned in order to ensure that dipole-dipole interactions induce predominantly dispersive effects. Then we further approximate our system employing the so-called “bubble picture” (Vuletic, 2006) for our effective two-level atoms (Sec. 2.2): we thus get an ensemble of two-level superatoms coupled to the cavity mode which is known as the driven Tavis-Cummings model (Sec. 2.3). We numerically evaluate the $g^{(2)}$ function of the light transmitted through the cavity (Sec. 2.4) and show that, depending on the cavity parameters, the transmitted light is bunched or antibunched (Sec. 2.5).

2.1 Effective two-level model

The starting point of our study is the Hamiltonian given in Chap. 1 for the system {atoms+cavity} under the usual RWA and Markov approximations:

$$H_{sys} = H_a + H_c + V_{a-c} + H_f$$

$$\begin{aligned} H_a &= -\Delta_e \sum_{n=1}^N \sigma_{ee}^{(n)} - \Delta_r \sum_{n=1}^N \sigma_{rr}^{(n)} + \frac{\Omega_{cf}}{2} \sum_{n=1}^N (\sigma_{re}^{(n)} + \sigma_{er}^{(n)}) + \sum_{m < n=1}^N \kappa_{mn} \sigma_{rr}^{(m)} \sigma_{rr}^{(n)} \\ H_c &= -\Delta_c a^\dagger a \\ V_{a-c} &= \sum_{n=1}^N g (a \sigma_{eg}^{(n)} + a^\dagger \sigma_{ge}^{(n)}) \\ H_f &= \alpha (a + a^\dagger) \end{aligned}$$

where we used the same notations as in Chap. 1. We also recall here the set of corresponding Heisenberg-Langevin equations:

¹This chapter is an edited version of (Grankin et al., 2014).

$$\frac{d}{dt}a = (i\Delta_c - \gamma_c)a - i\alpha - ig \sum_i^N \sigma_{ge}^{(i)} + a_{in} \quad (2.1)$$

$$\frac{d}{dt}\sigma_{ge}^{(i)} = (i\Delta_e - \gamma_e)\sigma_{ge}^{(i)} - i\frac{\Omega_{cf}}{2}\sigma_{gr}^{(i)} + iga(\sigma_{ee}^{(i)} - \sigma_{gg}^{(i)}) + F_{ge}^{(i)} \quad (2.2)$$

$$\frac{d}{dt}\sigma_{gr}^{(i)} = (i\Delta_r - \gamma_r)\sigma_{gr}^{(i)} - i\frac{\Omega_{cf}}{2}\sigma_{ge}^{(i)} + iga\sigma_{er}^{(i)} - i\sigma_{gr}^{(i)} \sum_{j \neq i}^N \kappa_{ij}\sigma_{rr}^{(j)} + F_{gr}^{(i)} \quad (2.3)$$

$$\begin{aligned} \frac{d}{dt}\sigma_{er}^{(i)} &= \{i(\Delta_r - \Delta_e) - \gamma_{er}\}\sigma_{er}^{(i)} + i\frac{\Omega_{cf}}{2}(\sigma_{rr}^{(i)} - \sigma_{ee}^{(i)}) + iga^\dagger\sigma_{gr}^{(i)} \\ &- i\sigma_{er}^{(i)} \sum_{j \neq i}^N \kappa_{ij}\sigma_{rr}^{(j)} + F_{er}^{(i)} \end{aligned} \quad (2.4)$$

Let us now simplify the system Eqs. (2.1-2.4). Discarding the non-linearity arising from the saturation of the transitions² we neglect the term $a\sigma_{er}^{(i)}$ in Eq. (2.3) and set $\sigma_{ee}^{(i)} - \sigma_{gg}^{(i)} \simeq -\mathbb{I}$ in Eq. (2.2). Averaging out the physically irrelevant fast oscillations of the atomic coherence $\sigma_{ge}^{(i)}$ (at frequency Δ_e) we can identify the latter with its steady-state expression

$$\sigma_{ge}^{(i)} \simeq \frac{\Omega_{cf}}{2(\Delta_e + i\gamma_e)}\sigma_{gr}^{(i)} + \frac{g}{(\Delta_e + i\gamma_e)}a + \frac{i}{(\Delta_e + i\gamma_e)}F_{ge}^{(i)}$$

Finally, substituting this relation into Eqs.(2.1,2.3) one gets

$$\frac{d}{dt}a = (i\tilde{\Delta}_c - \tilde{\gamma}_c)a - i\alpha + ig_{\text{eff}} \left(\sum_i \sigma_{gr}^{(i)} \right) + \tilde{a}_{in} \quad (2.5)$$

$$\frac{d}{dt}\sigma_{gr}^{(i)} = (i\tilde{\Delta}_r - \tilde{\gamma}_r)\sigma_{gr}^{(i)} + ig_{\text{eff}}a - i\sigma_{gr}^{(i)} \left(\sum_{j \neq i}^N \kappa_{ij}\sigma_{rr}^{(j)} \right) + \tilde{F}_{gr}^{(i)} \quad (2.6)$$

where (Grankin et al., 2014):

$$\begin{aligned} \tilde{\Delta}_c &= \Delta_c - \Delta_e \frac{g^2 N}{(\Delta_e^2 + \gamma_e^2)} \\ \tilde{\gamma}_c &= \gamma_c + \gamma_e \frac{g^2 N}{(\Delta_e^2 + \gamma_e^2)} \end{aligned}$$

²As pointed out in Chap. 1, we indeed expect Rydberg induced nonlinearities to be much stronger than saturation effects and therefore linearize the system apart from interatomic interactions.

2. Rydberg-induced quantum optical nonlinearities in the dispersive regime

$$\begin{aligned}\tilde{\Delta}_r &= \Delta_r - \Delta_e \frac{\Omega_{cf}^2}{4(\Delta_e^2 + \gamma_e^2)} \\ \tilde{\gamma}_r &= \gamma_r + \gamma_e \frac{\Omega_{cf}^2}{4(\Delta_e^2 + \gamma_e^2)} \\ g_{\text{eff}} &= \frac{g\Omega_{cf}}{2(\Delta_e + i\gamma_e)} \approx \frac{g\Omega_{cf}}{2\Delta_e}\end{aligned}$$

are the parameters for the effective two-level model and $\tilde{a}_{in}, \tilde{F}_{gr}^{(i)}$ are the modified Langevin noise operators

$$\begin{aligned}\tilde{a}_{in} &= a_{in} + \frac{g}{(\Delta_e + i\gamma_e)} \sum_i F_{ge}^{(i)} \approx a_{in} + \frac{g}{\Delta_e} \sum_i F_{ge}^{(i)} \\ \tilde{F}_{gr}^{(i)} &= F_{gr}^{(i)} + \frac{\Omega_{cf}}{2(\Delta_e + i\gamma_e)} F_{ge}^{(i)} \approx F_{gr}^{(i)} + \frac{\Omega_{cf}}{2\Delta_e} F_{ge}^{(i)}\end{aligned}$$

Finally, we get the effective Hamiltonian

$$\begin{aligned}\tilde{H} &= -\tilde{\Delta}_r \left(\sum_{n=1}^N \sigma_{rr}^{(n)} \right) + \sum_{m < n=1}^N \kappa_{mn} \sigma_{rr}^{(m)} \sigma_{rr}^{(n)} \\ &\quad - \tilde{\Delta}_c a^\dagger a + \alpha (a + a^\dagger) + g_{\text{eff}} \left\{ a \left(\sum_{n=1}^N \sigma_{rg}^{(n)} \right) + h.c. \right\}\end{aligned}$$

Performing the adiabatic elimination of the detuned intermediate level, we reduce the system to an ensemble of effective two-level atoms coupled to a cavity mode which interact via dipole-dipole interactions in exactly the same way as in the original system.

2.2 Rydberg bubble approximation

We may simplify the system further by introducing the Rydberg bubble approximation (Guerlin et al., 2010). In this approach, the strong Rydberg interactions are assumed to effectively split the sample into \mathcal{N}_b bubbles $\{\mathcal{B}_{\alpha=1, \dots, \mathcal{N}_b}\}$ each of which contains $n_b = \left(\frac{N}{\mathcal{N}_b}\right)$ atoms but can only accommodate for a single Rydberg excitation, delocalized over the bubble (Vuletic, 2006). Note that the number of atoms per bubble n_b is approximately given by (Parigi et al., 2012; Stanojevic et al., 2013)

$$n_b = \frac{2\pi^2 \rho_{\text{at}}}{3} \sqrt{\frac{|C_6|}{\Delta_r - \Omega_{cf}^2/(4\Delta_e)}} \quad (2.7)$$

where ρ_{at} is the atomic density. Each bubble can therefore be viewed as an effective spin $\frac{1}{2}$ whose Hilbert space is spanned by

$$\begin{aligned} |-\alpha\rangle = |G_\alpha\rangle &\equiv \bigotimes_{i_\alpha \in \mathcal{B}_\alpha} |g_{i_\alpha}\rangle \\ |+\alpha\rangle = |R_\alpha\rangle &\equiv \frac{1}{\sqrt{n_b}} \{|rg \dots g\rangle + \dots + |g \dots gr\rangle\} \end{aligned}$$

namely the ground state of the bubble \mathcal{B}_α and its symmetric singly-Rydberg-excited state, respectively. Introducing the bubble Pauli operators $s_-^{(\alpha)} = |-\alpha\rangle\langle +\alpha|$ – the operator $s_-^{(\alpha)}$ corresponds to the lowering operator of the spin and the annihilation of a Rydberg excitation, one can write

$$\begin{aligned} \sum_{n=1}^N \sigma_{gr}^{(n)} &= \sum_{\alpha=1}^{\mathcal{N}_b} \sum_{i_\alpha \in \mathcal{B}_\alpha} \sigma_{gr}^{(i_\alpha)} \\ &\approx \sum_{\alpha=1}^{\mathcal{N}_b} s_-^{(\alpha)} \left\langle -\alpha \left| \sum_{i_\alpha \in \mathcal{B}_\alpha} \sigma_{gr}^{(i_\alpha)} \right| +\alpha \right\rangle \\ &\approx \sqrt{n_b} \sum_{\alpha=1}^{\mathcal{N}_b} s_-^{(\alpha)} \\ &= \sqrt{n_b} J_- \end{aligned}$$

where we introduced the collective angular momentum $J_- \equiv \sum_{\alpha=1}^{\mathcal{N}_b} s_-^{(\alpha)}$. In the same way,

$$\begin{aligned} \sum_{n=1}^N \sigma_{rr}^{(n)} &= \sum_{\alpha=1}^{\mathcal{N}_b} \sum_{i_\alpha \in \mathcal{B}_\alpha} \sigma_{rr}^{(i_\alpha)} \\ &\approx \sum_{\alpha=1}^{\mathcal{N}_b} |+\alpha\rangle\langle +\alpha| \left\langle +\alpha \left| \sum_{i_\alpha \in \mathcal{B}_\alpha} \sigma_{rr}^{(i_\alpha)} \right| +\alpha \right\rangle \\ &\approx \sum_{\alpha=1}^{\mathcal{N}_b} \left(\frac{1}{2} + s_z^{(\alpha)} \right) \\ &\approx \left(\frac{\mathcal{N}_b}{2} + J_z \right) \end{aligned}$$

2. Rydberg-induced quantum optical nonlinearities in the dispersive regime

where we used $|+\alpha\rangle\langle+\alpha| \equiv \left(\frac{1}{2} + s_z^{(\alpha)}\right)^3$. Finally, as shown in (Guerlin et al., 2010), the Hamiltonian of the system takes the approximate form

$$\tilde{H} \approx -\tilde{\Delta}_c a^\dagger a + \alpha (a + a^\dagger) - \tilde{\Delta}_r \left(\frac{\mathcal{N}_b}{2} + J_z \right) + g_{\text{eff}} \sqrt{n_b} (a J_+ + a^\dagger J_-) \quad (2.8)$$

which represents the interaction of the large spin J_- with the cavity mode a , known as the driven (and dissipative) Tavis-Cummings model (Tavis and Cummings, 1968), that we study in the next section in more details.

2.3 Tavis-Cummings Hamiltonian

We first analyze the spectral properties of the Hamiltonian Eq. (2.8) without the driving term:

$$\tilde{H}_{TC} \approx -\tilde{\Delta}_c a^\dagger a - \tilde{\Delta}_r \left(\frac{\mathcal{N}_b}{2} + J_z \right) + g_{\text{eff}} \sqrt{n_b} (a J_+ + a^\dagger J_-) \quad (2.9)$$

The nonlinearity of this model arises from the finiteness of the Hilbert space spanned by the spin degree of freedom, as we shall now show.

As can be easily demonstrated, the total number of excitations is an integral of motion, *i.e.* $[\tilde{H}_{TC}, \hat{N}] = 0$, where $\hat{N} \equiv a^\dagger a + \left(\frac{\mathcal{N}_b}{2} + J_z\right)$. Therefore, the Hilbert space is split into subspaces of definite excitation number N_{ex} , spanned by the vectors $\{|n, N_{ex} - n\rangle, n = 0, \dots, N_{ex}\}$, where by $|n, k\rangle \equiv |n\rangle \otimes |j = \frac{\mathcal{N}_b}{2}; m = -\frac{\mathcal{N}_b}{2} + k\rangle$ we denote the state that contains n photonic excitations and the collective atomic spin J_z projection is equal to $-\frac{\mathcal{N}_b}{2} + k$. Since these subspaces are not coupled by Eq. (2.9), the matrix representation of \tilde{H}_{TC} , truncated at $N_{ex} = 2$ can be put in the block-diagonal form

³The derivation of the spin Hamiltonian provided here is based on the *ad hoc* representation of the sample as a collection of superatoms with a pre-defined position (Stanojevic and Côté, 2009; Robicheaux and Hernández, 2005). In each superatom, we restrict the basis to the set of allowed states. This is a simplified derivation. One can resort to a more rigorous treatment based on the restriction to the states of the *whole ensemble*, allowed by the interaction Hamiltonian. These states are given by (Guerlin et al., 2010) $|E_n\rangle = \frac{1}{\sqrt{\mathcal{A}}} \sum_{i_1, \dots, i_n \in \text{allowed}} |r_{i_1}, \dots, r_{i_n}\rangle$ where \mathcal{A} is the number of allowed states (It can be seen as a symmetric superposition of bubble states centered at different atoms). The matrix form of the collective raising (lowering) operator restricted to the set of allowed states $|E_n\rangle$ coincides with that of the momentum raising (lowering) operator J_- in the basis $\{|\frac{n_b}{2}, -\frac{n_b}{2} + n\rangle\}$. The system therefore behaves as a spin coupled to the cavity mode (Tavis-Cummings model) which agrees with and therefore legitimates the bubble picture.

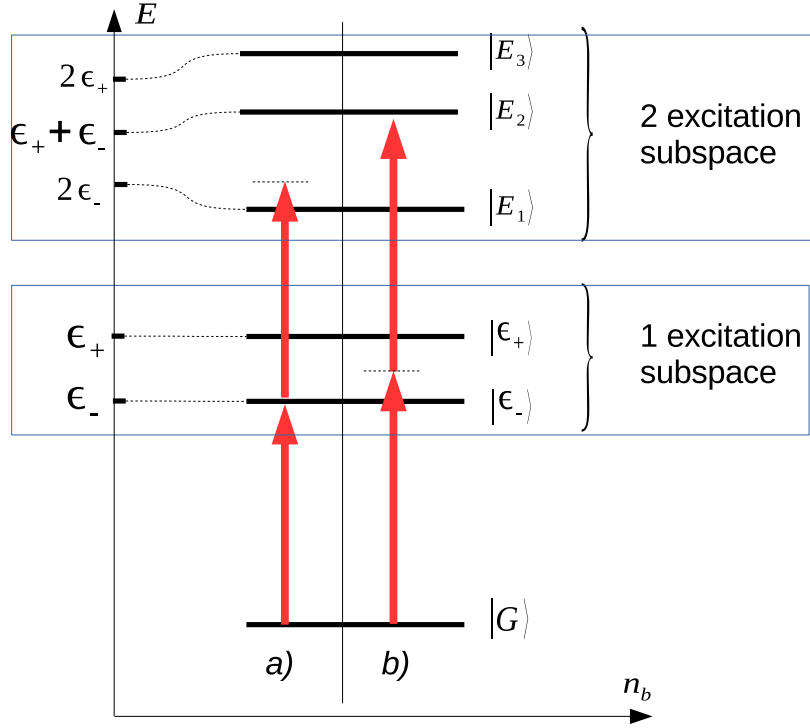


Figure 2.1: Schematic level structure of the Tavis-Cummings Hamiltonian for $\mathcal{N}_b > 1$ being externally excited so that a) single photon component is resonant, b) 2-photon component is resonant.

$$\tilde{H}_{TC} = \left(\begin{array}{ccc|ccc} 0 & 0 & 0 & 0 & 0 & 0 \\ 0 & -\tilde{\Delta}_c & g_{\text{eff}}\sqrt{N} & 0 & 0 & 0 \\ 0 & g_{\text{eff}}\sqrt{N} & -\tilde{\Delta}_r & 0 & 0 & 0 \\ \hline 0 & 0 & 0 & -2\tilde{\Delta}_c & \sqrt{2}g_{\text{eff}}\sqrt{N} & 0 \\ 0 & 0 & 0 & \sqrt{2}g_{\text{eff}}\sqrt{N} & -\tilde{\Delta}_c - \tilde{\Delta}_r & \sqrt{2}g_{\text{eff}}\sqrt{N - n_b} \\ 0 & 0 & 0 & 0 & \sqrt{2}g_{\text{eff}}\sqrt{N - n_b} & -2\tilde{\Delta}_r \end{array} \right) \quad (2.10)$$

The eigenenergies in the single excitation subspace are easily found to be $\epsilon_{\pm} = \frac{1}{2} \left(-\tilde{\Delta}_c - \tilde{\Delta}_r \pm \sqrt{4g_{\text{eff}}^2 N + (\tilde{\Delta}_c - \tilde{\Delta}_r)^2} \right)$. When the blockade sphere is very small and consequently the number of atoms per bubble Eq. (2.7) is also small, *i.e.* $n_b \rightarrow 0$, one checks that the quantities $2\epsilon_+, \epsilon_+ + \epsilon_-, 2\epsilon_-$ are eigenvalues of the two-excitation block of Eq. (2.10). The spectrum is thus harmonic with the possibility of existence of excitations of two kinds: since we assume that $n_b \rightarrow 0$ the basis spanned by the spin degree of freedom indeed becomes almost infinite and in this case the system behaves

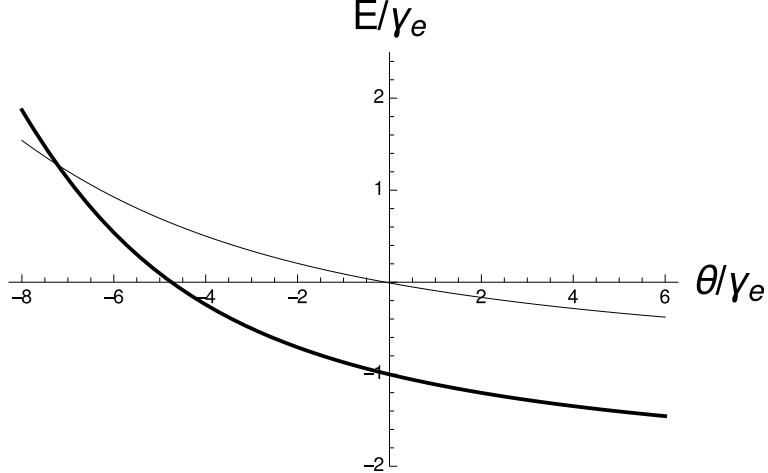


Figure 2.2: The structure of nearly-resonant eigenvalues of the Tavis-Cummings Hamiltonian as a function of the reduced detuning $\theta \equiv (\Delta_c - \Delta_c^{(0)})/\gamma_e$. Thin and thick lines represent eigenvalues of (2.10) in the single and two-excitation subspaces the respectively.

as two uncoupled harmonic oscillators with frequencies ϵ_+, ϵ_- . These modes “ \pm ” are also known as normal modes of the system. By contrast, when the number of atoms n_b per bubble is finite, the term $\sqrt{2}g_{\text{eff}}\sqrt{N - n_b}$ in the two-excitation block in Eq. (2.10) breaks the harmonicity of the level structure. We denote as E_1, E_2, E_3 the corresponding eigenvalues of the Hamiltonian in the two-excitation subspace.

In the low excitation regime, feeding terms can be perturbatively added to the Hamiltonian Eq. (2.9), without changing its level structure and all the properties of the transmitted light can therefore be explained by the configuration of its eigenvalues. In particular, as shown on Fig. 2.1, due to the anharmonicity of the level structure, the single and two-photon components of the light are not simultaneously resonant: it is thus possible to tune the cavity parameters to effectively filter one of them, therefore modifying the quantum statistics of transmitted light.

The next sections are devoted to the investigation of the different possible statistical behaviors of the system.

2.4 Calculation of the $g^{(2)}$ function

In this section we present the two methods (numerical and analytic) we use to compute the $g^{(2)}$ function of the system. In Schrödinger picture we consider the master equation

for the reduced density matrix:

$$\begin{aligned}
 \partial_t \tilde{\rho} &= \mathcal{L} \tilde{\rho} \\
 &= -i \left[\tilde{H}, \tilde{\rho} \right] + \tilde{\gamma}_c \{ 2a \tilde{\rho} a^\dagger - a^\dagger a \tilde{\rho} - \tilde{\rho} a^\dagger a \} \\
 &\quad + \tilde{\gamma}_r \sum_{\alpha=1}^{\mathcal{N}_b} \left\{ 2s_-^{(\alpha)} \tilde{\rho} s_+^{(\alpha)} - s_+^{(\alpha)} s_-^{(\alpha)} \tilde{\rho} - \tilde{\rho} s_+^{(\alpha)} s_-^{(\alpha)} \right\}
 \end{aligned} \tag{2.11}$$

One can also write the Heisenberg-Langevin equations for the time-dependent operators $a(t), J_-(t)$

$$\partial_t a = \left(i\tilde{\Delta}_c - \tilde{\gamma}_c \right) a - i\alpha - ig_{\text{eff}} \sqrt{n_b} J_- + \tilde{a}_{in} \tag{2.12}$$

$$\partial_t J_- = \left(i\tilde{\Delta}_r - \tilde{\gamma}_r \right) J_- + 2ig_{\text{eff}} \sqrt{n_b} J_z a + \tilde{J}_{in} \tag{2.13}$$

where $\tilde{a}_{in}, \tilde{J}_{in} \equiv \sum_{n=1}^N \tilde{F}_{gr}^{(n)}$ are the Langevin forces associated to a and J_- , respectively. Note that we neglected the effect of extra dephasing due to, *e.g.*, collisions or laser fluctuations.

To study the quantum properties of the light transmitted through the cavity, we shall compute the function $g_{\text{out}}^{(2)}$, which characterizes the two-photon correlations. In the input-output formalism (Walls and Milburn, 2007), one shows that this function simply equals the $g^{(2)}$ function for the intracavity field (see App. C for details) given by

$$g^{(2)}(\tau) = \frac{\text{Tr} \{ a^\dagger a e^{\mathcal{L}\tau} [a \rho_{ss} a^\dagger] \}}{\text{Tr} [a^\dagger a \rho_{ss}]^2} \tag{2.14}$$

where ρ_{ss} denotes the steady state of the system defined by $\mathcal{L}\rho_{ss} = 0$, see Eq. (2.11).

In the regime of small feeding parameter α , one can compute ρ_{ss} numerically by propagating in time the initial state $\rho_0 \equiv |N_r = 0\rangle \langle N_r = 0| \otimes |n_c = 0\rangle \langle n_c = 0|$ (here $|N_r = 0, 1, \dots, \mathcal{N}_b\rangle$ represents the symmetric state in which $N_r \equiv \left(\frac{\mathcal{N}_b}{2} + \frac{J_z}{\hbar}\right)$ bubbles are excited, and $|n_c = 0, 1, \dots\rangle$ are the Fock states of the cavity mode). To this end, one applies the Liouvillian evolution operator $e^{\mathcal{L}t}$ in a truncated basis, restricted to states of low numbers of excitations (typically with $n_c + N_r \leq 6$). The steady state is reached in the limit of large times – ideally when $t \rightarrow \infty$. The denominator of the ratio Eq.(2.14) is directly obtained from ρ_{ss} . To compute its numerator, one first propagates in time $a \rho_{ss} a^\dagger$ from $t = 0$ to τ , using the same procedure as above, then applies the operator $a^\dagger a$ and takes the trace.

In the regime of weak feeding, it is also possible to get a perturbative expression for $g^{(2)}(0)$ by computing the expansion of $\langle a^\dagger a^\dagger a a \rangle_{ss}$ and $\langle a^\dagger a \rangle_{ss}$ in powers of α . To this end, one uses the Heisenberg equations of the system Eqs.(2.12,2.13) to derive the hierarchy of equations relating the different mean values and correlations $\langle \dots \rangle_{ss}$ up to the fourth order in α . After straightforward though lengthy algebra, one gets

2. Rydberg-induced quantum optical nonlinearities in the dispersive regime

an expression for $g^{(2)}(0)$ which is too cumbersome to be reproduced here but allows for faster calculations than the numerical approach. Such a fully analytical treatment, however, cannot, to our knowledge, be extended to $g^{(2)}(\tau > 0)$. For $\tau > 0$ we therefore entirely rely on numerical simulations presented in the next section.

2.5 Numerical results and discussion

We consider the physical setup presented in (Parigi et al., 2012), *i.e.* an ensemble of ^{87}Rb atoms, whose state space is restricted to the levels $|g\rangle = |5s_{1/2}; F = 2\rangle$, $|e\rangle = |5p_{3/2}; F = 3\rangle$ and $|r\rangle = |95d_{5/2}; F = 4\rangle$ with the decay rates $\gamma_e = 2\pi \times 3$ MHz, and $\gamma_r = 2\pi \times 0.03$ MHz. The other physical parameters must be designed so that strong nonlinearities may be observed at the single-photon level. In the specific system considered here, we find this is achieved for a cavity decay rate $\gamma_c = 2\pi \times 1$ MHz, a volume of the sample $V = 40\pi \times 15 \times 15 \mu\text{m}^3$, a sample density $n_{at} = 0.4 \mu\text{m}^{-3}$, a control laser Rabi frequency $\Omega_{cf} = 10\gamma_e$, a cooperativity $C = 1000$, a detuning of the intermediate level $\Delta_e = -35\gamma_e$, a detuning of the Rydberg level $\Delta_r = 0.4\gamma_e$, a cavity feeding rate $\alpha = 0.01\gamma_e$. For these parameters, the cavity detuning $\Delta_c^{(0)} \approx -6.1\gamma_e$ corresponds to the (numerically computed) maximal average number of photons in the cavity, *i.e.*, to the linear EIT resonance. Note that these physical parameters are experimentally realistic and feasible, though they are not the ones used in (Parigi et al., 2012) (in particular, C was much smaller).

Let us first focus on the second-order correlation function at zero time $g^{(2)}(0)$, represented on Fig. 2.3 a) as a function of the reduced detuning $\theta \equiv (\Delta_c - \Delta_c^{(0)})/\gamma_e$. One notes a super-Poissonian region near (B) $\theta_B = -4.9$ and a deep sub-Poissonian area centered on (A) $\theta_A = 0$. This suggests that around (A), photons are preferably transmitted one by one, while around (B) they are preferably transmitted by pairs. Note, however, that, as a ratio, $g^{(2)}(0)$ gives only information on the relative importance of pair and single-photon emissions. Its peaks therefore do not correspond to maxima of photon pair emission, but to the best compromises between $\langle a^\dagger a^\dagger a a \rangle_{ss}$ and $\langle a^\dagger a \rangle_{ss}^2$, as can be checked by comparison of Fig. 2.3 a) and b). Hence, pair emission might dominate in a regime where the number of photons coming out from the cavity is actually very small. We may now explain the exact positions of single- and two-photon resonances. As discussed in the previous section the level structure of the Hamiltonian we consider in the low excitation regime coincides with those of the Tavis-Cummings Hamiltonian. As can be seen from the comparison of figures 2.2 and 2.3 various single and two-photon resonances correspond to the zero-crossings of eigenvalues of Eq. (2.10) in their respective subspace.

We now investigate the behaviour of $g^{(2)}(\tau > 0)$ for two different values of the detuning, *i.e.* $\theta_B = -4.9$ and $\theta_A = 0$ which respectively correspond to the peak (B) and minimum (A) of $g^{(2)}(0)$. The numerical simulations we obtained are given in Fig. 2.4.

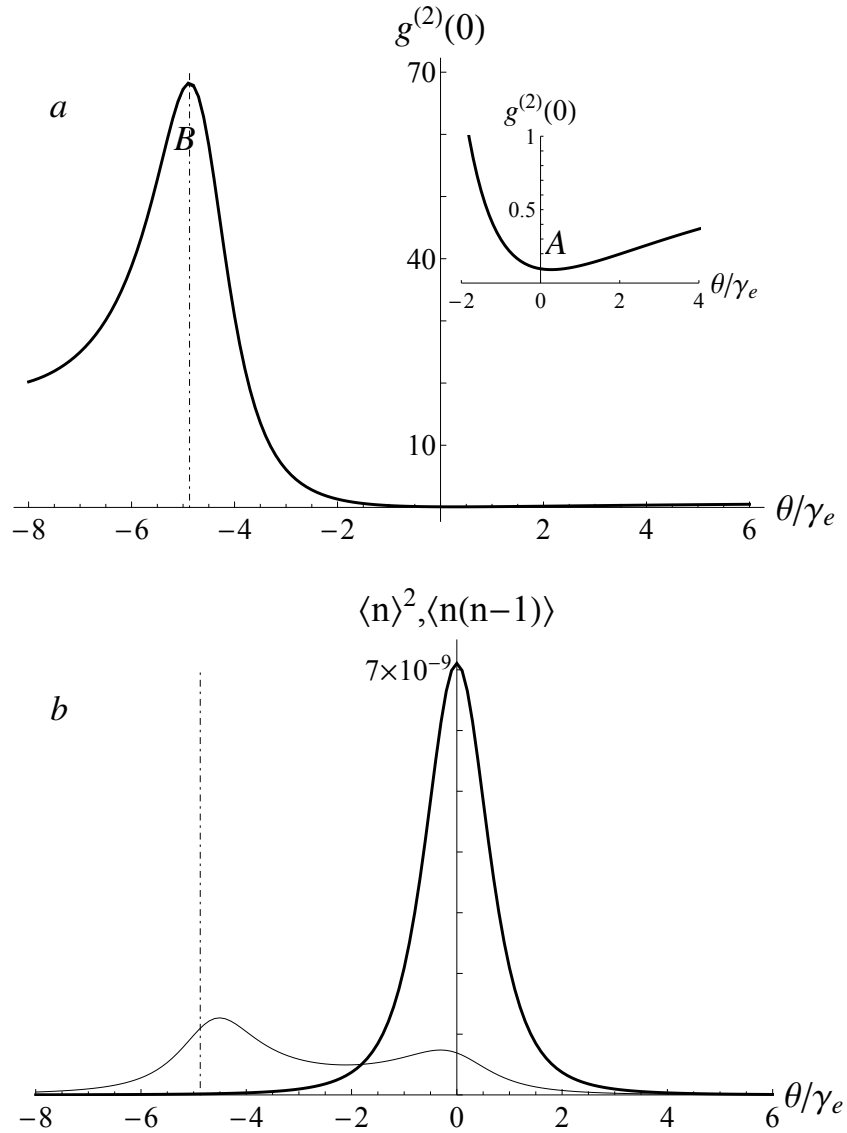


Figure 2.3: a) Second-order correlation function at zero time $g^{(2)}(0)$ (numerical and analytical plots coincide), as a function of the reduced detuning $\theta \equiv (\Delta_c - \Delta_c^{(0)})/\gamma_e$. In the neighborhood of the minimum (A) $\theta_A = 0$, a region with a sub-Poissonian statistics is observed (see inset); a super-Poissonian area is obtained around the peak (B) $\theta_B = -4.9$. b) Average number of pairs $\langle a^\dagger a^\dagger a a \rangle_{ss} = \langle n(n-1) \rangle_{ss}$ (thin line) and square of the average number of photons $\langle a^\dagger a \rangle_{ss}^2 = \langle n \rangle_{ss}^2$ in the steady state (thick line). The position of the peak of the correlation function $g^{(2)}(0)$ is signaled by a vertical line.

2. Rydberg-induced quantum optical nonlinearities in the dispersive regime

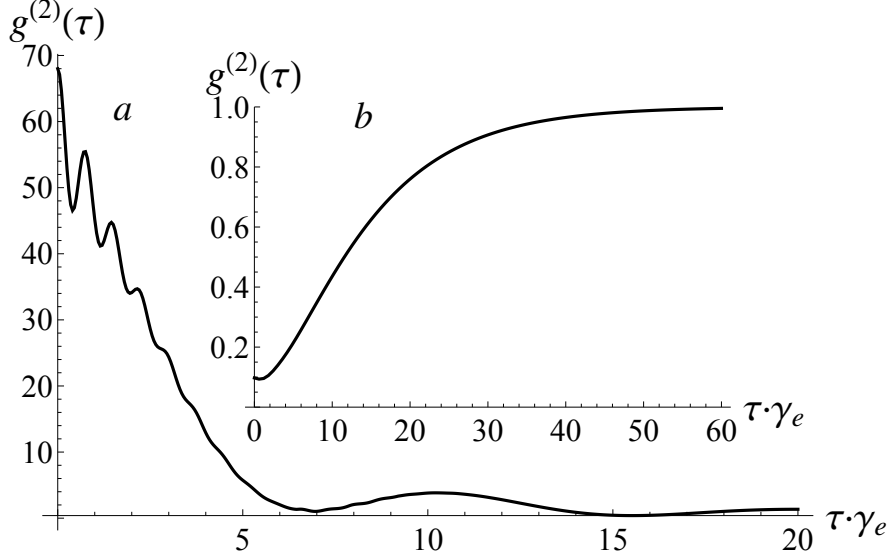


Figure 2.4: Temporal behaviour of $g^{(2)}(\tau)$ for a) $\theta_B = -4.9$ and b) $\theta_A = 0$. Note that we chose a dimensionless “time”-variable $\tau \times \gamma_e$ on the x -axis.

The plot relative to (B) exhibits damped oscillations, alternatively showing a bunched ($g^{(2)}(0) > g^{(2)}(\tau)$) or antibunched ($g^{(2)}(0) < g^{(2)}(\tau)$) behavior. The plot corresponding to (A) always remains on the antibunched side, though asymptotically tending to 1.

The features observed can be understood and satisfactorily accounted for by a simple three-level model. Indeed, due to the weakness of α , the system, in its steady state, is expected to contain at most two excitations (either photonic or atomic). Therefore, after a photon detection at $t = 0$, it contains at most one excitation which can be exchanged between the cavity field and atoms, as it has been known for long (Brecha et al., 1995; Brune et al., 1996). In other words, the operator $a\rho_{ss}a^\dagger$ can be expanded in the space restricted to the three states $\{|00\rangle \equiv |N_r = 0, n_c = 0\rangle, |01\rangle \equiv |N_r = 0, n_c = 1\rangle, |10\rangle \equiv |N_r = 1, n_c = 0\rangle\}$ and the effective non-Hermitian Hamiltonian for the system, in this subspace, takes the following form:

$$H_3 = \begin{bmatrix} 0 & \alpha & 0 \\ \alpha & -\tilde{\Delta}_c - i\tilde{\gamma}_c & g_{\text{eff}}\sqrt{N} \\ 0 & g_{\text{eff}}\sqrt{N} & -\tilde{\Delta}_r - i\tilde{\gamma}_r \end{bmatrix}$$

The oscillatory dynamical behavior observed for $g^{(2)}(t)$ in the specific cases (A,B) is correctly recovered by this Hamiltonian, which validates the schematic model we used and suggests it comprises the main physical processes at work.

2.6 Conclusion

In this chapter, we studied how the strong Rydberg-Rydberg van der Waals interactions in an atomic medium may affect the quantum statistical properties of an incoming light beam. In the dispersive regime, the system was shown to effectively behave as a large spin coupled to a damped harmonic oscillator, *i.e.* the assembly of Rydberg bubbles and the cavity mode, respectively. The strong anharmonicity of the atomic spin affects the quantum statistics of the outgoing light beam. To demonstrate this effect, we performed analytical and numerical calculations of the second-order correlation function $g^{(2)}(\tau \geq 0)$. The results we obtained on a specific physical example with rubidium atoms show indeed that the transmitted light presents either bunched or antibunched characters, depending on the detuning between the cavity mode and the probe field. This suggests that, in such a setup, one could design light of arbitrary quantum statistics through appropriately adjusting the physical parameters. The Rydberg bubble approach akin to that developed in this chapter was used in (Boddeda et al., 2016) to successfully reproduce the temporal behavior of the cavity transmission coefficient. In order to fit the experimental data an additional decay to a dark Rydberg manifold was added in a purely phenomenological way. More details can be found in App. A.

2. Rydberg-induced quantum optical nonlinearities in the dispersive regime

Chapter 3

Perturbative treatment at lowest-order

Contents

3.1	$g^{(2)}$ function in the perturbative regime	50
3.1.1	Factorization property	50
3.1.2	First order mean values	51
3.1.3	Second order mean values	51
3.1.4	Two-time correlation functions	53
3.2	Application to an experimental case.	53
3.2.1	Dispersive regime.	53
3.2.2	Resonant case	55
3.3	Effective non-linear three-boson model	57
3.3.1	Dispersive regime	60
3.3.2	Resonant case	60
3.4	Conclusion	60

3. Perturbative treatment at lowest-order

In Chap. 2 we investigated the dispersive regime of the system presented in Chap. 1, *i.e.* when the intermediate state is excited off-resonantly, $\Delta_e \gg \gamma_e$, and can therefore be adiabatically eliminated. This chapter¹ is devoted to the investigation of the general case, including the resonant configuration $\Delta_e = 0$, in the low feeding limit. The perturbative treatment we propose to tackle this new problem also allows us to avoid resorting to the free parameter “number of atoms per bubble” that we had to adjust in the previous chapter to fit the results of the semiclassical calculations. In Sec. 3.1, we present an analytic derivation of the correlation $g^{(2)}(\tau)$ function for the transmitted and reflected light, based on the factorization of the lowest perturbative order of operator product averages. It is important to note that this derivation is valid in both the dispersive and resonant regimes and therefore generalizes our previous results. In Sec. 3.2, we numerically investigate the dispersive ($\Delta_e \neq 0$) and resonant regimes ($\Delta_e \approx 0$) of the system; in particular, our treatment reveals novel features of the pair correlation function $g^{(2)}$ due to the interplay of the impedance matching and dipole-dipole interactions. In the Sec. 3.3, we propose an effective non-linear three-boson model for the coupled atom-cavity system: this Ansatz allows us to obtain the same results as the (more cumbersome) exhaustive treatment. In the dispersive regime, this Hamiltonian agrees with the one we obtained in Chap. 2 in the Rydberg-bubble approximation.

3.1 $g^{(2)}$ function in the perturbative regime

In order to compute the $g^{(2)}$ function of the transmitted or reflected light, we perturbatively expand all correlation functions with respect to the feeding rate α . This expansion is equivalent to the expansion in the number of excitations in the incoming light. In Subsec. 3.1.1 we use the latter fact along with the conservation of the total number of excitations to demonstrate the factorization property of the lowest non-vanishing perturbative order of operator product averages. This property restricts the calculation of $g^{(2)}(0)$ to the determination of first and second-order mean values in feeding discussed in Subsecs. 3.1.2 and 3.1.3. We finish this section by explicitly showing how to deduce the two-time correlation function $g^{(2)}(\tau)$ (Subsec. 3.1.4).

3.1.1 Factorization property

As we restrict ourselves to low feeding rates, we may expand $g^{(2)}(0)$ in powers of α . Here, we consider $g^{(2)}(0)$ at the lowest non-vanishing order in α : this requires to evaluate $\langle a^\dagger a^\dagger a a \rangle$, $\langle a^\dagger a^\dagger a \rangle$ and $\langle a^\dagger a \rangle$ at the fourth, third and second orders, respectively, as shown in App. C. This task is greatly simplified by the following remarkable factorization property, established in App. D:

¹This chapter is an edited version of (Grankin et al., 2015).

$$\begin{aligned}\langle a^\dagger(t) a(t) \rangle^{(2)} &= \langle a^\dagger(t) \rangle^{(1)} \langle a(t) \rangle^{(1)} \\ \langle a^\dagger(t_2) a^\dagger(t_1) a(t_1) \rangle^{(3)} &= \langle a^\dagger(t_2) a^\dagger(t_1) \rangle^{(2)} \langle a(t_1) \rangle^{(1)} \\ \langle a^\dagger(t_2) a^\dagger(t_1) a(t_1) a(t_2) \rangle^{(4)} &= \langle a^\dagger(t_2) a^\dagger(t_1) \rangle^{(2)} \langle a(t_1) a(t_2) \rangle^{(2)}\end{aligned}$$

where the superscript (k) denotes the order in α to which quantities are calculated. This is a consequence of the conservation of the excitation number by the full Hamiltonian of the system {atoms+cavity+baths}. Therefore, for instance, for the transmitted light,

$$g_t^{(2)}(0) = \left(\langle a^\dagger a^\dagger \rangle^{(2)} \langle a a \rangle^{(2)} \right) / \left(\langle a^\dagger \rangle^{(1)} \langle a \rangle^{(1)} \right)^2$$

and we merely need to determine $\langle a \rangle^{(1)}$ and $\langle a^2 \rangle^{(2)}$. Note that the factorization does not apply to products of the kind $\langle a^2 \rangle^{(2)}$, so that $\langle a^2 \rangle^{(2)} \neq \langle a \rangle^{(1)} \langle a \rangle^{(1)}$.

3.1.2 First order mean values

The mean values $\langle a \rangle^{(1)}$ and $\langle \sigma_{ge}^{(i)} \rangle^{(1)}$ are readily obtained through taking the steady state of the first-order averaged Heisenberg equations Eqs. (1.12-1.15)

$$\langle a \rangle^{(1)} = \frac{\alpha}{D_c - \frac{g^2 N}{\left(D_e - \frac{\Omega_{cf}^2}{4D_r} \right)}} \quad (3.1)$$

$$\langle \sigma_{ge}^{(i)} \rangle^{(1)} = \frac{\alpha g}{D_c \left(D_e - \frac{\Omega_{cf}^2}{4D_r} \right) - g^2 N} \quad (3.2)$$

$$\langle \sigma_{gr}^{(i)} \rangle^{(1)} = \frac{\alpha g \Omega_{cf}}{2D_r \left[D_c \left(D_e - \frac{\Omega_{cf}^2}{4D_r} \right) - g^2 N \right]} \quad (3.3)$$

3.1.3 Second order mean values

In a similar way, the second-order value $\langle a^2 \rangle^{(2)}$ is determined through solving the following closed system²

²This system is closed as a result of the expansion with respect to α .

3. Perturbative treatment at lowest-order

$$\langle a^2 \rangle^{(2)} = \frac{g\sqrt{N}}{D_c} \langle ab \rangle^{(2)} + \frac{\alpha}{D_c} \langle a \rangle^{(1)} \quad (3.4)$$

$$\begin{aligned} \langle ab \rangle^{(2)} &= \frac{\Omega_{cf}}{2(D_c + D_e)} \langle ac \rangle^{(2)} + \frac{g\sqrt{N}}{(D_c + D_e)} \langle aa \rangle^{(2)} \\ &+ \frac{g\sqrt{N}}{(D_c + D_e)} \langle bb \rangle^{(2)} + \frac{\alpha}{(D_c + D_e)} \langle b \rangle^{(1)} \end{aligned} \quad (3.5)$$

$$\langle ac \rangle^{(2)} = \frac{g\sqrt{N}}{(D_c + D_r)} \langle bc \rangle^{(2)} + \frac{\alpha}{(D_c + D_r)} \langle c \rangle^{(1)} + \frac{\Omega_{cf}}{2(D_c + D_r)} \langle ab \rangle^{(2)} \quad (3.6)$$

$$\langle bb \rangle^{(2)} = \frac{\Omega_{cf}}{2D_e} \langle bc \rangle^{(2)} + \frac{g\sqrt{N}}{D_e} \langle ab \rangle^{(2)} \quad (3.7)$$

$$\langle bc \rangle^{(2)} = \frac{\Omega_{cf}}{2(D_e + D_r)} \langle cc \rangle^{(2)} + \frac{g\sqrt{N}}{(D_e + D_r)} \langle ac \rangle^{(2)} + \frac{\Omega_{cf}}{2(D_e + D_r)} \langle bb \rangle^{(2)} \quad (3.8)$$

$$\langle cc \rangle^{(2)} = \frac{\Omega_{cf}g\sqrt{N}}{2} K \langle ac \rangle^{(2)} + \frac{\Omega_{cf}^2 g\sqrt{N}}{4D_e} K \langle ab \rangle^{(2)} \quad (3.9)$$

deduced from Eqs. (1.12-1.15) under the assumption of a homogeneous atomic medium, whose consequences are detailed in App. E. In this system, we introduced the collective atomic operators

$$b \equiv \frac{1}{\sqrt{N}} \sum_i \sigma_{ge}^{(i)} \quad c \equiv \frac{1}{\sqrt{N}} \sum_i \sigma_{gr}^{(i)}. \quad (3.10)$$

We note that the first-order mean values $\langle a \rangle^{(1)}$, $\langle b \rangle^{(1)}$ and $\langle c \rangle^{(1)}$ which appear in Eqs. (3.4, 3.5, 3.6), respectively, have been computed in Eqs. (3.1, 3.2, 3.3). The K coefficient is approximately given by (see App. E for details)

$$K \approx \frac{1}{\left(D_e + D_r - \frac{\Omega_{cf}^2}{4D_e}\right) D_r - \frac{\Omega_{cf}^2}{4}} \left(1 - \frac{V_b}{V}\right) \quad (3.11)$$

where

$$V_b = \frac{\sqrt{2}\pi^2}{3} \sqrt{\frac{-C_6}{D_r - \Omega_{cf}^2 / \left(4(D_e + D_r) - \frac{\Omega_{cf}^2}{D_e}\right)}} \quad (3.12)$$

will be interpreted as the Rydberg bubble volume in the dispersive regime in the next section. Though it is too cumbersome to be reproduced here, the solution for $\langle a^2 \rangle^{(2)}$ is simply obtained by matrix inversion, and the calculation of $g_t^{(2)}(0)$ and $g_r^{(2)}(0)$ can be straightforwardly programmed, e.g. in Mathematica.

The closed sets of equations for the single- Eqs. (3.1-3.3) and two- Eqs. (3.4-3.9) operator product averages are obtained in the steady state regime. The temporal

response can however be derived in Fourier space by replacing setting $\frac{d}{dt}$ by $-i\omega$ in the expressions of App. E. This would account for the linear and non-linear (Rydberg-induced) EIT dispersion. The intrinsic (saturation) nonlinearity of the EIT ladder scheme is neglected from our consideration as it is assumed to be very weak for the chosen regime of parameters.

3.1.4 Two-time correlation functions

As for $g_{t,r}^{(2)}(0)$, the calculation of the time-dependent correlation function $g_{t,r}^{(2)}(\tau)$ is greatly simplified (see App. C) by the factorization property derived in App. D, since we simply need to determine the quantity $\langle a(t+\tau)a(t) \rangle^{(2)}$. From Eqs. (1.12-1.15), one easily deduces the following differential system, at the lowest order in α ,

$$\begin{aligned} \frac{d}{d\tau} \begin{pmatrix} \langle a(t+\tau)a(t) \rangle^{(2)} \\ \langle b(t+\tau)a(t) \rangle^{(2)} \\ \langle c(t+\tau)a(t) \rangle^{(2)} \end{pmatrix} &= -i\alpha \langle a \rangle \begin{pmatrix} 1 \\ 0 \\ 0 \end{pmatrix} + \\ -i \begin{pmatrix} -D_c & g\sqrt{N} & 0 \\ g\sqrt{N} & -D_e & \frac{\Omega_{cf}}{2} \\ 0 & \frac{\Omega_{cf}}{2} & -D_r \end{pmatrix} \begin{pmatrix} \langle a(t+\tau)a(t) \rangle^{(2)} \\ \langle b(t+\tau)a(t) \rangle^{(2)} \\ \langle c(t+\tau)a(t) \rangle^{(2)} \end{pmatrix} \end{aligned}$$

which, together with the boundary condition

$$\begin{pmatrix} \langle a(t+\tau)a(t) \rangle^{(2)} \\ \langle b(t+\tau)a(t) \rangle^{(2)} \\ \langle c(t+\tau)a(t) \rangle^{(2)} \end{pmatrix}_{\tau=0} = \begin{pmatrix} \langle aa \rangle^{(2)} \\ \langle ba \rangle^{(2)} \\ \langle ca \rangle^{(2)} \end{pmatrix}$$

calculated above, allows us to determine $\langle a(t+\tau)a(t) \rangle$. Again, though involved, the expressions are straightforward to obtain and program.

3.2 Application to an experimental case.

3.2.1 Dispersive regime.

Let us now provide some numerical results obtained in the perturbative approach described above. We first investigate the dispersive regime, addressed in Chap. 2. We consider the same values for physical parameters of the system {atoms + cavity} as discussed in Chap. 1, except for the following tunable parameters, which are fixed so as to optimize the effect: the control laser Rabi frequency is $\Omega_{cf} = 10\gamma_e$, the detuning of the intermediate level is $\Delta_e = -35\gamma_e$, the detuning of the Rydberg level is $\Delta_r = 0.4\gamma_e$, the cavity feeding rate is $\alpha = 0.01\gamma_e$, and the Van der Waals coefficient is $C_6 = -8.83 \times 10^6 \gamma_e \mu\text{m}^6$. For these parameters, the maximal average number of

3. Perturbative treatment at lowest-order

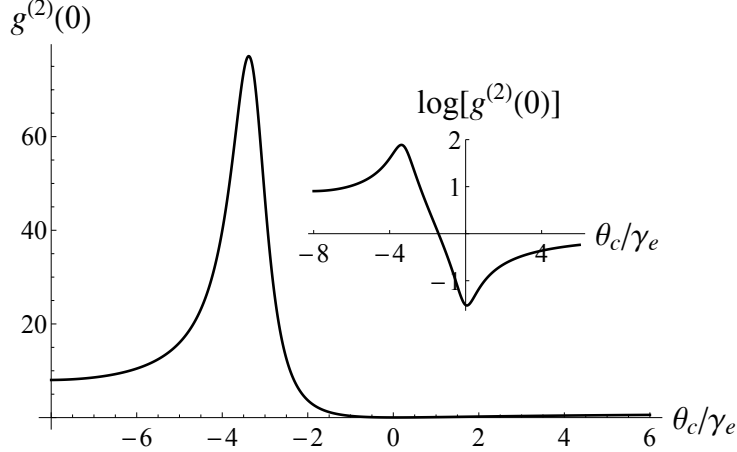


Figure 3.1: Second-order correlation function $g_t^{(2)}(0)$ for the transmitted light in the dispersive regime considered in Chap. 2 as a function of the renormalized cavity detuning $\theta_c/\gamma_e \equiv (\Delta_c - \Delta_c^{(0)})/\gamma_e$ where $\Delta_c^{(0)}$ is the detuning of the linear cavity. The shape of the plot is in good qualitative agreement with the results of the previous model. Inset : the same plot in logarithmic scale.

photons in the cavity is obtained for the cavity detuning $\Delta_c^{(0)} = -6.15 \gamma_e$ which is taken as a reference.

Under these conditions, Fig. 3.1 shows the second-order correlation function $g_t^{(2)}(0)$ as a function of the reduced cavity detuning $\theta_c \equiv (\Delta_c - \Delta_c^{(0)})/\gamma_e$, to be compared with Fig. 2.3 a) in Chap. 2. The two plots are in good qualitative agreement, but the position of the maximum is shifted from $\theta_c \approx -5$ to $\theta_c \approx -3.5$, for the same parameters. This basically originates from the definition of V_b in Chap. 2, differing from the present one by a factor $\sqrt{2}$. Fig. 3.2 shows the two-time second-order correlation function $g_t^{(2)}(\tau)$ as a function of time delay τ for two values of the detuning, *i.e.* $\theta_c \approx -3.5$ (maximum of $g_t^{(2)}(0)$) and $\theta_c \approx 0$ (minimum $g_t^{(2)}(0)$) : again, these plots are in good agreement with what we previously obtained in Chap. 2.

Let us note that in real experimental conditions, the atoms undergo not only radiative damping, but are also subject to extra dephasing γ_d on the Rydberg-ground state transition, due to laser frequency and intensity noise. This additional dephasing cannot be modeled in the Hamiltonian formalism presented in Appendix F, and thus the demonstration given in Appendix D for the factorization of mean values does not apply any more. However, since the radiative coherence damping is $\gamma_r \approx 0.01 \gamma_e$, the additional damping is $\gamma_d \approx 0.15 \gamma_e$, and the total number of atoms in the sample is $N \approx 10^4$, the experimental parameters satisfy the condition $\gamma_r \ll \gamma_d \ll N\gamma_r$. Under these circumstances, it is shown in Appendix F that the factorization remains valid, provided that the coherence radiative damping γ_r is replaced by the dephasing rate γ_d in the equations.

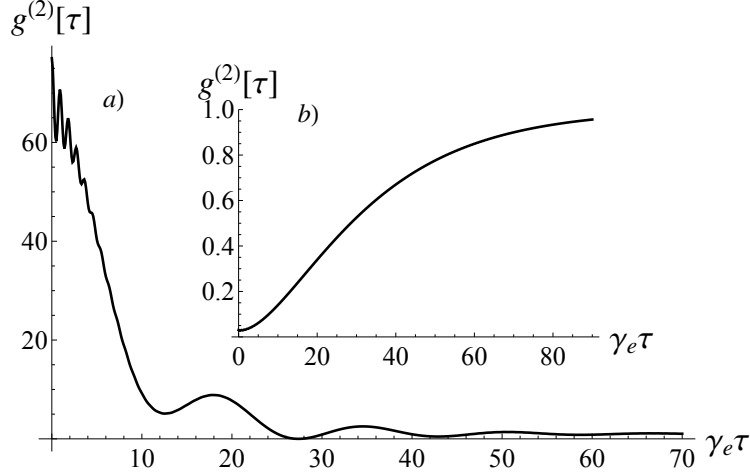


Figure 3.2: Unequal time second-order correlation function $g_t^{(2)}(\tau)$ for the transmitted light in the dispersive regime considered in Chap. 2 as a function of time. a) For $\theta_c/\gamma_e = -3.5$, $g_t^{(2)}(\tau)$ exhibits damped oscillations around the asymptotic value 1, alternatively showing bunching and antibunching. b) For $\theta_c/\gamma_e = 0$, $g_t^{(2)}(\tau)$ tends to 1 without crossing the asymptote. The results obtained in both cases are in good qualitative agreement with the results of the previous model.

3.2.2 Resonant case

In the previous subsection we confirmed results, obtained in the dispersive regime, in a more exhaustive way. Let us now consider the resonant case, which could not be treated in the previous chapter. As a new set of parameters, we take $\Delta_c = \Delta_e = \Delta_r = 0$, and assume that $\gamma_c^{(R)} \ll \gamma_c^{(L)}$. We also choose a higher principal number $n = 100$ for the Rydberg level, for which we take $\gamma_r = 0.1\gamma_e$. In addition, we fix $\gamma_c = 0.3\gamma_e$, $C = \frac{g^2 N}{2\gamma_e \gamma_c} \approx 30$ and $V = 50\pi \times 20 \times 20 \mu\text{m}^3$. In this regime, $V_b \approx \frac{\sqrt{2}\pi^2}{3} \sqrt{\frac{-C_6}{D_e}}$ is enhanced, and therefore magnified non-linear effects are expected.

As can be seen on Figure 3.3, there exists a value for which single photons are mostly absorbed $\langle a_{out}^{(L)\dagger} a_{out}^{(L)} \rangle = 0$, while pairs are reflected $\langle a_{out}^{(L)\dagger} a_{out}^{(L)\dagger} a_{out}^{(L)} a_{out}^{(L)} \rangle \neq 0$: this value can be computed and is found to be

$$\Omega_{cf} = 2\sqrt{\gamma_e \gamma_r (2C - 1)} = 2\gamma_e \sqrt{6} \approx 5\gamma_e$$

The time-dependence of $g_r^{(2)}(\tau)$ for the reflected light is also displayed for this choice of Rabi frequency: the reflected light is strongly bunched.

On the contrary, in a slightly detuned case, *i.e.* for $\Delta_e = -2\gamma_e$ and $\Delta_r = -0.1\gamma_e$, the other parameters remaining the same, one observes that around $\Omega_{cf} \approx 11\gamma_e$ pairs are absorbed $\langle a_{out}^{(L)\dagger} a_{out}^{(L)\dagger} a_{out}^{(L)} a_{out}^{(L)} \rangle = 0$ while single photons are reflected $\langle a_{out}^{(L)\dagger} a_{out}^{(L)} \rangle \neq 0$ (see Fig. 3.4). The time-dependence of $g_r^{(2)}(\tau)$ is also shown on Fig. 3.4 for $\Omega_{cf} \approx 11\gamma_e$: the reflected light is antibunched, asymptotically becoming uncorrelated at large times.

3. Perturbative treatment at lowest-order

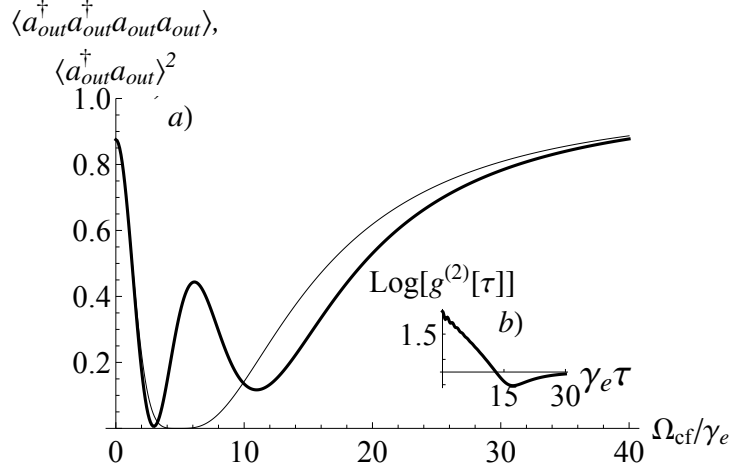


Figure 3.3: *Resonant case* $\Delta_c = \Delta_e = \Delta_r = 0$. a) The quantities $\langle a_{out}^{(L)\dagger} a_{out}^{(L)\dagger} a_{out}^{(L)} a_{out}^{(L)} \rangle$ (thick line) and $\langle a_{out}^{(L)\dagger} a_{out}^{(L)} \rangle$ (thin line), renormalized by the intensity of the incoming light, are represented as functions of the normalized control field Rabi frequency Ω_{cf}/γ_e . For $\Omega_{cf} = 2\sqrt{\gamma_e \gamma_r (2C - 1)} \approx 5\gamma_e$, photon pairs are reflected, *i.e.* $\langle a_{out}^{(L)\dagger} a_{out}^{(L)\dagger} a_{out}^{(L)} a_{out}^{(L)} \rangle \neq 0$, while single photons are absorbed, *i.e.* $\langle a_{out}^{(L)\dagger} a_{out}^{(L)} \rangle \approx 0$. b) Unequal time second-order correlation function $g_r^{(2)}(\tau)$ in logarithmic scale, for $\Omega_{cf} \approx 5\gamma_e$: the reflected light is strongly bunched.

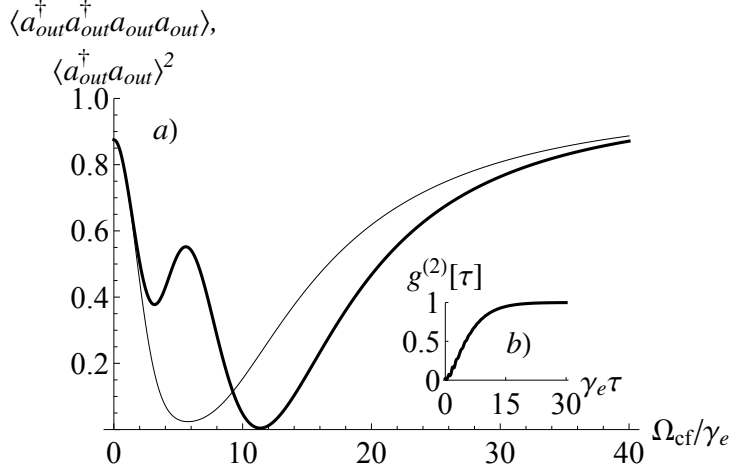


Figure 3.4: *Slightly detuned case* $\Delta_c = 0$, $\Delta_e = -2\gamma_e$, $\Delta_r = -0.1\gamma_e$. a) The quantities $\langle a_{out}^{(L)\dagger} a_{out}^{(L)\dagger} a_{out}^{(L)} a_{out}^{(L)} \rangle$ (thick line) and $\langle a_{out}^{(L)\dagger} a_{out}^{(L)} \rangle$ (thin line), renormalized by the intensity of the incoming light, are represented as functions of the normalized control field Rabi frequency Ω_{cf}/γ_e . For $\Omega_{cf} \approx 11\gamma_e$, photon pairs are absorbed, *i.e.* $\langle a_{out}^{(L)\dagger} a_{out}^{(L)\dagger} a_{out}^{(L)} a_{out}^{(L)} \rangle = 0$, while single photons are reflected, *i.e.* $\langle a_{out}^{(L)\dagger} a_{out}^{(L)} \rangle \neq 0$. b) Unequal time second-order correlation function $g_r^{(2)}(\tau)$, for $\Omega_{cf} \approx 11\gamma_e$: reflected light is antibunched, asymptotically becoming uncorrelated.

These new features are specific of the near-resonant regime, and could not be revealed by our previous work. They may be interpreted as different “impedance matching”³ conditions for single photons and pairs, leading to very large non-linear losses, acting at the single photon level.

In the last two sections, we described how to compute the correlation function in the low excitation regime, valid not only in the dispersive regime but even in the resonant case. Though exact and computable, the analytic expressions we get are cumbersome and do not easily lend themselves to physical interpretation. As we will see in the next section, one can however describe the physics of the system by a simpler model, in the low excitation number approximation. In this regime, according to the well-known Holstein-Primakoff approximation (Holstein and Primakoff, 1940), it is indeed possible to treat b and c as bosonic operators. To recover the results of the previous section to the lowest order, one moreover needs to introduce an effective non-linear dispersive term in the Hamiltonian together with a non-linear decay: the expressions we find have the advantage of being physically more transparent.

3.3 Effective non-linear three-boson model

In this section, we propose an effective model which is designed to correctly reproduce the physics of the system in the perturbative regime. Besides being simpler than the original formulation, this Ansatz also lends itself to a more transparent physical interpretation, as we shall see.

In the low excitation regime, *i.e.* for numbers of excitations much lower than the total number of atoms N , if initially prepared in a collective symmetric atomic state (*e.g.* the ground state), the system essentially remains in a symmetric subspace – that is with respect to permutations of atoms. It is therefore enough to focus on the effective action of the Hamiltonian H and the dissipation operator \mathcal{D} onto this subspace. Let us first consider the action of b (defined in Eq. 3.10) onto the collective symmetric atomic state $|m, n\rangle \equiv |N_e = m; N_r = n; N_g = N - m - n\rangle$ containing m excitations ‘ e ’ and n excitations ‘ r ’. Neglecting m and n with respect to N , one readily gets $b|m, n\rangle \approx \sqrt{m}|(m-1), n\rangle$ and $b^\dagger|m, n\rangle \approx \sqrt{(m+1)}|(m+1), n\rangle$. Hence $b^\dagger b|m, n\rangle = m|m, n\rangle = \sum_{n=1}^N \sigma_{ee}^{(n)}|m, n\rangle$ and $[b, b^\dagger] \approx 1$ and the term $(-\Delta_e \sum_{n=1}^N \sigma_{ee}^{(n)})$ in the Hamiltonian can be replaced by $-\Delta_e b^\dagger b$. The same results can be established for c : in particular, the term $(-\Delta_r \sum_{n=1}^N \sigma_{rr}^{(n)})$ in the Hamiltonian can be replaced by $-\Delta_r c^\dagger c$. Moreover, in the low excitation regime, bosonic operators b and c can be considered independent – their commutators being of order $O(\frac{m}{N}, \frac{n}{N})$. In the same approximation framework, the term $\sum_{n=1}^N (\sigma_{re}^{(n)} + \sigma_{er}^{(n)})$, involved in the interaction between atoms and control

³Analogously to classical systems, here, impedance matching designates the regime when no reflection of the incoming wave is observed.

3. Perturbative treatment at lowest-order

field, is replaced by $(bc^\dagger + b^\dagger c)$ – the action of these two operators onto the same collective symmetric state indeed coincides up to $O(\frac{m}{N}, \frac{n}{N})$ contributions. Similarly, the Liouvillian operators corresponding to spontaneous decays from intermediate and Rydberg levels take the collective forms

$$\begin{aligned}\mathcal{D}_e(\rho) &= \frac{\gamma_e}{2} (2b\rho b^\dagger - \rho b^\dagger b - b^\dagger b\rho) \\ \mathcal{D}_r(\rho) &= \frac{\gamma_r}{2} (2c\rho c^\dagger - \rho c^\dagger c - c^\dagger c\rho)\end{aligned}$$

The dipole-dipole interaction term is more tricky: it indeed couples the symmetric subspace both to itself and the nonsymmetric subspace. The restriction of V_{int} to the symmetric subspace yields the approximate form $\frac{\bar{\kappa}}{2}c^\dagger c^\dagger cc$ where $\bar{\kappa}$ denotes the average pair interaction. The complementary term $V_{S-A} = V_{int} - \frac{\bar{\kappa}}{2}c^\dagger c^\dagger cc$ therefore represents the coupling of symmetric and nonsymmetric subspaces. Since it requires multiple Rydberg excitations, the effect of this coupling remains small in the low excitation regime. It, however, has two consequences : *i*) it changes the coupling strength $\bar{\kappa}$ into a new value denoted κ_r , which takes into account self-coupling of the symmetric subspace through the nonsymmetric subspace via terms of the form $(V_{S-A})^2$, *ii*) it induces a non-linear decay due to the enhanced spontaneous emission experienced by nonsymmetric states which are uncoupled to the cavity field and therefore do not fulfill EIT conditions. The form we choose for this non-linear decay is

$$\mathcal{D}_{nl}(\rho) = \frac{\kappa_i}{2} (2cc\rho c^\dagger c^\dagger - \rho c^\dagger c^\dagger cc - c^\dagger c^\dagger cc\rho)$$

Though it seems arbitrary at this stage, this choice will be mathematically justified later by the fact that it allows us to recover the Heisenberg equations Eqs. (3.4-3.9) obtained in the previous Section. The expression of κ_i will be determined later by identification with Eqs. (3.4-3.9) ; it is also physically sound since it affects only multiply Rydberg-excited states inducing their decay to the ground level.

At this point, the Hamiltonian for our effective three-boson model writes

$$\begin{aligned}H_{eff} &= -\Delta_c a^\dagger a + \alpha (a + a^\dagger) - \Delta_e b^\dagger b \\ &\quad - \Delta_r c^\dagger c + g\sqrt{N} (ab^\dagger + b^\dagger a) \\ &\quad + \frac{\Omega_{cf}}{2} (bc^\dagger + b^\dagger c) + \frac{\kappa_r}{2} c^\dagger c^\dagger cc\end{aligned}$$

with the dissipation Liouvillian $\mathcal{D}[\rho] = \mathcal{D}_e(\rho) + \mathcal{D}_r(\rho) + \mathcal{D}_{nl}(\rho)$. We shall now determine κ_i and κ_r by identifying the corresponding steady state averages for the second order correlation functions. From the full Liouville-von Neumann equation of the system $\partial_t \rho = -\frac{i}{\hbar} [H_{eff}, \rho] + \mathcal{D}[\rho]$ one readily derives the following Bloch equations

$$\frac{d}{dt} \langle a \rangle = iD_c \langle a \rangle - i\alpha - ig\sqrt{N} \langle b \rangle \quad (3.13)$$

$$\frac{d}{dt} \langle b \rangle = iD_e \langle b \rangle - ig\sqrt{N} \langle a \rangle - i\frac{\Omega_{cf}}{2} \langle c \rangle \quad (3.14)$$

$$\frac{d}{dt} \langle c \rangle = iD_r \langle c \rangle - i\frac{\Omega_{cf}}{2} \langle b \rangle - i\kappa \langle c^+ cc \rangle \quad (3.15)$$

where we introduced the notation $\kappa \equiv \kappa_r - i\kappa_i$, κ_r and κ_i being real. From this set of equations, one gets the same steady state value $\langle a \rangle^{(1)}$ as in Eq. (3.1). At second order in α , the set of equations for two-operator steady-state averages is derived in the same way (here we omit superscripts ^(1,2) for simplicity)

$$\begin{aligned} \langle aa \rangle &= \frac{g\sqrt{N}}{D_c} \langle ab \rangle + \frac{\alpha}{D_c} \langle a \rangle \\ \langle ab \rangle &= \frac{\Omega_{cf}}{2(D_c + D_e)} \langle ac \rangle + \frac{g\sqrt{N}}{(D_c + D_e)} \langle aa \rangle + \frac{g\sqrt{N}}{(D_c + D_e)} \langle bb \rangle + \frac{\alpha}{(D_c + D_e)} \langle b \rangle \\ \langle ac \rangle &= \frac{g\sqrt{N}}{(D_c + D_r)} \langle bc \rangle + \frac{\alpha}{(D_c + D_r)} \langle c \rangle + \frac{\Omega_{cf}}{2(D_c + D_r)} \langle ab \rangle \\ \langle bb \rangle &= \frac{\Omega_{cf}}{2D_e} \langle bc \rangle + \frac{g\sqrt{N}}{D_e} \langle ab \rangle \\ \langle bc \rangle &= \frac{\Omega_{cf}}{2(D_e + D_r)} \langle cc \rangle + \frac{g\sqrt{N}}{(D_e + D_r)} \langle ac \rangle + \frac{\Omega_{cf}}{2(D_e + D_r)} \langle bb \rangle \\ \langle cc \rangle &= \frac{\Omega_{cf}}{2(D_r - \frac{\kappa}{2})} \langle bc \rangle \end{aligned}$$

which agrees with Eqs. (3.4-3.9) but for the last equation. If, however, we eliminate $\langle bc \rangle$ and $\langle bb \rangle$ from the last three equations, we obtain

$$\langle cc \rangle = \frac{\frac{\Omega_{cf}}{2} g\sqrt{N}}{(D_r - \frac{\kappa}{2}) \left(D_r + D_e - \frac{\Omega_{cf}^2}{4D_e} \right) - \frac{\Omega_{cf}^2}{4}} \left(\langle ac \rangle + \frac{\Omega_{cf}}{2D_e} \langle ab \rangle \right)$$

Finally, for our model to correctly reproduce the physics of the original system, the value we got for $\langle cc \rangle$ must coincide with Eq. (3.9) which requires that

$$K = \frac{1}{(D_r - \frac{\kappa}{2}) \left(D_r + D_e - \frac{\Omega_{cf}^2}{4D_e} \right) - \frac{\Omega_{cf}^2}{4}}$$

and, upon recalling Eq. (3.11),

$$\kappa = 2 \left(\frac{V_b}{V - V_b} \right) \left(\frac{\Omega_{cf}^2}{4 \left(D_r + D_e - \frac{\Omega_{cf}^2}{4D_e} \right)} - D_r \right)$$

We thus obtain the analytic expressions of the parameters κ_r and κ_i , respectively characterizing the non-linear dispersion and absorption of the c -boson, which make our model system precisely reproduce the results of the original problem in the steady state and in the lowest order of the feeding parameter α .

Let us now investigate the physical content of the previous model by considering two limiting cases.

3.3.1 Dispersive regime

In the dispersive regime addressed in the Chap. 2, $|D_{e,r}| \gg \Omega_{cf}$, whence $V_b \approx \frac{\sqrt{2\pi^2}}{3} \sqrt{\frac{|C_6|}{\Delta_r}}$, $\kappa_r \approx -\frac{2\Delta_r}{(N_b-1)}$ and $\kappa_i \approx 0$, where we introduced $\mathcal{N}_b \equiv \frac{V}{V_b}$. This result agrees with what we previously obtained in the Rydberg bubble approximation and therefore confirms its validity: we observe a shift due to the non-linear dispersive behavior of the c -boson, but no non-linear absorption since the intermediate level is too far detuned. Moreover, in the bubble picture, the parameter \mathcal{N}_b was interpreted as the number of Rydberg bubbles the sample may accommodate; as suggested above, this allows us to interpret V_b as the bubble volume.

3.3.2 Resonant case

If we now go to the opposite regime, *i.e.* the resonant case for which $\Delta_e = \Delta_r = 0$, $\gamma_e \gg \gamma_r$ and $\Omega_{cf}^2 \gg \gamma_e^2$, we obtain $V_b \approx \frac{\pi^2}{3} (1 - i) \sqrt{\frac{|C_6|}{\gamma_e}}$ and therefore the non-linearity parameters are

$$\kappa_r = -\kappa_i \approx -\frac{2\pi^2}{3V} \sqrt{\gamma_e |C_6|}$$

We now have both dispersion *and* absorption. From the expression of κ_i , it is clear that absorption results from an interplay of the spontaneous emission from the intermediate state and the Rydberg-Rydberg interactions.

3.4 Conclusion

In this chapter, we have studied the strong quantum optical non-linearities induced by Rydberg-Rydberg dipole-dipole interactions in an atomic medium. We provided a new perturbative treatment of the problem, based on the factorization of the lowest-order of operator product averages. This calculation enabled us to recover and extend our previous results: we could validate the approach based on the Rydberg bubble picture, as

well as investigate the resonant, absorptive, regime. In particular, our numerical simulations showed that strong Rydberg-induced non-linearities lead to different impedance matching conditions for single photons and photon pairs.

Moreover we proposed an effective model which yields the same results as the full calculation at the lowest order in the feeding parameter; this model also sheds light on the origin of the dispersion and absorption, as well as makes a bridge between the Rydberg bubble and perturbative approaches. In (Boddeda et al., 2016), the effective bosonic model was used to reproduce the non-linear behavior of the cavity transmission. Under the “mean-field” approximation (equivalent to all bosons being in coherent states) the model was shown to correctly reproduce the experimental data. More details can be found in App. A.

In the next chapter, we present an approach inspired from the many-body physics which allows us to go beyond the lowest order terms in expansion of correlation functions.

3. Perturbative treatment at lowest-order

Chapter 4

Schwinger-Keldysh contour formalism.

Contents

4.1	Introduction	64
4.1.1	Bosonic representation of the Hamiltonian	64
4.1.2	Contour-ordered representation of correlation functions	65
4.2	Wick's theorem and Green's functions	70
4.2.1	Wick's theorem	70
4.2.2	Green's functions	71
4.3	First order quantities	75
4.4	Factorization of averages in the lowest order	77
4.5	Intensity correlation function	79
4.5.1	$g^{(2)}$ function	79
4.5.2	T matrix	85
4.5.3	Relation to the decoupled case	86
4.5.4	Numerical results	88
4.6	$G^{(1)}$ correlation function	91
4.6.1	Elastic contribution	93
4.6.2	Inelastic contribution to $G_{out}^{(1)}$	96
4.6.3	Transmission spectrum	98
4.7	Conclusions	99

4. Schwinger-Keldysh contour formalism.

In Chap. 3 we considered the perturbative expansion of correlation functions to the lowest order in the feeding rate α . The extension of this method to higher orders leads to cumbersome expressions which are difficult to deal with. In this chapter¹ we consider the system in the so-called Schwinger-Keldysh contour formalism. Based on a contour-ordered representation of the relevant correlation functions (Sec. 4.1), it allows for a systematic perturbative expansion via Wick's theorem (Sec. 4.2). As a perturbation we will consider both feeding and dipole-dipole interaction Hamiltonians. We will perform a complete resummation with respect to the latter, for each correlation function that we encounter in this chapter. Using this method we re-derive results of Chap. 3 (Secs. 4.3,4.4,4.5) in an analytic compact form and go beyond by deriving analytic expressions for elastic and inelastic components of the cavity transmission spectrum (Sec. 4.6). We also identify a polaritonic resonance structure, to our knowledge unreported so far, that we physically interpret.

4.1 Introduction

In this section, we introduce the basic tools we shall use throughout this chapter. In Subsec. 4.1.1, we present the bosonic representation of the system's Hamiltonian, explained in more detail in App. B. In Subsec. 4.1.2, we show how to use the so-called Schwinger-Keldysh contour idea to express generic correlation functions in a form particularly well suited for the perturbative expansion we perform in subsequent sections.

4.1.1 Bosonic representation of the Hamiltonian

In the perturbative treatment we perform in the next sections, we shall make an extensive use of Wick's theorem. To this end, it is convenient to represent our system in terms of bosons. The idea, presented in detail in App. B and only briefly sketched here, is to associate each atom $i = 1, \dots, N$ in the ensemble with two independent bosonic annihilation operators $\{b_i, c_i\}$ whose truncations to single-excitation subspace coincide with the lowering operators $\sigma_{ge}^{(i)}$ and $\sigma_{gr}^{(i)}$, respectively. This approximation is valid in the regime of large atom numbers and weak coupling $g \ll \gamma_c^R, \gamma_e$. In that representation, the Hamiltonian of the full system described in Chap. 1 now takes the form $H = H_0 + H_{int}$ where

¹The results of this chapter are presented in the preprint (Grankin et al., 2016) submitted for publication.

$$\begin{aligned}
H_0 &= H_{at} + V_{a-c} + H_{cav} + H_{bath} + V_{cav-bath} + V_{at-bath} \\
H_{int} &= H_{dd} + H_f \\
H_{dd} &= \frac{1}{2} \sum_{m,n}^N \kappa_{mn} c_m^\dagger c_n^\dagger c_m c_n \\
H_f &= \alpha (a + a^\dagger) \\
H_{at} &= \sum_{n=1}^N \left\{ -\Delta_e b_n^\dagger b_n - \Delta_r c_n^\dagger c_n + \frac{\Omega_{cf}}{2} (b_n^\dagger c_n + b_n c_n^\dagger) \right\} \\
V_{a-c} &= \sum_{n=1}^N g (a b_n^\dagger + a^\dagger b_n) \\
H_{cav} &= -\Delta_c a^\dagger a \\
H_{bath} &= \sum_{\lambda=L,R} \int d\omega \omega B_{\lambda,\omega}^\dagger B_{\lambda,\omega} + \int d\omega \omega \sum_{n=1}^N (D_{n,\omega}^\dagger D_{n,\omega} + C_{n,\omega}^\dagger C_{n,\omega}) \\
V_{cav-bath} &= \sum_{\lambda=L,R} \int d\omega g_b(\omega) [B_{\lambda,\omega} a^\dagger + B_{\lambda,\omega}^\dagger a] \\
V_{at-bath} &\approx \sum_{n=1}^N \int d\omega [g_c(\omega) C_{n,\omega} b_n^\dagger + g_d(\omega) D_{n,\omega} c_n^\dagger + \text{H.c.}]
\end{aligned}$$

4.1.2 Contour-ordered representation of correlation functions

4.1.2.1 Multitime-correlation functions in the interaction picture

²Throughout this dissertation, we have focused on evaluating correlation functions of the light either transmitted through or reflected from the cavity, which can be experimentally obtained via multitime measurements of the light outgoing from the setup. Input-output theory shows that, under Markov approximation, these functions simply relate to the intracavity field correlation functions, themselves coupled to the atomic correlation functions via Heisenberg-Langevin equations. The generic form for such correlation functions is

$$\left\langle \tilde{\mathcal{T}} \left\{ \prod_{i=1}^r \mathcal{O}_{H,i}^\dagger(t_i) \right\} \mathcal{T} \left\{ \prod_{j=r+1}^{r+s} \mathcal{O}_{H,j}(t_j) \right\} \right\rangle \quad (4.1)$$

where $\mathcal{O}_{H,i}(t) \equiv e^{iH(t-t_0)} \mathcal{O}_i e^{-iH(t-t_0)}$ is an arbitrary operator of our system, expressed in the Heisenberg picture with respect to the Hamiltonian H given in the previous subsection. In (4.1) \mathcal{T} and $\tilde{\mathcal{T}}$ stand for the chronological and anti-chronological time-

²This subsection essentially follows (Stefanucci and van Leeuwen, 2013; Rammer, 2007).

4. Schwinger-Keldysh contour formalism.

ordering operators defined respectively as:

$$\mathcal{T}(A(t_1)B(t_2)) = \begin{cases} A(t_1)B(t_2); & t_1 > t_2 \\ B(t_2)A(t_1); & t_2 > t_1 \end{cases} \quad (4.2)$$

$$\tilde{\mathcal{T}}(A(t_1)B(t_2)) = \begin{cases} A(t_1)B(t_2); & t_2 > t_1 \\ B(t_2)A(t_1); & t_1 > t_2 \end{cases} \quad (4.3)$$

We also notice that averaging in 4.1 is performed over the initial state of the system (at $t = t_0$), that we assume to be the vacuum $\rho_0 = |\mathcal{O}\rangle\langle\mathcal{O}|$ ($\langle\cdots\rangle \equiv \text{Tr}[\rho_0\cdots]$), *i.e.* the state which does not contain any excitation, either in the baths or in the system {cavity+atoms}. Many physically relevant quantities involve correlation functions of the form (4.1), as for example the $g^{(2)}(\tau)$ function of the transmitted light (See App. C) or the squeezing spectrum which requires the determination of $\langle\mathcal{T}\{a(t)a(t')\}\rangle, \langle\tilde{\mathcal{T}}\{a^\dagger(t)a^\dagger(t')\}\rangle$.

Let us now transform (4.1) into the interaction picture with respect to H_0 . For any operator $\mathcal{O}_H(t) \equiv e^{iH(t-t_0)}\mathcal{O}e^{-iH(t-t_0)}$ in the Heisenberg picture we may write

$$\mathcal{O}_H(t) = V^\dagger(t, t_0)\mathcal{O}_{H_0}(t)V(t, t_0) \quad (4.4)$$

where we introduced $V(t, t_0) \equiv e^{iH_0(t-t_0)}e^{-iH(t-t_0)}$. By time derivation of the previous definition we get

$$\begin{aligned} \frac{d}{dt}V(t, t_0) &= -iH_{int}(t)V(t, t_0) \\ H_{int}(t) &\equiv e^{iH_0(t-t_0)}H_{int}e^{-iH_0(t-t_0)} \end{aligned} \quad (4.5)$$

and deduce through recursive integration that $V = \sum_{n=0}^{+\infty} V^{(n)}$, where $V^{(0)}(t, t_0) = 1$ and

$$\begin{aligned} V^{(n>1)}(t, t_0) &= (-i)^n \int_{t_0}^t \dots \int_{t_0}^{t_2} dt_1 \dots dt_n H_{int}(t_n) \dots H_{int}(t_1) \\ &= \frac{(-i)^n}{n!} \mathcal{T} \left\{ \left(\int_{t_0}^t ds H_{int}(s) \right)^n \right\} \end{aligned}$$

where \mathcal{T} is the chronological time-ordering operator (see Eq. 4.2). Please note that the $n!$ factor in the denominator appears from permutations of the time arguments. Finally combining all terms in the expansion of $V(t, t_0)$ we get

$$V(t, t_0) = \mathcal{T} \left\{ e^{-i \int_{t_0}^t ds H_{int}(s)} \right\} \quad (4.6)$$

and

$$V^\dagger(t, t_0) = \tilde{\mathcal{T}} \left\{ e^{-i \int_t^{t_0} ds H_{int}(s)} \right\} \quad (4.7)$$

At this point it is worth noticing, that following (Abrikosov et al., 1975; Stefanucci and van Leeuwen, 2013; Rammer, 2007; Kamenev, 2011), we do not provide any prescription for same-time values of (4.2). In order to make the chronological time-ordering coincide with normal ordering when $t = t'$, we shall implicitly assume that, under \mathcal{T} , the time arguments of creation operators are shifted further in time by the infinitesimal quantity 0^+ such that, e.g.

$$\begin{aligned} \mathcal{T} \left\{ \int_{t_0}^t ds H_{dd}(s) \right\} &= \mathcal{T} \left\{ \frac{1}{2} \sum_{m,n} \kappa_{mn} \int ds c_m^\dagger(s+0^+) c_n^\dagger(s+0^+) c_m(s) c_n(s) \right\} \\ &= \left\{ \frac{1}{2} \sum_{m,n} \kappa_{mn} \int ds c_m^\dagger(s) c_n^\dagger(s) c_m(s) c_n(s) \right\} \end{aligned}$$

For the same reason, under $\tilde{\mathcal{T}}$, the time arguments of creation operators will be added the infinitesimal quantity 0^- so that:

$$\begin{aligned} \tilde{\mathcal{T}} \left\{ \int_{t_0}^t ds H_{dd}(s) \right\} &= \tilde{\mathcal{T}} \left\{ \frac{1}{2} \sum_{m,n} \kappa_{mn} \int ds c_m^\dagger(s+0^-) c_n^\dagger(s+0^-) c_m(s) c_n(s) \right\} \\ &= \left\{ \frac{1}{2} \sum_{m,n} \kappa_{mn} \int ds c_m^\dagger(s) c_n^\dagger(s) c_m(s) c_n(s) \right\} \end{aligned}$$

Combining (4.4, 4.6, 4.7) we may rewrite (4.4) under the following form:

$$\mathcal{O}_H(t) = \tilde{\mathcal{T}} \left\{ e^{-i \int_t^{t_0} ds H_{int}(s)} \right\} \mathcal{O}_{H_0}(t) \mathcal{T} \left\{ e^{-i \int_{t_0}^t ds H_{int}(s)} \right\} \quad (4.8)$$

Consider now, without loss of generality, that all creation and annihilation operators in (4.1) are already arranged anti-chronologically and chronologically, respectively, *i.e.* $t_1 < t_2 < \dots < t_r, t_{r+1} > t_{r+2} > \dots > t_{r+s}$. Substituting (4.8) into (4.1) we get:

4. Schwinger-Keldysh contour formalism.

$$\begin{aligned}
& \left\langle \mathcal{O}_1^\dagger(t_1) \mathcal{O}_2^\dagger(t_2) \dots \mathcal{O}_r^\dagger(t_r) \mathcal{O}_{r+1}(t_{r+1}) \dots \mathcal{O}_{r+s}(t_{r+s}) \right\rangle \quad (4.9) \\
&= \text{Tr} \left[\begin{aligned} & \rho_0 V^\dagger(t_1, t_0) \mathcal{O}_{H_0,1}^\dagger(t_1) V^\dagger(t_2, t_1) \mathcal{O}_{H_0,2}^\dagger(t_2) \dots V^\dagger(t_r, t_{r-1}) \mathcal{O}_{H_0,r}^\dagger(t_r) V(t_r, t_0) \\ & \times V^\dagger(t_{r+1}, t_0) \mathcal{O}_{H_0,r+1}(t_{r+1}) V(t_{r+1}, t_{r+2}) \dots \mathcal{O}_{H_0,r+s}(t_{r+s}) V(t_{r+s}, t_0) \end{aligned} \right] \\
&= \text{Tr} \left[\begin{aligned} & \rho_0 V^\dagger(t_1, t_0) \mathcal{O}_{H_0,1}^\dagger(t_1) \dots \mathcal{O}_{H_0,r}^\dagger(t_r) V^\dagger(\infty, t_r) \\ & \times V(\infty, t_{r+1}) \mathcal{O}_{H_0,r+1}(t_{r+1}) \dots \mathcal{O}_{H_0,r+s}(t_{r+s}) V(t_{r+s}, t_0) \end{aligned} \right]
\end{aligned}$$

where in the last line we used the unitarity of the V operator. Finally we assume further that the evolution of the system began at $t_0 = -\infty$. The latter condition is consistent with the steady state calculation.

Reintroducing time-ordering operators in Eq. (4.9) we get

$$\begin{aligned}
& \left\langle \tilde{\mathcal{T}} \left\{ \prod_{i=1}^r \mathcal{O}_{H,i}^\dagger(t_i) \right\} \mathcal{T} \left\{ \prod_{j=r+1}^{r+s} \mathcal{O}_{H,j}(t_j) \right\} \right\rangle \quad (4.10) \\
&= \text{Tr} \left[\begin{aligned} & \rho_0 \tilde{\mathcal{T}} \left\{ V^\dagger(t_1, \infty) \mathcal{O}_{H_0,1}^\dagger(t_1) \dots \mathcal{O}_{H_0,r}^\dagger(t_r) V^\dagger(\infty, t_r) \right\} \\ & \times \mathcal{T} \left\{ V(\infty, t_{r+1}) \mathcal{O}_{H_0,r+1}(t_{r+1}) \dots \mathcal{O}_{H_0,r+s}(t_{r+s}) V(t_{r+s}, \infty) \right\} \end{aligned} \right] \\
&= \text{Tr} \left[\begin{aligned} & \rho_0 \tilde{\mathcal{T}} \left\{ \mathcal{O}_{H_0,1}^\dagger(t_1) \dots \mathcal{O}_{H_0,r}^\dagger(t_r) e^{-i \int_{+\infty}^{-\infty} ds H_{int}(s)} \right\} \\ & \times \mathcal{T} \left\{ \mathcal{O}_{H_0,r+1}(t_{r+1}) \dots \mathcal{O}_{H_0,r+s}(t_{r+s}) e^{-i \int_{-\infty}^{+\infty} ds H_{int}(s)} \right\} \end{aligned} \right]
\end{aligned}$$

4.1.2.2 Schwinger-Keldysh contour-ordering

Eq. (4.10) suggests to introduce a new variable, which does not merely follow the real axis $(-\infty, \infty)$ but rather a contour \mathcal{C} made of two branches $\mathcal{C}_+ = (-\infty, +\infty)$ and $\mathcal{C}_- = (+\infty, -\infty)$ (Fig. 4.1). A contour-ordering operator $\mathcal{T}_{\mathcal{C}}$ can be defined, accordingly, by

$$\forall z_1, z_2 \in \mathcal{C} : \mathcal{T}_{\mathcal{C}} \{A(z_1) B(z_2)\} = \begin{cases} A(z_1) B(z_2); & z_1 > z_2 \\ B(z_2) A(z_1); & z_2 > z_1 \end{cases}$$

or, to be more explicit,

$$\mathcal{T}_{\mathcal{C}} \{A(z_1) B(z_2)\} = \begin{cases} A(z_1) B(z_2); & \text{if } z_1 \in \mathcal{C}_-, z_2 \in \mathcal{C}_+ \\ B(z_2) A(z_1); & \text{if } z_1 \in \mathcal{C}_+, z_2 \in \mathcal{C}_- \\ \mathcal{T} \{A(z_1) B(z_2)\}; & \text{if } z_1 \in \mathcal{C}_+, z_2 \in \mathcal{C}_+ \\ \tilde{\mathcal{T}} \{A(z_1) B(z_2)\}; & \text{if } z_1 \in \mathcal{C}_-, z_2 \in \mathcal{C}_- \end{cases}$$

Finally, introducing the notation $\mathcal{O}_{\pm,i} \equiv \mathcal{O}_{H_0,i}(t_i \in \mathcal{C}_{\pm})$, we may rewrite (4.10) under the form:

$$\begin{aligned}
& \left\langle \tilde{\mathcal{T}} \left\{ \prod_{i=1}^r \mathcal{O}_{H,i}^\dagger(t_i) \right\} \mathcal{T} \left\{ \prod_{j=r+1}^{r+s} \mathcal{O}_{H,j}(t_j) \right\} \right\rangle \\
&= \left\langle \mathcal{T}_C \left\{ \prod_{i=1}^r \prod_{j=r+1}^{r+s} \mathcal{O}_{-,i}^\dagger(t_i) \mathcal{O}_{+,j}(t_j) e^{-i \int_C ds H_{int}(s)} \right\} \right\rangle \quad (4.11)
\end{aligned}$$

The so-called Schwinger-Keldysh contour formalism we have just introduced allows one to expand e.g. correlation functions in powers of the perturbation in a more systematic and practical way than “conventional” approaches thanks to Wick’s theorem for contour-ordered quantities, as we shall see in the next section.

For the sake of simplicity, we introduce the operator $A_q = \frac{1}{\sqrt{2\pi}} \int_{-\infty}^{\infty} (a_+ - a_-) ds$ in Eq. (4.11), where the q subscript stands for the so-called “quantum” variable (Kamenev, 2011)³:

$$\begin{aligned}
& \left\langle \mathcal{T}_C \left\{ e^{-i(\int_C H_{dd}) - i\sqrt{2\pi}\alpha(A_q + A_q^\dagger)} \prod_{i=1}^r \mathcal{O}_{-,i}^\dagger(t_i) \prod_{j=r+1}^{r+s} \mathcal{O}_{+,j}(t_j) \right\} \right\rangle \\
&= \sum_n \frac{(-i\sqrt{2\pi}\alpha)^n}{n!} \left\langle \mathcal{T}_C \left\{ e^{-i(\int_C H_{dd})} (A_q + A_q^\dagger)^n \prod_{i=1}^r \mathcal{O}_{-,i}^\dagger(t_i) \prod_{j=r+1}^{r+s} \mathcal{O}_{+,j}(t_j) \right\} \right\rangle \\
&= \sum_{n,k} \frac{(-i\sqrt{2\pi}\alpha)^n}{(n-k)!k!} \left\langle \mathcal{T}_C \left\{ e^{-i(\int_C H_{dd})} A_q^{n-k} A_q^{\dagger k} \prod_{i=1}^r \prod_{j=r+1}^{r+s} \mathcal{O}_{-,i}^\dagger(t_i) \mathcal{O}_{+,j}(t_j) \right\} \right\rangle \quad (4.12)
\end{aligned}$$

In the next section, we shall consider the perturbative expansion of Eq. (4.12) with respect to H_{dd} which yields the following double perturbation series

$$\sum_{n,k,p} \frac{(-i\sqrt{2\pi}\alpha)^n}{(n-k)!k!} \left\langle \mathcal{T}_C \left\{ \frac{(-i \int_C H_{dd})^p}{p!} A_q^{n-k} A_q^{\dagger k} \prod_{i=1}^r \prod_{j=r+1}^{r+s} \mathcal{O}_{-,i}^\dagger(t_i) \mathcal{O}_{+,j}(t_j) \right\} \right\rangle \quad (4.13)$$

Thanks to Wick’s theorem, recalled in the next section, we shall be able to fully resum the first few terms in α (up to $n = 4$) with respect to H_{dd} .

³This definition is made for the sake of convenience. The term “quantum variable” can be motivated by the following decomposition of the forward and backward operators: $a_+(t) \equiv \langle a(t) \rangle + \delta a_+(t)$, $a_-(t) \equiv \langle a(t) \rangle + \delta a_-(t)$, where $\langle \delta a_{+,-} \rangle = 0$. Therefore the so-called quantum variable $a_q \equiv \frac{1}{\sqrt{2}}(a_+ - a_-) = \frac{1}{\sqrt{2}}(\delta a_+ - \delta a_-)$ indeed represents quantum fluctuations around the mean field.

4. Schwinger-Keldysh contour formalism.

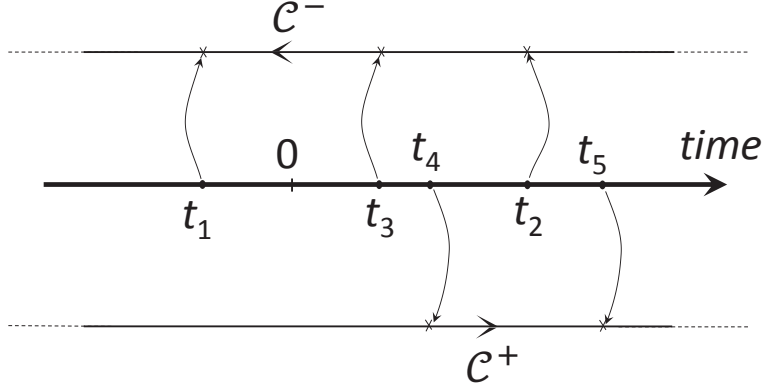


Figure 4.1: Representation of contour-ordering for the multitime correlation function $\langle \tilde{\mathcal{T}} \{ \mathcal{O}^1(t_1) \mathcal{O}^2(t_2) \mathcal{O}^3(t_3) \} \mathcal{T} \{ \mathcal{O}^4(t_4) \mathcal{O}^5(t_5) \} \rangle$.

4.2 Wick's theorem and Green's functions

In this section we recall the Wick's theorem for bosonic statistics which applies to our system. Then we define and give the main properties of the Green's functions which appear as the basic element of the perturbative expansion we get from Wick's theorem.

4.2.1 Wick's theorem

Following (Rammer, 2007), we recall the Wick's theorem for contour-ordered quantities specific to the bosonic statistics.

The generic term of the double perturbative expansion of Eq. (4.13) is an expectation value in the vacuum state ρ_0 of a contour-ordered string of creation and annihilation operators

$$\mathcal{S} = \left\langle \mathcal{T}_C \left\{ e_{p+q}^\dagger(z_{p+q}) \cdots e_{p+1}^\dagger(z_{p+1}) e_p(z_p) \cdots e_1(z_1) \right\} \right\rangle \quad (4.14)$$

where e_1, e_2, \dots, e_{p+q} are bosonic annihilation operators in the interaction picture with respect to H_0 . Applied to our system, Wick's theorem states that such a contour-ordered string can be decomposed into a sum over all possible pairwise products of creation and annihilation operators⁴ in the string in Eq. (4.14)

⁴We notice that Wick's theorem is actually demonstrated for independent bosons (Rammer, 2007). In our case, bosons are not independent but we may set ourselves in these conditions as follows. The Hamiltonian H_0 is quadratic in bosonic operators, *i.e.* it can be written as $H_0 = \sum_{i,j} h_{ij} \zeta_i^\dagger \zeta_j$ where we sum over all the possible operators of the system ($\forall i, j : [\zeta_i, \zeta_j^\dagger] = \delta_{ij}$). We introduce the new operators $\xi_i = \sum U_i^j \zeta_j$, where U stands for the unitary transformation which diagonalizes the matrix

$$\mathcal{S} = \sum_{a.p.p} \prod_{k,l} \left\langle \mathcal{T}_C \left\{ e_l(z_l) e_k^\dagger(z_k) \right\} \right\rangle \quad (4.15)$$

The quantity $G_{e_k e_l}^{(C)}(z_l, z_k) = -i \left\langle \mathcal{T}_C \left\{ e_l(z_l) e_k^\dagger(z_k) \right\} \right\rangle$ is called the unperturbed contour-ordered Green's function for the operators e_k and e_l . The next subsection shall be devoted to its determination.

It is important to notice that an implicit part of the theorem's statement is that the number of creation and annihilation operators should be equal, the corresponding expectation value otherwise vanishes. This remark allows us to simplify the general formula Eq. (4.13) for the correlation function as follows. In this formula we have $k + r + 2p$ creation operators (recalling that $H_{dd} = \frac{1}{2} \sum_{ij} \kappa_{ij} c_i^\dagger c_j^\dagger c_i c_j$) and $n - k + s + 2p$ annihilation operators. According to the remarks above, we can restrict the series Eq. (4.13) to the terms which satisfy $k + r + 2p = n - k + s + 2p$, or equivalently $k = \frac{n+s-r}{2}$. Defining $D = s - r$ we finally have

$$\sum_{n: \frac{n+D}{2} \in \mathbb{Z}, p} \frac{(-i\sqrt{2\pi}\alpha)^n}{\left(\frac{n+D}{2}\right)! \left(\frac{n-D}{2}\right)!} \left\langle \mathcal{T}_C \left\{ \frac{(-i \int_C H_{dd})^p}{p!} A_q^{\frac{n-D}{2}} A_q^{\dagger \frac{n+D}{2}} \prod_{i=1}^r \prod_{j=r+1}^{r+s} \mathcal{O}_{-,i}^\dagger(t_i) \mathcal{O}_{+,j}(t_j) \right\} \right\rangle \quad (4.16)$$

where in the summation over n we specified that k should be an integer. For future reference and for the sake of conciseness we shall use the formally resummed version of this formula with respect to p

$$\sum_{n: \frac{n+D}{2} \in \mathbb{Z}} \frac{(-i\sqrt{2\pi}\alpha)^n}{\left(\frac{n+D}{2}\right)! \left(\frac{n-D}{2}\right)!} \left\langle \mathcal{T}_C \left\{ e^{-i(\int_C H_{dd})} A_q^{\frac{n-D}{2}} A_q^{\dagger \frac{n+D}{2}} \prod_{i=1}^r \prod_{j=r+1}^{r+s} \mathcal{O}_{-,i}^\dagger(t_i) \mathcal{O}_{+,j}(t_j) \right\} \right\rangle \quad (4.17)$$

Finally it is worth noticing that the theorem completes the mathematical apparatus required for the perturbative expansion of the correlation functions.

4.2.2 Green's functions

The crucial concept of this chapter is the contour-ordered Green's function $G_{e_k e_l}^{(C)}(z_l, z_k) = -i \left\langle \mathcal{T}_C \left\{ e_l(z_l) e_k^\dagger(z_k) \right\} \right\rangle$ which naturally emerges from Wick's theorem. Physically it characterizes the system's response at some time z_l to the creation of a single excitation at time z_k .

h_{ij} . These new operators are themselves bosonic, *i.e.* $[\xi_i, \xi_j^\dagger] = \delta_{ij}$ and since $H_0 = \sum_i \omega_i \xi_i^\dagger \xi_i$, they are independent and therefore satisfy the theorem's hypothesis. Finally transforming bosons back to the initial basis we get Eq. (4.15).

4. Schwinger-Keldysh contour formalism.

Depending on the respective positions of the arguments z_k and z_l on the contour, $G_{e_k e_l}^{(C)} [z_l, z_k]$ coincides with one of the four following real-time Green's functions:

$$\begin{cases} G_{e_k e_l}^{T} (z_l - z_k) &= G_{e_k e_l}^{(C)} [z_l, z_k]; \text{ when } z_l, z_k \in \mathcal{C}_+ \\ G_{e_k e_l}^{\tilde{T}} (z_l - z_k) &= G_{e_k e_l}^{(C)} [z_l, z_k]; \text{ when } z_l, z_k \in \mathcal{C}_- \\ G_{e_k e_l}^{>} (z_l - z_k) &= G_{e_k e_l}^{(C)} [z_l, z_k]; \text{ when } z_k \in \mathcal{C}_+, z_l \in \mathcal{C}_- \\ G_{e_k e_l}^{<} (z_l - z_k) &= G_{e_k e_l}^{(C)} [z_l, z_k]; \text{ when } z_k \in \mathcal{C}_-, z_l \in \mathcal{C}_+ \end{cases}$$

where we implicitly assumed the time invariance of $G^{T, \tilde{T}, >, <}$ (resulting from the fact that H_0 is time-independent).

Note that, while (z_k, z_l) are contour arguments in $G_{e_k e_l}^{(C)} (z_l, z_k)$, they must be understood as “real” time arguments in the functions $G^T, G^{\tilde{T}}, G^>, G^<$. It can also be shown (Stefanucci and van Leeuwen, 2013) that⁵ $G_{xy}^{\tilde{T}} [t' - t] = -[G_{yx}^T [t - t']]^* = -[G_{xy}^T [t - t']]^*$, or equivalently in temporal Fourier space $G_{xy}^{\tilde{T}} [\omega] = -[G_{xy}^T [\omega]]^*$. Moreover, the different Green's functions are related by $G_{xy}^{>} [\omega] + G_{xy}^{<} [\omega] = G_{xy}^T [\omega] + G_{xy}^{\tilde{T}} [\omega]$. This can be further simplified by noticing that, since H_0 preserves the excitation number and the state we average on is the vacuum ρ_0 , then $G_{xy}^{<} [\omega] = 0$ for any pair of operators (x, y) ; therefore $G_{xy}^{>} [\omega] = 2i \text{Im} [G_{xy}^T [\omega]]$. As it can be seen, all four Green's functions are not independent. As a consequence defining the so-called “quantum” variable $x_q(t) \equiv \frac{1}{\sqrt{2}} (x_+(t) - x_-(t))$ (where as usual $x_{\pm}(t) = x_{H_0}(t \in \mathcal{C}_{\pm})$) we get for any pair of two operators (x, y) : $\langle \mathcal{T}_C \{x_q(t) y_q^\dagger(t')\} \rangle = 0$.

In the remainder of this subsection we determine G_{xy}^T for all possible pairs of operators (x, y) , from which all other Green's functions can be deduced.

4.2.2.1 Time-ordered Green's functions

In this subsection we shall determine time-ordered Green's functions of the form $G^T(t_k - t_l) = -i \langle \mathcal{T} \{e_k(t_k) e_l^\dagger(t_l)\} \rangle$ where e_k, e_l are either atomic or photonic annihilation operators expressed in the interaction picture with respect to H_0 . Their expression can be deduced from the Heisenberg-Langevin equations of the system, generated by H_0 alone:

$$\frac{d}{dt} a = -\Gamma_c a - i\alpha - ig \sum_i^N b_i + \sqrt{2\gamma_c} a_{in} \quad (4.18)$$

$$\frac{d}{dt} b_i = -\Gamma_e b_i - i\frac{\Omega_{cf}}{2} c_i - iga + \sqrt{2\gamma_e} b_{i,in} \quad (4.19)$$

$$\frac{d}{dt} c_i = -\Gamma_r c_i - i\frac{\Omega_{cf}}{2} b_i + \sqrt{2\gamma_r} c_{i,in} \quad (4.20)$$

⁵The second equality follows from the unitarity of the Hamiltonian.

In this section we use complex decay rates $\Gamma_x \equiv \gamma_x + i\Delta_x$ where $x = c, e, r$ for simplicity. We now introduce the collective spinwaves $b_{\vec{k}} \equiv \frac{1}{\sqrt{N}} \sum_j e^{i\vec{k}r_j} b_j$, $c_{\vec{k}} \equiv \frac{1}{\sqrt{N}} \sum_j e^{i\vec{k}r_j} c_j$ defined in App. B which allow us to split the system of Eqs. (4.18-4.20) into a set of independent subsystems, *i.e.*

$$\frac{d}{dt}a = -\Gamma_c a - i\alpha - ig\sqrt{N}b_0 + \sqrt{2\gamma_c}a_{in} \quad (4.21)$$

$$\frac{d}{dt}b_0 = -\Gamma_e b_0 - i\frac{\Omega_{cf}}{2}c_i - ig\sqrt{N}a + \sqrt{2\gamma_e}b_{0,in} \quad (4.22)$$

$$\frac{d}{dt}c_0 = -\Gamma_r c_0 - i\frac{\Omega_{cf}}{2}b_0 + \sqrt{2\gamma_r}c_{0,in} \quad (4.23)$$

and, for $\vec{k} \neq 0$

$$\frac{d}{dt}b_{\vec{k}} = -\Gamma_e b_{\vec{k}} - i\frac{\Omega_{cf}}{2}c_{\vec{k}} + \sqrt{2\gamma_e}b_{\vec{k},in} \quad (4.24)$$

$$\frac{d}{dt}c_{\vec{k}} = -\Gamma_r c_{\vec{k}} - i\frac{\Omega_{cf}}{2}b_{\vec{k}} + \sqrt{2\gamma_r}c_{\vec{k},in} \quad (4.25)$$

We define the matrix⁶

$$\hat{G}^T [t, t'] \equiv -i \langle \mathcal{T} \left(\vec{X}(t) \times \vec{X}^\dagger(t') \right) \rangle \quad (4.26)$$

where

$$\vec{X}(t) \equiv \begin{pmatrix} a(t) \\ b_0(t) \\ c_0(t) \\ \left\{ b_{\vec{k}}(t) \right\}_{\vec{k} \neq 0} \\ \left\{ c_{\vec{k}}(t) \right\}_{\vec{k} \neq 0} \end{pmatrix}$$

and $\vec{X}^\dagger(t)$ is the transconjugated vector $\left(a^\dagger(t), b_0^\dagger(t), c_0^\dagger(t), \left\{ b_{\vec{k}}^\dagger(t), c_{\vec{k}}^\dagger(t) \right\} \right)$, that is more explicitly,

$$\hat{G}^T [t, t'] \equiv -i \begin{pmatrix} \langle \mathcal{T} \{ a(t) a^\dagger(t') \} \rangle & \langle \mathcal{T} \{ a(t) b_0^\dagger(t') \} \rangle & \langle \mathcal{T} \{ a(t) c_0^\dagger(t') \} \rangle & \langle \mathcal{T} \{ a(t) b_{\vec{k}}^\dagger(t') \} \rangle & \langle \mathcal{T} \{ a(t) c_{\vec{k}}^\dagger(t') \} \rangle \\ \langle \mathcal{T} \{ b_0(t) a^\dagger(t') \} \rangle & \langle \mathcal{T} \{ b_0(t) b_0^\dagger(t') \} \rangle & \langle \mathcal{T} \{ b_0(t) c_0^\dagger(t') \} \rangle & \langle \mathcal{T} \{ b_0(t) b_{\vec{k}}^\dagger(t') \} \rangle & \langle \mathcal{T} \{ b_0(t) c_{\vec{k}}^\dagger(t') \} \rangle \\ \langle \mathcal{T} \{ c_0(t) a^\dagger(t') \} \rangle & \langle \mathcal{T} \{ c_0(t) b_0^\dagger(t') \} \rangle & \langle \mathcal{T} \{ c_0(t) c_0^\dagger(t') \} \rangle & \langle \mathcal{T} \{ c_0(t) b_{\vec{k}}^\dagger(t') \} \rangle & \langle \mathcal{T} \{ c_0(t) c_{\vec{k}}^\dagger(t') \} \rangle \\ \langle \mathcal{T} \{ b_{\vec{k}}(t) a^\dagger(t') \} \rangle & \langle \mathcal{T} \{ b_{\vec{k}}(t) b_0^\dagger(t') \} \rangle & \langle \mathcal{T} \{ b_{\vec{k}}(t) c_0^\dagger(t') \} \rangle & \langle \mathcal{T} \{ b_{\vec{k}}(t) b_{\vec{k}}^\dagger(t') \} \rangle & \langle \mathcal{T} \{ b_{\vec{k}}(t) c_{\vec{k}}^\dagger(t') \} \rangle \\ \langle \mathcal{T} \{ c_{\vec{k}}(t) a^\dagger(t') \} \rangle & \langle \mathcal{T} \{ c_{\vec{k}}(t) b_0^\dagger(t') \} \rangle & \langle \mathcal{T} \{ c_{\vec{k}}(t) c_0^\dagger(t') \} \rangle & \langle \mathcal{T} \{ c_{\vec{k}}(t) b_{\vec{k}}^\dagger(t') \} \rangle & \langle \mathcal{T} \{ c_{\vec{k}}(t) c_{\vec{k}}^\dagger(t') \} \rangle \end{pmatrix}$$

⁶Note that the time-ordering applies only to operators but not to vectors

4. Schwinger-Keldysh contour formalism.

From Eqs. (4.21-4.23,4.24,4.25) we deduce the matrix equation (Rammer, 2007)

$$\partial_t \hat{G}^T [t, t'] = \hat{M} \times \hat{G} [t, t'] - i\delta(t - t') \mathbb{I} \quad (4.27)$$

where \hat{M} has the following block-diagonal structure in the basis $(a, b_0, c_0, \{b_k, c_k\})$:

$$\hat{M} = \begin{bmatrix} \hat{M}_0 & 0 \\ 0 & \{\hat{M}_{\vec{k}}\}_{\vec{k} \neq 0} \end{bmatrix} \quad (4.28)$$

where

$$\hat{M}_0 = \begin{pmatrix} -\Gamma_c & -ig\sqrt{N} & 0 \\ -ig\sqrt{N} & -\Gamma_e & -i\frac{\Omega_{cf}}{2} \\ 0 & -i\frac{\Omega_{cf}}{2} & -\Gamma_r \end{pmatrix} \quad (4.29)$$

$$\hat{M}_{\vec{k}} = \begin{pmatrix} -\Gamma_e & -i\frac{\Omega_{cf}}{2} \\ -i\frac{\Omega_{cf}}{2} & -\Gamma_r \end{pmatrix} \quad (4.30)$$

Switching to the temporal Fourier space ($\hat{G}^T [\omega] \equiv -i \int d\omega e^{i\omega t} \langle \mathcal{T} (\vec{X}^\dagger(t) \times \vec{X}(0)) \rangle$) we get:

$$-i\omega \hat{G}^T [\omega] = \hat{M} \cdot \hat{G}^T [\omega] - i\mathbb{I}$$

or equivalently:

$$\hat{G}^T [\omega] = (\omega - i\hat{M})^{-1}$$

Finally, using the expression of \hat{M} (4.28) we get a block-diagonal form for $\hat{G}^T [\omega]$

$$\hat{G}^T [\omega] = \begin{bmatrix} \hat{G}_0^T [\omega] & 0 \\ 0 & \{\hat{G}_{\vec{k}}^T [\omega]\} \end{bmatrix}$$

where

$$\hat{G}_0^T [\omega] = \begin{pmatrix} \omega + i\Gamma_c & -g\sqrt{N} & 0 \\ -g\sqrt{N} & \omega + i\Gamma_e & -\frac{\Omega_{cf}}{2} \\ 0 & -\frac{\Omega_{cf}}{2} & \omega + i\Gamma_r \end{pmatrix}^{-1} \quad (4.31)$$

$$\hat{G}_{\vec{k}}^T [\omega] = \begin{pmatrix} \omega + i\Gamma_e & -\frac{\Omega_{cf}}{2} \\ -\frac{\Omega_{cf}}{2} & \omega + i\Gamma_r \end{pmatrix}^{-1} \quad (4.32)$$

The explicit calculation of $\hat{G}_0^T [\omega]$ and $\hat{G}_{\vec{k}}^T [\omega]$ can be readily performed, for example, using Mathematica. The exact expression of the full \hat{G}^T does not present much interest

here: we will provide specific matrix elements where needed.

Recalling the properties of the Green's functions $\hat{G}^T, \hat{G}^>$ specified in the introduction to this subsection we may straightforwardly deduce that they exhibit the same block-diagonal structure as \hat{G}^T .

In the following sections we present the calculation of correlation functions using the formalism presented above. For all physical quantities of interest, we will perform the expansion and full resummation of Eq. (4.17) with respect to H_{dd} , for the first few orders (up to the fourth order) in the feeding rate α : therefore, unless specified, the term ‘‘order’’ will refer to the order in power of α . In Sec. 4.3 we derive the first order averages for cavity and atomic variables. In Sec. 4.4 we demonstrate the factorization of the lowest order correlation functions. Using this property we re-derive the results of the Chap. 3 in Sec. 4.5, but, here, in an analytic form. In Sec. 4.6 we go beyond the lowest order and derive the analytic expression of the transmission spectrum of the cavity, distinguishing its elastic and inelastic parts. We give a physical explanation to the inelastic part using a simple polaritonic picture.

4.3 First order quantities

In this section we derive results for the first order cavity mode average $\langle a \rangle^{(1)}$. Applying the general expression Eq. (4.17) to $\langle a(t) \rangle^{(1)}$ we get:

$$\langle a(t) \rangle^{(1)} = \left(-i\sqrt{2\pi\alpha} \right) \left\langle \mathcal{T}_{\mathcal{C}} \left\{ e^{-i(\int_{\mathcal{C}} H_{dd})} A_q^\dagger a_+(t) \right\} \right\rangle \quad (4.33)$$

Being of the first order with respect to the feeding rate α , this correlation function could be derived from, e.g., the Heisenberg-Langevin equations presented in Chap. 3. In order to introduce the formalism we, however, prefer to provide a detailed derivation.

By separating the forward and backward parts of the contour $\int_{\mathcal{C}} H_{dd} = \int_{\mathcal{C}_+} H_{dd} + \int_{\mathcal{C}_-} H_{dd}$ and expanding with respect to each of them separately we get from (4.33):

$$\langle a(t) \rangle^{(1)} = \left(-i\sqrt{2\pi\alpha} \right) \sum_{p,q} \left\langle \mathcal{T}_{\mathcal{C}} \left\{ \frac{\left(-i \int_{\mathcal{C}_+} H_{dd} \right)^p}{p!} \frac{\left(-i \int_{\mathcal{C}_-} H_{dd} \right)^q}{q!} A_q^\dagger a_+(t) \right\} \right\rangle \quad (4.34)$$

We first consider the term $\left(-i \int_{\mathcal{C}_-} H_{dd} \right)^q$ in Eq. (4.34), which, according to the definition of H_{dd} , contains $2q$ creation operators and $2q$ annihilation operators belonging to the backward part of the contour \mathcal{C} .

According to Wick's theorem we shall now consider all possible pairings of these annihilation/creation operators to get the generic term of the expansion. We will first provide two important rules that we shall use extensively in the remainder of the chapter. We start by making the simple but very important remark: since H_0 conserves the

4. Schwinger-Keldysh contour formalism.

number of excitations and the state we average on is the vacuum ρ_0 , then the average of a normal ordered product of annihilation e_k and a creation operator e_l^\dagger vanishes, *i.e.* $\langle e_l^\dagger(z_l) e_k(z_k) \rangle = 0$; as a consequence:

R1 the contraction $\langle \mathcal{T}_C \{ e_k(z_k) e_l^\dagger(z_l) \} \rangle$ vanishes unless $z_k > z_l$ on the contour \mathcal{C} .

Another consequence of the excitation number conservation by H_0 and ρ_0 being in the vacuum state, is that for any $k \geq 1$

$$\left\langle \mathcal{T}_C \left\{ \left(-i \int_{\mathcal{C}_\pm} H_{dd}(s) ds \right)^k \right\} \right\rangle = 0$$

which implies:

R2

$$\left\langle \mathcal{T}_C \left\{ \exp \left(-i \int_{\mathcal{C}_\pm} H_{dd}(s) ds \right) \right\} \right\rangle = 1$$

Applying the rule R1 we deduce that all creation and annihilation operators in $\left(-i \int_{\mathcal{C}_-} H_{dd} \right)^q$ should be contracted with each other. According to rule R2 a contraction arrangement in which the $(2q)$ operators of $\left(-i \int_{\mathcal{C}_-} H_{dd} \right)^q$ are paired with each other, and therefore disconnected from the remaining terms $\left(-i \int_{\mathcal{C}_+} H_{dd} \right)^p A_q^\dagger a_+(t)$, will give a vanishing contribution to the overall average, unless $q = 0$. This simple but fundamental remark will be used further; let us notice that it allows one to discard the terms in the perturbation series corresponding to the so-called disconnected diagrams (Abrikosov et al., 1975). The same kind of argument holds for $\left(-i \int_{\mathcal{C}_+} H_{dd} \right)^p$ and we, therefore, may discard all terms except for $q, p = 0$:

$$\langle a(t) \rangle^{(1)} = \left(-i\sqrt{2\pi\alpha} \right) \langle \mathcal{T}_C \{ A_q^\dagger a_+(t) \} \rangle$$

which further simplifies recalling that $A_q^\dagger \equiv \frac{1}{\sqrt{2\pi}} \int ds \left(a_+^\dagger - a_-^\dagger \right)$:

$$\langle a(t) \rangle^{(1)} = (-i\alpha) \left\langle \mathcal{T}_C \left\{ \int ds \left(a_+^\dagger - a_-^\dagger \right) a_+(t) \right\} \right\rangle \quad (4.35)$$

Let us now consider the Fourier transform of the Eq. (4.35):

$$\begin{aligned}
 \frac{1}{\sqrt{2\pi}} \int e^{i\omega t} dt \langle a(t) \rangle^{(1)} &= \frac{(-i\alpha)}{\sqrt{2\pi}} \int e^{i\omega t} \left\langle \mathcal{T}_C \left\{ \int ds a_+^\dagger(s) a_+(t) \right\} \right\rangle \\
 &= \frac{(-i\alpha)}{\sqrt{2\pi}} \int e^{i\omega t} \int ds iG_{aa}^T[t, s] \\
 &= \frac{(-i\alpha)}{\sqrt{2\pi}} \int e^{i\omega t} \int ds iG_{aa}^T[t-s] \\
 &= \left(-i\alpha\sqrt{2\pi} \right) iG_{aa}[\omega] \delta(\omega)
 \end{aligned}$$

The term $\left\langle \mathcal{T}_C \left\{ \int ds a_+^\dagger(s) a_+(t) \right\} \right\rangle$ vanished due to the rule R1. The delta function in this expression results from the system being in the steady state (we assume that the evolution starts at $t_0 = -\infty$). Using the expression Eq. (4.31) we deduce:

$$\begin{aligned}
 \langle a(t) \rangle^{(1)} &= (-i\alpha) iG_{aa}[0] \\
 &= \frac{(-i\alpha)}{\Gamma_c + \frac{g^2 N}{\left(\Gamma_e + \frac{\Omega_{cf}^2}{4\Gamma_r} \right)}}
 \end{aligned}$$

Here we recover the standard cavity-EIT response formula.

We may derive other averages in the same way:

$$\begin{aligned}
 \langle b_0(\omega) \rangle^{(1)} &= \left(-i\alpha\sqrt{2\pi} \right) iG_{b_0a}[0] \delta(\omega) \\
 \langle c_0(\omega) \rangle^{(1)} &= \left(-i\alpha\sqrt{2\pi} \right) iG_{c_0a}[0] \delta(\omega)
 \end{aligned}$$

4.4 Factorization of averages in the lowest order

In this subsection we consider the expression for correlation function in the general contour-ordered form Eq. (4.17). Restricting ourselves to the lowest non-vanishing order in α , that is $n = r + s^7$, where r , and s are the numbers of creation and annihilation operators, respectively, we get:

⁷The results from employing the equality between the number of creation and annihilation operators in Eq. (4.17)

4. Schwinger-Keldysh contour formalism.

$$\begin{aligned}
& \left\langle \tilde{\mathcal{T}} \left\{ \prod_{i=1}^r \mathcal{O}_i^\dagger(t_i) \right\} \mathcal{T} \left\{ \prod_{j=r+1}^{r+s} \mathcal{O}_j(t_j) \right\} \right\rangle \\
&= \frac{(-i\sqrt{2\pi}\alpha)^{r+s}}{r!s!} \left\langle \mathcal{T}_{\mathcal{C}} \left\{ e^{-i\int_{\mathcal{C}}(H_{dd})} (A_q)^r (A_q^\dagger)^s \prod_{i=1}^r \mathcal{O}_{-,i}^\dagger(t_i) \prod_{j=r+1}^{r+s} \mathcal{O}_{+,j}(t_j) \right\} \right\rangle
\end{aligned} \tag{4.36}$$

Let us now expand the expression Eq. (4.36) in powers of $\int_{\mathcal{C}_+}(H_{dd})$ and $\int_{\mathcal{C}_-}(H_{dd})$ analogously to the previous subsection:

$$\frac{(-i\sqrt{2\pi}\alpha)^{r+s}}{r!s!} \sum_{p,q} \frac{(-i)^{p+q}}{p!q!} \left\langle \mathcal{T}_{\mathcal{C}} \left\{ \left\{ \int_{\mathcal{C}_+}(H_{dd}) \right\}^p \left\{ \int_{\mathcal{C}_-}(H_{dd}) \right\}^q A_q^r A_q^{\dagger s} \dots \times \prod_{i=1}^r \mathcal{O}_{-,i}^\dagger(t_i) \prod_{j=r+1}^{r+s} \mathcal{O}_{+,j}(t_j) \right\} \right\rangle \tag{4.37}$$

Recalling the expression for the Hamiltonian of the dipole-dipole interactions $H_{dd} = \frac{1}{2} \sum_{m,n} \kappa_{mn} c_n^\dagger c_m^\dagger c_n c_m$, we deduce that each term of the sum in (4.37) contains $(2p+s)$ annihilation operators that belong to the forward part (\mathcal{C}_+) of the contour. From the rule R1 given in the previous subsection, they can only be contracted with the s operators A_q^\dagger and $2p$ creation operators within $\left\{ -i \int_{\mathcal{C}_+}(H_{dd}) \right\}^p$. The same remark applies to the $(2q+r)$ annihilation operators belonging to the \mathcal{C}_- branch of the contour: they can only be contracted with the r operators A_q and the $2q$ annihilation operators in $\left\{ -i \int_{\mathcal{C}_-}(H_{dd}) \right\}^q$. Therefore, in Eq. (4.37) the two sums over p and q factorize, or, more explicitly:

$$\begin{aligned}
& \frac{(-i\sqrt{2\pi}\alpha)^{r+s}}{r!s!} \sum_{p,q} \frac{(-i)^{p+q}}{p!q!} \left\langle \mathcal{T}_{\mathcal{C}} \left\{ \left\{ \int_{\mathcal{C}_+}(H_{dd}) \right\}^p \left\{ \int_{\mathcal{C}_-}(H_{dd}) \right\}^q A_q^r A_q^{\dagger s} \dots \times \prod_{i=1}^r \mathcal{O}_{-,i}^\dagger(t_i) \prod_{j=r+1}^{r+s} \mathcal{O}_{+,j}(t_j) \right\} \right\rangle \\
&= \frac{(-i\sqrt{2\pi}\alpha)^r}{r!} \sum_q \frac{(-i)^q}{q!} \left\langle \mathcal{T}_{\mathcal{C}} \left\{ \left(\int_{\mathcal{C}_-} H_{dd} \right)^q A_q^r \prod_{i=1}^r \mathcal{O}_{-,i}^\dagger(t_i) \right\} \right\rangle \\
&\times \frac{(-i\sqrt{2\pi}\alpha)^s}{s!} \sum_p \frac{(-i)^p}{p!} \left\langle \mathcal{T}_{\mathcal{C}} \left\{ \left(\int_{\mathcal{C}_+} H_{dd} \right)^p A_q^{\dagger s} \prod_{j=r+1}^{r+s} \mathcal{O}_{+,j}(t_j) \right\} \right\rangle \\
&= \left\langle \tilde{\mathcal{T}} \left\{ \prod \mathcal{O}_{+,j}(t_j) \right\} \right\rangle^{(s)} \left\langle \mathcal{T} \left\{ \prod \mathcal{O}_{+,j}(t_j) \right\} \right\rangle^{(r)}
\end{aligned}$$

where the superscript as usual denotes the order in expansion in α . Here we therefore recover the factorization property of averages discussed in Chap. 3, though in an alternative way. It is important to stress that this property does not apply to averages beyond the lowest non-vanishing order (leading to some interesting physical effects, as will be shown in the Subsec. 4.6.2).

4.5 Intensity correlation function

In this subsection we partially re-derive the results obtained in Chap 3 on the $g^{(2)}$ function. It allows us to introduce various tools that we will use to compute quantities beyond the lowest order approximation.

4.5.1 $g^{(2)}$ function

Using the results of the previous subsections we may write for the intensity correlation function at the lowest non-vanishing order:

$$\begin{aligned} g^{(2)}(\tau) &= \frac{\langle \tilde{\mathcal{T}} \{a^\dagger(0) a^\dagger(\tau)\} \mathcal{T} \{a(\tau) a(0)\} \rangle^{(4)}}{\left(\langle a^\dagger(0) a(0) \rangle^{(2)} \right)^2} \\ &= \frac{\left| \langle \mathcal{T} \{a(\tau) a(0)\} \rangle^{(2)} \right|^2}{\left| \langle a \rangle_{ss}^{(1)} \right|^4} \end{aligned}$$

The denominator of this expression was already computed in Sec. 4.3, therefore, in this section we shall focus on $\langle \mathcal{T} (a(t) a(t')) \rangle^{(2)}$. We use (4.36) with $r = 0$ and $s = 2$ and get:

$$\langle \mathcal{T} \{a(t) a(t')\} \rangle^{(2)} = \frac{(-i\sqrt{2\pi}\alpha)^2}{2!} \left\langle \mathcal{T}_{\mathcal{C}} \left\{ e^{-i(\int_{\mathcal{C}_+} H_{dd})} (A_q^\dagger)^2 a_+(t) a_+(t') \right\} \right\rangle \quad (4.38)$$

Note that here we omitted the $e^{-i(\int_{\mathcal{C}_-} H_{dd})}$ factor under the contour ordering as only its 0th order in expansion contributes to the average (see Sec. 4.3). We also notice that Eq. (4.38) contains only “+” operators and therefore its Wick’s expansion comprises only time-ordered Green’s functions. We therefore keep only the \mathcal{C}_+ part of the contour (for shortness we will omit “+” indices in this section):

$$\langle \mathcal{T} (a(t) a(t')) \rangle^{(2)} = \frac{(-i\alpha)^2}{2!} \left\langle \mathcal{T} \left\{ e^{-i\frac{1}{2} \sum_{m,n} \kappa_{mn} \int ds c_n^\dagger c_m^\dagger c_n c_m} \left(\int ds a^\dagger(s) \right)^2 a(t) a(t') \right\} \right\rangle \quad (4.39)$$

In order to evaluate this expression we now perform the perturbative expansion with respect to H_{dd} . It appears to be more convenient to express the Hamiltonian in the spinwave picture derived in App. B.2:

$$H_{dd} = \frac{1}{2} \sum_{\vec{q}, \vec{k}_1, \vec{k}_2} U_{\vec{q}} c_{\vec{k}_2 - \vec{q}}^\dagger c_{\vec{q} + \vec{k}_1}^\dagger c_{\vec{k}_1} c_{\vec{k}_2}$$

4. Schwinger-Keldysh contour formalism.

A. Zeroth order The zeroth order in expansion of Eq. (4.39) in H_{dd} yields:

$$\begin{aligned}
\langle \mathcal{T} (a(t) a(t')) \rangle^{(2,0)} &= \frac{(-i\alpha)^2}{2!} \left\langle \mathcal{T} \left\{ \left(\int ds a^\dagger(s) \right)^2 a(t) a(t') \right\} \right\rangle \\
&= (-i\alpha)^2 \left(\int ds_1 iG_{aa}[t-s_1] \int ds_2 iG_{aa}[t'-s_2] \right) \\
&= (-i\alpha)^2 iG_{aa}[\omega=0] iG_{aa}[\omega=0] \\
&\equiv \langle a(t) \rangle^{(1)} \langle a(t') \rangle^{(1)}
\end{aligned}$$

where the superscript (p,q) denotes the p -th order in expansion in α and q -th in H_{dd} (we also recall here the definition of $\langle a(t) \rangle^{(1)} \equiv (-i\alpha) iG_{aa}[0]$). The factorization of $\langle \mathcal{T} (a(t) a(t')) \rangle^{(2,0)}$ constitutes an obvious consequence of the fact that at zeroth order in H_{dd} the system is completely linear.

B. First order Let us now consider the first order in expansion in dipole-dipole interactions:

$$\begin{aligned}
&\langle \mathcal{T} \{a(t) a(t')\} \rangle^{(2,1)} \tag{4.40} \\
&= \sum_{\vec{q}, \vec{k}_1, \vec{k}_2} \frac{-iU_{\vec{q}} (-i\alpha)^2}{2} \left\langle \mathcal{T} \left\{ \int ds c_{\vec{k}_2 - \vec{q}}^\dagger c_{\vec{q} + \vec{k}_1}^\dagger c_{\vec{k}_1} c_{\vec{k}_2} \left(\int ds' a^\dagger(s') \right)^2 a(t) a(t') \right\} \right\rangle
\end{aligned}$$

According to Wick's theorem, we now have to review all possible ways to pair creation and annihilation operators in (4.40). Let us first make a few remarks which allow us to discard vanishing contractions.

As shown in Subsection 4.2.2, the matrix representation $\hat{G}^T[\omega]$ of the time-ordered Green's function show a block-diagonal structure in the basis $\{a_0, b_0, c_0, \{b_{\vec{k} \neq 0}, c_{\vec{k} \neq 0}\}\}$ which implies that the Green's functions $G_{xy}^T(t-t') = -i \langle \mathcal{T} \{x(t) y^\dagger(t')\} \rangle$ vanishes unless x and y simultaneously belong to the same set, either $\{a_0, b_0, c_0\}$ or $\{b_{\vec{k} \neq 0}, c_{\vec{k} \neq 0}\}$. Therefore:

R3 Only contractions of operators all picked either in the set $\{a, b_0, c_0\}$ or in the set $\{b_{\vec{k} \neq 0}, c_{\vec{k} \neq 0}\}$ give non-vanishing contractions.

Moreover we recall our convention for same-time expectation values, evaluated on the \mathcal{C}_\pm branches (see Sec. 4.1): the time argument of the creation operators are assumed to be infinitesimally shifted by 0^\pm , such that the chronological coincides with normal ordering. Therefore:

R4 Same-time contractions vanish, in particular, $\left\langle \mathcal{T}_{\mathcal{C}_{\pm}} \left\{ c_k(t) c_k^{\dagger}(t + 0^{\pm}) \right\} \right\rangle = 0$.

Taking these remarks into account we get:

$$\begin{aligned} & \langle \mathcal{T} \{a(t) a(t')\} \rangle^{(2,1)} \\ &= -i \times U_0 (-i\alpha)^2 \int ds_1 ds_2 ds_3 G_{ac_0}[t, s_1] G_{ac_0}[t', s_1] G_{c_0a}[s, s_2] G_{c_0a}[s, s_3] \end{aligned} \quad (4.41)$$

Fourier transforming of Eq. (4.41) with respect to both t and t' we get:

$$\begin{aligned} & \langle \mathcal{T} \{a(\omega_{out,1}) a(\omega_{out,2})\} \rangle^{(2,1)} \\ &= \frac{1}{2\pi} \int dt dt' e^{i\omega_{out,1}t} e^{i\omega_{out,2}t'} \langle \mathcal{T} \{a(t) a(t')\} \rangle^{(2,1)} \\ &= \left(-i\sqrt{2\pi}\alpha\right)^2 \left(-i \times \frac{U_0}{2\pi}\right) \delta(\omega_{out,1} + \omega_{out,2}) G_{ac_0}^T[\omega] G_{ac_0}^T[\omega'] \left(G_{c_0a}^T[0]\right)^2 \end{aligned} \quad (4.42)$$

Note that the operator \mathcal{T} appearing in $\langle \mathcal{T} \{a(\omega_{out,1}) a(\omega_{out,2})\} \rangle^{(2,1)}$ does not refer to any hypothetical ordering in the frequency space; it is a mere notation meant to remind that this quantity was obtained by Fourier transforming the average of a time-ordered product in real time space.

C. Second order Consider now the second order in expansion in H_{dd} :

$$\begin{aligned} & \langle \mathcal{T} \{a(t) a(t')\} \rangle^{(2,2)} \\ &= \left(-i\sqrt{2\pi}\alpha\right)^2 \sum_{\vec{q}, \vec{k}_1, \vec{k}_2, \vec{k}'_1, \vec{k}'_2, \vec{q}'} \left(\frac{-iU_{-\vec{q}}}{2\pi}\right) \left(\frac{-iU_{\vec{q}'}}{2\pi}\right) \\ &\times \left\langle \mathcal{T} \left\{ a(t) a(t') \int ds_1 c_{\vec{k}_2 - \vec{q}}^{\dagger}(s) c_{\vec{q} + \vec{k}_1}^{\dagger}(s) c_{\vec{k}_1}(s) c_{\vec{k}_2}(s) \right. \right. \\ &\quad \left. \left. \times \int ds_2 c_{\vec{k}'_2 - \vec{q}'}^{\dagger}(s_2) c_{\vec{q}' + \vec{k}'_1}^{\dagger}(s_2) c_{\vec{k}'_1}(s_2) c_{\vec{k}'_2}(s_2) \left(\frac{1}{\sqrt{2\pi}} \int ds a^{\dagger}(s)\right)^2 \right\} \right\rangle \end{aligned}$$

Using the same remarks as made above for the first order and recalling that, according to the rule R2, the contribution of “disconnected diagrams” (*i.e.* the contraction arrangement in which the $(4p)$ atomic operators of $\left(-i \int_{\mathcal{C}_+} H_{dd}\right)^p$ are paired with each other and therefore are disconnected from the other terms) vanishes, we get in the temporal Fourier space:

4. Schwinger-Keldysh contour formalism.

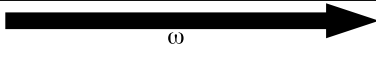
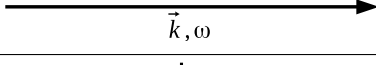
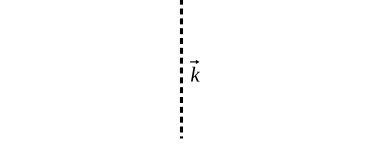
Green's function	Diagrammatic representation
$G_{ac_0}[\omega], G_{c_0a}[\omega]$	
$G_{c_{\vec{k}}c_{\vec{k}}}[\omega]$	
$U_{\vec{k}}$	

Table 4.1: Diagrammatic representation of Green's functions and interacting potential.

$$\begin{aligned}
& \langle \mathcal{T} \{ a(\omega_{out,1}) a(\omega_{out,2}) \} \rangle^{(2,2)} \\
&= \left(-i\sqrt{2\pi}\alpha \right)^2 \delta(\omega_{out,1} + \omega_{out,2}) G_{ac_0}^T[\omega_{out,1}] G_{ac_0}^T[\omega_{out,2}] \times \\
&\times \sum_{\vec{q}} \left(\frac{-iU_{-\vec{q}}}{2\pi} \right) \left(\frac{iU_{\vec{q}}}{2\pi} \right) \left(\int d\omega G_{c_{\vec{q}},c_{\vec{q}}}^T[\omega] G_{c_{-\vec{q}},c_{-\vec{q}}}^T[-\omega] \right) \\
&\times \left(G_{c_0a}^T[0] \right)^2 \tag{4.43}
\end{aligned}$$

D. Feynman diagrams The expansion can be performed further. Higher-order terms in H_{dd} reveal a self-similar form and lend themselves to a diagrammatic representation. Table 4.1 summarizes the equivalence rules we use to build diagrams in Fourier space: Green's functions of different kinds are represented by different arrows, while the interaction potential is represented by a vertical dashed line; it is moreover implicit that, for each loop in a diagram, integration (summation) should be performed over internal variables (indices) and that the overall expression obtained should be multiplied by the factor $(-i\sqrt{2\pi}\alpha)^2 \delta(\omega_{out,1} + \omega_{out,2}) \left(\frac{-i}{2\pi}\right)^p$ where p is the order in H_{dd} , *i.e.* the number of dashed vertical lines. Note that we do not distinguish $G_{ac_0}[\omega]$ and $G_{c_0a}[\omega]$ graphically since their expressions coincide (see Eq. (4.31)).

It is easy to see that diagrams (a), (b), (c) in Fig. 4.2, which represent $\langle \mathcal{T} \{ a(\omega_{out,1}) a(\omega_{out,2}) \} \rangle^{(2,p)}$ for $p = 1, 2, 3$, have four thick lines in common. These thick lines represent the conversion of a photon from the cavity mode to the symmetric Rydberg polariton and back. As there is no integration over the arguments of the corresponding Green's function we can factorize them (Fig. 4.2 (d)). The remaining part of the correlation function is denoted by T_0 ; its perturbative expansion is diagrammatically represented in Fig. 4.2 (e).

We now write the expression that corresponds to the diagram (d) in Fig 4.2:

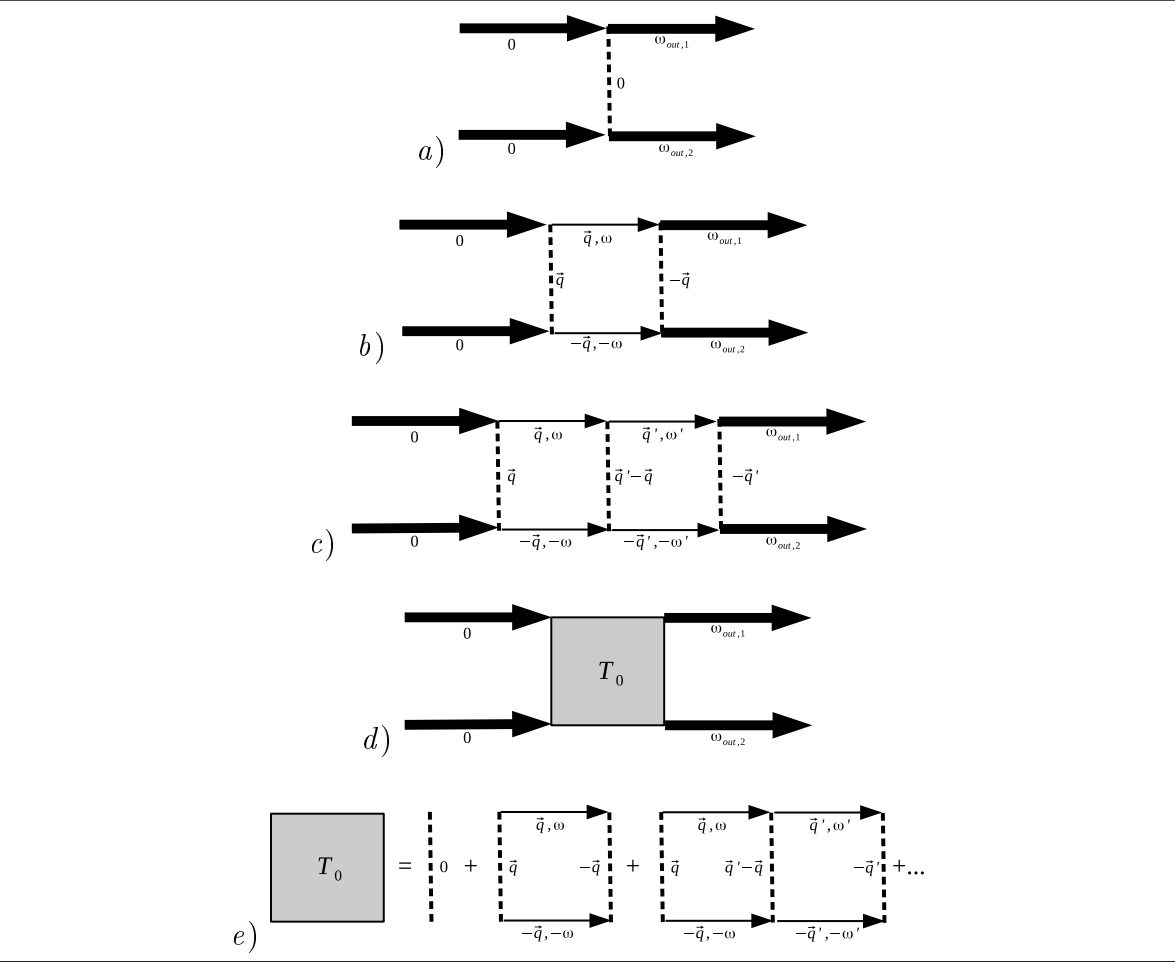


Figure 4.2: Feynman diagrams corresponding to *a)* first order, *b)* second order, *c)* third order contributions in H_{dd} . *d)* Schematic representation of the sum of all orders starting with the first. *e)* diagrammatic representation of the perturbative expansion of T_0 .

4. Schwinger-Keldysh contour formalism.

$$\begin{aligned} & \sum_p \langle \mathcal{T} \{ a(\omega_{out,1}) a(\omega_{out,2}) \} \rangle^{(2,p)} \\ &= \left(-i\sqrt{2\pi}\alpha \right)^2 \delta(\omega_{out,1} + \omega_{out,2}) G_{ac_0}^T[\omega_{out,1}] G_{ac_0}^T[\omega_{out,2}] \frac{(-iT_0)}{2\pi} \left(G_{c_0a}^T[0] \right)^2 \end{aligned} \quad (4.44)$$

where T_0 is (by direct translation of Fig. 4.2 (e))

$$T_0 = U_0 + i \sum_{\vec{q}} U_{-\vec{q}} S_{\vec{q}} U_{\vec{q}} + i^2 \sum_{\vec{q}} U_{-\vec{q}} S_{\vec{q}} \sum_{\vec{q}'} U_{\vec{q}-\vec{q}'} S_{\vec{q}'} U_{\vec{q}'} + \dots \quad (4.45)$$

and $S_{\vec{q}} \equiv \frac{1}{2\pi} \int d\omega G_{c_{\vec{q}}, c_{-\vec{q}}}^T[\omega] G_{c_{-\vec{q}}, c_{\vec{q}}}^T[-\omega]$.

We may now give a simple interpretation to the overall formula Eq. (4.44) by inspecting its different terms. The last term on the right side of Eq. (4.45), $\left(G_{c_0a}^T[0] \right)^2$, stands for the conversion of two incoming photons into symmetric Rydberg polaritons. Resulting from the resummation of diagrams of all perturbative orders in H_{dd} , the term $\frac{(-iT_0)}{2\pi}$ represents the action of the Rydberg dipole-dipole-interaction-induced non-linearity on the two symmetric polaritons, provided they return to the symmetric subspace. Finally the term $G_{ac_0}^T[\omega_{out,1}] G_{ac_0}^T[\omega_{out,2}]$ represents the conversion of two symmetric polaritons back to the cavity mode photons.

E. Analytic expression of $g^{(2)}(0)$ According to the results above, we finally get the following analytic expression for the second-order correlation function $g^{(2)}(0)$:

$$\begin{aligned} g^{(2)}(0) &= \frac{\langle a^\dagger(0) a^\dagger(0) a(0) a(0) \rangle^{(4)}}{\left(\langle a^\dagger(0) a(0) \rangle^{(2)} \right)^2} \\ &= \left| 1 + \frac{\frac{i\alpha^2}{2\pi} \int d\omega G_{ac_0}^T[\omega] G_{ac_0}^T[-\omega] T_0 \left(G_{c_0a}^T[0] \right)^2}{\left(\langle a(0) \rangle^{(1)} \right)^2} \right|^2 \end{aligned} \quad (4.46)$$

where

$$\begin{aligned} \langle a(t) \rangle^{(1)} &= (-i\alpha) iG_{aa}[0] \\ &= \frac{(-i\alpha)}{\Gamma_c + \frac{g^2 N}{\left(\Gamma_e + \frac{\Omega_{cf}^2}{4\Gamma_r} \right)}} \end{aligned}$$

The ‘‘simplicity’’ of Eq. (4.46) is misleading. The main difficulty is enclosed in the explicit determination of T_0 to which the next subsection is devoted.

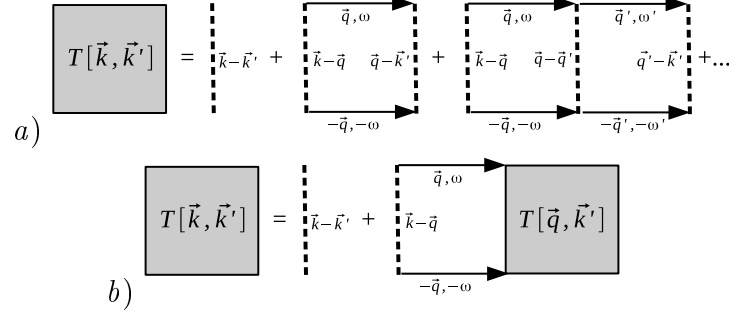


Figure 4.3: Diagrammatic representation of $T[\vec{k}, \vec{k}']$ in a) perturbative form, b) self-consistent form.

4.5.2 T matrix

As shown in the previous section, T_0 describes the combination of all possible interaction-induced scattering processes in which two incoming Rydberg polaritons are converted back to the same symmetric spinwaves. This quantity actually appears as a specific value of a more general function which describes the scattering of two arbitrary (*i.e.* not necessarily symmetric) Rydberg polaritons only constrained by the conservation of the sum of the wavevectors. To be more explicit we denote this latter function by $T[\vec{k}, \vec{k}', \vec{P}]$ where $\vec{k} = \frac{\vec{k}_{in,1} - \vec{k}_{in,2}}{2}$ and $\vec{k}' = \frac{\vec{k}_{out,1} - \vec{k}_{out,2}}{2}$ are the differences of the incoming/outgoing spinwave's wavevectors $\vec{k}_{(in/out),1}, \vec{k}_{(in/out),2}$ respectively, and $\vec{P} = \vec{k}_{in,1} + \vec{k}_{in,2}$ is their (necessarily conserved) sum. The symmetry of the coupling between the cavity mode and the atoms restricts the possible values of the wavevectors: we are therefore entitled to consider only the $\vec{P} = 0$ component, and denote $T[\vec{k}, \vec{k}', \vec{P} = 0] \equiv T[\vec{k}, \vec{k}']$.

The diagrammatic representation of $T[\vec{k}, \vec{k}']$ (given in Fig.4.3 a)) is similar to the one obtained for T_0 . From the diagrammatic structure it is easy to infer its self-consistent definition shown in Fig.4.3 b). The corresponding equation is readily obtained using the correspondence rules specified in the previous subsection:

$$T[\vec{k}, \vec{k}'] = U_{\vec{k}-\vec{k}'} + i \sum_{\vec{q}} U_{\vec{k}-\vec{q}} S_{\vec{q}} T[\vec{q}, \vec{k}'] \quad (4.47)$$

Let us recall the expression for $S_{\vec{q}} \equiv \frac{1}{2\pi} \int d\omega G_{c_{\vec{q}}, c_{\vec{q}}}^T[\omega] G_{c_{-\vec{q}}, c_{-\vec{q}}}^T[-\omega]$. As shown in Sec. 4.2.2, all Green's functions $G_{c_{\vec{q}}, c_{\vec{q}}}$ have the same expression for $\vec{q} \neq 0$; we therefore define $S_{\vec{q} \neq 0} \equiv S$. Using the latter remark we rewrite Eq. 4.47:

4. Schwinger-Keldysh contour formalism.

$$T \left[\vec{k}, \vec{k}' \right] = U_{\vec{k}-\vec{k}'} + i \sum_{\vec{q}} U_{\vec{k}-\vec{q}} S T \left[\vec{q}, \vec{k}' \right] + i U_{\vec{k}} (S_0 - S) T \left[0, \vec{k}' \right] \quad (4.48)$$

It is convenient to represent this equation in a matrix form. We therefore define matrices:

$$\widehat{T}_{\vec{k}, \vec{k}'} \equiv T \left[\vec{k}, \vec{k}' \right] \quad (4.49)$$

$$\widehat{U}_{\vec{k}, \vec{k}'} \equiv U_{\vec{k}-\vec{k}'} \quad (4.50)$$

$$\mathcal{P}_{\vec{k}, \vec{k}'}^{(0)} \equiv \delta \left(\vec{k} \right) \delta \left(\vec{k}' \right)$$

where $\mathcal{P}^{(0)}$ is the projector on the zeroth spinwave. With these definitions Eq. (4.48) takes the form:

$$\widehat{T} = \widehat{U} + i S \widehat{U} \cdot \widehat{T} + i (S_0 - S) \widehat{U} \cdot \mathcal{P}^{(0)} \cdot \widehat{T}$$

$$\widehat{T} = \left(1 - i S \widehat{U} \right)^{-1} \cdot \widehat{U} \cdot \left(\mathbb{I} + i (S_0 - S) \mathcal{P}^{(0)} \cdot \widehat{T} \right) \quad (4.51)$$

There is no obvious straightforward way to extract \widehat{T} from Eq. (4.51) in the general case. We may however relate \widehat{T} to its value in the *hypothetical* configuration when the atoms decouple from the cavity, *i.e.* when atom-cavity coupling coefficient vanishes *i.e.* $g = 0$.

4.5.3 Relation to the decoupled case

When $g = 0$, the atoms do not interact with the cavity field. From Eqs. (4.31,4.32) in the latter condition we infer that $G_{c_{\vec{q}}c_{\vec{q}}}^T[\omega] = G_{c_0c_0}^T[\omega]$ whence $S = S_0$. In this specific configuration, the matrix \widehat{T} , that we shall denote $\widehat{\overset{\circ}{T}}$, to distinguish it from the general case, obeys:

$$\widehat{\overset{\circ}{T}} = \widehat{U} + i S \widehat{U} \cdot \widehat{\overset{\circ}{T}} \quad (4.52)$$

or equivalently:

$$\widehat{\overset{\circ}{T}} = \left(1 - i S \widehat{U} \right)^{-1} \cdot \widehat{U}$$

From Eq. (4.51) we get the relation between the T - matrices for the general and hypothetical cases:

$$\widehat{T} = \widehat{\overset{\circ}{T}} \cdot \left(\mathbb{I} + i (S_0 - S) \mathcal{P}^{(0)} \cdot \widehat{\overset{\circ}{T}} \right) \quad (4.53)$$

Let us multiply both sides of Eq. (4.53) by $\mathcal{P}^{(0)}$ from the left:

$$\mathcal{P}^{(0)} \cdot \hat{T} = \mathcal{P}^{(0)} \cdot \hat{T} + i(S_0 - S) \mathcal{P}^{(0)} \cdot \hat{T}_0 \cdot \mathcal{P}^{(0)} \cdot \hat{T}$$

Solving this equation with respect to $\mathcal{P}^{(0)} \cdot \hat{T}$ and defining $\mathcal{P}^{(0)} \cdot \hat{T} \cdot \mathcal{P}^{(0)} \equiv \hat{T}_0 \mathcal{P}^{(0)}$ we get:

$$\mathcal{P}^{(0)} \cdot \hat{T} = \frac{\mathcal{P}^{(0)} \cdot \hat{T}}{1 - i(S_0 - S) \hat{T}_0}$$

Substituting this expression in Eq. (4.53) we finally get the expression for the T matrix:

$$\hat{T} = \hat{T} + i(S_0 - S) \frac{\hat{T} \cdot \mathcal{P}^{(0)} \cdot \hat{T}}{1 - i(S_0 - S) \hat{T}_0} \quad (4.54)$$

Since we are interested in determining $T_0 = T[0, 0] = \text{Tr} \left\{ \mathcal{P}^{(0)} \cdot \hat{T} \cdot \mathcal{P}^{(0)} \right\}$ we multiply Eq. (4.54) by $\mathcal{P}^{(0)}$ on the left and right sides and get:

$$T_0 = \frac{\hat{T}_0}{1 - i\hat{T}_0(S_0 - S)} \quad (4.55)$$

The advantage of this relation is that \hat{T}_0 can be evaluated exactly. We start with Eq. (4.52) and recalling the definitions of matrices \hat{T} and \hat{U} Eqs. (4.49, 4.50) we have:

$$\hat{T} \left[\vec{k}, \vec{k}' \right] = U_{\vec{k}-\vec{k}'} + iS \sum_{\vec{q}} U_{\vec{k}-\vec{q}} \hat{T} \left[\vec{q}, \vec{k}' \right]$$

Let us now transform $T \left[\vec{k}, \vec{k}' \right]$ to the real space using $U_{\vec{K}} = \frac{1}{N} \sum_m^N \kappa(\vec{r}_m) e^{i\vec{K}\vec{r}_m}$ (see App. B.2) :

$$\begin{aligned} T[\vec{r}, \vec{r}'] &\equiv \frac{1}{N} \sum_{\vec{k}, \vec{k}'} e^{-i\vec{k}\vec{r}} e^{i\vec{k}'\vec{r}'} \hat{T} \left[\vec{k}, \vec{k}' \right] \\ &= \frac{1}{N} \sum_{\vec{k}, \vec{k}'} e^{-i\vec{k}\vec{r}} e^{i\vec{k}'\vec{r}'} U_{\vec{k}-\vec{k}'} \\ &+ iS \frac{1}{N} \sum_{\vec{k}, \vec{k}'} e^{-i\vec{k}\vec{r}} e^{i\vec{k}'\vec{r}'} \sum_{\vec{q}} U_{\vec{k}-\vec{q}} \hat{T} \left[\vec{q}, \vec{k}' \right] \\ &= \kappa(\vec{r}) \delta_{\vec{r}, \vec{r}'} + iS \kappa(\vec{r}) \hat{T}[\vec{r}, \vec{r}'] \end{aligned}$$

where \vec{r} and \vec{r}' denote the real space conjugate coordinates to \vec{k} and \vec{k}' , respectively, and $\kappa(R) = \frac{C_6}{R^6}$. Finally we get:

4. Schwinger-Keldysh contour formalism.

$$\mathring{T}[\vec{r}, \vec{r}'] = \frac{\kappa(r)}{1 - iS\kappa(\vec{r})} \delta_{\vec{r}, \vec{r}'}$$

Using this expression and transforming back to the spinwave space we get $\mathring{T}[0, 0] = \frac{1}{N} \sum_i \frac{\kappa(\vec{r}_i)}{1 - iS\kappa(\vec{r}_i)}$. We notice that we already encountered expressions of this kind in Chap. 3.

We may approximately turn \mathring{T}_0 into an integral assuming the size of the sample to be sufficiently big :

$$\begin{aligned} \mathring{T}_0 &\approx \frac{1}{V} \int_V d^3R \frac{\kappa(R)}{1 - iSV(R)} \\ &= \frac{1}{V} \int_V d^3R \frac{\frac{C_6}{R^6}}{1 - iS\frac{C_6}{R^6}} \\ &= \frac{4\pi}{V} \int_0^\infty dR \times R^2 \frac{\frac{C_6}{R^6}}{1 - iS\frac{C_6}{R^6}} \\ &= \frac{2\pi^2}{3V} C_6 \sqrt{\frac{i}{C_6 S}} \end{aligned}$$

Assume now that $C_6 < 0$ we have:

$$\mathring{T}_0 = -\frac{2\pi^2}{3V} \sqrt{\frac{-i|C_6|}{S}} \quad (4.56)$$

Now combining Eqs. (4.55,4.56) we finally have:

$$T_0 = \frac{-\frac{2\pi^2}{3V} \sqrt{\frac{-i|C_6|}{S}}}{1 + i(S_0 - S) \frac{2\pi^2}{3V} \sqrt{\frac{-i|C_6|}{S}}} \quad (4.57)$$

Substituting this expression into Eq. (4.44) we can get an expression for the non-linear part of the pair correlation function in Fourier space. We may also use it directly as it gives the main part of the spectrum of the transmitted light, or to recover results of the Chap. 3.

4.5.4 Numerical results

In this paragraph we provide the numerical results we obtained for the $g^{(2)}(0)$ function of the light transmitted through the cavity, using the method developed in the current chapter. We compare these results with those obtained in Chap. 3. We also define and compute the squeezing spectrum $\Xi[\omega, \theta]$ of the transmitted light.

Intensity correlation function In the previous subsection we obtained all the components required to derive the $g^{(2)}$ function.

We first recall that (Eq. 4.46):

$$\begin{aligned} \langle \mathcal{T} \{a(\omega) a(\omega')\} \rangle^{(2)} &= \langle a(\omega) \rangle^{(1)} \langle a(\omega') \rangle^{(1)} \\ &+ i\alpha^2 \delta(\omega + \omega') G_{ac_0}^T[\omega] G_{ac_0}^T[\omega'] T_0 (G_{c_0a}^T[0])^2 \end{aligned} \quad (4.58)$$

which, in the time domain, yields:

$$\begin{aligned} \langle \mathcal{T} \{a(t) a(t')\} \rangle^{(2)} &= \frac{1}{2\pi} \int d\omega d\omega' e^{-i\omega t} e^{-i\omega' t'} \langle \mathcal{T} \{a(\omega) a(\omega')\} \rangle^{(2)} \\ &= \left(\langle a(t) \rangle^{(1)} \right)^2 + \frac{i\alpha^2}{2\pi} \int d\omega e^{-i\omega(t-t')} G_{ac_0}^T[\omega] G_{ac_0}^T[-\omega] T_0 (G_{c_0a}^T[0])^2 \end{aligned}$$

For comparison with results obtained in Chap. 3 we set $t = t'$ and get

$$\langle \mathcal{T} \{a(t) a(t)\} \rangle^{(2)} \equiv \left(\langle a(t) \rangle^{(1)} \right)^2 + \frac{i\alpha^2}{2\pi} \int d\omega G_{ac_0}^T[\omega] G_{ac_0}^T[-\omega] T_0 (G_{c_0a}^T[0])^2$$

Integration is performed analytically in App. G, as well the explicit calculation of S and S_0 .

In Fig. 4.4 we provide plots of $g^{(2)}(0)$ function obtained through the perturbative method of Chap. 3 and in the contour approach described in the current chapter, both in the resonant (a) and detuned regimes (b). The agreement between the two methods is such that no difference can be discerned on the figures. As already noted in the previous chapter, the nonlinearity is weaker in the far detuned regime than on exact resonance.

Squeezing spectrum Optical non-linearities are known to lead to squeezing of light, such as, e.g., in the parametric oscillator model Hamiltonian (Walls and Milburn, 2007). Light squeezing is powerful means to perform measurements beyond the quantum limit. In the multimode case, squeezing can be quantitatively characterized by the squeezing spectrum, which can be physically measured via homodyne detection (Lvovsky, 2014).

The calculation presented in the current chapter also allows us to easily determine the squeezing spectrum of the transmitted light (at second order in feeding). According to (Walls and Milburn, 2007) the squeezing spectrum is given by

$$\zeta(\omega, \theta) = 1 + \int dt e^{-i\omega t} \langle : X_\theta^{out}(t), X_\theta^{out}(0) : \rangle \quad (4.59)$$

where the quadrature operator is defined by $X_\theta^{out}(t) \equiv a_{out}(t) e^{-i\theta} + a_{out}^\dagger(t) e^{i\theta}$, $\langle : \dots : \rangle$

4. Schwinger-Keldysh contour formalism.

denotes the normal ordering of operators and $\langle A, B \rangle \equiv \langle AB \rangle - \langle A \rangle \langle B \rangle$. We can therefore put (4.59) under the form

$$\begin{aligned}
& \zeta(\omega, \theta) \\
&= 1 + \int dt e^{-i\omega t} \left\langle : a_{out}(t) e^{-i\theta} + a_{out}^\dagger(t) e^{i\theta}, a_{out}(0) e^{-i\theta} + a_{out}^\dagger(0) e^{i\theta} : \right\rangle \\
&= 1 + 2\gamma_c^{(R)} \int dt e^{-i\omega t} \langle \mathcal{T} \{a(t), a(0)\} \rangle e^{-2i\theta} + 2\gamma_c^{(R)} \int dt e^{-i\omega t} \langle \tilde{\mathcal{T}} \{a^\dagger(t), a^\dagger(0)\} \rangle e^{2i\theta} \\
&+ 2\gamma_c^{(R)} \int dt e^{-i\omega t} \langle a^\dagger(0), a(t) \rangle + 2\gamma_c^{(R)} \int dt e^{-i\omega t} \langle a^\dagger(t), a(0) \rangle \tag{4.60}
\end{aligned}$$

where we used the input-output formalism to relate the transmitted and intracavity field operators ($a_{out} = \sqrt{2\gamma_c^{(R)}} a(t) - a_{in}(t)$). Restricting ourselves to the second order in feeding rate α , we may use the factorization property of averages, from which we deduce, for example, $\langle a^\dagger(0), a(t) \rangle^{(2)} \equiv \langle a^\dagger(0) a(t) \rangle^{(2)} - \langle a^\dagger(0) \rangle^{(1)} \langle a(t) \rangle^{(1)} = 0$. Therefore Eq. (4.60) greatly simplifies:

$$\begin{aligned}
\zeta^{(2)}(\omega, \theta) &= 1 + 2\gamma_c^{(R)} \int dt e^{-i\omega t} \langle \mathcal{T} \{a(t), a(0)\} \rangle^{(2)} e^{-2i\theta} \\
&+ 2\gamma_c^{(R)} \int dt e^{-i\omega t} \langle \tilde{\mathcal{T}} \{a^\dagger(t), a^\dagger(0)\} \rangle^{(2)} e^{2i\theta} \tag{4.61}
\end{aligned}$$

The second term in this equation is actually the complex conjugate of the third one:

$$\begin{aligned}
\left(\int dt e^{-i\omega t} \langle \tilde{\mathcal{T}} \{a^\dagger(t), a^\dagger(0)\} \rangle^{(2)} e^{2i\theta} \right)^* &= \int dt e^{i\omega t} \langle \mathcal{T} \{a(t), a(0)\} \rangle^{(2)} e^{-2i\theta} \\
&= \int dt e^{-i\omega t} \langle \mathcal{T} \{a(t), a(0)\} \rangle^{(2)} e^{-2i\theta}
\end{aligned}$$

where in the last line we used the time inversion symmetry of time ordered products. Using Eq. (4.58) we therefore finally get :

$$\begin{aligned}
\zeta^{(2)}(\omega, \theta) &= 1 + 2\gamma_c^{(R)} \int d\omega' \langle \mathcal{T} \{a(-\omega), a(\omega')\} \rangle^{(2)} e^{-2i\theta} + \mathbf{c.c.} \\
&= 1 + 2\Re \left[2\gamma_c^{(R)} \int d\omega' \langle \mathcal{T} \{a(-\omega), a(\omega')\} \rangle^{(2)} e^{-2i\theta} \right] \\
&= 1 + 4\gamma_c^{(R)} \alpha^2 \Re \left[i G_{ac_0}^T[-\omega] G_{ac_0}^T[\omega] T_0 (G_{c_0a}^T[0])^2 e^{-2i\theta} \right] \tag{4.62}
\end{aligned}$$

According to Eq. (4.62) the maximal squeezing which can be achieved with respect to θ is, for any ω ,

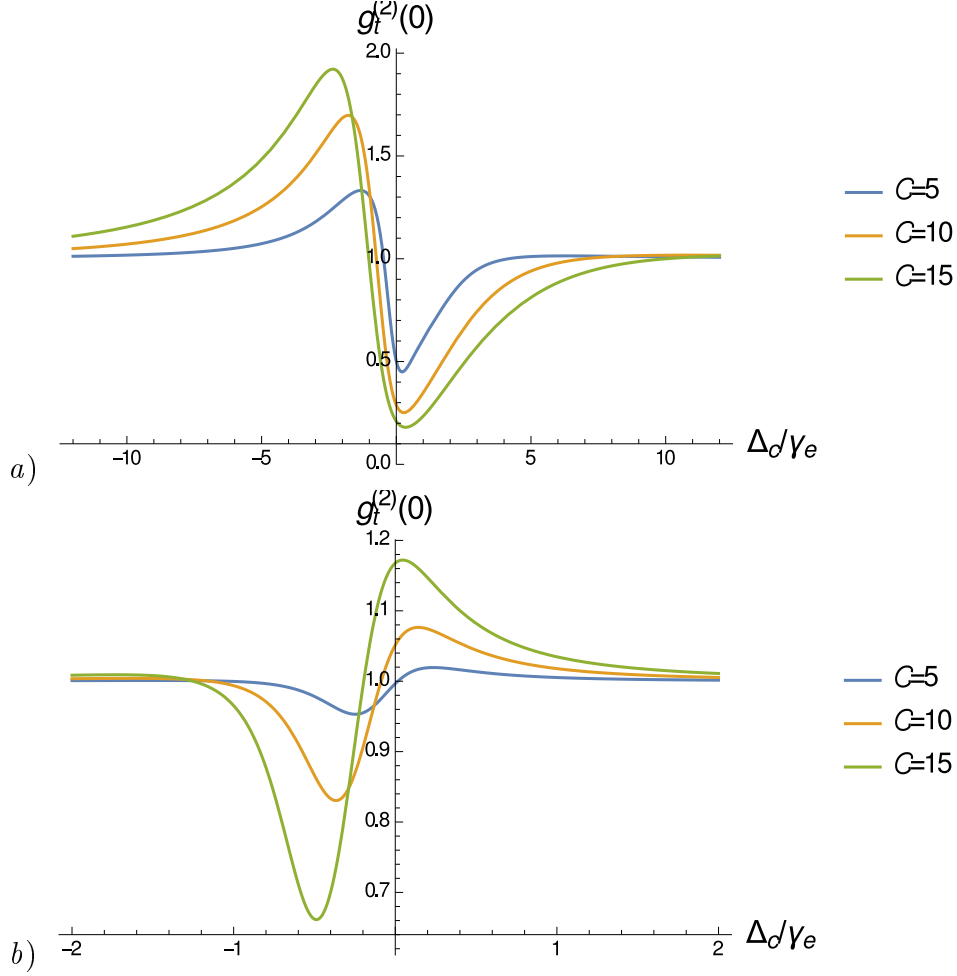


Figure 4.4: Intensity correlation functions of the transmitted light $g_t^{(2)}(0)$ assuming $n = 100$ and $\Omega_{cf} = 3\gamma_e$ for different values of cooperativity (provided on the plot) for a) the resonant case ($\Delta_e = 0, \Delta_r = 0$), b) detuned case $\Delta_e = -25\gamma_e, \Delta_r = 0$.

$$\Xi^{(2)}(\omega) = 1 - 4\gamma_c^{(R)}\alpha^2 \left| G_{ac_0}^T[-\omega] G_{ac_0}^T[\omega] T_0 (G_{c_0a}^T[0])^2 \right|$$

In our calculation we *a priori* assumed that α is small and therefore the latter expression cannot significantly differ from unity. Fig. 4.5 shows the deviation from unity of the maximum of squeezing spectrum, *i.e.* $1 - \Xi^{(2)}(\omega)$, using the same parameters as in the previous paragraph and $\alpha = 0.1\gamma_e$.

4.6 $G^{(1)}$ correlation function

In this section we use the Schwinger-Keldysh contour formalism in order to compute the $G_{out}^{(1)}(t, t') = \langle a_{out}^{(R)\dagger}(t) a_{out}^{(R)}(t') \rangle$ correlation function of the light transmitted through the

4. Schwinger-Keldysh contour formalism.

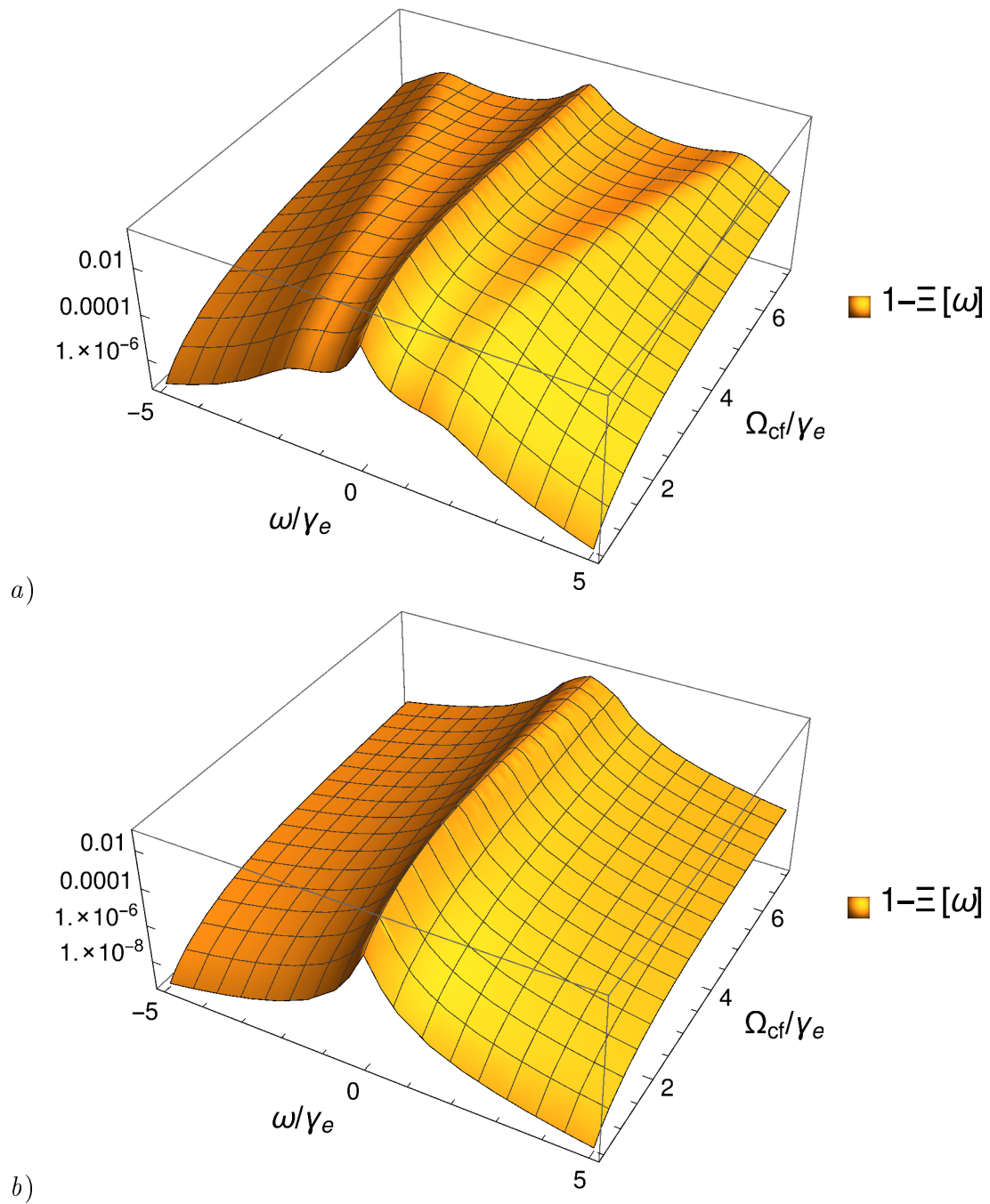


Figure 4.5: Maximum squeezing spectra $1 - \Xi^{(2)}[\omega]$ as a function of the control field Rabi frequency for *a*) the resonant case ($\Delta_e = 0, \Delta_r = 0$), *b*) detuned case $\Delta_e = -25\gamma_e$, $\Delta_r = 0$, $\alpha = 0.1\gamma_e$.

cavity at the fourth order in feeding. This quantity could not have been analytically determined within the formalism used in Chap. 3 and it will allow us, in the next subsection, to compute the transmission spectrum.

Using the input-output relation for the right mirror of the cavity $a_{out}^{(R)}(t) = \sqrt{2\gamma_c^{(R)}} a(t) - a_{in}^{(R)}(t)$ we readily deduce:

$$\begin{aligned} \langle a_{out}^{(R)\dagger}(t) a_{out}^{(R)}(t') \rangle &= \left\langle \left(\sqrt{2\gamma_c^{(R)}} a^\dagger(t) - a_{in}^{\dagger(R)}(t) \right) \left(\sqrt{2\gamma_c^{(R)}} a(t') - a_{in}^{(R)}(t') \right) \right\rangle \\ &= 2\gamma_c^{(R)} \langle a^\dagger(t) a(t') \rangle \end{aligned} \quad (4.63)$$

where we took into account that the bath to the right of the cavity is in vacuum state (or equivalently $a_{in}^{(R)}(t')$ gives zero contribution). The right handside of Eq. (4.63) can be computed using the formalism developed in the current chapter.

At second order in feeding $\langle a^\dagger(t) a(t') \rangle^{(2)} = \langle a^\dagger(t) \rangle^{(1)} \langle a(t') \rangle^{(1)}$ due to the factorization property. At fourth order in feeding this property does not hold any longer and we must resort to the general formula (4.17) to get:

$$\langle a^\dagger(t) a(t') \rangle^{(4)} = \frac{(-i\sqrt{2\pi\alpha})^4}{4} \left\langle \mathcal{T}_{\mathcal{C}} \left\{ e^{-i(\int_{\mathcal{C}} H_{dd})} A_q^2 A_q^{\dagger 2} a_-^\dagger(t) a_+(t') \right\} \right\rangle \quad (4.64)$$

Note that we placed the operators $a_-^\dagger(t)$ and $a_+(t)$ on the \mathcal{C}_- and \mathcal{C}_+ branches, respectively, in order to impose the normal ordering $a^\dagger(t) a(t')$ whatever t and t' are. We now expand the correlation function Eq. (4.64) with respect to the dipole-dipole interactions, separating the forward and backward branches of the contour \mathcal{C} as follows:

$$\begin{aligned} &\langle a^\dagger(t) a(t') \rangle^{(4)} \\ &= \frac{(-i\sqrt{2\pi\alpha})^4}{4} \sum_{p,q} \frac{(-i)^{p+q}}{p!q!} \left\langle \mathcal{T}_{\mathcal{C}} \left\{ \left(\int_{\mathcal{C}_+} ds H_{dd}(s) \right)^p \left(\int_{\mathcal{C}_-} ds H_{dd}(s) \right)^q \right. \right. \\ &\times \left. \left. A_q^2 A_q^{\dagger 2} a_-^\dagger(t) a_+(t') \right\} \right\rangle \end{aligned} \quad (4.65)$$

In the following paragraphs, we split the sum into two main sub-series which exhibit physically different contributions to the $G_{out}^{(1)}$ function at fourth order in feeding.

4.6.1 Elastic contribution

In this subsection, we consider the partial resummation $\mathcal{E}(t, t') = \sum_{p=0, q>0} + \sum_{p>0, q=0}$ of Eq. ($G^{(1)}$ correlation function) which will be shown to constitute the so-called elastic part of the $G_{out}^{(1)}$ function.

4. Schwinger-Keldysh contour formalism.

Consider first the partial sum of Eq. (4.65) including the terms $p \neq 0, q = 0$:

$$\frac{(-i\sqrt{2\pi\alpha})^4}{4} \sum_p \frac{(-i)^p}{p!} \left\langle \mathcal{T}_C \left\{ \left(\frac{1}{2} \sum_{m,n} \kappa_{mn} \int_{\mathcal{C}_+} ds c_n^\dagger c_m^\dagger c_n c_m \right)^p A_q^2 A_q^{\dagger 2} a_-^\dagger(t) a_+(t') \right\} \right\rangle \quad (4.66)$$

From the rule **R1** (see Subsec. 4.3) we see that the operator $a_-^\dagger(t)$ does not have other candidates for contraction than A_q . Since $\langle a^\dagger(t) \rangle^{(1)} = (-\sqrt{2\pi i \alpha}) \langle \mathcal{T}_C \{ a_-^\dagger(t) A_q \} \rangle$ (see Sec. 4.3),

$$\frac{(-i\sqrt{2\pi\alpha})^3}{2} \sum_p \frac{(-i)^p}{p!} \left\langle \mathcal{T}_C \left\{ \left(\frac{1}{2} \sum_{m,n} \kappa_{mn} \int_{\mathcal{C}_+} ds c_n^\dagger c_m^\dagger c_n c_m \right)^p A_q A_q^{\dagger 2} a_+(t') \right\} \right\rangle \times \langle a^\dagger(t) \rangle^{(1)} \quad (4.67)$$

The first term in Eq. (4.67) will now be shown to be equal to $\langle a(t) \rangle^{(3)}$. From the general formula Eq. (4.17) we indeed have

$$\begin{aligned} & \langle a(t) \rangle^{(3)} \\ \equiv & \frac{(-i\sqrt{2\pi\alpha})^3}{2!} \sum_{p,q} \frac{(-i)^{p+q}}{p!q!} \left\langle \mathcal{T}_C \left\{ \left(\frac{1}{2} \sum_{m,n} \kappa_{mn} \int_{\mathcal{C}_+} c_n^\dagger c_m^\dagger c_n c_m \right)^p \right. \right. \\ & \left. \left. \times \left(\frac{1}{2} \sum_{m,n} \kappa_{mn} \int_{\mathcal{C}_-} c_n^\dagger c_m^\dagger c_n c_m \right)^q A_q A_q^{\dagger 2} a_+(t) \right\} \right\rangle \end{aligned}$$

In the expression above one of the operators c_n^\dagger, c_m^\dagger belonging the \mathcal{C}_- branch does not have any partner for contraction (according to the rule **R1**). Therefore only the $q = 0$ term will contribute to the sum and

$$\langle a(t) \rangle^{(3)} \equiv \frac{(-i\sqrt{2\pi\alpha})^3}{2!} \left\langle \mathcal{T}_C \left\{ e^{-i\frac{1}{2} \sum_{m,n} \kappa_{mn} \int_{\mathcal{C}_+} ds c_n^\dagger c_m^\dagger c_n c_m} A_q A_q^{\dagger 2} a_+(t) \right\} \right\rangle \quad (4.68)$$

We indeed recover the expression obtained in Eq. (4.67). Analogously, the partial sum of the terms ($p = 0, q \neq 0$) yields $\langle a^\dagger(t) \rangle^{(3)} \langle a(t') \rangle^{(1)}$. Finally we get

$$\mathcal{E} = \langle a^\dagger(t) \rangle^{(3)} \langle a(t') \rangle^{(1)} + \langle a^\dagger(t) \rangle^{(1)} \langle a(t') \rangle^{(3)}$$

We shall now determine the expression for $\langle a(t) \rangle^{(3)}$. Let us perform an expansion of Eq. (4.68) with respect to H_{dd} . Due to the symmetry properties of the system, it is more convenient to work in the spatial Fourier space. We therefore get:

$$\begin{aligned} \langle a(t) \rangle^{(3)} &= \\ &= \frac{(-i\sqrt{2\pi\alpha})^3}{2!} \sum_p \frac{1}{p!} \left\langle \mathcal{T}_C \left\{ \left(-\frac{i}{2} \sum_{\vec{q}, \vec{k}_1, \vec{k}_2} U_{\vec{q}} \int_{\mathcal{C}_+} c_{\vec{k}_2 - \vec{q}}^\dagger c_{\vec{q} + \vec{k}_1}^\dagger c_{\vec{k}_1} c_{\vec{k}_2} \right)^p A_q A_q^{\dagger 2} a_+(t) \right\} \right\rangle \end{aligned}$$

As expected, the zeroth order ($p = 0$) of this expansion is zero since it necessarily involves the vanishing contraction of two “quantum” operators A_q and A_q^\dagger (see Sec. 4.2.2). Applying rules R1, R2, R3, R4, the first order term ($p = 1$) takes the form:

$$\begin{aligned} \langle a(t) \rangle^{(3,1)} &= \\ &= \frac{(-i\sqrt{2\pi\alpha})^3}{2!} \frac{-i}{2} \sum_{\vec{q}, \vec{k}_1, \vec{k}_2} U_{\vec{q}} \left\langle \mathcal{T}_C \left\{ \int_{\mathcal{C}_+} c_{\vec{k}_2 - \vec{q}}^\dagger c_{\vec{q} + \vec{k}_1}^\dagger c_{\vec{k}_1} c_{\vec{k}_2} A_q A_q^{\dagger 2} a_+(t) \right\} \right\rangle \\ &= (-i\alpha)^3 (-iU_0) \int ds_1 ds_2 ds_3 iG_{ac_0}^T(t-s) \left(-iG_{ac_0}^{\tilde{T}}[s_3-s] \right) iG_{c_0a}^T(s-s_1) iG_{c_0a}^T(s-s_2) \end{aligned}$$

where we used

$$\begin{aligned} \left\langle \mathcal{T}_C \left\{ A_q c_{+, \vec{k}}^\dagger(t) \right\} \right\rangle &= \frac{1}{\sqrt{2\pi}} \int ds \left\langle \mathcal{T}_C \left\{ (a_+(s) - a_-(s)) c_{+, \vec{k}}^\dagger(t) \right\} \right\rangle \\ &= \frac{1}{\sqrt{2\pi}} \int ds \left\{ iG_{ac_0}^T[s, t] - iG_{ac_0}^>[s, t] \right\} \delta_{\vec{k}, 0} \\ &= \frac{1}{\sqrt{2\pi}} \int ds \left\{ -iG_{ac_0}^{\tilde{T}}[s, t] \right\} \delta_{\vec{k}, 0} \end{aligned}$$

Therefore, switching to the frequency domain

$$\langle a(\omega) \rangle^{(3,1)} = \left(-i\sqrt{2\pi\alpha} \right)^3 \left(-iG_{ac_0}^T[0] iG_{ac_0}^{\tilde{T}}[0] \right) (-iU_0) \left(iG_{c_0a}^T[0] \right)^2$$

We can determine the second order term ($p = 2$) in Eq. (4.68) in a similar way and get:

$$\begin{aligned} \langle a(\omega) \rangle^{(3,2)} &= \left(-i\sqrt{2\pi\alpha} \right)^3 \left(-iG_{ac_0}^T[0] iG_{ac_0}^{\tilde{T}}[0] \right) \times \\ &\times \left\{ \sum_{\vec{q}} (-iU_{\vec{q}}) (-iU_{-\vec{q}}) \left(\int d\omega iG_{\vec{q}, \vec{q}}^T[\omega] iG_{-\vec{q}, -\vec{q}}^T[-\omega] \right) \right\} \\ &\times \left(iG_{c_0a}^T[0] \right)^2 \end{aligned}$$

Higher-order terms ($p \geq 3$) can be diagrammatically generated and resummed so that

4. Schwinger-Keldysh contour formalism.

we get

$$\langle a(\omega) \rangle^{(3)} = \sum_p \langle a(\omega) \rangle^{(3,p)} = \left(-i\sqrt{2\pi\alpha} \right)^3 \delta(\omega) \left(-iG_{ac_0}^T [0] iG_{ac_0}^{\tilde{T}} [0] \right) \left(\frac{-iT_0}{2\pi} \right) \left(iG_{c_0a}^T [0] \right)^2 \quad (4.69)$$

where T_0 was defined in Eq. (4.45). Gathering Eqs. (4.69,4.33) we finally get in the frequency domain

$$\begin{aligned} \mathcal{E}(\omega, \omega') &= \langle a^\dagger(\omega) \rangle^{(1)} \langle a(\omega') \rangle^{(3)} + \text{c.c.} \\ &= -2\pi\alpha^4 \delta(\omega') \delta(\omega) G_{aa}^* [0] \left(G_{ac_0}^T [0] G_{ac_0}^{\tilde{T}} [0] \right) T_0 \left(G_{c_0a}^T [0] \right)^2 + \text{c.c.} \end{aligned}$$

Since $\langle a^\dagger(\omega) \rangle^{(3)} \propto \delta(\omega)$, $\langle a(\omega') \rangle^{(1)} \propto \delta(\omega')$, we see that $\mathcal{E}(\omega, \omega')$ corresponds to the elastic part of the $G_{out}^{(1)}$ function at fourth order in feeding.

$$\left\langle a_{out}^{(R)\dagger}(\omega) a_{out}^{(R)}(\omega') \right\rangle_{el} \propto \delta(\omega) \delta(\omega')$$

which is due to photons propagating through cavity without changing their frequency. Note that this fourth order elastic contribution is actually a correction of the (necessarily elastic) second order spectrum.

4.6.2 Inelastic contribution to $G_{out}^{(1)}$

In this subsection, we consider the partial resummation of the terms of Eq. ($G^{(1)}$ correlation function) $\mathcal{I}(t, t') \equiv \sum_{p>0, q>0} \langle a^\dagger(t) a(t') \rangle^{(4)} - \mathcal{E}(t, t')$ and show this brings nonlinearity-induced inelastic features which were absent at lower orders.

We have

$$\mathcal{I}(t, t') = \frac{(-i\sqrt{2\pi\alpha})^4}{4} \sum_{p>0, q>0} \left\langle \mathcal{T}_C \left\{ \frac{1}{p!} \left(-i \int_{C_+} ds H_{dd}(s) \right)^p \frac{1}{q!} \left(-i \int_{C_-} ds H_{dd}(s) \right)^q \right. \right. \\ \left. \left. \times A_q^2 A_q^{\dagger 2} a_-^\dagger(t) a_+(t') \right\} \right\rangle$$

Let us first consider the term ($p = 1, q = 1$) still using the H_{dd} in the spinwave basis:

$$\begin{aligned}
 & \mathcal{I}_{1,1}(t, t') \\
 &= \frac{(-i\sqrt{2\pi}\alpha)^4}{4} \left\langle \mathcal{T}_C \left\{ \left(-i\frac{1}{2} \sum_{\vec{q}, \vec{k}_1, \vec{k}_2} \int ds U_{\vec{q}} c_{\vec{k}_2 - \vec{q}, +}^\dagger c_{\vec{q} + \vec{k}_1, +}^\dagger c_{\vec{k}_1, +} c_{\vec{k}_2, +} \right) \right. \right. \\
 & \times \left. \left. \left(-i\frac{1}{2} \sum_{\vec{q}', \vec{k}'_1, \vec{k}'_2} U_{\vec{q}'} \int ds c_{\vec{k}'_2 - \vec{q}', -}^\dagger c_{\vec{q}' + \vec{k}'_1, -}^\dagger c_{\vec{k}'_1, -} c_{\vec{k}'_2, -} \right) A_q^2 A_q^{\dagger 2} a_-^\dagger(t) a_+(t') \right\} \right\rangle \quad (4.70)
 \end{aligned}$$

We first notice that in Eq. (4.70) operators $c_{\vec{k}_1, +} c_{\vec{k}_2, +}$ and $c_{\vec{k}'_2 - \vec{q}', -}^\dagger c_{\vec{q}' + \vec{k}'_1, -}^\dagger$ can only be contracted with $A_q^{\dagger 2}$ and A_q^2 respectively (using rules R1, R2, R3, R4). Recalling that $A_q \equiv \frac{1}{\sqrt{2\pi}} \int ds (a_+(s) - a_-(s))$ we have:

$$\begin{aligned}
 \left\langle \mathcal{T}_C \left\{ c_{\vec{k}, +}(t) A_q^\dagger \right\} \right\rangle &= \frac{i}{\sqrt{2\pi}} \int ds G_{c_0 a}^T(t-s) \delta_{\vec{k}, 0} \\
 \left\langle \mathcal{T}_C \left\{ c_{\vec{k}, -}^\dagger(t) A_q \right\} \right\rangle &= \frac{-i}{\sqrt{2\pi}} \int ds G_{c_0 a}^{\bar{T}}(s-t) \delta_{\vec{k}, 0}
 \end{aligned}$$

therefore

$$\begin{aligned}
 \mathcal{I}_{1,1}(t, t') &= \frac{(-i\sqrt{2\pi}\alpha)^4}{4} \left\langle \mathcal{T}_C \left\{ \left(-i \int_{\mathcal{C}_+} dz_1 \sum_{\vec{q}} U_{\vec{q}} c_{-\vec{q}}^\dagger c_{\vec{q}}^\dagger \right) \left(i \int_{-\mathcal{C}_-} dz_2 \sum_{\vec{q}'} U_{\vec{q}'} c_{-\vec{q}'} c_{\vec{q}'} \right) \right. \right. \\
 & \times \left. \left. a_-^\dagger(t) a_+(t') \right\} \right\rangle \left(\int \frac{ds}{\sqrt{2\pi}} i G_{c_0 a}^T[z_1, s] \right)^2 \left(- \int \frac{ds}{\sqrt{2\pi}} i G_{ac_0}^{\bar{T}}[s, z_2] \right)^2 \quad (4.71)
 \end{aligned}$$

In this expression, according to rule R1, $a_-^\dagger(t)$ and $a_+(t')$ can only be contracted with one of $c_{\vec{q}, -}$ and $c_{\vec{q}, +}^\dagger$ operators respectively. Therefore:

$$\begin{aligned}
 & (-i\sqrt{2\pi}\alpha)^4 \left\langle \mathcal{T}_C \left\{ \left(-i \int_{\mathcal{C}_+} dz_1 U_0 c_0^\dagger \right) \left(i \int_{-\mathcal{C}_-} dz_2 U_0 c_0 \right) \right\} \right\rangle \quad (4.72) \\
 & \times i G_{c_0 a}^{\bar{T}}[z_2, t] i G_{ac_0}^T[t', z_1] \left(\int \frac{ds}{\sqrt{2\pi}} i G_{c_0 a}^T[z_1, s] \right)^2 \left(- \int \frac{ds}{\sqrt{2\pi}} i G_{ac_0}^{\bar{T}}[s, z_2] \right)^2
 \end{aligned}$$

and finally, recalling the definition of the greater Green's function $\forall (z_1 \in \mathcal{C}_-, z_2 \in \mathcal{C}_+)$, $\left\langle \mathcal{T}_C \left\{ c_0(z_2) c_0^\dagger(z_1) \right\} \right\rangle = i G_{c_0, c_0}^>[z_2, z_1]$ we have

4. Schwinger-Keldysh contour formalism.

$$\begin{aligned} \mathcal{I}_{1,1}(t, t') &= \left(-i\sqrt{2\pi\alpha}\right)^4 (-iU_0)(iU_0) \int_{-\infty}^{\infty} dz_1 dz_2 iG_{c_0c_0}^> [z_2, z_1] iG_{c_0a}^{\tilde{T}} [z_2, t] \\ &\times iG_{ac_0}^T [t', z_1] \left(\int \frac{ds}{\sqrt{2\pi}} iG_{c_0a}^T [z_1, s] \right)^2 \left(- \int \frac{ds}{\sqrt{2\pi}} iG_{ac_0}^{\tilde{T}} [s, z_2] \right)^2 \end{aligned} \quad (4.73)$$

or equivalently in frequency domain

$$\begin{aligned} &\left(-i\sqrt{2\pi\alpha}\right)^4 \delta(\omega - \omega') \left(-i\frac{U_0}{2\pi}\right) \left(i\frac{U_0}{2\pi}\right) iG_{c_0c_0}^> [-\omega] iG_{c_0a}^{\tilde{T}} [\omega'] \\ &\times iG_{ac_0}^T [\omega] (iG_{c_0a}^T [0])^2 (iG_{ac_0}^{\tilde{T}} [0])^2 \end{aligned} \quad (4.74)$$

Continuing the procedure and resumming for $p, q > 0$, we get:

$$\begin{aligned} \mathcal{I}(\omega, \omega') &= -\alpha^4 \delta(\omega - \omega') |T_0|^2 iG_{c_0c_0}^> [-\omega] G_{c_0a}^{\tilde{T}} [\omega'] \\ &\times G_{ac_0}^T [\omega] (G_{c_0a}^T [0])^2 (G_{ac_0}^{\tilde{T}} [0])^2 \end{aligned} \quad (4.75)$$

4.6.3 Transmission spectrum

In this subsection we use the results, derived above to investigate the spectrum of the transmitted light

$$\mathcal{S}^{out}(\omega) \equiv \int d\omega' G_{out}^{(1)}(\omega, \omega')$$

We shall be particularly interested in the inelastic part ($\mathcal{S}_i^{out} \equiv 2\gamma_c^R \int_{-\infty}^{\infty} d\nu \mathcal{I}(\omega, \nu)$, see Eq. (4.75)), which is represented in Fig. 4.6 in resonant ($\Delta_c = \Delta_e = \Delta_r = 0$) as well as detuned ($\Delta_c = -3\gamma_e, \Delta_e = 0, \Delta_r = 0$) configurations. For both regimes we assume a cloud cooperativity $C = 5$, and $\gamma_c^R = 0.3\gamma_e \gg \gamma_c^L$ and $\gamma_r = 0.15\gamma_e$ for the cavity and Rydberg decays respectively. All parameters are expressed in units of the intermediate state decay rate $\gamma_e = 2\pi \times 3\text{MHz}$.

As can be seen on Fig. 4.6 the spectrum has several resonances which depend on the control field Rabi frequency. The resonance structure shown in Fig. 4.6 (a) (resonant case) resembles the level pattern of the Hamiltonian in the single excitation subspace

$$\begin{pmatrix} 0 & g\sqrt{N} & 0 \\ g\sqrt{N} & 0 & \frac{\Omega}{2} \\ 0 & \frac{\Omega}{2} & 0 \end{pmatrix}$$

In the detuned case, the structure shown on Fig. 4.6 (b) is more complicated; resonances can still be identified as the eigenvalues $\epsilon_1, \epsilon_2, \epsilon_3$ of the Hamiltonian

$$\begin{pmatrix} -\Delta_c & g\sqrt{N} & 0 \\ g\sqrt{N} & -\Delta_e & \frac{\Omega}{2} \\ 0 & \frac{\Omega}{2} & -\Delta_r \end{pmatrix} \quad (4.76)$$

but taken with positive and negative signs. The physical explanation of this effect can be given according to the level structure of the considered system, shown in Fig. 4.7 (Ourjountsev et al., 2011). The system can be seen as to be excited by two photons of the probe laser frequency ω_p . Eq. (4.75) shows that the strength of dipole-dipole interactions does not affect the ω -dependence of the inelastic component at fourth order since H_{dd} enters Eq. (4.75) only via the overall factor T_0 . Doubly excited states decay via dissipative terms Eq. (1.11) to the three symmetric polaritons: the resonance frequencies of the emitted photon pairs are therefore $\omega_p \pm \epsilon_1$, $\omega_p \pm \epsilon_2$ and $\omega_p \pm \epsilon_3$, respectively, or, in the frame rotating at the probe frequency ω_p , $\pm\epsilon_1$, $\pm\epsilon_2$ and $\pm\epsilon_3$.

4.7 Conclusions

In this chapter, we investigated the quantum optical nonlinearities induced by a cavity Rydberg EIT medium in the Schwinger-Keldysh contour approach. We transformed all operators of the system into the interaction picture, and used the contour-ordered form for correlation functions. We expanded them perturbatively with respect to both feeding and dipole-dipole interactions. The resummation of series can be performed employing the Wick's theorem for contour-ordered quantities. For that we defined and derived all possible Green's functions of the system. As dipole-dipole interactions can *a priori* be arbitrarily strong, we are compelled to resum all order of magnitude in H_{dd} for each order of expansion in the feeding Hamiltonian. Using this approach we could derive a compact analytic expression for the squeezing spectrum of the transmitted light and the $g_t^{(2)}$ function at lowest non-vanishing order in feeding. Then we derived the analytic expression of the spectrum of the light transmitted through the cavity beyond the lowest order in feeding which were not accessible to the methods presented in previous chapters. Besides an elastic part, associated to photons going through the cavity without frequency change, the spectrum also comprises an inelastic contribution which contains several resonances that we explained by a simple polaritonic picture.

Throughout this chapter, we assumed a constant feeding of the system, for simplicity: the formalism actually allows for time-dependent wavepacket inputs. We moreover want to emphasize that, though rarely employed in this context (another example of application of such techniques in quantum optics is provided in (Fleischhauer and Yelin, 1999)), the contour formalism is a powerful tool for quantum optics which could be used, e.g., to compute higher-order correlation functions of the system or thoroughly analyze subtle effects in Rydberg atomic ensembles such as thermalization (Ates et al., 2012) or phase transition (Löw et al., 2009).

4. Schwinger-Keldysh contour formalism.

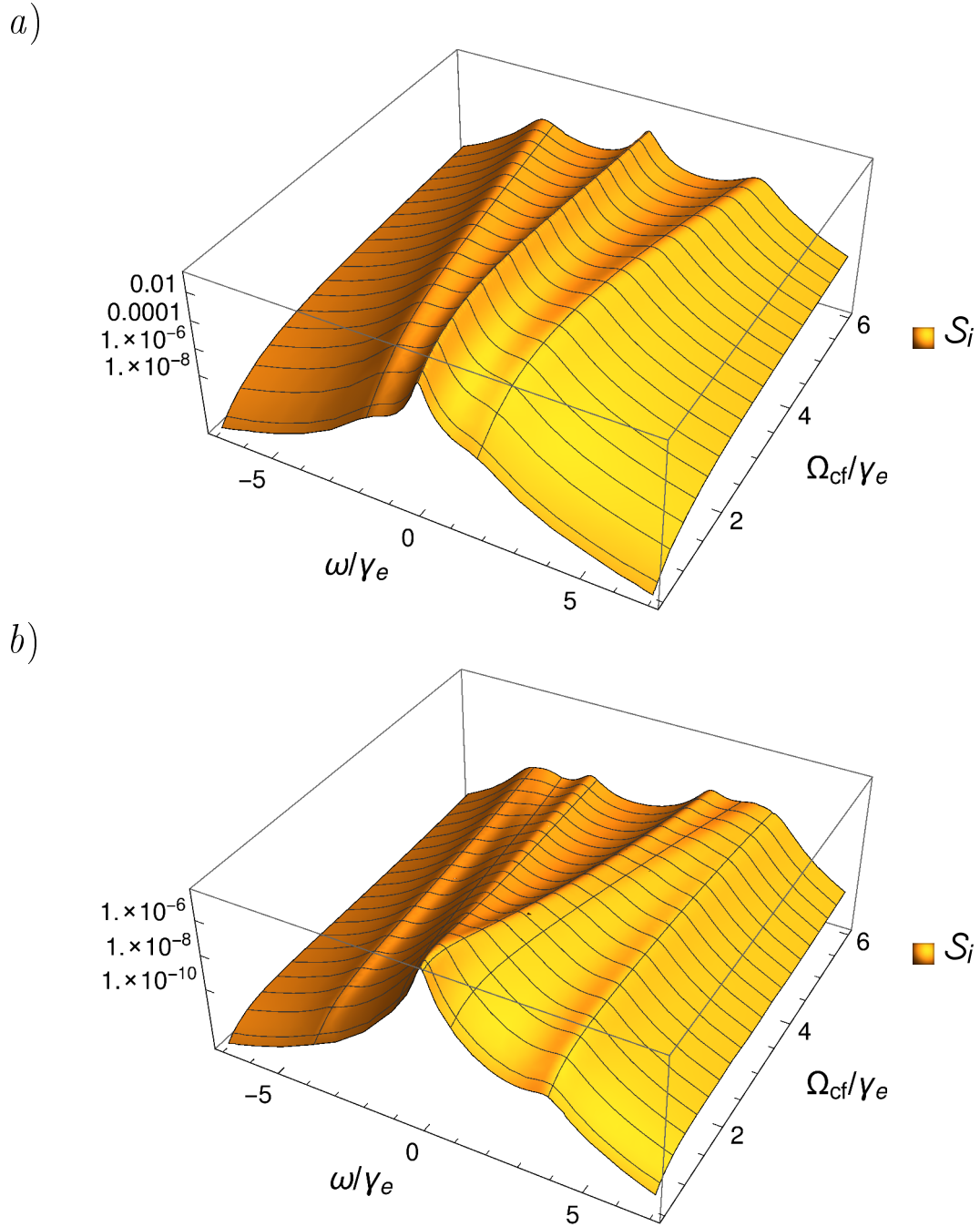


Figure 4.6: Inelastic component of the cavity transmission spectrum $\mathcal{S}_i \equiv 2\gamma_c^R \int d\nu \langle a^\dagger(\omega), a(\nu) \rangle$ in logarithmic scale as a function of Ω_{cf} and the frequency (in the frame rotating at ω_p) for: a) the resonant case $\Delta_c = \Delta_e = \Delta_r = 0$, b) the detuned case. The transverse curves give $(\pm\epsilon_1, \pm\epsilon_2, \pm\epsilon_3)$ as functions of Ω_{cf} (see main text).

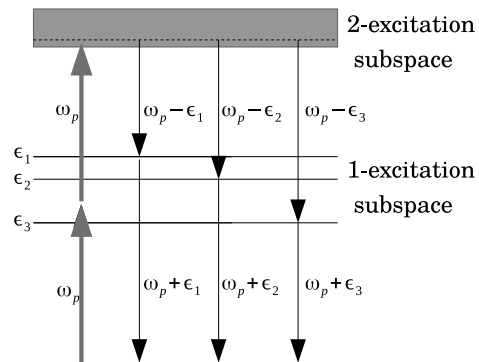


Figure 4.7: The level structure of the Hamiltonian of the system, restricted to two excitations. The structure of the doubly excited manifold is represented schematically.

4. Schwinger-Keldysh contour formalism.

Chapter 5

Photonic phase gate

Contents

5.1	Presentation of the protocol	104
5.2	Photon scattering on the cavity	107
5.2.1	Dynamical equations	107
5.2.2	Reference situation	108
5.2.3	Cavity with non-interacting two-level atoms	109
5.3	Gate operation	111
5.3.1	Evolution of $ 00\rangle, 10\rangle$	111
5.3.2	Evolution of $ 01\rangle$	111
5.3.3	Evolution of $ 11\rangle$	112
5.4	Numerical results	115
5.4.1	Choi-Jamiolkowsky fidelity	115
5.4.2	Dual rail encoding	117
5.5	Conclusions	118

5. Photonic phase gate

In this chapter¹, we present a novel scheme for high-fidelity photonic controlled-phase gates based on the Rydberg blockade in an atomic ensemble loaded in an optical cavity. The setup we consider, represented on Fig. 5.1, is very similar to that described in Chap. 1: it comprises a ladder-type three-level Rydberg medium, placed in an optical cavity whose left mirror is partially transmissive while the right mirror is perfectly reflecting. In our scenario, the π phase factor is induced by the reflection of the target photonic qubit on the cavity, conditioned by the presence of an intracavity stored polariton, associated with the control qubit. The resulting gate can be implemented with cavities of moderate finesse allowing for highly efficient and robust processing of quantum information encoded in photons.

After describing the gate protocol in Sec. 5.1, we introduce the formalism required to study the scattering of an incident photon on the cavity in Sec. 5.2. We apply this formalism to quantitatively characterize the respective evolution of the logical qubit states in Sec. 5.3. In the last section, we present numerical results we obtained for the gate fidelity, based on the expressions of the scattering coefficients derived previously.

5.1 Presentation of the protocol

For simplicity, we first describe the operation in the so-called “single-rail” approach, according to which a qubit is encoded in a pulse prepared in a superposition of vacuum $|0\rangle$ and single-photon $|1\rangle$ states. In Sec. 5.4, we shall extend it to the dual-rail encoding where a qubit is encoded as a photon prepared in one of two, spatially distinct possible modes.

In the single-rail version outlined in Figs. 5.1 a) and b), the gate operates as follows. The pulse encoding the control qubit is sent towards the cavity where it gets stored as a Rydberg polariton of type $|r\rangle$, via a strong-laser-assisted ladder-type storage process (Gorshkov et al., 2007). The $|r\rangle$ excitation is then transferred to another Rydberg state $|r'\rangle$ by a microwave pulse². At that stage, the ensemble therefore contains a single atom in state $|r'\rangle$ if the first pulse did contain a photon. Note that we do not take into account possible losses during the storage process and hence assume that, in the latter case, the resulting state of the ensemble is $\frac{1}{\sqrt{N}} \sum_i |g_1, \dots, r'_i, \dots, g_N\rangle$.

The pulse encoding the target qubit is then sent towards the cavity. It is important to notice, that, as shown on Fig. 5.1, the $|r'\rangle$ state is not coupled to the control field. We now consider the following two possible cases. **A.** If the first pulse contained no photon, the second pulse is scattered under Rydberg EIT conditions (we assume all transitions

¹This chapter is an edited version of (Das et al., 2016; 2015)

²It is important to note that, here, $|r\rangle$ and $|r'\rangle$ are assumed to be of the same parity, so that r and r' -excited atoms interact via Van der Waals Hamiltonian $\propto \frac{1}{r^6}$. Transferring the excitation from $|r\rangle$ to $|r'\rangle$ therefore requires a two-photon process. Alternatively, one could also directly convert the control photon as an $|r'\rangle$ excitation by using a different control field laser for the storage step, which drives the transition $|e\rangle \leftrightarrow |r'\rangle$.

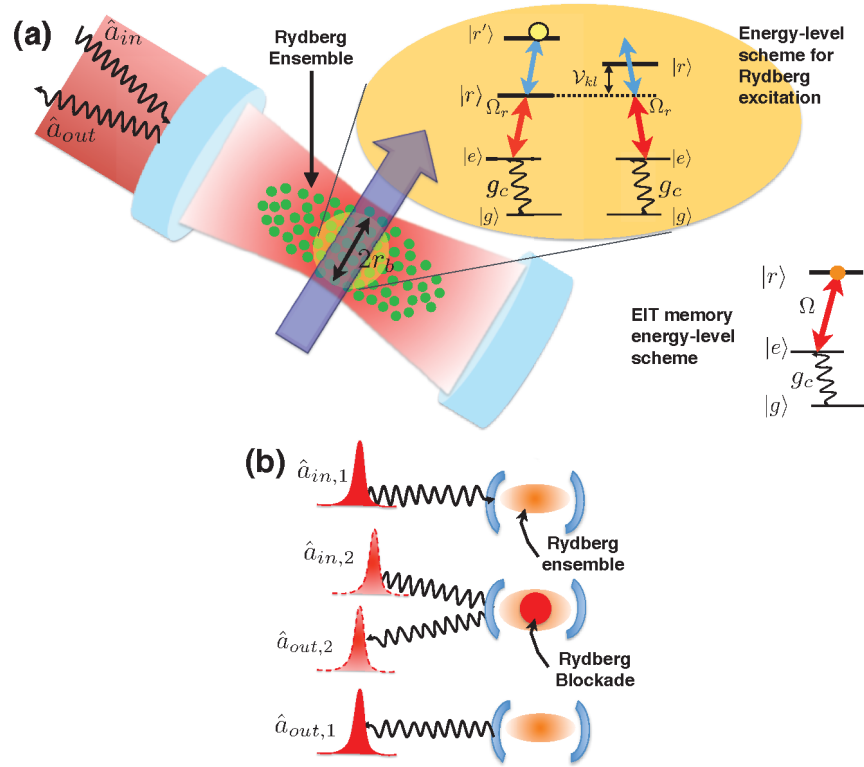


Figure 5.1: Schematic outline of the phase gate (a) An input single photon pulse along with a driving field induces a two-photon transition to the Rydberg state $|r\rangle$ which is subsequently transferred to another Rydberg state $|r'\rangle$. Due to Rydberg interactions V_{kl} among the atoms, other Rydberg states $|r\rangle$ within the range of the interaction potential, given by, the blockade radius of r_b , become off-resonant allowing no further excitation. (b) When an initial photon pulse is stored in the Rydberg ensemble, the second incoming photon cannot enter the cavity and is scattered off, which ideally induces a phase flip of π on the scattered photons.

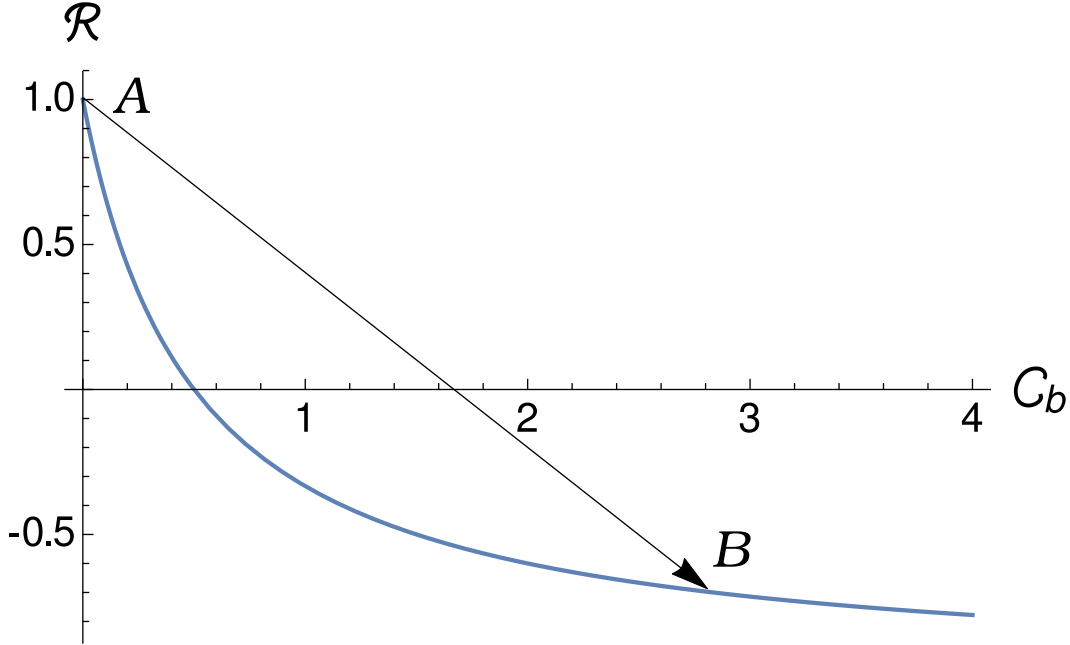


Figure 5.2: Reflection coefficient of the cavity \mathcal{R} as a function of the cooperativity C_b of atoms within the blockade sphere.

are resonantly driven: $\Delta_c = 0$, $\Delta_e = 0$, $\Delta_r = 0$) . **B**. If the first pulse contained a photon, the delocalized excitation in $|r'\rangle$ induces an energy shift on the state $|r\rangle$ in the atoms around, which can prevent the second photon from entering, and imprints on the wavefunction an additional π phase, compared to the case A. A naive explanation of this effect is provided on Fig. 5.2. If no excitation is initially stored in the cavity (case A), the reflection coefficient for the second photon, treated in the long pulse approximation (steady state) is conventionally taken to be ³ $\mathcal{R} = 1$, provided the cloud is transparent (perfect EIT). In that case the photon indeed merely enters the cavity, is reflected from the right mirror and leaves the cavity through the left mirror. By contrast, in case B, the stored excitation breaks EIT in its neighbourhood, transforming the blockaded atoms around into resonant two-level systems. The collective response of these atoms changes the cavity reflection coefficient into⁴ $\mathcal{R} = \frac{1-2C_b}{1+2C_b}$, where $C_b = \frac{g^2 n_b}{2\gamma_c \gamma_e}$ is the cooperativity of (n_b) atoms inside the blockade sphere (see Fig. 5.2). For sufficiently large values of C_b , the photon can not enter the cavity any longer, and is reflected from the left mirror, acquiring the desired π phase (shown by black arrow), *i.e.* $\mathcal{R} \rightarrow -1$.

For future reference, let us introduce the qubit encoding :

³This actually corresponds to defining \mathcal{R} such that $a_{out} = -\mathcal{R}a_{in}$ where a_{in} and a_{out} are the incoming and outgoing mode annihilation operators.

⁴This result can be readily obtained from the Heisenberg-Langevin equations, assuming the cavity is filled with resonant two-level atoms with the cooperativity C_b .

$$|00\rangle \equiv |\emptyset\rangle \quad (5.1)$$

$$|01\rangle \equiv \int d\omega \beta(\omega) b_\omega^\dagger |\emptyset\rangle \quad (5.2)$$

$$|10\rangle \equiv S^\dagger |\emptyset\rangle \quad (5.3)$$

$$|11\rangle \equiv S^\dagger \int d\omega \beta(\omega) b_\omega^\dagger |\emptyset\rangle \quad (5.4)$$

where $|\emptyset\rangle \equiv |g_1, \dots, g_N\rangle \otimes |0\rangle$ is the vacuum state of the system {atoms+baths}, $S^\dagger \equiv \frac{1}{\sqrt{N}} \sum_i \sigma_{r'g}^{(i)}$ (where as usual $\sigma_{\mu\nu}^{(i)} \equiv |\mu_i\rangle \langle \nu_i|$ with μ, ν taking values from $\{g, e, r, r'\}$) is the stored r' -polariton creation operator and b_ω^\dagger is the creation operator of the electromagnetic bath mode of frequency ω . We moreover assume that the function $\beta(\omega)$ which defines the temporal mode of the incoming photon satisfies the normalization condition $\int d\omega |\beta(\omega)|^2 = 1$.

To evaluate the performances of the gate defined above, we must be able to quantitatively describe the scattering of a photon on the cavity in which an r' excitation may be stored. In the next section we introduce the general formalism which shall allow us to compute the scattering coefficients in the four cases corresponding to the four logical states of the two incoming qubits.

5.2 Photon scattering on the cavity

In this section, we provide the general equations which govern the dynamics of the system and show, on a simple example, how to deduce the scattering coefficient for an incoming photon.

5.2.1 Dynamical equations

The Hamiltonian of the full system (including the bath modes) we consider here reads:

$$\begin{aligned} H &= \frac{\Omega_{cf}}{2} \sum_i (\sigma_{er}^{(i)} + \sigma_{re}^{(i)}) + g \sum_i (a^\dagger \sigma_{ge}^{(i)} + a \sigma_{eg}^{(i)}) + \sum_{ij} V_{ij} \sigma_{r'r'}^{(i)} \sigma_{rr}^{(j)} \\ &+ g_b \int d\omega b_\omega^\dagger a + g_b^* \int d\omega b_\omega a^\dagger + \int d\omega \omega b_\omega^\dagger b_\omega \\ &+ H_{at-bath} \end{aligned} \quad (5.5)$$

where the last term in the first line of Eq. (5.5) stands for the dipole-dipole-induced shift $V_{ij} = \frac{\tilde{C}_6}{r_{ij}^6}$ of the doubly excited state $|r_i, r'_j\rangle$. We notice, that according to the qubit encoding Eqs. (5.1-5.4), there can never be two atoms simultaneously excited in the

5. Photonic phase gate

state $|r\rangle$. This is why we implicitly omitted the term $H_{dd} = \frac{1}{2} \sum_{k,l} V_{ij} \sigma_{rr}^{(k)} \sigma_{rr}^{(l)}$ in Eq. (5.5).

We now perform Markov approximation and eliminate all bath modes. The resulting Heisenberg-Langevin equations are given by:

$$\frac{d}{dt}a = -\gamma_c a - ig \sum_i \sigma_{ge}^{(i)} + \sqrt{2\gamma_c} a_{in} \quad (5.6)$$

$$\frac{d}{dt}\sigma_{ge}^{(i)} = -\gamma_e \sigma_{ge}^{(i)} + iga \left(2\sigma_{ee}^{(i)} + \sigma_{rr}^{(i)} + \sigma_{r'r'}^{(i)} - 1 \right) - i\frac{\Omega_{cf}}{2} \sigma_{gr}^{(i)} \quad (5.7)$$

$$\frac{d}{dt}\sigma_{gr}^{(i)} = iga\sigma_{er}^{(i)} - i\frac{\Omega_{cf}}{2}\sigma_{ge}^{(i)} - i\sigma_{gr}^{(i)} \sum_k V_{ij} \sigma_{r'r'}^{(k)} \quad (5.8)$$

$$\frac{d}{dt}\sigma_{gr'}^{(i)} = iga\sigma_{er'}^{(i)} - i\sigma_{gr'}^{(i)} \sum_k V_{ik} \sigma_{rr}^{(k)} \quad (5.9)$$

We implicitly neglected Langevin forces in Eqs. (5.7-5.9) as, for the atomic operators, bath is assumed to be in the vacuum state initially.

We moreover set $\gamma_r, \gamma_{r'} \rightarrow 0$, since the time of the experiment is assumed to be much shorter than the lifetimes of the Rydberg states. As said in the previous section, we shall also assume that the storage and retrieval of photons into the atomic ensemble are perfect (which strictly speaking requires infinite cooperativity (Gorshkov et al., 2007)). Therefore, the only step which may limit the performance of the gate is the imperfect reflection of the target photon on the cavity which can lead to distortion of the photon shape and/or photon loss. This may be quantitatively characterized by a coefficient relating the actual scattered state to a reference state, as we shall now focus on.

5.2.2 Reference situation

In order to characterize the effect of a possibly stored Rydberg excitation in the ensemble on the scattering on an incoming photon we need to take a reference configuration in which atoms play no role. We therefore consider the imaginary situation in which the coupling strength g is artificially set to zero in Eq. (5.5). In this reference situation the bath and cavity mode are decoupled from the atomic ensemble and evolve according to the Hamiltonian⁵:

$$\bar{H} = \int d\omega \omega b_\omega^\dagger b_\omega + \bar{g}_b \int d\omega b_\omega \bar{a}^\dagger + \bar{g}_b^* \int d\omega b_\omega^\dagger \bar{a}$$

Moreover since we are not interested in quantitatively accounting for the possible distortion of the wavepacket due to the cavity response, we shall assume its decay rate $\bar{\gamma}_c$ is much bigger than the spectral width of the incoming photon ($\bar{\gamma}_c \rightarrow \infty$) or equivalently

⁵All barred quantities correspond to the reference situation.

the coupling strength to the bath modes g_b is infinite. This assumption legitimates the steady state approximation for the cavity field in Eq. (5.6):

$$\bar{a}(\omega) \underset{\bar{\gamma}_c \rightarrow \infty}{\approx} \frac{\sqrt{2\bar{\gamma}_c} \bar{a}_{in}(\omega)}{\bar{\gamma}_c}$$

The input-output relation that corresponds to the reference situation above is therefore

$$\begin{aligned} \bar{a}_{out}(\omega) &= \frac{2\bar{\gamma}_c \bar{a}_{in}(\omega)}{\bar{\gamma}_c} - \bar{a}_{in}(\omega) \\ &= \bar{a}_{in}(\omega) \end{aligned}$$

Since in the reference situation the photon does not entangle with the atoms, its state $|\bar{\phi}(t_f)\rangle$ can be evaluated independently at time t_f after the scattering took place and is given by (using $\bar{a}_{out}(\omega) \equiv b_\omega(t_f) e^{i\omega t_f}$ and $\bar{a}_{in}(\omega) \equiv b_\omega$ (Walls and Milburn, 2007))

$$\begin{aligned} |\bar{\phi}(t_f)\rangle &= e^{-i\bar{H}t_f} \int \beta(\omega) b_\omega^\dagger |\emptyset\rangle \\ &= \int \beta(\omega) b_\omega^\dagger(t_f) |\emptyset\rangle \\ &= \int \beta(\omega) \bar{a}_{out}^\dagger(\omega) e^{i\omega t_f} |\emptyset\rangle \\ &= \int \beta(\omega) \bar{a}_{in}^\dagger(\omega) e^{i\omega t_f} |\emptyset\rangle \\ |\bar{\phi}(t_f)\rangle &= - \int \beta(\omega) b_\omega^\dagger e^{i\omega t_f} |\emptyset\rangle \end{aligned} \tag{5.10}$$

5.2.3 Cavity with non-interacting two-level atoms

In this subsection, we introduce the formalism that we shall use in the next sections to analyze the gate performance on the simple example of a cavity filled with non-interacting two-level atoms. The Hamiltonian for this system can be readily obtained from Eq. (5.5) with $\Omega_{cf} = 0$

$$H_{2lev} \underset{\Omega_{cf} \rightarrow 0}{\equiv} H$$

Assuming the same initial state is $|\phi_0\rangle = \int d\omega \beta(\omega) b_\omega^\dagger |\emptyset\rangle$ as above, the state of the full system at time t_f is given by:

$$|\phi(t_f)\rangle = e^{-iHt_f} |\phi_0\rangle$$

5. Photonic phase gate

To compare the actual scattering process to the reference situation we now consider the following scalar product, henceforth referred to as “scattering coefficient”:

$$\begin{aligned}
& \langle \bar{\phi}(t_f) | \phi(t_f) \rangle \\
&= - \left\langle \emptyset \left| \left\{ \int d\omega' b_{\omega'} e^{i\omega' t_f} \beta^*(\omega') \right\} e^{-iH_{2lev} t_f} \right| \phi_0 \right\rangle \\
&= - \left\langle \emptyset \left| \left\{ \int d\omega' e^{-iH_{2lev} t_f} e^{iH_{2lev} t_f} b_{\omega'} e^{-iH_{2lev} t_f} e^{i\omega' t_f} \beta^*(\omega') \right\} \right| \phi_0 \right\rangle \\
&= - \left\langle \emptyset \left| \int d\omega' b_{\omega'}(t_f) e^{i\omega' t_f} \beta^*(\omega') \int d\omega b_{\omega}^{\dagger} \beta(\omega) \right| \phi_0 \right\rangle \\
&= - \left\langle \emptyset \left| \int d\omega' a_{out}(\omega') \beta^*(\omega') \right| \phi_0 \right\rangle
\end{aligned}$$

where we implicitly used the following relation and definitions:

$$\begin{aligned}
e^{-iH_{2lev} t} |\emptyset\rangle &= |\emptyset\rangle \\
b_{\omega'}(t_f) &\equiv e^{iH_{2lev} t_f} b_{\omega'} e^{-iH_{2lev} t_f} \\
a_{out}(\omega) &\equiv b_{\omega}(t_f) e^{i\omega t_f}
\end{aligned}$$

Moreover, for a cavity filled with non-interacting atoms, the linearized set of Heisenberg-Langevin equations for a in Fourier space yields $a(\omega) = \frac{\sqrt{2}\gamma_c}{\gamma_c + \frac{g^2 N}{\gamma_e - i\omega} - i\omega} a_{in}(\omega)$, whence

$$\begin{aligned}
& \langle \bar{\phi}(t_f) | \phi(t_f) \rangle \\
&= - \left\langle \emptyset \left| \int d\omega a_{out}(\omega) \beta^*(\omega) \right| \phi_0 \right\rangle \tag{5.11}
\end{aligned}$$

$$\begin{aligned}
&= - \left\langle \emptyset \left| \int d\omega \left(\sqrt{2}\gamma_c a(\omega) - a_{in}(\omega) \right) \beta^*(\omega) \right| \phi_0 \right\rangle \\
&= \int d\omega \frac{\gamma_c - \frac{g^2 N}{\gamma_e - i\omega} + i\omega}{\gamma_c + \frac{g^2 N}{\gamma_e - i\omega} - i\omega} |\beta(\omega)|^2 \tag{5.12}
\end{aligned}$$

where we used $a_{in}(\omega) |\phi_0\rangle \equiv b_{\omega} \int d\omega' b_{\omega'}^{\dagger} \beta(\omega') |\emptyset\rangle = -\beta(\omega) |\emptyset\rangle$ ⁶.

Finally we consider two limiting cases of the formula (5.12). If the number of atoms in the ensemble is very large (*i.e.* $N \rightarrow \infty$) the absorption in the cavity is increased and

$$\langle \bar{\phi} | \phi \rangle_{N \rightarrow \infty} \approx -1$$

⁶We note that from Eq. (5.12) in the long-pulse (steady state) limit, *i.e.* $|\beta(\omega)|^2 = \delta(\omega)$, we recover the formula for \mathcal{R} used in Sec. 5.1.

On the other hand if the number of atoms is very small ($N \rightarrow 0$), that is in the empty cavity case we find

$$\langle \bar{\phi} | \phi \rangle_{N \rightarrow 0} = \int d\omega \frac{\gamma_c + i\omega}{\gamma_c - i\omega} |\beta(\omega)|^2 \underset{|\beta(\omega)|^2 \rightarrow \delta(\omega)}{\approx} 1$$

In the next section we shall apply the same technique to evaluate the scattering coefficient relative to the full system and deduce a quantitative characterization of the gate performance.

5.3 Gate operation

In this section, we investigate the performance of the gate described in Sec. 5.1. Given the qubit encoding Eqs. (5.1-5.4) we will compute the scattering coefficient $\langle \bar{\phi}(t_f) | \phi(t_f) \rangle$ for each of the four following initial states:

- $|00\rangle$ –no stored excitation, no incoming photon
- $|10\rangle$ –one stored excitation and no incoming photon
- $|01\rangle$ –no stored excitation and one incoming photon
- $|11\rangle$ –one stored excitation and one incoming photon

We demonstrate that, following the naive picture presented in the introduction (Sec. 5.1), for sufficiently large cooperativity per blockade sphere the evolution with respect to H Eq. (5.5) achieves the desired control phase gate operation.

5.3.1 Evolution of $|00\rangle, |10\rangle$

We start this section by considering the trivial cases $|00\rangle$ and $|10\rangle$, corresponding to no incoming photon, an excitation being stored or not in the cavity. Obviously, in those cases the real and reference situations lead to the same evolution, *i.e.*, $\langle \bar{00}(t_f) | 00(t_f) \rangle = \langle \bar{10}(t_f) | 10(t_f) \rangle = 1$.

5.3.2 Evolution of $|01\rangle$

We now consider the initial state $|01\rangle$ *i.e.* when target photon scatters on the cavity which initially contains no excitation. The “real” and “reference” states of the bath are therefore the same, as in the previous case. The only difference comes from the cavity dynamics. From Heisenberg-Langevin equations:

$$\begin{aligned}\frac{d}{dt}a &= -\gamma_c a - ig \sum_i \sigma_{ge}^{(i)} + \sqrt{2\gamma_c} a_{in} \\ \frac{d}{dt}\sigma_{ge}^{(i)} &= -\gamma_e \sigma_{ge}^{(i)} - iga - i\frac{\Omega_{cf}}{2}\sigma_{gr}^{(i)} \\ \frac{d}{dt}\sigma_{gr}^{(i)} &= -i\frac{\Omega_b}{2}\sigma_{ge}^{(i)}\end{aligned}$$

we get in Fourier space

$$a(\omega) = \frac{\sqrt{2\gamma_c}}{\left(\gamma_c - i\omega + \frac{g^2 N}{\left(\gamma_e - i\omega + i\frac{\Omega_{cf}}{4\omega}\right)}\right)} a_{in}(\omega)$$

and upon recalling Eq. (5.10), we finally compute the desired scattering coefficient

$$\begin{aligned}\langle \overline{01}(t_f) | 01(t_f) \rangle &= -\left\langle \emptyset \left| \int d\omega a_{out}(\omega) \beta^*(\omega) \right| 01 \right\rangle \\ &= -\left\langle \emptyset \left| \int d\omega \left(\sqrt{2\gamma_c} a(\omega) - a_{in}(\omega) \right) \beta^*(\omega) \right| 01 \right\rangle \\ &= -\left\langle \emptyset \left| \int d\omega \left(\frac{\gamma_c + i\omega - \frac{g^2 N}{\left(\gamma_e - i\omega + i\frac{\Omega_{cf}}{4\omega}\right)}}{\gamma_c - i\omega + \frac{g^2 N}{\left(\gamma_e - i\omega + i\frac{\Omega_{cf}}{4\omega}\right)}} \right) a_{in}(\omega) \beta^*(\omega) \right| 01 \right\rangle \\ \langle \overline{01}(t_f) | 01(t_f) \rangle &= \int d\omega |\beta(\omega)|^2 \frac{\gamma_c + i\omega - \frac{g^2 N}{\left(\gamma_e - i\omega + i\frac{\Omega_{cf}}{4\omega}\right)}}{\gamma_c - i\omega + \frac{g^2 N}{\left(\gamma_e - i\omega + i\frac{\Omega_{cf}}{4\omega}\right)}}\end{aligned}$$

Let us remark that setting $\Omega_{cf} = 0$ we recover the expression obtained in Eq. (5.12)

5.3.3 Evolution of $|11\rangle$

In this case, the initial state of the system is defined by $|11\rangle = S^\dagger \int d\omega b_\omega^\dagger \beta(\omega) |\emptyset\rangle$. The state of the system at time t_f in the reference and real situations are given by:

$$|\overline{11}(t_f)\rangle = -S^\dagger \int d\omega b_\omega^\dagger e^{-i\omega t_f} \beta(\omega) |\emptyset\rangle \quad (5.13)$$

$$|11(t_f)\rangle = e^{-iHt_f} S^\dagger \int d\omega b_\omega^\dagger \beta(\omega) |\emptyset\rangle \quad (5.14)$$

respectively. In Eq. (5.13) we implicitly used the fact that in the reference configuration, the polariton does not evolve in time. The scattering coefficient is therefore given by:

$$\begin{aligned} & \langle \overline{11}(t_f) | 11(t_f) \rangle \\ &= -\left\langle \emptyset \left| S \int d\omega b_\omega e^{i\omega t_f} \beta(\omega) e^{-iHt_f} \right| 11 \right\rangle \\ &= -\left\langle \emptyset \left| S(t_f) \int d\omega b_\omega(t_f) e^{i\omega t_f} \beta^*(\omega) \right| 11 \right\rangle \\ &= -\left\langle \emptyset \left| S(t_f) \int d\omega a_{out}(\omega) \beta^*(\omega) \right| 11 \right\rangle \\ &= -\left\langle \emptyset \left| S(t_f) \int d\omega \left(\sqrt{2\gamma_c} a(\omega) - a_{in}(\omega) \right) \beta^*(\omega) \right| 11 \right\rangle \\ &= -\sqrt{2\gamma_c} \int d\omega \beta^*(\omega) \langle \emptyset | S(t_f) a(\omega) | 11 \rangle - \left(\int d\omega |\beta(\omega)|^2 \right) \langle \emptyset | S(t_f) S^\dagger | \emptyset \rangle \\ &= -\sqrt{2\gamma_c} \int d\omega \beta^*(\omega) \langle \emptyset | S(t_f) a(\omega) | 11 \rangle - 1 \end{aligned}$$

where we employed

$$\begin{aligned} S(t_f) &\equiv e^{iHt_f} S e^{-iHt_f} \\ b_\omega(t_f) &\equiv e^{iHt_f} b_\omega e^{-iHt_f} \\ a_{out}(\omega) &\equiv b_\omega(t_f) e^{i\omega t_f} \\ \langle \emptyset | e^{-iHt_f} &= \langle \emptyset | \\ \int d\omega |\beta(\omega)|^2 &= 1 \\ \langle \emptyset | S(t_f) S^\dagger | \emptyset \rangle &= 1 \end{aligned}$$

We now compute $\langle \emptyset | S(t_f) a(\omega) | 11 \rangle$. First, we notice that the term $\langle \emptyset | S(t_f) a(\omega) | 11 \rangle$ can be put under the form:

$$\langle \emptyset | S(t_f) a(\omega) | 11 \rangle = \frac{1}{N} \sum_{i,j} \left\langle \emptyset \left| \sigma_{gr'}^{(i)}(t_f) a(\omega) \right| r'_j, 1_\beta \right\rangle$$

5. Photonic phase gate

where $|r'_j, 1_\beta\rangle \equiv \sigma_{r'_j g}^{(j)} \int d\omega \beta(\omega) b_\omega^\dagger |\mathcal{O}\rangle$. Moreover $\langle \mathcal{O} | \sigma_{gr'}^{(i)}(t_f) a(\omega) | r'_j, 1_\beta \rangle$ is readily obtained through Fourier transforming the following differential system, derived from the Heisenberg-Langevin equations:

$$\begin{aligned} \frac{d}{dt} \langle \mathcal{O} | \sigma_{gr'}^{(i)}(t_f) a(t) | r'_j, 1_\beta \rangle &= -\gamma_c \langle \mathcal{O} | \sigma_{gr'}^{(i)}(t_f) a(t) | r'_j, 1_\beta \rangle \\ &\quad - ig \sum_k \langle \mathcal{O} | \sigma_{gr'}^{(i)}(t_f) \sigma_{ge}^{(k)}(t) | r'_j, 1_\beta \rangle \\ &\quad - \sqrt{2\gamma_c} \beta(t) \langle \mathcal{O} | \sigma_{gr'}^{(i)}(t_f) | r'_j, 1_\beta \rangle \\ \frac{d}{dt} \langle \mathcal{O} | \sigma_{gr'}^{(i)}(t_f) \sigma_{ge}^{(k)}(t) | r'_j, 1_\beta \rangle &= -\gamma_e \langle \mathcal{O} | \sigma_{gr'}^{(i)}(t_f) \sigma_{ge}^{(k)}(t) | r'_j, 1_\beta \rangle \\ &\quad + ig(\delta_{kj} - 1) \langle \mathcal{O} | \sigma_{gr'}^{(i)}(t_f) a(t) | r'_j, 1_\beta \rangle \\ &\quad - i\frac{\Omega_{cf}}{2} \langle \mathcal{O} | \sigma_{gr'}^{(i)}(t_f) \sigma_{gr}^{(k)}(t) | r'_j, 1_\beta \rangle \\ \frac{d}{dt} \langle \mathcal{O} | \sigma_{gr'}^{(i)}(t_f) \sigma_{gr}^{(k)}(t) | r'_j, 1_\beta \rangle &= -i\frac{\Omega_b}{2} \langle \mathcal{O} | \sigma_{gr'}^{(i)}(t_f) \sigma_{ge}^{(k)}(t) | r'_j, 1_\beta \rangle \\ &\quad - iV_{kj} \langle \mathcal{O} | \sigma_{gr'}^{(i)}(t_f) \sigma_{gr}^{(k)}(t) | r'_j, 1_\beta \rangle \end{aligned}$$

We find

$$\langle \mathcal{O} | \sigma_{gr'}^{(i)}(t_f) a(\omega) | r'_j, 1_\beta \rangle = -\frac{\sqrt{2\gamma_c} \beta(\omega) \delta_{ij}}{\left(\gamma_c - i\omega + \frac{g^2 N}{\gamma_e} \frac{1}{N} \sum_{k \neq j} \frac{\gamma_e}{\left(\gamma_e - i\omega - i\frac{\Omega_{cf}^2}{4(V_{kj} - \omega)} \right)} \right)}$$

and therefore

$$\langle \mathcal{O} | S(t_f) a(\omega) | 11 \rangle = -\frac{1}{N} \sum_i \frac{\sqrt{2\gamma_c} \beta(\omega)}{\left(\gamma_c - i\omega + \frac{g^2 N}{\gamma_e} \frac{1}{N} \sum_{k \neq i} \frac{\gamma_e}{\left(\gamma_e - i\omega - i\frac{\Omega_{cf}^2}{4(V_{ki} - \omega)} \right)} \right)}$$

Assuming the sample is homogeneous, with no edge effects, and defining

$$\frac{V_b(\omega)}{V} \equiv \frac{1}{N} \sum_{k \neq i} \frac{\gamma_e}{\left(\gamma_e - i\omega - i\frac{\Omega_{cf}^2}{4(V_{ki} - \omega)} \right)}$$

where assumed that the latter expression does not depend on the i index, we get

$$\langle \emptyset | S(t_f) a(\omega) | 11 \rangle \approx - \frac{\sqrt{2\gamma_c} \beta(\omega)}{\left(\gamma_c - i\omega + \frac{g^2 N}{\gamma_e} \frac{V_b(\omega)}{V} \right)}$$

Finally, we obtain the following scattering coefficient:

$$\langle \overline{11}(t_f) | 11(t_f) \rangle = 2\gamma_c \int d\omega \frac{|\beta(\omega)|^2}{\left(\gamma_c - i\omega + \frac{g^2 N}{\gamma_e} \frac{V_b(\omega)}{V} \right)} - 1$$

If we further assume the photon wavepacket is long enough (steady state approximation), we get the simplified form

$$\begin{aligned} \langle \overline{11}(t_f) | 11(t_f) \rangle &\approx \frac{2\gamma_c}{\left(\gamma_c + \frac{g^2 N}{\gamma_e} \frac{V_b}{V} \right)} - 1 \\ &= \frac{\gamma_c - \frac{g^2 N}{\gamma_e} \frac{V_b}{V}}{\gamma_c + \frac{g^2 N}{\gamma_e} \frac{V_b}{V}} \\ &= \frac{1 - 2C_b}{1 + 2C_b} \end{aligned}$$

where we introduced $C_b \equiv \frac{g^2 N}{2\gamma_e \gamma_c} \frac{V_b(0)}{V} = \frac{g^2}{2\gamma_e \gamma_c} n_b$ which can be interpreted as the cooperativity per blockade sphere (n_b is the number of atoms per bubble).

In the next section we shall use the results obtained above for the different initial states to evaluate the gate fidelity in experimentally feasible situations.

5.4 Numerical results

In this section, we quantitatively estimate the performance of the gate protocol by means of the so-called Choi-Jamiolkowski fidelity, that we readily compute using the results of the previous section. Then we introduce the dual-rail encoding version of the protocol, where both logic states $|0\rangle$ and $|1\rangle$ are physically encoded in two states of a single photon propagating along two spatially distinct paths. This encoding allows for postselection, therefore correcting possible photon-loss-induced errors during the gate operation. Finally, we evaluate fidelities for the single- and dual-rail versions of the protocol as functions of the cooperativity per blockade volume.

5.4.1 Choi-Jamiolkowsky fidelity

To evaluate the performance of the proposed C-PHASE gate we shall calculate its Choi-Jamiolkowski fidelity (Choi, 1975; Jamiolkowski, 1972). Since, in general, we have $C > C_b$, the fidelity will be mainly limited by the target photon scattering process

5. Photonic phase gate

and we may therefore safely ignore the imperfections of the storage/retrieval of the control photon. With the above solution to the scattering problem we have a complete characterization of the gate dynamics.

To translate this into the Choi-Jamiolkowski fidelity, we consider the input state $|\Phi\rangle \equiv \frac{1}{2}(|00\rangle|00\rangle + |01\rangle|01\rangle + |10\rangle|10\rangle + |11\rangle|11\rangle)$ of a system of four qubits, two of which, e.g. the third and the fourth ones, are subject to the gate, while the other two are left alone. The final state ($t = t_f$) is therefore given by $|\Phi_{real}\rangle = (\mathbb{I} \otimes e^{-iHt_f}) |\Phi\rangle$ which represents the evolution of the third and fourth qubits under the Hamiltonian Eq. (5.5). By contrast, the state resulting from the action of the ideal C-PHASE gate on $|\Phi\rangle$ can be expressed by means of the evolved reference states $|\bar{ij}\rangle(t_f)$ (see Sec. 5.2) as:

$$|\Phi_{ideal}\rangle = \mathbb{I} \otimes U e^{-iH_{ref}t_f} |\Phi\rangle = \sum_{ij=0,1} \langle ij | \text{CPHASE} | ij \rangle |ij\rangle |\bar{ij}\rangle(t_f)$$

with

$$\text{CPHASE} = \begin{pmatrix} 1 & 0 & 0 & 0 \\ 0 & 1 & 0 & 0 \\ 0 & 0 & 1 & 0 \\ 0 & 0 & 0 & -1 \end{pmatrix}$$

The fidelity is therefore given by:

$$\begin{aligned} F_{cj} &\equiv |\langle \Phi_{ideal} | \Phi_{real} \rangle|^2 & (5.15) \\ &= \frac{1}{16} |\langle \bar{00}(t_f) | 00(t_f) \rangle + \langle \bar{01}(t_f) | 01(t_f) \rangle + \langle \bar{10}(t_f) | 10(t_f) \rangle - \langle \bar{11}(t_f) | 11(t_f) \rangle|^2 \\ &= \frac{1}{16} |2 + \langle \bar{10}(t_f) | 10(t_f) \rangle - \langle \bar{11}(t_f) | 11(t_f) \rangle|^2 \\ &= \frac{1}{16} \left| 2 + \int d\omega |\beta(\omega)|^2 \frac{\gamma_c + i\omega - \frac{g^2 N}{\left(\gamma_e - i\omega + i\frac{\Omega_{cf}^2}{4\omega}\right)}}{\gamma_c - i\omega + \frac{g^2 N}{\left(\gamma_e - i\omega + i\frac{\Omega_{cf}^2}{4\omega}\right)}} - \int d\omega |\beta(\omega)|^2 \frac{\gamma_c + i\omega - \frac{g^2 N}{\gamma_e} \frac{V_b(\omega)}{V}}{\left(\gamma_c - i\omega + \frac{g^2 N}{\gamma_e} \frac{V_b(\omega)}{V}\right)} \right|^2 \end{aligned}$$

The steady state limit ($|\beta(\omega)|^2 \rightarrow \delta(\omega)$) of this expression yields

$$F_{cj} \equiv \frac{1}{16} \left| 3 - \frac{1 - 2C_b}{1 + 2C_b} \right|^2 \quad (5.16)$$

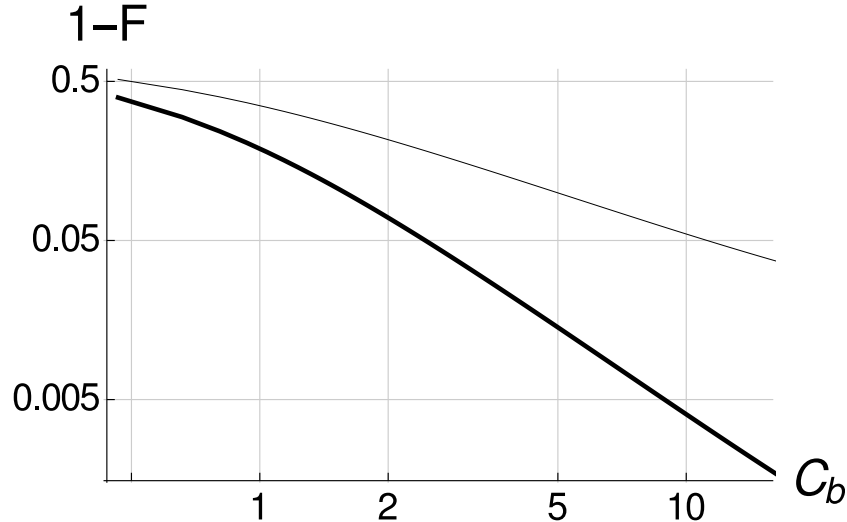


Figure 5.3: Choi-Jamiolkowski fidelity (thin line) and postselected swap fidelity (thick line) as functions of the blocked cooperativity C_b for a spectrally narrow pulse $|\beta(\omega)|^2 \rightarrow \delta(\omega)$.

where $C_b \equiv \frac{g^2 N V_b}{\gamma_e V}$ (see Sec. 5.3). As can be seen from Eq. (5.16), in the limit of big cooperativity per blockade sphere, the fidelity approaches unity ($1 - F_{cj} \propto \frac{1}{|C_b|}$) (see Fig. 5.3). Therefore, as discussed in the introduction (Sec. 5.1), the cavity-enhanced blocked cooperativity is the main figure of merit for the gate.

5.4.2 Dual rail encoding

In the dual-rail encoding, both logical states $|0\rangle$ and $|1\rangle$ are encoded in two states of a single photon propagating along two spatially distinct paths. A schematic of the dual-rail C-PHASE gate is shown in Fig. 5.1 (c). The first photon pulse in the upper two arms of the figure is first stored in one of the memories consisting of a Rydberg ensemble placed in each arm (in the case polarization encoding, two such memories might be realized by two different internal states of the same ensemble). A second photon pulse is then scattered from the Rydberg ensemble if it is in state $|1\rangle$ (upper rail in the figure). This scattering ideally induces a phase change of π if there was a photon stored in the Rydberg ensemble, *i.e.*, if both qubits were in state $|1\rangle$.

As opposed to the single-rail implementation, the dual-rail allows one to condition the gate's operation on getting two photons in the output. Since the dominant source of error in the single-rail implementation is the photon loss, this offers a substantial increase in the fidelity with only a minor failure probability of the gate. We consider the conditional fidelity of a maximally entangled two-qubit state resulting from an entanglement swap realized with the gate using the full circuit drawn in Fig. 5.1 (c). Neglecting again the error due to finite storage efficiency, we find that this fidelity is (see App. H for more details):

$$\begin{aligned}
 F_{swap} & \tag{5.17} \\
 &= \frac{1}{16P_{suc}} \left| 2 + \int d\omega |\beta(\omega)|^2 \left(\frac{\gamma_c + i\omega - \frac{g^2 N}{\left(\gamma_e - i\omega + i\frac{\Omega_{cf}^2}{4\omega}\right)}}{\gamma_c - i\omega + \frac{g^2 N}{\left(\gamma_e - i\omega + i\frac{\Omega_{cf}^2}{4\omega}\right)}} - \frac{\gamma_c + i\omega - \frac{g^2 N}{\gamma_e} \frac{V_b(\omega)}{V}}{\gamma_c - i\omega + \frac{g^2 N}{\gamma_e} \frac{V_b(\omega)}{V}} \right) \right|^2
 \end{aligned}$$

where

$$\begin{aligned}
 P_{suc} & \\
 &= \frac{1}{4} \left(2 + \left| \int d\omega |\beta(\omega)|^2 \frac{\gamma_c + i\omega - \frac{g^2 N}{\left(\gamma_e - i\omega + i\frac{\Omega_{cf}^2}{4\omega}\right)}}{\gamma_c - i\omega + \frac{g^2 N}{\left(\gamma_e - i\omega + i\frac{\Omega_{cf}^2}{4\omega}\right)}} \right|^2 + \left| \int d\omega |\beta(\omega)|^2 \frac{\gamma_c + i\omega - \frac{g^2 N}{\gamma_e} \frac{V_b(\omega)}{V}}{\gamma_c - i\omega + \frac{g^2 N}{\gamma_e} \frac{V_b(\omega)}{V}} \right|^2 \right)
 \end{aligned}$$

Note that, compared to F_{c_j} in Eq. (5.15), the only difference is due to the conditioning with the success probability $P_{suc} < 1$.

Let us now consider the steady state limit of Eq. 5.17:

$$F_{swap} = \frac{\left| 3 - \frac{1-2C_b}{1+2C_b} \right|^2}{4 \left(3 + \left| \frac{1-2C_b}{1+2C_b} \right|^2 \right)}$$

In the limit of a long pulse, we thus see that the conditional gate error $1 - F_{swap} \propto \frac{1}{|C_b|^2}$ for $C_b \gg 1$ is much smaller than for the single rail. This comes at only a minor cost in the failure probability $1 - P_{suc} \propto \frac{1}{|C_b|}$. The resulting dual-rail fidelities are plotted in Fig. 5.3 as a function of the parameter C_b . For $C_b \approx 8$, the (postselected) fidelity is found to be larger than 0.99.

5.5 Conclusions

In this chapter, we proposed an efficient method to implement a C-PHASE gate for photonic qubits. The gate combines the advantages of cavity-defined optical modes and cavity-enhanced light-matter interactions with the strong Rydberg blockade obtainable in atomic ensembles. As a direct application, the proposed gate can be used to improve the communication rate of quantum repeaters. More generally it may serve as a building block for photonic quantum networks (Das et al., 2016).

Chapter 6

Outlook

In this dissertation, we theoretically studied the reflection and transmission of an optical cavity filled with an ensemble of ladder-type three-level atoms, whose lower transition, from the ground to the low-lying intermediate states, is driven by the cavity mode, while the upper transition, from the intermediate to a Rydberg excited states, is driven by a strong control field. Because of the large dipole-dipole interactions between Rydberg atoms, the response of the setup is expected to be strongly nonlinear, allowing for optical nonlinearities even at the single-photon level, which constitute the key ingredient of photonic quantum information processing.

We investigated both the resonant and dispersive regimes of the setup, *i.e.* when the transition from the ground to intermediate states is resonant with the cavity mode or not, and demonstrated that a quasi-classical input beam can be made highly non-classical when reflected from or transmitted through the cavity. Strong correlations between photons were shown to appear, manifesting themselves in the behavior of the pair-correlation function and revealing effective intracavity photon-photon interactions. Depending on the physical parameters of the system, its response can be drastically different to the single- and two-photon components of the incident light which, effectively turns the setup into a filter that operates in the quantum regime. Resorting to many-body physics techniques, namely to the Schwinger-Keldysh contour formalism, we were able to compute correlation functions beyond the lowest non-vanishing order in the excitation number. We also demonstrated that, due to dipole-dipole interactions, the light transmitted through the cavity becomes non-monochromatic: along with the broadening, it was indeed shown to acquire sidebands, whose frequencies are defined by the intracavity polariton energies. Finally we demonstrated that, combined with the photon storage techniques, our setup can operate as a high fidelity C-PHASE gate.

Several aspects of the problem remain to be addressed in the future.

Throughout this dissertation our calculations were restricted to the weak cavity feeding regime. More specifically, all our results were obtained by discarding the Fock components of the incoming coherent light beam with more than two photons. Many phenomena are however expected to take place beyond the two-photon regime, as re-

6. Outlook

cently demonstrated in free-space configuration (Bienias and Büchler, 2016; Jachymski et al., 2016). The method presented in Chap. 4 actually may be extended to higher excitation numbers, by means of the multi-particle scattering theory developed by Faddeev (Faddeev, 1961). Well-known in few-body physics, this theory allows to regroup Feynman diagrams for photon components higher than two in a systematic way which facilitates their subsequent resummation.

In this thesis, we generally considered the steady state regime of the cavity feeding. Many applied problems, however, may involve time-dependent incoming photon wavepacket. The latter regime can be well addressed by a straightforward modification of the formalism, presented in Chap. 4.

As shown in App. A, while the experimentally observed behavior of the setup is well reproduced by our theoretical model when S-Rydberg states are excited, it significantly differs in the case of D states. Elucidating that point will surely require to go beyond the simple three-level model we employed throughout this dissertation and incorporate extra states not directly addressed by the laser but coupled to the Rydberg state considered in our protocol, whose effect would be to “shelve” excitation.

Finally, within the past few years, much effort has been devoted to developing quantum platforms using interacting photons to simulate various models taken from condensed matter physics (Carusotto and Ciuti, 2013). In particular, it has recently been suggested to use dispersive EIT with a Rydberg medium coupled to different degenerate spatial modes of a linear optical cavity to implement crystalline order and fractional quantum Hall states of light (Sommer et al., 2015). The latter proposal actually relies on an *ad hoc* effective interaction potential between dark-state polaritons. The “*ab initio*” approach we used in Chap. 4 may allow us to clarify the range of applicability of such an approximate description and to go beyond by considering, e.g., the resonant regime of EIT.

Appendix A

Transmission of an intracavity Rydberg medium: experimental results vs theoretical methods

In this appendix, we present variants of the models developed in Chaps. 2 and 3, which were recently put forward (Boddeda et al., 2016) to account for different features of the transmission spectrum of a cavity filled with a Rydberg EIT medium, experimentally observed at IOGS.

In the first section, we derive a mean-field description from the bosonic model proposed in Chap. 3 which satisfactorily reproduces the experimental data obtained in the case of S-Rydberg states but fails for D-Rydberg states. To deal with the latter, in Sec. A.2, we elaborate on the Rydberg bubble model, used in Chap. 2 that we combine with a phenomenological decay towards an extra shelving Rydberg state; the resulting model successfully fits the data upon adjusting the free parameters.

A.1 S-Rydberg state

In this section, we present a mean-field approximation of the three-boson model developed in Chap. 3, and show that it satisfactorily accounts for the transmission of an S-excited Rydberg EIT medium, experimentally observed at IOGS.

A.1.1 Presentation of the model

As shown in Eqs. (3.13-3.15), the expectation values $\langle a \rangle$, $\langle b \rangle$, $\langle c \rangle$ for the cavity mode annihilation operator and the collective atomic operators

A. Transmission of an intracavity Rydberg medium: experimental results vs theoretical methods

$$b = \frac{1}{\sqrt{N}} \sum_i \sigma_{ge}^{(i)}$$

$$c = \frac{1}{\sqrt{N}} \sum_i \sigma_{gr}^{(i)}$$

are governed by the following dynamical equations:

$$\frac{d}{dt} \langle a \rangle = (i\Delta_c - \gamma_c) \langle a \rangle - ig\sqrt{N} \langle b \rangle - i\alpha \quad (\text{A.1})$$

$$\frac{d}{dt} \langle b \rangle = (i\Delta_e - \gamma_{ge}) \langle b \rangle - i\sqrt{N}g \langle a \rangle - i\frac{\Omega_{cf}}{2} \langle c \rangle \quad (\text{A.2})$$

$$\frac{d}{dt} \langle c \rangle = (i\Delta_r - \gamma_{gr}) \langle c \rangle - i\frac{\Omega_{cf}}{2} \langle b \rangle - i\kappa \langle c^\dagger cc \rangle \quad (\text{A.3})$$

where the complex constant κ characterizes the effect of dipole-dipole Rydberg interactions, and is given by

$$\kappa = -2 \left(\frac{V_b}{V - V_b} \right) \left(\frac{\Omega_{cf}^2}{4(D_e + D_r - \frac{\Omega_{cf}^2}{4(D_e)})} - (D_r) \right)$$

with

$$V_b = \frac{\sqrt{2}\pi^2}{3} \sqrt{\frac{C_6}{D_e - \frac{\Omega_{cf}^2}{4(D_e + D_r - \frac{\Omega_{cf}^2}{4D_e})}}} \quad (\text{A.4})$$

where $D_k \equiv \Delta_k + i\gamma_{gk}$ for $k = e, r$, V_b is the volume of a blockade sphere and V is the total volume of the cloud.

If the ratio V_b/V is small (high Rydberg bubble number regime) the state of the system can be approximately considered as coherent. We therefore apply to Eqs. (A.1-A.3) the so-called mean field approximation: it implies that the state of each boson is coherent and we therefore replace operators by the corresponding complex numbers: $a \rightarrow \langle a \rangle$, $b \rightarrow \langle b \rangle$, $c \rightarrow \langle c \rangle$. The corresponding system of equations is given by:

$$\frac{d}{dt} \langle a \rangle = (i\Delta_c - \gamma_c) \langle a \rangle - ig\sqrt{N} \langle b \rangle - i\alpha \quad (\text{A.5})$$

$$\frac{d}{dt} \langle b \rangle = (i\Delta_e - \gamma_{ge}) \langle b \rangle - i\sqrt{N}g \langle a \rangle - i\frac{\Omega_{cf}}{2} \langle c \rangle \quad (\text{A.6})$$

$$\frac{d}{dt} \langle c \rangle = (i\Delta_r - \gamma_{gr}) \langle c \rangle - i\frac{\Omega_{cf}}{2} \langle b \rangle - i\kappa |\langle c \rangle|^2 \langle c \rangle \quad (\text{A.7})$$

This system can be numerically solved in order to deduce the cavity transmission $T = \frac{\gamma_c^2 |\langle a \rangle|^2}{\alpha^2}$.

A.1.2 Comparison with the experimental data

In Fig. A.1.2 we provide the experimental results for the stationary cavity transmission spectrum using the following set of parameters $\Delta_c - \Delta_e = -3.2\text{MHz}$, $\Delta_r - \Delta_e = -1.2\text{MHz}$, $\gamma_r = 2\pi \times 0.42\text{MHz}$, $\gamma_c = 2\pi \times 10\text{MHz}$, $\Omega_{cf} = 2\pi \times 10\text{MHz}$, $C = 8$ (Boddeda et al., 2016).

Due to the dipole-dipole interactions of S-excited Rydberg atoms, the spectrum depends on the intensity of the incoming field. The results are fitted by the solution of Eqs. (A.5 - A.7) which appear to be in a reasonably good agreement.

As soon as D states are employed, however, the mean-field description fails to reproduce the behavior of the cavity transmission: in particular, in the case of D states, when the cavity is locked on resonance and a constant probe beam is sent through it, the transmission decreases on a slow ($10\mu s$) time scale. This feature does not show up with S-states, and is not accounted for by the mean-field model. We therefore need to develop a different phenomenological model model that we present in the next section.

A.2 D-Rydberg state

Here, we present the phenomenological model which was developed to account for the cavity transmission, in the case of *D*-Rydberg-state-excited samples. This model combines a modified version of the Rydberg bubble picture used in Chap. 2 with a phenomenological decay towards a shelving Rydberg state. The decay rate, left as a free parameter, can be adjusted in order to successfully reproduce the experimental data for both the static and dynamical transmission of the setup.

A.2.1 Presentation of the model

We assume that the Rydberg blockade phenomenon effectively splits the atomic sample into independent and equivalent “bubbles” which can at most accommodate for one Rydberg excitation. Accordingly, the two-photon transition towards the Rydberg level $|r\rangle$ essentially couples the two collective symmetric states

$$\begin{aligned} |G\rangle &\equiv |g \cdots g\rangle \\ |R\rangle &\equiv \frac{1}{\sqrt{n_b}} \sum_{i=1}^{n_b} \sigma_{rg}^{(i)} |G\rangle = \frac{1}{\sqrt{n_b}} (|rg \cdots g\rangle + \cdots |g \cdots gr\rangle) \end{aligned}$$

where n_b denotes the number of atoms in a Rydberg bubble, and the corresponding lowering operator is the Pauli-like matrix $\sigma_{GR} \equiv |G\rangle \langle R|$ (we also define $\sigma_{RR} \equiv |R\rangle \langle R|$ and $\sigma_{RG} \equiv |R\rangle \langle G|$). Note that n_b can be evaluated by $n_b = N \times \left| \frac{V_b}{V} \right|$, where N is the total number of atoms in the sample, V is the total volume of the sample and V_b is the

A. Transmission of an intracavity Rydberg medium: experimental results vs theoretical methods

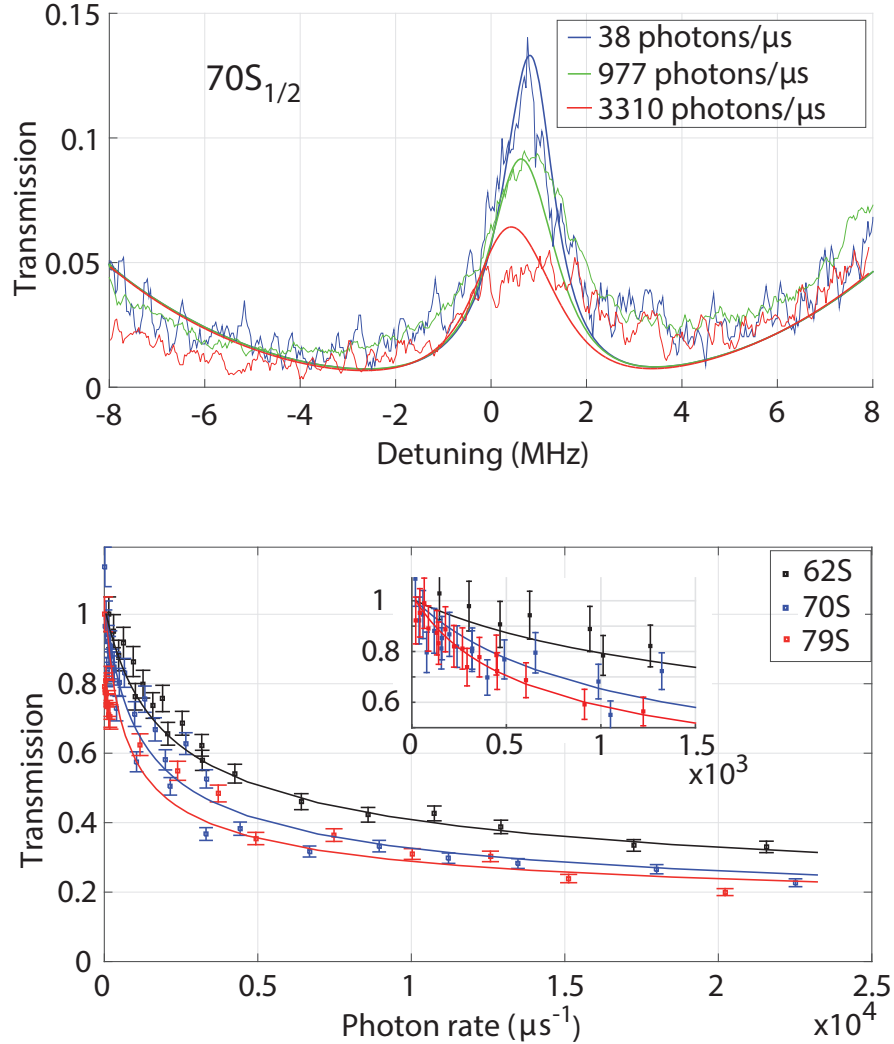


Figure A.1: a) The cavity transmission spectrum is plotted for various incoming probe photon rates for $70S_{1/2}$ Rydberg state of rubidium atom ^{87}Rb . (b) Cavity transmission at the center of the transparency window as a function of the probe photon rate, for various Rydberg levels. Each curve has been normalized to help their comparison and the inset gives a closer look of the transmission at low photon rates. One can observe the reduction of the transparency with higher photon rate due to the Rydberg blockade effect. The theory is in quite good agreement with the data at any detuning or Rydberg state.

volume of a Rydberg bubble whose expression was given in Eq. A.4.

In a Rydberg bubble, the intermediate state can, by contrast, be arbitrarily populated ; we, however, further assume that we remain in the low excitation regime (corresponding to moderate cavity feeding rates) so that the transition to the intermediate state is never saturated. In this approximation scheme, the collective lowering operator

$$\beta \equiv \frac{1}{\sqrt{n_b}} \sum_{i=1}^{n_b} \sigma_{ge}^{(i)}$$

can be satisfactorily considered bosonic, *i.e.* $[\beta, \beta^\dagger] \approx 1$.

Here, in order to account for the dynamical behavior observed experimentally, we moreover introduce an extra Rydberg state, denoted by $|s\rangle$, to which the state $|r\rangle$ decays: this implies that, in a bubble, the collective states $|R\rangle$ and $|S\rangle \equiv \frac{1}{\sqrt{n_b}} (|sg \cdots g\rangle + \cdots |g \cdots gs\rangle)$ are coupled by a Lindblad-like operator.

To simplify the treatment, we furthermore assume the cavity mode to be classical, that is we replace a by its expectation value $\langle a \rangle$ whose time evolution is therefore ruled by the equation

$$\frac{d}{dt} \langle a \rangle = i(\Delta_c + i\gamma_c) \langle a \rangle - i \left(\frac{N}{n_b} \right) g\sqrt{n_b} \langle \beta \rangle - i\alpha$$

Note that the second term of the right hand side of this equation arises from the coupling of the cavity mode with the ensemble of $\left(\frac{N}{n_b} \right)$ Rydberg bubbles with the magnified coupling strength $g\sqrt{n_b}$. The first term accounts for the detuning and decay of the cavity, while the last one results from the feeding by the probe field. In this semi-classical approximation, bubbles do not entangle with the cavity mode and therefore cannot get entangled with each other: the atomic sample can hence be described by the tensor product density matrix $\rho \otimes \cdots \otimes \rho$ where ρ is the density matrix of any of the bubbles (they are all equivalent). The semi-classical dynamical equation for ρ now writes $\frac{d}{dt} \rho = -i[H, \rho] + \mathcal{D}_l(\rho) + \mathcal{D}_{nl}(\rho)$ where single-bubble Hamiltonian and decay operators are given by

$$\begin{aligned} H &= -\Delta_r |R\rangle \langle R| - \Delta_e \beta^\dagger \beta \\ &\quad + \left\{ \left(\frac{\Omega_{cf}}{2} \sigma_{RG} + g\sqrt{n_b} \langle a \rangle^* \right) \beta + \text{h.c.} \right\} \\ \mathcal{D}_l(\rho) &= \gamma_e (2\beta\rho\beta^\dagger - \beta^\dagger\beta\rho - \rho\beta^\dagger\beta) \\ &\quad + \gamma_r (2\sigma_{GR}\rho\sigma_{RG} - \sigma_{RR}\rho - \rho\sigma_{RR}) \\ &\quad + \gamma_s (2\sigma_{GS}\rho\sigma_{SG} - \sigma_{SS}\rho - \rho\sigma_{SS}) \\ \mathcal{D}_{nl}(\rho) &= \xi \langle \sigma_{RR} \rangle (2\sigma_{SR}\rho\sigma_{RS} - \sigma_{RR}\rho - \rho\sigma_{RR}) \end{aligned}$$

Note that the phenomenological extra non-linear decay $\mathcal{D}_{nl}(\rho)$ we introduced is time

A. Transmission of an intracavity Rydberg medium: experimental results vs theoretical methods

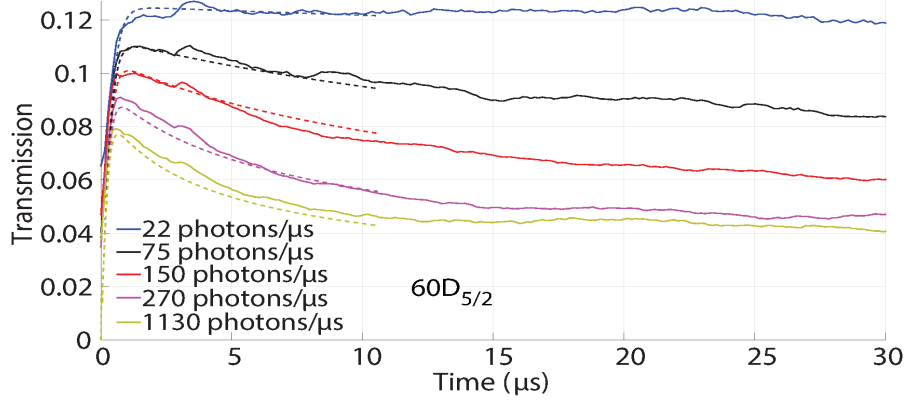


Figure A.2: Cavity transmission in EIT conditions (probe and control fields are on resonance) for $60D_{5/2}$ Rydberg state of rubidium atom. In addition to a decrease in transmission with the probe photon rate due to the Rydberg blockade, we observe a transmission decay over time for D states.

dependent through $\langle \sigma_{RR} \rangle (t)$; its rate is moreover governed by the *ad hoc* free parameter ξ , whose value can be tuned so as to reproduce the experimental results.

A.2.2 Experimental results vs theoretical methods

The experimental results for the time-dependent $T(t) = \gamma_c^2 |\langle a(t) \rangle|^2 / \alpha^2$ cavity transmission are shown on Fig. A.2 (Boddeda et al., 2016) using the same set of parameters as in Sec. A.1.2. The proper choice of the ξ parameter allows us to fit the experimental curves for all intensities. Besides, with the same value of ξ we recover the cavity transmission spectrum for the whole range of frequencies of the incident light as shown in Fig. A.3.

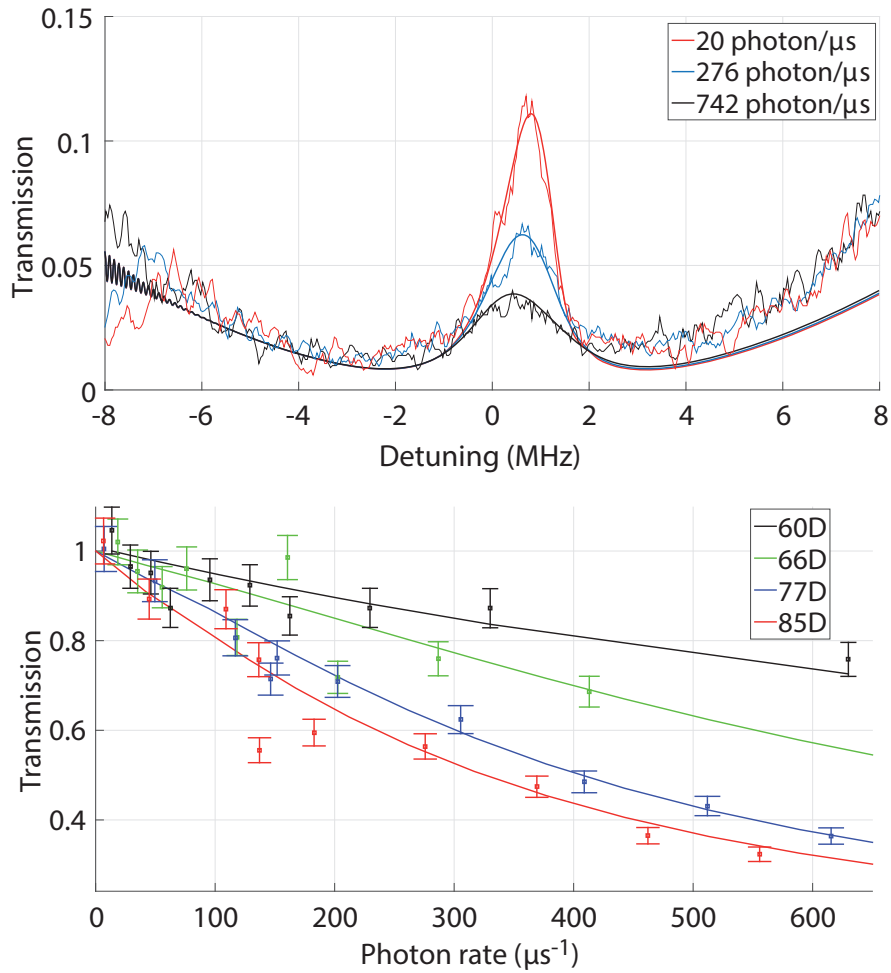


Figure A.3: (a) The cavity transmission spectrum is plotted for various incoming photon rates for $85D_{5/2}$ Rydberg state of rubidium atom ^{87}Rb (b) Cavity transmission at the center of the transparency window as a function of the incoming photon rate, for various Rydberg levels. The model including long-lived Rydberg atoms agrees well with the observed transmission data.

A. Transmission of an intracavity Rydberg medium: experimental results vs theoretical methods

Appendix B

Bosonic representation

B.1 Bosonic representation

In order to use Wick's theorem in Chap. 4 it is convenient to represent our system in terms of bosons.

Let us first illustrate the basic principle of this mapping on the simple example of a single atom coupled to two classical fields, driving the lower ($g \leftrightarrow e$) and upper ($e \leftrightarrow r$) transitions with the respective Rabi frequencies Ω_p and Ω_{cf} . Analogously to Chap. 1 we may write the Hamiltonian of this system in the RWA approximation under the form

$$H_{1at} = -\Delta_e \sigma_{ee} - \Delta_r \sigma_{rr} + \frac{\Omega_{cf}}{2} (\sigma_{er} + \sigma_{re}) + \frac{\Omega_p}{2} (\sigma_{ge} + \sigma_{eg})$$

or equivalently, in the matrix form (using the basis $\{|g\rangle, |e\rangle, |r\rangle\}$):

$$H_{1at} \rightarrow \begin{pmatrix} 0 & \frac{\Omega_p}{2} & 0 \\ \frac{\Omega_p}{2} & -\Delta_e & \frac{\Omega_{cf}}{2} \\ 0 & \frac{\Omega_{cf}}{2} & -\Delta_r \end{pmatrix} \quad (\text{B.1})$$

Let us now introduce two independent bosonic operators b and c ($[b, b^\dagger] = 1$, $[c, c^\dagger] = 1, [b, c] = 0, [b, c^\dagger] = 0$) that we shall identify with lowering operators σ_{ge} and σ_{gr} respectively, in the Hilbert space restricted to zero and one excitation. We moreover introduce the anharmonic Hamiltonian:

$$\begin{aligned} \tilde{H} &= -\Delta_e b^\dagger b - \Delta_r c^\dagger c + \frac{\Omega_p}{2} (b^\dagger + b) + \frac{\Omega_{cf}}{2} (c^\dagger b + b^\dagger c) \\ &+ \tilde{H}_{sat} \end{aligned} \quad (\text{B.2})$$

with

$$\tilde{H}_{sat} \equiv \frac{U_\infty}{2} b^\dagger b^\dagger b b + \frac{U_\infty}{2} c^\dagger c^\dagger c c + U_\infty b^\dagger b c^\dagger c$$

where U_∞ is some real-valued constant. We now show that, in certain circumstances,

B. Bosonic representation

the two Hamiltonians Eqs. (B.2,B.3) coincide. Consider the matrix representation of \tilde{H} in the basis $(|0, 0\rangle, |1, 0\rangle, |0, 1\rangle, |2, 0\rangle, |1, 1\rangle, |0, 2\rangle, \dots)$ where $|m, n\rangle \equiv \frac{(b^\dagger)^m (c^\dagger)^n}{\sqrt{m!} \sqrt{n!}} |0, 0\rangle$:

$$\begin{pmatrix} 0 & \frac{\Omega_p}{2} & 0 & 0 & 0 & 0 & \dots \\ \frac{\Omega_p}{2} & -\Delta_e & \frac{\Omega_{cf}}{2} & \frac{\Omega_p}{2}\sqrt{2} & 0 & 0 & \dots \\ 0 & \frac{\Omega_{cf}}{2} & -\Delta_r & 0 & \frac{\Omega_p}{2} & 0 & \dots \\ 0 & \frac{\Omega_p}{2}\sqrt{2} & 0 & -2\Delta_e + U_\infty & \frac{\Omega_{cf}}{2}\sqrt{2} & 0 & \dots \\ 0 & 0 & \frac{\Omega_p}{2} & \frac{\Omega_{cf}}{2}\sqrt{2} & -\Delta_e - \Delta_r + U_\infty & \frac{\Omega_{cf}}{2}\sqrt{2} & \dots \\ 0 & 0 & 0 & 0 & \frac{\Omega_{cf}}{2}\sqrt{2} & -2\Delta_r + U_\infty & \dots \\ \vdots & \vdots & \vdots & \vdots & \vdots & \vdots & \ddots \end{pmatrix} \quad (\text{B.3})$$

where vertical and horizontal lines separate subspaces with different excitation numbers. In Eq. B.3, diagonal elements in the subspaces with more than two excitations contain U_∞ . If $U_\infty = 0$, we merely recover a system of two coupled harmonic oscillators. By contrast, if we set $U_\infty \rightarrow \infty$ the subspaces with more than two excitations will become highly off-resonant and inaccessible from the zero and single excitation subspaces. Hence, the Hamiltonian \tilde{H} will effectively reduce to H_{1at} (Eq. (B.1)). It is worth noticing that \tilde{H}_{sat} accounts for the non-linearity due to the saturation of atomic transitions.

We may now extrapolate the representation to the N -atom ensemble described in Chap. 1 by defining two bosons b_i, c_i for each atom $i = 1, \dots, N$. The full Hamiltonian $H = H_0 + H_{int}$ contains the natural evolution part H_0 and the ‘‘interaction’’ part H_{int} which stands for the external feeding and quartic in operators:

$$H_0 = H_{at} + V_{a-c} + H_{cav} + H_{bath} + V_{cav-bath} + V_{at-bath} \quad (\text{B.4})$$

$$H_{int} = H_{dd} + H_{sat} + H_f \quad (\text{B.5})$$

$$H_{dd} = \frac{1}{2} \sum_{m,n}^N \kappa_{mn} c_m^\dagger c_n^\dagger c_m c_n \quad (\text{B.6})$$

$$H_f = \alpha (a + a^\dagger) \quad (\text{B.7})$$

$$H_{sat} = U_\infty \sum_n \left\{ \frac{1}{2} b_n^\dagger b_n^\dagger b_n b_n + \frac{1}{2} c_n^\dagger c_n^\dagger c_n c_n + b_n^\dagger b_n c_n^\dagger c_n \right\} \quad (\text{B.8})$$

$$H_{at} = \sum_{n=1}^N \left\{ -\Delta_e b_n^\dagger b_n - \Delta_r c_n^\dagger c_n + \frac{\Omega_{cf}}{2} (b_n^\dagger c_n + b_n c_n^\dagger) \right\} \quad (\text{B.9})$$

$$V_{a-c} = \sum_{n=1}^N g (ab_n^\dagger + a^\dagger b_n) \quad (\text{B.10})$$

$$H_{cav} = -\Delta_c a^\dagger a \quad (\text{B.11})$$

$$H_{bath} = \sum_{\lambda=L,R} \int d\omega \omega B_{\lambda,\omega}^\dagger B_{\lambda,\omega} + \int d\omega \omega \sum_{n=1}^N (D_{n,\omega}^\dagger D_{n,\omega} + C_{n,\omega}^\dagger C_{n,\omega}) \quad (\text{B.12})$$

$$V_{cav-bath} = \sum_{\lambda=L,R} \int d\omega g_b(\omega) [B_{\lambda,\omega} a^\dagger + B_{\lambda,\omega}^\dagger a] \quad (\text{B.13})$$

$$V_{at-bath} \approx \sum_{n=1}^N \int d\omega [g_c(\omega) C_{n,\omega} b_n^\dagger + g_d(\omega) D_{n,\omega} c_n^\dagger + \text{H.c.}] \quad (\text{B.14})$$

We notice that H_{sat} is the sum of single-atom Hamiltonians: since, throughout this dissertation, we consider the weak coupling regime ($g \ll \gamma_c^R, \gamma_e$), this term does not contribute to the non-linear behavior of the system. Contrary to H_{sat} , H_{dd} involves many atoms and therefore constitutes the leading contribution. We therefore completely neglect the H_{sat} non-linearity in our calculations.

B.2 Spinwave basis

In this section, we introduce the collective modes known as ‘‘spinwaves’’ which play a crucial role due to the symmetries of the problem and lead to a simpler expression of the full Hamiltonian.

First, we assume that atoms occupy the vertices of a 3D square lattice of spacing δ . In all calculations we will eventually set the limit $\delta \rightarrow 0$ and therefore consider a continuous medium but we will keep the discrete sums in all expressions for the sake of convenience. The discrete Fourier transform allows us to relate the direct space bosonic operators b_j and c_j to the reciprocal space collective (so-called) spinwave operators $b_{\vec{k}}, c_{\vec{k}}$:

$$c_{\vec{k}} = \frac{1}{\sqrt{N}} \sum_j e^{i\vec{k}\vec{r}_j} c_j \leftrightarrow c_j = \frac{1}{\sqrt{N}} \sum_{\vec{k}} e^{-i\vec{k}\vec{r}_j} c_{\vec{k}} \quad (\text{B.15})$$

$$b_{\vec{k}} = \frac{1}{\sqrt{N}} \sum_j e^{i\vec{k}\vec{r}_j} b_j \leftrightarrow b_j = \frac{1}{\sqrt{N}} \sum_{\vec{k}} e^{-i\vec{k}\vec{r}_j} b_{\vec{k}} \quad (\text{B.16})$$

where \vec{r}_i is the position of the i -th atom and $k_{x,y,z} = -\frac{\pi}{\delta}, -\frac{\pi}{\delta} + \frac{2\pi}{L_{x,y,z}}, \dots, \frac{\pi}{\delta}$ are the components of the \vec{k} vector, where $L_{x,y,z}$ is the lattice dimension in the $\{x, y, z\}$ direction. One readily shows

B. Bosonic representation

$$\begin{aligned}
\left[c_{\vec{k}}, c_{\vec{k}'}^\dagger \right] &= \frac{1}{N} \sum_{m,n} e^{i\vec{k}\vec{r}_m} e^{-i\vec{k}'\vec{r}_n} [c_m, c_n^\dagger] \\
&= \frac{1}{N} \sum_m e^{i\vec{k}\vec{r}_m} e^{-i\vec{k}'\vec{r}_m} \\
&= \delta_{\vec{k},\vec{k}'} \\
\left[b_{\vec{k}}, b_{\vec{k}'}^\dagger \right] &= \delta_{\vec{k},\vec{k}'}
\end{aligned}$$

We now rewrite the dipole-dipole interactions Hamiltonian in terms of the spinwaves operators defined above

$$H_{dd} = \frac{1}{2N^2} \sum_{m,n} \kappa_{mn} \sum_{\vec{k}''', \vec{k}'', \vec{k}', \vec{k}} e^{i(\vec{k}''' - \vec{k})\vec{r}_n} e^{i(\vec{k}'' - \vec{k}')\vec{r}_m} c_{\vec{k}'''} c_{\vec{k}''} c_{\vec{k}'} c_{\vec{k}} \quad (\text{B.17})$$

Imposing the periodic boundary conditions to κ_{mn} , we obtain

$$\begin{aligned}
\frac{1}{N^2} \sum_{m,n} \kappa_{mn} e^{i(\vec{k}''' - \vec{k})\vec{r}_n} e^{i(\vec{k}'' - \vec{k}')\vec{r}_m} &= U_{\vec{k}'' - \vec{k}'} \frac{1}{N} \sum_n e^{i(\vec{k}'' - \vec{k}' + \vec{k}''' - \vec{k})\vec{r}_n} \\
&= U_{\vec{k}'' - \vec{k}'} \delta(\vec{k}'' - \vec{k}' + \vec{k}''' - \vec{k}) \quad (\text{B.18})
\end{aligned}$$

where we defined the Fourier transform of the interaction matrix κ_{mn} as $\frac{1}{N} \sum_m \kappa_{nm} e^{i\vec{K}\vec{r}_m} = U_{\vec{K}} e^{i\vec{K}\vec{r}_n}$. Substituting B.18 to B.17 we get

$$H_{dd} = \sum_{\vec{k}', \vec{k}, \vec{q}} U_{\vec{q}} c_{\vec{k}' - \vec{q}} c_{\vec{k}' + \vec{q}} c_{\vec{k}'} c_{\vec{k}} \quad (\text{B.19})$$

where summations can be taken within any period of the lattice and will be omitted for the sake of conciseness.

Analogously, we can rewrite the natural Hamiltonian H_0 (Eq. (B.4)) under the form

$$\begin{aligned}
 H_0 &= H_{at} + V_{a-c} + H_{cav} + H_{bath} + V_{cav-bath} + V_{at-bath} \\
 V_{a-c} &= g\sqrt{N} \left(ab_0^\dagger + a^\dagger b_0 \right) \\
 H_{at} &= \sum_{n=1}^N \left\{ -\Delta_e b_n^\dagger b_n - \Delta_r c_n^\dagger c_n + \frac{\Omega_{cf}}{2} (b_n^\dagger c_n + b_n c_n^\dagger) \right\} \\
 &= \sum_{n=1}^N \sum_{\vec{k}, \vec{k}'} \frac{1}{N} e^{i(\vec{k}-\vec{k}')r_n} \left\{ -\Delta_e b_{\vec{k}}^\dagger b_{\vec{k}'} - \Delta_r c_{\vec{k}}^\dagger c_{\vec{k}'} + \frac{\Omega_{cf}}{2} (b_{\vec{k}}^\dagger c_{\vec{k}'} + b_{\vec{k}} c_{\vec{k}'}^\dagger) \right\} \\
 &= \sum_{\vec{k}, \vec{k}'} \delta_{\vec{k}, \vec{k}'} \left\{ -\Delta_e b_{\vec{k}}^\dagger b_{\vec{k}'} - \Delta_r c_{\vec{k}}^\dagger c_{\vec{k}'} + \frac{\Omega_{cf}}{2} (b_{\vec{k}}^\dagger c_{\vec{k}'} + b_{\vec{k}} c_{\vec{k}'}^\dagger) \right\} \\
 &= \sum_{\vec{k}} \left\{ -\Delta_e b_{\vec{k}}^\dagger b_{\vec{k}} - \Delta_r c_{\vec{k}}^\dagger c_{\vec{k}} + \frac{\Omega_{cf}}{2} (b_{\vec{k}}^\dagger c_{\vec{k}} + b_{\vec{k}} c_{\vec{k}}^\dagger) \right\} \\
 H_{bath} &= \sum_{\lambda=L,R} \int d\omega \omega B_{\lambda,\omega}^\dagger B_{\lambda,\omega} + \int d\omega \omega \sum_{n=1}^N \left(D_{\vec{k},\omega}^\dagger D_{\vec{k},\omega} + C_{\vec{k},\omega}^\dagger C_{\vec{k},\omega} \right) \quad (\text{B.20}) \\
 V_{at-bath} &\approx \sum_{n=1}^N \int d\omega \left[g_c(\omega) C_{\vec{k},\omega} b_{\vec{k}}^\dagger + g_d(\omega) D_{\vec{k},\omega} c_{\vec{k}}^\dagger + \text{H.c.} \right] \quad (\text{B.21})
 \end{aligned}$$

where $C_{\vec{k},\omega} \equiv \frac{1}{\sqrt{N}} \sum_j e^{i\vec{k}\vec{r}_j} C_{j,\omega}$, $D_{\vec{k},\omega} \equiv \frac{1}{\sqrt{N}} \sum_j e^{i\vec{k}\vec{r}_j} D_{j,\omega}$.

Deriving Heisenberg equations from the expression above, we conclude that the Hamiltonian H_0 does not couple the spinwaves $\vec{k} = 0$ (symmetric) and $\vec{k} \neq 0$.

Appendix C

The second-order correlation function $g^{(2)}$ of the reflected/transmitted light

In this appendix we provide technical details regarding the calculation of the $g^{(2)}(\tau)$ function of the transmitted and reflected lights. We denote by $a_{out}^{(R,L)}$ the annihilation operators of the “out” mode to the right or to the left of the cavity, respectively.

Let us first consider the transmitted light. By definition, assuming the $g_t^{(2)}$ function is computed in the steady state, we have:

$$g_t^{(2)}(\tau) \equiv \frac{\left\langle a_{out}^{(R)\dagger}(0) a_{out}^{(R)\dagger}(\tau) a_{out}^{(R)}(\tau) a_{out}^{(R)}(0) \right\rangle}{\left\langle a_{out}^{(R)\dagger} a_{out}^{(R)} \right\rangle^2} \quad (\text{C.1})$$

there the average is computed in the state $|\psi(t = -\infty)\rangle \equiv |in\rangle = e^{-\frac{1}{2}\langle n \rangle} e^{\int d\omega \alpha(\omega) b_{L,\omega}^\dagger} |\emptyset\rangle$ where $b_{L,\omega}^\dagger$ is the creation operator of the bath mode of frequency ω and $|\emptyset\rangle$ is the state with no excitations in the system. From the input-output relation for the right mirror $a_{out}^{(R)} + a_{in}^{(R)} = \sqrt{2\gamma_c^{(R)}} a$ we may write for (C.1)

$$g_t^{(2)}(\tau) = \frac{\left\langle a^\dagger(0) \left(\sqrt{2\gamma_c^{(R)}} a^\dagger(\tau) - a_{in}^{\dagger(R)}(\tau) \right) \left(a(\tau) - a_{in}^{(R)}(\tau) \right) \left(\sqrt{2\gamma_c^{(R)}} a(0) \right) \right\rangle}{(2\gamma_c^{(R)}) \langle a^\dagger a \rangle^2} \quad (\text{C.2})$$

where we implicitly used the fact that $a_{in}^{(R)}(0) |in\rangle = 0$. For the further development of (C.2) we may use the standard commutation relation for the Langevin noise operator a_{in} and any operator of the system \hat{x} (Walls and Milburn, 2007):

$$\left[\hat{x}(t'), \sqrt{2\gamma_c^R} a_{in}(t) \right] = 2\gamma\theta(t' - t) [\hat{x}(t'), a(t)] \quad (\text{C.3})$$

where $\theta(t)$ is the Heaviside step function. Using now the latter formula we finally have

C. The second-order correlation function $g^{(2)}$ of the reflected/transmitted light

for the transmitted light assuming $\tau > 0$:

$$g_t^{(2)}(\tau) = \frac{\langle a^\dagger(0) a^\dagger(\tau) a(\tau) a(0) \rangle}{\langle a^\dagger a \rangle^2} \quad (\text{C.4})$$

We now consider the reflected light on the left side (L) of the cavity:

$$g_r^{(2)}(\tau) \equiv \frac{\langle a_{out}^{(L)\dagger}(0) a_{out}^{(L)\dagger}(\tau) a_{out}^{(L)}(\tau) a_{out}^{(L)}(0) \rangle}{\langle a_{out}^{(L)\dagger} a_{out}^{(L)} \rangle^2}$$

Similarly, by using the following input-output relation for the left mirror:¹

$$a_{out}^{(L)} + a_{in}^{(L)} - i \frac{\alpha}{\sqrt{2\gamma_c^{(L)}}} = \sqrt{2\gamma_c^{(L)}} a$$

one gets

$$\begin{aligned} & \langle a_{out}^{(L)\dagger}(0) a_{out}^{(L)\dagger}(\tau) a_{out}^{(L)}(\tau) a_{out}^{(L)}(0) \rangle = (2\gamma_c^{(L)})^2 \langle a^\dagger(0) a^\dagger(\tau) a(\tau) a(0) \rangle + \\ & + 2i\gamma_c^{(L)}\alpha [\langle a^\dagger(0) a^\dagger(\tau) a(\tau) \rangle + \langle a^\dagger(0) a^\dagger(\tau) a(0) \rangle - \langle a^\dagger(0) a(\tau) a(0) \rangle - \langle a^\dagger(\tau) a(\tau) a(0) \rangle] \\ & + \alpha^2 (2\langle a^\dagger a \rangle + \langle a^\dagger(\tau) a(0) \rangle + \langle a^\dagger(0) a(\tau) \rangle - \langle a^\dagger(0) a^\dagger(\tau) \rangle - \langle a(\tau) a(0) \rangle) \\ & + i \frac{\alpha^3}{\gamma_c^{(L)}} (\langle a^\dagger \rangle - \langle a \rangle) + \frac{\alpha^4}{(2\gamma_c^{(L)})^2} \end{aligned}$$

$$\text{and } \langle a_{out}^{(L)\dagger} a_{out}^{(L)} \rangle = 2\gamma_c^{(L)} \langle a^\dagger a \rangle + i\alpha (\langle a^\dagger \rangle - \langle a \rangle) + \frac{\alpha^2}{2\gamma_c^{(L)}}$$

where we omitted the time arguments for those averages which do not depend on τ .

We may also notice that the factorization property discussed in App. D for the intracavity (field) operators also applies to the correlation functions of the transmitted or reflected lights, *i.e.* we may write in the lowest order in α :

$$\langle a_{out}^{(L,R)\dagger}(0) a_{out}^{(L,R)\dagger}(\tau) a_{out}^{(L,R)}(\tau) a_{out}^{(L,R)}(0) \rangle^{(4)} = \langle a_{out}^{(L,R)\dagger}(0) a_{out}^{(L,R)\dagger}(\tau) \rangle^{(2)} \langle a_{out}^{(L,R)}(\tau) a_{out}^{(L,R)}(0) \rangle^{(2)}.$$

¹Note that the term $i \frac{\alpha}{\sqrt{2\gamma_c^{(L)}}}$ is responsible for the displacement from the vacuum due to the coherent feeding while the bath modes are assumed to be in vacuum.

Appendix D

Factorization of correlation functions.

In this appendix, we give the technical details regarding the derivation of the factorization of the intracavity field operator correlation functions at lowest non-vanishing order in cavity feeding rate, that we extensively use in Chap. 3.

Here, we suppose that the bath interacting with the cavity is initially in the following continuous-mode coherent state (incoming quasi-classical field)

$$|\alpha\rangle = e^{-\frac{1}{2}\langle n \rangle} e^{\sqrt{\langle n \rangle} B_\alpha^\dagger} |0\rangle$$

where $\int |\alpha(t)|^2 dt = \langle n \rangle$ and $B_\alpha^\dagger = \frac{1}{\sqrt{\langle n \rangle}} \int d\omega \alpha(\omega) B^\dagger(\omega)$ is a superposition of bath mode creation operators $B^\dagger(\omega)$ (Loudon, 2000). Note that with this definition, B_α is a bosonic operator, *i.e.* $[B_\alpha, B_\alpha^\dagger] = 1$. The atoms and cavity field are initially in their ground state denoted by $|G\rangle \equiv |g \dots g\rangle \otimes |0\rangle$.

Let us consider, for instance, the quantity $\langle \alpha, G | a^\dagger(t_1) a^\dagger(t_2) a(t_2) a(t_1) | G, \alpha \rangle$, for $t_2 > t_1$, where $|G, \alpha\rangle$ denotes the initial state of the whole system {atoms+cavity+baths}¹,

$$\begin{aligned} & \langle \alpha, G | a^\dagger(t_1) a^\dagger(t_2) a(t_2) a(t_1) | G, \alpha \rangle \\ &= e^{-\langle n \rangle} \sum_{k,l} \frac{\langle n \rangle^{\frac{k+l}{2}}}{\sqrt{k!l!}} \langle k, G | a^\dagger(t_1) a^\dagger(t_2) a(t_2) a(t_1) | G, l \rangle \end{aligned} \quad (\text{D.1})$$

Expanding this expression with respect to $|\alpha|$ (which is equivalent to expanding in the number of excitations present in the system), one finds that the lowest non-vanishing contribution is the fourth order term $k = l = 2$. For the system considered the identity operator can be represented in the following way $\mathcal{I} = \bigotimes_i \mathcal{I}_i$ where $\mathcal{I}_i = \sum_q |q_i\rangle \langle q_i|$ are the identity operators on each degree of freedom of the system, and $|q_i\rangle$'s denote q -th basis vector of i -th degree of freedom. Inserting this identity operator between $a^\dagger(t_2)$ and $a(t_2)$ of the quantity (D.1) yields:

¹The baths coupled to the atoms are supposed empty and their state is not explicitly written.

D. Factorization of correlation functions.

$$e^{-\langle n \rangle} \sum_{k,l} \frac{\langle n \rangle^{\frac{k+l}{2}}}{\sqrt{k!l!}} \langle k, G | a^\dagger(t_1) a^\dagger(t_2) \rangle \quad (D.2)$$

$$\left\{ \bigotimes_i \sum_q |q_i\rangle \langle q_i| \right\} a(t_2) a(t_1) |G, l\rangle$$

For the lowest non-vanishing term $k = 2, l = 2$:

$$a(t_2) a(t_1) |G, 2\rangle = e^{iHt_2} a e^{iH(t_1-t_2)} a |G, 2(t_1)\rangle$$

where H is the Hamiltonian of the full system including baths Eq. (1.1) and $|G, 2(t_1)\rangle \equiv e^{-iHt_1} |G, 2\rangle$ (note that this state can contain excited atoms and/or cavity photons). The state $a |G, 2(t_1)\rangle$ can at most contain one excitation, and so can the state $e^{iH(t_1-t_2)} a |G, 2(t_1)\rangle$ due to the conservation of excitation number. Hence $e^{iHt_2} a e^{iH(t_1-t_2)} a |G, 2(t_1)\rangle$ can only have component on $|G, 0\rangle$. Finally the fourth order expression of (D.2) reads:

$$\begin{aligned} & e^{-\langle n \rangle} \frac{\langle n \rangle^2}{2} \langle 2, G | a^\dagger(t_1) a^\dagger(t_2) a(t_2) a(t_1) |G, 2\rangle \\ &= e^{-\langle n \rangle} \frac{\langle n \rangle^2}{2} |\langle 2, G | a^\dagger(t_1) a^\dagger(t_2) |G, 0\rangle|^2 \\ &= \langle \alpha, G | a^\dagger(t_1) a^\dagger(t_2) |G, 0\rangle_2 \langle G, 0 | a(t_2) a(t_1) |G, \alpha\rangle_2 \end{aligned}$$

where we used that $e^{-\frac{\langle n \rangle}{2}} \frac{\langle n \rangle}{\sqrt{2}} \langle 2, G | a^\dagger(t_1) a^\dagger(t_2) |G, 0\rangle$ and $e^{-\frac{\langle n \rangle}{2}} \frac{\langle n \rangle}{\sqrt{2}} \langle 0, G | a(t_2) a(t_1) |G, 2\rangle$ are equal to the second order expansion in $|\alpha\rangle$ of quantities $\langle \alpha, G | a^\dagger(t_1) a^\dagger(t_2) |G, \alpha\rangle$ and $\langle \alpha, G | a^\dagger(t_1) a^\dagger(t_2) |G, \alpha\rangle$ respectively, that we denoted by $\langle \dots \rangle_2$.

To compute $\langle \alpha, G | a^\dagger(t_1) a^\dagger(t_2) a(t_2) a(t_1) |G, \alpha\rangle$ in the lowest order it is thus enough to calculate $\langle a(t_2) a(t_1) \rangle \equiv \langle \alpha, G | a(t_2) a(t_1) |G, \alpha\rangle$.

The same argument holds for more general mean values such as

$$\langle \alpha, G | a^\dagger(t_1) a^\dagger(t_2) \dots a^\dagger(t_p) a(t_{p+1}) \dots a(t_{p+q-1}) a(t_{p+q}) | \alpha, G \rangle^{(p+q)}$$

and in particular

$$\begin{aligned} \langle a^\dagger(t) a(t) \rangle^{(2)} &= \langle a^\dagger(t) \rangle^{(1)} \langle a(t) \rangle^{(1)} \\ \langle a^\dagger(t_2) a^\dagger(t_1) a(t_1) \rangle^{(3)} &= \langle a^\dagger(t_2) a^\dagger(t_1) \rangle^{(2)} \langle a(t_1) \rangle^{(1)} \\ \langle a^\dagger(t_2) a^\dagger(t_1) a(t_1) a(t_2) \rangle^{(4)} &= \langle a^\dagger(t_2) a^\dagger(t_1) \rangle^{(2)} \langle a(t_1) a(t_2) \rangle^{(2)} \end{aligned}$$

Appendix E

Calculation of $\langle aa \rangle^{(2)}$

In this appendix we sketch the calculation of the correlation function $\langle a(t) a(t) \rangle$ in the second order in the cavity feeding rate α that we need in Chap. 3. to compute the pair correlation function $g^{(2)}$.

The system of equations for the same-time two-operator products in the second order in α is readily derived from Heisenberg-Langevin equations Eqs. (5.6-5.9). For notational convenience here, we do not explicitly write superscripts ^(1,2), nor the time argument since we only deal with same-time mean values : hence $\langle aa \rangle$ should be understood as $\langle a(t) a(t) \rangle^{(2)}$ and $\langle \sigma_{ge}^{(i)} \rangle$ as $\langle \sigma_{ge}^{(i)}(t) \rangle^{(1)}$ etc. We thus find

$$\begin{aligned}
 \frac{d}{dt} \langle aa \rangle &= 2D_c \langle aa \rangle - 2ig \sum_i \langle a\sigma_{ge}^{(i)} \rangle - 2i\alpha \langle a \rangle \\
 \frac{d}{dt} \langle a\sigma_{ge}^{(i)} \rangle &= (D_c + D_e) \langle a\sigma_{ge}^{(i)} \rangle - i\frac{\Omega_b}{2} \langle a\sigma_{gr}^{(i)} \rangle - ig \langle aa \rangle - ig \sum_j \langle \sigma_{ge}^{(j)} \sigma_{ge}^{(i)} \rangle - i\alpha \langle \sigma_{ge}^{(i)} \rangle \\
 \frac{d}{dt} \langle a\sigma_{gr}^{(i)} \rangle &= (D_c + D_r) \langle a\sigma_{gr}^{(i)} \rangle - ig \sum_j \langle \sigma_{ge}^{(j)} \sigma_{gr}^{(i)} \rangle - i\alpha \langle \sigma_{gr}^{(i)} \rangle - i\frac{\Omega_b}{2} \langle a\sigma_{ge}^{(i)} \rangle \\
 \frac{d}{dt} \langle \sigma_{ge}^{(j)} \sigma_{ge}^{(i)} \rangle &= 2D_e \langle \sigma_{ge}^{(j)} \sigma_{ge}^{(i)} \rangle - i\frac{\Omega_b}{2} \langle \sigma_{ge}^{(j)} \sigma_{gr}^{(i)} \rangle - i\frac{\Omega_b}{2} \langle \sigma_{gr}^{(j)} \sigma_{ge}^{(i)} \rangle - ig \langle a\sigma_{ge}^{(j)} \rangle - ig \langle a\sigma_{ge}^{(i)} \rangle \\
 \frac{d}{dt} \langle \sigma_{ge}^{(j)} \sigma_{gr}^{(i)} \rangle &= (D_e + D_r) \langle \sigma_{ge}^{(j)} \sigma_{gr}^{(i)} \rangle - i\frac{\Omega_b}{2} \langle \sigma_{gr}^{(j)} \sigma_{gr}^{(i)} \rangle - ig \langle a\sigma_{gr}^{(i)} \rangle - i\frac{\Omega_b}{2} \langle \sigma_{ge}^{(j)} \sigma_{ge}^{(i)} \rangle \\
 \frac{d}{dt} \langle \sigma_{gr}^{(j)} \sigma_{gr}^{(i)} \rangle &= (2D_r - i\kappa_{i,j}) \langle \sigma_{gr}^{(j)} \sigma_{gr}^{(i)} \rangle - i\frac{\Omega_b}{2} \langle \sigma_{ge}^{(j)} \sigma_{gr}^{(i)} \rangle - i\frac{\Omega_b}{2} \langle \sigma_{gr}^{(j)} \sigma_{ge}^{(i)} \rangle
 \end{aligned}$$

Assuming that the medium is homogeneous, *i.e.* that for all (i, j) , $\langle \sigma_{ge}^{(j)} \sigma_{gr}^{(i)} \rangle = \langle \sigma_{ge}^{(i)} \sigma_{gr}^{(j)} \rangle$ and $\langle a\sigma_{ge}^{(i)} \rangle = \langle a\sigma_{ge}^{(j)} \rangle$, in the steady-state this system yields

E. Calculation of $\langle aa \rangle^{(2)}$

$$\begin{aligned}
\langle aa \rangle &= \frac{g}{D_c} \sum_i \langle a\sigma_{ge}^{(i)} \rangle + \frac{\alpha}{D_c} \langle a \rangle \\
\langle a\sigma_{ge}^{(i)} \rangle &= \frac{\Omega_b}{2(D_c + D_e)} \langle a\sigma_{gr}^{(i)} \rangle + \frac{g}{(D_c + D_e)} \langle aa \rangle + \frac{g}{(D_c + D_e)} \sum_j \langle \sigma_{ge}^{(j)} \sigma_{ge}^{(i)} \rangle \\
&\quad + \frac{\alpha}{(D_c + D_e)} \langle \sigma_{ge}^{(i)} \rangle \\
\langle a\sigma_{gr}^{(i)} \rangle &= \frac{g}{(D_c + D_r)} \sum_j \langle \sigma_{ge}^{(j)} \sigma_{gr}^{(i)} \rangle + \frac{\alpha}{(D_c + D_r)} \langle \sigma_{gr}^{(i)} \rangle + \frac{\Omega_b}{2(D_c + D_r)} \langle a\sigma_{ge}^{(i)} \rangle \\
\langle \sigma_{ge}^{(j)} \sigma_{ge}^{(i)} \rangle &= \frac{\Omega_b}{2D_e} \langle \sigma_{ge}^{(j)} \sigma_{gr}^{(i)} \rangle + \frac{g}{D_e} \langle a\sigma_{ge}^{(i)} \rangle \\
\langle \sigma_{ge}^{(j)} \sigma_{gr}^{(i)} \rangle &= \frac{\Omega_b}{2(D_e + D_r)} \langle \sigma_{gr}^{(j)} \sigma_{gr}^{(i)} \rangle + \frac{g}{(D_e + D_r)} \langle a\sigma_{gr}^{(i)} \rangle + \frac{\Omega_b}{2(D_e + D_r)} \langle \sigma_{ge}^{(j)} \sigma_{ge}^{(i)} \rangle \\
\langle \sigma_{gr}^{(j)} \sigma_{gr}^{(i)} \rangle &= \frac{\Omega_b}{2(D_r - \frac{\kappa_{i,j}}{2})} \langle \sigma_{ge}^{(j)} \sigma_{gr}^{(i)} \rangle
\end{aligned}$$

Note that the first-order values $\langle a \rangle \equiv \langle a \rangle^{(1)}$, $\langle \sigma_{ge}^{(i)} \rangle \equiv \langle \sigma_{ge}^{(i)} \rangle^{(1)}$, $\langle \sigma_{gr}^{(i)} \rangle \equiv \langle \sigma_{gr}^{(i)} \rangle^{(1)}$ have been determined through solving the first-order steady state system, see Eqs. (3.1-3.3) in the main text.

Summing the above equations over atom numbers (i, j) yields a system on averages of the collective operators $b \equiv \frac{1}{\sqrt{N}} \sum_i \sigma_{ge}^{(i)}$ and $c \equiv \frac{1}{\sqrt{N}} \sum_i \sigma_{gr}^{(i)}$ and field operator a , which is *almost* closed but for the last equation which will now be considered and approximated.

Eliminating $\langle \sigma_{ge}^{(j)} \sigma_{gr}^{(i)} \rangle$ and $\langle \sigma_{ge}^{(j)} \sigma_{ge}^{(i)} \rangle$ from the last three equations we get

$$\begin{aligned}
\langle \sigma_{gr}^{(j)} \sigma_{gr}^{(i)} \rangle &= \\
&\frac{\Omega_b g}{2 \left\{ (D_r - \frac{\kappa_{i,j}}{2}) \left[(D_e + D_r) - \frac{\Omega_b^2}{4D_e} \right] - \frac{\Omega_b^2}{4} \right\}} \langle a\sigma_{gr}^{(i)} \rangle \\
&+ \frac{\Omega_b^2 g}{4D_e \left\{ (D_r - \frac{\kappa_{i,j}}{2}) \left[(D_e + D_r) - \frac{\Omega_b^2}{4D_e} \right] - \frac{\Omega_b^2}{4} \right\}} \langle a\sigma_{ge}^{(i)} \rangle
\end{aligned}$$

We now sum over i and j indices and divide this equation by N to get

$$\langle cc \rangle = \frac{\Omega_b g}{2} \sum_i K_i \langle a\sigma_{gr}^{(i)} \rangle + \frac{\Omega_b^2 g}{4D_e} \sum_i K_i \langle a\sigma_{ge}^{(i)} \rangle$$

where we introduced the coefficient

$$K_i \equiv \frac{1}{N} \sum_j \frac{1}{\left(D_e + D_r - \frac{\Omega_b^2}{4D_e}\right) \left(D_r - \frac{\kappa_{i,j}}{2}\right) - \frac{\Omega_b^2}{4}}.$$

Making the approximation that K_i does not depend on i , *i.e.* $K_i \approx K$, we get:

$$\langle cc \rangle \approx \frac{\Omega_b g \sqrt{N}}{2} K \langle ac \rangle + \frac{\Omega_b^2 g \sqrt{N}}{4D_e} K \langle ab \rangle$$

To estimate K we consider that the sample is a sphere of radius R

$$\begin{aligned} K &= \frac{1}{N} \sum_j \frac{1}{\left(D_e + D_r - \frac{\Omega_b^2}{4D_e}\right) \left(D_r - \frac{\kappa_{i,j}}{2}\right) - \frac{\Omega_b^2}{4}} \\ &\approx \frac{4\pi}{\frac{4\pi}{3} R^3} \int_0^R \frac{r^2}{\left(D_e + D_r - \frac{\Omega_b^2}{4D_e}\right) \left(D_r - \frac{C_6}{2r^6}\right) - \frac{\Omega_b^2}{4}} dr \\ &= \frac{3}{R^3} \int_0^R \frac{r^2}{\left(D_e + D_r - \frac{\Omega_b^2}{4D_e}\right) \left(D_r - \frac{C_6}{2r^6}\right) - \frac{\Omega_b^2}{4}} dr \end{aligned}$$

For large values of R , K does not depend on the geometry

$$\begin{aligned} K &\underset{R \rightarrow \infty}{\sim} \frac{1}{\left(D_e + D_r - \frac{\Omega_b^2}{4D_e}\right) D_r - \frac{\Omega_b^2}{4}} \\ &\times \left(1 - \frac{\sqrt{2}\pi^2}{3V} \sqrt{\frac{C_6}{\frac{\Omega_b^2}{4\left(D_e + D_r - \frac{\Omega_b^2}{4D_e}\right)} - D_r}} \right) \end{aligned}$$

Finally the desired closed system is

E. Calculation of $\langle aa \rangle^{(2)}$

$$\begin{aligned}
\langle aa \rangle &= \frac{g\sqrt{N}}{D_c} \langle ab \rangle + \frac{\alpha}{D_c} \langle a \rangle \\
\langle ab \rangle &= \frac{\Omega_b}{2(D_c + D_e)} \langle ac \rangle + \frac{g\sqrt{N}}{(D_c + D_e)} \langle aa \rangle + \frac{g\sqrt{N}}{(D_c + D_e)} \langle bb \rangle + \frac{\alpha}{(D_c + D_e)} \langle b \rangle \\
\langle ac \rangle &= \frac{g\sqrt{N}}{(D_c + D_r)} \langle bc \rangle + \frac{\alpha}{(D_c + D_r)} \langle c \rangle + \frac{\Omega_b}{2(D_c + D_r)} \langle ab \rangle \\
\langle bb \rangle &= \frac{\Omega_b}{2D_e} \langle bc \rangle + \frac{g\sqrt{N}}{D_e} \langle ab \rangle \\
\langle bc \rangle &= \frac{\Omega_b}{2(D_e + D_r)} \langle cc \rangle + \frac{g\sqrt{N}}{(D_e + D_r)} \langle ac \rangle + \frac{\Omega_b}{2(D_e + D_r)} \langle bb \rangle \\
\langle cc \rangle &= \frac{\Omega_b g\sqrt{N}}{2} K \langle ac \rangle + \frac{\Omega_b^2 g\sqrt{N}}{4D_e} K \langle ab \rangle
\end{aligned} \tag{E.1}$$

which allows us to determine $\langle aa \rangle$. The analytical solution is too cumbersome to be displayed but can be readily obtained by matrix inversion.

Appendix F

Factorization in the presence of extra dephasing

In this appendix, we show in which conditions the factorization of field operator products described in Appendix D remains valid in the presence of extra dephasing due to laser frequency and intensity noise. Such dephasing is correctly accounted for by adding the term $-\gamma_d \sigma_{gr}^{(n)} + F_{gr}^{(d)}$ in the Heisenberg-Langevin equation Eq. (1.14) on $\sigma_{gr}^{(n)}$, where $F_{gr}^{(d)}$ is an extra Langevin force and $\gamma_d \approx 0.15 \times \gamma_e$, $\gamma_r \approx 0.01 \times \gamma_e$ and $\gamma_e = 2\pi \times 3$ MHz in the experimental setup studied at IOGS.

In the absence of interatomic interactions, because laser and cavity fields address the atoms symmetrically, the ensemble evolves in the subspace of symmetric states. The atomic system essentially remains in this subspace, even when the interactions are taken into account, if the number of Rydberg excitations in the sample is much less than the total number of Rydberg bubbles the ensemble can accommodate for. Such symmetric superpositions actually not only contain “allowed” components (*i.e.* with Rydberg atoms further than a Rydberg bubble radius apart) but also “forbidden” components (with Rydberg atoms closer than a Rydberg bubble radius). Their number is, however, very small compared to that of “allowed” configurations and they will therefore only slightly alter the outcome of dissipative dynamics of the system.

Under these assumptions, let us show in which conditions the mean value $\langle c^\dagger c \rangle$ factorizes at lowest order. Focusing on the dissipative part¹ of Bloch equations for $\sigma_{gr}^{(i)}$

¹Due to the presence of extra dephasing, the coherent collective excitations are turned into a statistical mixture which does not allow for the factorization of averages. Here we derive a condition when the coherent symmetric (which is coupled to the cavity mode) component of population dominates over the statistical mixture. We set $\Omega_{cf} \rightarrow 0$, $g = 0$, $\kappa_{ij} \rightarrow 0$ in Eq. (1.14) in order to study the effect of dephasing separately. We also implicitly assume that initially the atoms are prepared in the symmetric coherent state.

F. Factorization in the presence of extra dephasing

and $\sigma_{rr}^{(i)}$ (note that for the latter, there is no extra dephasing) we get

$$\begin{aligned}\frac{d}{dt} \langle \sigma_{gr}^{(i)} \rangle|_d &= -(\gamma_r + \gamma_d) \langle \sigma_{gr}^{(i)} \rangle \\ \frac{d}{dt} \langle \sigma_{rg}^{(i)} \sigma_{gr}^{(j)} \rangle|_{d, i \neq j} &= -2(\gamma_r + \gamma_d) \langle \sigma_{rg}^{(i)} \sigma_{gr}^{(j)} \rangle \\ \frac{d}{dt} \langle \sigma_{rr}^{(i)} \rangle|_d &= -2\gamma_r \langle \sigma_{rr}^{(i)} \rangle\end{aligned}$$

and recalling that $c \equiv \frac{1}{\sqrt{N}} \sum_i \sigma_{gr}^{(i)}$, we get $\langle c^\dagger c \rangle = \frac{1}{N} \sum_i \langle \sigma_{rr}^{(i)} \rangle + \frac{1}{N} \sum_{i \neq j} \langle \sigma_{rg}^{(i)} \sigma_{gr}^{(j)} \rangle$ whence

$$\begin{aligned}\left. \frac{d \langle c^\dagger c \rangle}{dt} \right|_d &= \frac{1}{N} \sum_i \left. \frac{d \langle \sigma_{rr}^{(i)} \rangle}{dt} \right|_d + \frac{1}{N} \sum_{i \neq j} \left. \frac{d \langle \sigma_{rg}^{(i)} \sigma_{gr}^{(j)} \rangle}{dt} \right|_d \\ &= -\frac{2\gamma_r}{N} \sum_i \langle \sigma_{rr}^{(i)} \rangle - \frac{2}{N} (\gamma_r + \gamma_d) \sum_{i \neq j} \langle \sigma_{rg}^{(i)} \sigma_{gr}^{(j)} \rangle \\ &= \frac{2\gamma_d}{N} \sum_i \langle \sigma_{rr}^{(i)} \rangle - \frac{2}{N} (\gamma_r + \gamma_d) \sum_{i,j} \langle \sigma_{rg}^{(i)} \sigma_{gr}^{(j)} \rangle\end{aligned}$$

and

$$\left. \frac{d \langle c^\dagger c \rangle}{dt} \right|_d = \frac{2\gamma_d}{N} \sum_i \langle \sigma_{rr}^{(i)} \rangle - 2(\gamma_r + \gamma_d) \langle c^\dagger c \rangle$$

When there are n_r Rydberg excitations in the sample, with $n_r \ll N_b \ll N$ (N_b is the maximum number of Rydberg excitations the sample can contain), one has $\langle c^\dagger c \rangle \approx \sum_i \langle \sigma_{rr}^{(i)} \rangle \approx n_r$ whence

$$\left. \frac{d \langle c^\dagger c \rangle}{dt} \right|_d \approx -2 \left[\gamma_r + \gamma_d \left(1 - \frac{1}{N} \right) \right] \langle c^\dagger c \rangle$$

For $\gamma_r \ll \gamma_d \ll N\gamma_r$, one therefore has

$$\left. \frac{d \langle c^\dagger c \rangle}{dt} \right|_d \approx -2\gamma_d \langle c^\dagger c \rangle$$

so, from the point of view of $c^\dagger c$, everything works as if the system was radiatively damped with the rate γ_d . In the same conditions, we moreover have

$$\left. \frac{d \langle c \rangle}{dt} \right|_d \approx -\gamma_d \langle c \rangle$$

and again, from the point of view of c , everything works as if the system was radiatively damped with the rate γ_d . Moreover, since all other dynamical equations (for population, coherence and field operator mean values) remain formally the same as in the purely radiative damping, the factorization procedure remains valid for $\langle a^\dagger a \rangle$ provided that

$\gamma_r \ll \gamma_d \ll N\gamma_r$ and the radiative coherence decay γ_r is effectively replaced by the dephasing decay rate γ_d .

This result can also be extended to higher order quantities $\langle (a^\dagger)^m a^p \rangle$.

Appendix G

Computation of integrals

Throughout Chap. 4, we encounter various integrals, which, as we show in this appendix can be computed in a unified manner. For example let us consider the following integral:

$$S_{\vec{q}} = \frac{1}{2\pi} \int_{-\infty}^{\infty} d\omega G_{c_{\vec{q}}c_{\vec{q}}}^T[\omega] G_{c_{-\vec{q}}c_{-\vec{q}}}^T[-\omega] \quad (\text{G.1})$$

where $G_{c_{\vec{q}}c_{\vec{q}}}^T$ is the Green's function defined in Eq. (4.26). The latter may contain several poles, and therefore the direct calculation of (G.1) using the residue theorem is somewhat cumbersome. There is, however, an alternative and easier way, as we shall now show.

Let us construct the tensor product $\vec{G}_{\vec{q}}^T[\omega] \otimes \vec{G}_{-\vec{q}}^T[-\omega]$ where the matrices $\hat{G}_{\vec{q}}^T$ are defined in Eqs. (4.31-4.32) which contain Green's functions of all possible kinds, and let us define $\hat{S}_{\vec{q}}$ as

$$\hat{S}_{\vec{q}} \equiv \frac{1}{2\pi} \int_{-\infty}^{\infty} d\omega \hat{G}_{\vec{q}}^T[\omega] \otimes \hat{G}_{-\vec{q}}^T[-\omega] \quad (\text{G.2})$$

Note that $\hat{S}_{\vec{q}}$ obviously includes Eq. (G.1). $\hat{S}_{\vec{q}}$ can also be expressed as an integral over time as follows:

$$\begin{aligned} \hat{S}_{\vec{q}} &\equiv \frac{1}{2\pi} \int_{-\infty}^{\infty} d\omega d\tau d\tau' e^{-i\omega\tau} \hat{G}_{\vec{q}}^T[\tau] \otimes e^{i\omega\tau'} \hat{G}_{-\vec{q}}^T[\tau'] \\ &= \int_{-\infty}^{\infty} d\tau \hat{G}_{\vec{q}}^T[\tau] \otimes \hat{G}_{-\vec{q}}^T[\tau] \end{aligned}$$

The matrix $\hat{G}_{\vec{q}}^T[\tau]$ obeys (see Eq. (4.27))

$$\begin{cases} \frac{d}{d\tau} \hat{G}_{\vec{q}}^T = M_{\vec{q}} \times \hat{G}_{\vec{q}}^T; & \tau > 0 \\ \hat{G}_{\vec{q}}^T = 0; & \tau < 0 \end{cases} \quad (\text{G.3})$$

G. Computation of integrals

where the matrix $M_{\bar{q}}$ is defined in Eq. (4.29-4.30). Solving Eq. (G.3) we get: $\hat{G}_{\bar{q}}^T[\tau > 0] = e^{M_{\bar{q}}\tau} \hat{G}_{\bar{q}}^T[0^+] = -ie^{M_{\bar{q}}\tau}$. Substituting this relation to Eq. (G.2) we have:

$$\begin{aligned}
\hat{S}_{\bar{q}} &\equiv \int_0^\infty d\tau \hat{G}_{\bar{q}}^T[\tau] \otimes \hat{G}_{-\bar{q}}^T[\tau] \\
&= - \int_0^\infty d\tau e^{M_{\bar{q}}\tau} \otimes e^{M_{-\bar{q}}\tau} \\
&= - \int_0^\infty d\tau e^{(M_{\bar{q}} \otimes \mathcal{I} + \mathcal{I} \otimes M_{-\bar{q}})\tau} \\
&= (M_{\bar{q}} \otimes \mathcal{I} + \mathcal{I} \otimes M_{-\bar{q}})^{-1}
\end{aligned}$$

The inversion of the matrix is much easier from the computational point of view and can be easily performed *e.g.* in Mathematica. We therefore provide the final expression for the integral Eq. (G.1):

$$S = -\frac{\frac{4\Gamma_e^2}{\Omega_{cf}^2 + 4\Gamma_e\Gamma_r} + 1}{2(\Gamma_e + \Gamma_r)} \quad (\text{G.4})$$

The expression for $S_0 \equiv \frac{1}{2\pi} \int_{-\infty}^\infty d\omega G_{c_0c_0}^T[\omega] G_{c_0c_0}^T[-\omega]$ is much more cumbersome:

$$\frac{\Gamma_c\Omega_{cf}^4 + 4\Omega_{cf}^2(\Gamma_c^3 + \Gamma_c(\Gamma_e^2 + 2\Gamma_e\Gamma_r + g^2N) + \Gamma_c^2(\Gamma_e + \Gamma_r) + g^2N\Gamma_r) + 16(\Gamma_c + \Gamma_e)(\Gamma_c\Gamma_e + g^2N)((\Gamma_c + \Gamma_r)(\Gamma_e + \Gamma_r) + g^2N)}{2(\Gamma_c\Omega_{cf}^2 + 4\Gamma_r(\Gamma_c\Gamma_e + g^2N))(4(\Gamma_c + \Gamma_e)((\Gamma_c + \Gamma_r)(\Gamma_e + \Gamma_r) + g^2N) + \Omega_{cf}^2(\Gamma_e + \Gamma_r))}$$

Appendix H

C-PHASE gate

This appendix is an extended preprint version of the article (Das et al., 2016).

Photonic Controlled-Phase Gates Through Rydberg Blockade in Optical Cavities

Sumanta Das^{1,*}, Andrey Grankin^{2,†}, Ivan Iakoupov¹, Etienne Brion³, Johannes Borregaard^{1,4}, Rajiv Boddeda², Imam Usmani², Alexei Ourjoutsev², Philippe Grangier², and Anders S. Sørensen¹

¹ *The Niels Bohr Institute, University of Copenhagen, Blegdamsvej 17, DK-2100 Copenhagen Ø, Denmark*

² *Laboratoire Charles Fabry, Institut d'Optique, CNRS, Univ Paris-Sud, Campus Polytechnique, RD 128, 91127 Palaiseau cedex, France*

³ *Laboratoire Aimé Cotton, CNRS, Université Paris Sud, ENS Cachan, 91405 Orsay, France.*

⁴ *Department of Physics, Harvard University, Cambridge, MA 02138, USA*

(Dated: September 16, 2015)

We propose a novel scheme for high fidelity photonic controlled-phase gates using Rydberg blockade in an ensemble of atoms in an optical cavity. The gate operation is obtained by first storing a photonic pulse in the ensemble and then scattering a second pulse from the cavity, resulting in a phase change depending on whether the first pulse contained a single photon. We show that the combination of Rydberg blockade and optical cavities effectively enhances the optical non-linearity created by the strong Rydberg interaction and makes the gate operation more robust. The resulting gate can be implemented with cavities of moderate finesse allowing for highly efficient processing of quantum information encoded in photons. As an illustration, we show how the gate can be employed to increase the communication rate of quantum repeaters based on atomic ensembles.

PACS numbers:

Keywords:

Large bandwidth, fast propagation and the non-interacting nature of photons, make them ideal for communicating quantum information over long distances [1]. In contrast, strong photon-photon interactions are desirable for processing of quantum information encoded in the photons, especially if both high fidelity and high efficiency are needed. To satisfy these requirements one needs a highly non-linear medium. Typically, the strength of photon-photon interactions mediated by a non-linear medium is very weak at the single-photon level where photonic quantum logic gates are operating [2]. As a consequence, the implementation of photonic quantum gates remains an unsolved challenge and requires novel means of efficient light-matter interaction. To enhance light-matter interactions, a viable solution is to use ensembles of atoms, e.g., configured for electromagnetically induced transparency (EIT) [3]; this can be further improved by placing the ensemble in an optical cavity, but these ensemble based approaches do not increase the essential photonic non-linearity. In recent years, there has been intense efforts to realize light-matter interactions via, non-linear interactions in a variety of medium, ranging from atoms [4–10] and atom like systems [11–14] to superconducting qubits [15–17].

A promising approach towards creating strong quantum nonlinearities is to exploit excitation blockade in Rydberg EIT systems [18–25]. Several quantum effects like strong optical non-linearities and control of light by light [22–28], deterministic single-photon sources [29], and the generation of entanglement and atomic quantum gates [30–34] have been investigated. The strong nonlinearity originates from the fact that the Rydberg interaction prevents multiple excitations within a blocked radius r_b [35, 36]. The ensemble then behaves as a two-level *superatom* consisting of N_b atoms within a radius r_b [35, 36]. If the optical depth d_b corresponding to the superatom is sufficiently large, $d_b \gg 1$ [22], a strong optical nonlinearity at the single-photon level can be achieved in the EIT configuration [18–25]. Reaching such an optical depth is,

however, challenging, which limits the effectiveness of photonic quantum gates.

An enhanced optical nonlinearity was recently demonstrated by placing the ensemble inside an optical cavity [26], but a direct application of this nonlinearity for quantum gates is non-trivial since the outgoing optical modes are highly distorted and entangled by the interaction [37–39]. In this letter, we propose a novel scheme for achieving a high fidelity *photonic controlled-phase (CP) gate with a Rydberg EIT ensemble* trapped inside an optical cavity of moderate finesse. In our scheme, the photons are incident at different times thus avoiding the problem of mode distortion while still allowing the cavity enhancement of the interaction. The use of a cavity has several major advantages compared to ensembles in free space, since it enhanced light-atom coupling in the ensemble and also effectively increases the non-linearity. In our proposal, the parameter characterizing the Rydberg blockade is $C_b \sim \mathcal{F}d_b$, where $C_b = N_b\mathcal{C}$, with $\mathcal{C} \ll 1$ being the single atom cooperativity, and \mathcal{F} is the cavity finesse. Hence the effect of the Rydberg interaction is increased by the cavity finesse \mathcal{F} , whereas the low value of \mathcal{C} is compensated by a high value of N_b . In addition, the cavity is also useful for controlling the mode structure thereby enabling high input-output efficiencies [40]. We show that the proposed gate can have a promising (heralded) error scaling as $1/C_b^2$, and demonstrate how it can be used to improve quantum repeaters based on atomic ensembles even for moderate interaction strengths $C_b \sim 10$. The proposed CP gate can thus be directly integrated into quantum communication circuitry thereby providing a building block for future quantum networks. The Rydberg interaction [36] for our proposal can either be long range dipolar or van der Waals interactions, but for simplicity, we only consider the latter.

We first outline the basic idea of our gate, which goes along the line of Ref. [41], except that the single trapped atom is replaced by a Rydberg ensemble. In contrast to Ref. [41],

and many others, we thus do *not* require the strong-coupling regime of cavity QED, and can work with cavities of moderate finesse. This enables input-output efficiency near unity since the cavity losses can be completely negligible compared to the mirror's transmission [40]. For simplicity, we first describe the operation for single-rail qubits where a qubit is encoded in a photon pulse containing a superposition of vacuum $|0\rangle$ and a single photon $|1\rangle$. Later, we generalize it to a more useful dual-rail encoding where the qubit is encoded as a photon in one of two possible modes.

In the single-rail version outlined in Figs. 1(a) and (b), a first photon pulse is stored in a cavity containing a Rydberg EIT ensemble [42]. Here a classical driving field from an excited state $|e\rangle$ to a Rydberg state $|r\rangle$ enables the storage of incoming photons in $|r\rangle$ through the interaction of the cavity field with the transition from the ground state $|g\rangle$ to $|e\rangle$. The excitation in state $|r\rangle$ is then transferred to another Rydberg state $|r'\rangle$ by a microwave pulse so that the ensemble contains a single atom in state $|r'\rangle$ if the first pulse contained a single incoming photon. The second pulse is then incident on the cavity. If the first pulse contained vacuum $|\emptyset\rangle$, the second pulse is scattered under Rydberg EIT conditions and leaves the cavity with the same phase. If the first pulse contained a photon, the atom in $|r'\rangle$ shifts the position of the state $|r\rangle$ in the remaining atoms. As we will show, this prevents the second pulse from entering the cavity resulting in a phase flip on the $|1\rangle$ component of the second pulse. This evolution thus realizes a CP gate which, together with single qubit operations, is universal for quantum information processing.

We now present a theoretical treatment to evaluate the performance of the CP gate. The initial state of the single photon pulse can be expressed as $\int d\omega \phi(\omega) \hat{a}_\omega^\dagger e^{-i\omega t} |\emptyset\rangle$, where $\phi(\omega)$ is the normalized pulse shape, \hat{a}_ω^\dagger is the one-dimensional field operators satisfying the standard bosonic commutation relations and $|\emptyset\rangle$ denotes the vacuum of all the optical modes. The frequency integrand ω of the incoming photon is referenced to the cavity frequency ω_c , which in turn is nearly resonant to the $|e\rangle \rightarrow |g\rangle$ transition (see Fig. 1(a)). The cavity is assumed to be one-sided with a standing-wave field. The dynamics of the system can be described in the quantum jump approach through the no-jump Hamiltonian $\mathcal{H} = \mathcal{H}_s + \mathcal{H}_I$. Here \mathcal{H}_s consists of the decays and the free energy terms [43] while,

$$\begin{aligned} \mathcal{H}_I = & - \sum_l \hbar \left[\frac{\Omega_l}{2} |r_l\rangle \langle e_l| + i\mathcal{G}_l |e_l\rangle \langle g_l| \hat{b} \right] + \text{H.c.} \\ & + \sum_k \hbar \mathcal{V}_{kl} |r'_k\rangle \langle r'_k| \otimes |r_l\rangle \langle r_l|, \end{aligned} \quad (1)$$

Here the coupling strengths of the l^{th} atom with the driving field and the incoming single photon pulse is respectively Ω_l and \mathcal{G}_l , while \mathcal{V}_{kl} is the van der Waals interaction among the Rydberg excitations of atoms k and l . We solve the Schrödinger equation for the scattering stage assuming constant Ω_l in Fourier space to find the reflection co-efficient. The (amplitude) reflection coefficient with the stored Rydberg excitation in atom k is given by $\mathcal{R}_k(\omega) = (2\kappa \mathbf{S}_k(\omega) - 1)$

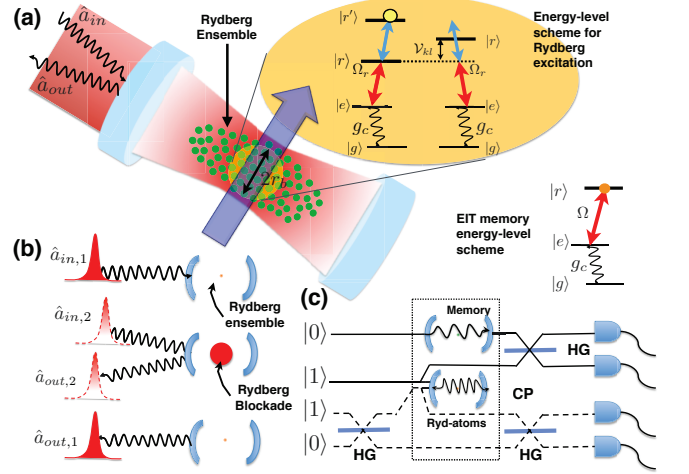


FIG. 1: Schematic outline of the phase gate (a) An input single photon pulse along with a driving field induces a two-photon transition to the Rydberg state $|r\rangle$ which is subsequently transferred to another Rydberg state $|r'\rangle$. Due to Rydberg interactions \mathcal{V}_{kl} among the atoms, other Rydberg states $|r\rangle$ within the range of the interaction potential, given by, the blockade radius of r_b , become off-resonant allowing no further excitation. (b) When an initial photon pulse is stored in the Rydberg ensemble, the second incoming photon cannot enter the cavity and is scattered off, which ideally induces a phase flip of π on the scattered photons. (c) Dual-rail implementation of a CP gate (dotted box). A Bell state measurement can be implemented by combining the CP gate with Hadamard gates (HG).

where,

$$\mathbf{S}_k(\omega) = \left(\kappa - i\omega + \sum_l \frac{|\mathcal{G}_l|^2}{(\Gamma_{el} - i\tilde{\Delta}_l) + \frac{|\Omega_l/2|^2}{\Gamma_{rl} + i(\delta_l + \mathcal{V}_{kl} - \omega)}} \right)^{-1} \quad (2)$$

where the detunings are $\Delta_l = \omega_{e_l} - \omega_c$, $\tilde{\Delta}_l = \Delta_l + \omega$ and $\delta_l = (\omega_{r_l} - \omega_e) - \omega_c$ with $\hbar\omega_{e_l(r_l)}$ and $\Gamma_{e_l(r_l)}$ being the energy and width of the excited (Rydberg) state $|e\rangle(|r\rangle)$ in atom l and κ is the cavity field decay rate. The reflection coefficient $\mathcal{R}_g(\omega)$ [43] for no stored excitation is evaluated by setting $\mathcal{V}_{kl} = 0$.

To get an understanding of the scattering we study the behavior of the reflection coefficient for resonant interactions $\delta_l = \Delta_l = 0$ and long lived Rydberg excitations ($\Gamma_{r_l} = 0$). For simplicity, we assume equal couplings and driving strengths on all atoms $\mathcal{G}_l = \mathcal{G}$ and $\Omega_l = \Omega$ (for the general case see [43]). Furthermore, if the photon pulse has a suitably long duration we can put $\omega \approx 0$ (see below). With these assumptions, we find from Eq. (S14) that $\mathcal{R}_g = 1$ for no stored excitation; this is the perfect EIT condition. When an excitation is stored, the reflection coefficient becomes

$$\mathcal{R}_k = \left(\frac{2}{1 + C_v^*} - 1 \right), \quad (3)$$

where $C_v^* = C_b + iC'_b = C \sum_l 1 / \left[1 + \frac{|\Omega/2|^4}{\mathcal{V}_{kl}^2 \Gamma_e^2} \right] + iC \sum_l \frac{|\Omega/2|^2}{\mathcal{V}_{kl} \Gamma_e} / \left[1 + \frac{|\Omega/2|^4}{\mathcal{V}_{kl}^2 \Gamma_e^2} \right]$ quantifies the effective coopera-

tivity of the blockade, while $\mathcal{C} = |\mathcal{G}|^2/(\kappa\Gamma_e)$ is the single atom cooperativity. Each atom l in the volume blocked by the $|r'_k\rangle$ excitation, *i.e.* such that $\mathcal{V}_{kl} \gg |\Omega/2|^2/\Gamma_e$, will contribute with \mathcal{C} in \mathcal{C}_b . On the other hand, those atoms for which $\mathcal{V}_{kl} \ll |\Omega/2|^2/\Gamma_e$ will have a negligible contribution to \mathcal{C}_b , and hence \mathcal{C}_b gives the effective cooperativity of the blockade ensemble. The imaginary part depends on the shape of the interaction but for a uniform $1/r^6$ interaction at resonance in a uniform cloud we find that $|\mathcal{C}'_b| = \mathcal{C}_b$ [43] (r is the distance between atoms k and l).

We now discuss the key feature of our work - the implementation of a photonic CP gate via scattering from a Rydberg ensemble in either a single-rail or dual-rail encoding. The single-rail implementation uses the encoding discussed in the introduction and is shown schematically in Fig. 1 (b). A first qubit is encoded in the vacuum and single photon state, $|\mathcal{O}\rangle$ and $|1\rangle = \int d\omega \phi(\omega) \hat{a}_\omega^\dagger e^{-i\omega t} |\mathcal{O}\rangle$, respectively, of a first incoming pulse. This pulse is stored in the Rydberg ensemble such that the logical states $|0\rangle$ and $|1\rangle$ are mapped onto the ensemble being in the joint ground state $|0\rangle = |g^N\rangle |\mathcal{O}\rangle$ and a Rydberg polariton $|1\rangle = \sum_k \alpha_k |g^{N-1}, r'_k\rangle |\mathcal{O}\rangle$. This is achieved using the well established techniques of storage in atomic ensembles, which is known to have an error $1/N\mathcal{C}$ for any slowly varying pulse shape provided a temporally varying control field is used during storage [3, 19], followed by microwave π -pulse between $|r_k\rangle$ and $|r'_k\rangle$. A second incoming photon pulse is then reflected from the cavity. This reflection can be from either an ensemble in the EIT configuration (ensemble in $|0\rangle$), or from a blocked ensemble ($|1\rangle$). As can be seen from Eq. (S17) there is exactly a π phase shift between the two situations: $\mathcal{R}_g = 1$ for $\mathcal{C}_v^* = 0$ and $\mathcal{R}_k = -1$ for $|\mathcal{C}_v^*| \gg 1$. Finally, the first stored pulse is retrieved from the ensemble.

To evaluate the performance we calculate the Choi-Jamiolkowski fidelity of the gate. Since, in general, we have $N\mathcal{C} > \mathcal{C}_b$, the fidelity of the operation will mainly be limited by the gate and we shall ignore imperfections during the storage. The fidelity can then be determined by [43],

$$F_{\text{CJ}} = \frac{1}{16} \left| 2 + \int d\omega |\phi(\omega)|^2 \mathcal{R}_g(\omega) - \sum_k \int d\omega |\alpha_k|^2 |\phi(\omega)|^2 \mathcal{R}_k(\omega) \right|^2. \quad (4)$$

To account for errors due to imperfect Rydberg blockade, we evaluate the above fidelity and find

$$F_{\text{CJ}} = 1 - \frac{(1 + \mathcal{C}_b)}{(1 + \mathcal{C}_b)^2 + \mathcal{C}_b'^2} - \frac{N\mathcal{C}\Gamma_e^2}{|\Omega/2|^4} (\Delta\omega)^2 - \left(\frac{1}{\kappa} + \frac{N\mathcal{C}\Gamma_e}{|\Omega/2|^2} \right)^2 (\Delta\omega)^2 \quad (5)$$

Here the third and fourth term are gate errors due to the finite frequency width $\Delta\omega^2$ of the incoming pulse. These terms arise predominately from the EIT bandwidth, which is much narrower than the variations of the blocked reflection coefficient. For a narrow pulse $\Delta\omega \rightarrow 0$, the fidelity is only limited

by the cooperativity of the blocked ensemble $1 - F_{\text{CJ}} \propto 1/\mathcal{C}_b$. Hence, as discussed in the introduction, it is the cavity enhanced blocked cooperativity, which is the main figure of merit for the gate.

In the dual-rail encoding, both logical states $|0\rangle$ and $|1\rangle$ are represented by photons, but in two different paths. A schematic of the dual-rail CP gate is shown in Fig. 1(c). The first photon pulse in the upper two arms of the figure is first stored in a memory consisting of a Rydberg ensemble placed in each arm (for a polarization encoding such two memories might be realized by two different internal states of the same ensemble). A second photon pulse is then scattered from the Rydberg ensemble if it is in state $|1\rangle$ (upper rail in the figure). This scattering ideally induces a phase change of π if there was a photon stored in the Rydberg ensemble, *i.e.* if both qubits were in state $|1\rangle$. As opposed to the single-rail implementation, the dual-rail implementation has the possibility of conditioning on getting two photons in the output. Since the dominant error in the single-rail implementation is the loss of photons, this possibility allows for a substantial increase in the fidelity with only a minor failure probability of the gate. In view of a possible application of the gate for quantum repeaters, discussed below, we consider the conditional fidelity of an EPR pair resulting from an entanglement swap realized with the gate using the full circuit in Fig. 1(c). Neglecting again the error due to finite storage efficiency, we find that this fidelity is [43]

$$F_{\text{swap}} = \frac{\int d\omega |\phi(\omega)|^2 |2 + \mathcal{R}_g(\omega) - \sum_k |c_k|^2 \mathcal{R}_k(\omega)|^2}{16P_{\text{suc}}} \quad (6)$$

where the success probability of the process is $P_{\text{suc}} = \int d\omega |\phi(\omega)|^2 (2 + |\mathcal{R}_g(\omega)|^2 + |\sum_k |c_k|^2 \mathcal{R}_k(\omega)|^2)/4$. Note that compared to F_{CJ} in Eq. (S19), the only difference is due to the conditioning with a success probability $P_{\text{suc}} < 1$ and the way the mode function is treated. The latter is related to the fact that Eq. (S19) is the fidelity with a specific mode function. Keeping only the leading order contribution to the dispersion, we find the fidelity and success probability of the CP gate

$$F_{\text{swap}} = 1 - \frac{1}{[\mathcal{C}_b^2 + \mathcal{C}_b'^2]} - \frac{3\mathcal{C}_b^2 - \mathcal{C}_b'^2}{4[\mathcal{C}_b^2 + \mathcal{C}_b'^2]^2} (\Delta\omega)^2, \quad (7)$$

$$P_{\text{suc}} = 1 - \frac{\mathcal{C}_b}{(1 + \mathcal{C}_b)^2 + \mathcal{C}_b'^2} - \frac{N\mathcal{C}\Gamma_e^2}{|\Omega/2|^4} (\Delta\omega)^2 \quad (8)$$

Here the fourth term is again the leading order error from the spectral width of the pulse. In the limit of a narrow pulse $\Delta\omega \rightarrow 0$, we see that the conditional gate error $1 - F_{\text{swap}} \propto 1/(\mathcal{C}_b)^2$ for $\mathcal{C}_b \gg 1$ is much smaller than for the single-rail. This comes at only a minor cost in the failure probability $1 - P_{\text{suc}} \propto 1/\mathcal{C}_b$. The resulting dual-rail fidelities are plotted in Fig. 2 as a function of the parameter \mathcal{C}_b . For $\mathcal{C}_b \approx 8$, the (post-selected) fidelity is found to be larger than 0.99

In order to get realistic predictions, we use the experimental conditions of Ref. [26], with $\Gamma_e \approx (2\pi)3\text{MHz}$ and

$\kappa \approx (2\pi)10\text{MHz}$ (corresponding to a finesse $\mathcal{F} \approx 120$) but a smaller beam waist $w_0 = 15\mu\text{m}$. This gives a single atom cooperativity $\mathcal{C} = 0.025$ and we take $N\mathcal{C} = 20$ corresponding to a combined storage and retrieval efficiency of 90%. We assume a Rydberg line width $\gamma_r = (2\pi)60\text{kHz}$ [44] corresponding to a coherence time of $\tau_r = 1/\gamma_r = 2.65\mu\text{s}$ (note that if the two ensembles in the dual-rail encoding are read out with the same laser the scheme becomes insensitive to phase fluctuations). With a pulse duration of $T = 1/\Delta\omega = 300\text{ns}$ and a driving strength of $\Omega = (2\pi)36\text{MHz}$ the error due to finite bandwidth in Eq. (S22) is below 2%. Taking the interaction $\mathcal{V} = (2\pi)8.31 \cdot 10^6/r^6\text{MHz}\mu\text{m}^6$ corresponding to two atoms with a Rydberg quantum number $n_r = 90$ and an atomic density of $n = 0.25\mu\text{m}^{-3}$, one has $\mathcal{C}_b \sim 8.1$ [43] which is sufficient to obtain high fidelities as show in Fig. 2. Here, we ignore any effect of sample inhomogeneities, but this can be taken into account by suitable redefinitions of \mathcal{C}_b and \mathcal{C}'_b [43].

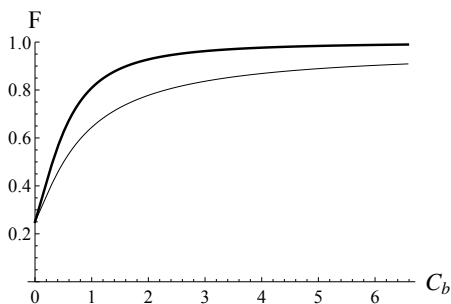


FIG. 2: Choi-Jamiolkowski fidelity (thin line) and post-selected swap fidelity (thick line) as functions of the blockaded cooperativity \mathcal{C}_b for a spectrally narrow pulse $\Delta\omega \rightarrow 0$. We assume $|\mathcal{C}'_b| = \mathcal{C}_b$.

As a particular application of the gate, we consider long distance quantum cryptography based on quantum repeaters. We considered the ensemble based quantum repeater protocol proposed in Ref. [46], but replace the entanglement swapping with the procedure shown in Fig. 1(c). We calculate the secret key rate per repeater station as described in Ref. [45] (assuming the distributed states to be Werner states) and compare the results to the original protocol (see Fig. 3). At the lowest level of the protocol, single excitations are stored in atomic ensembles using a Raman scheme and we include double excitation errors to lowest order similar to Ref. [46]. The performance of the protocol depends strongly on the repetition rate of this operation. Regardless of the repetition rate, the CP gate enables significantly higher communication rates since it allows near perfect Bell state measurements (for $\mathcal{C}_b \gg 1$) whereas swapping operations based on linear optics have a maximal success probability of 50%. In Fig. 3, we also show the rate obtainable if single excitations are initially created perfectly and deterministically in the atomic ensembles, e.g., by exploiting Rydberg blockade [29]. We find that for such a protocol, a cooperativity of $\mathcal{C}_b \sim 25$ is sufficient to obtain a secret key rate of 1.5 Hz over 1000 km using 33 repeater stations.

In conclusion, we have proposed an efficient method to im-

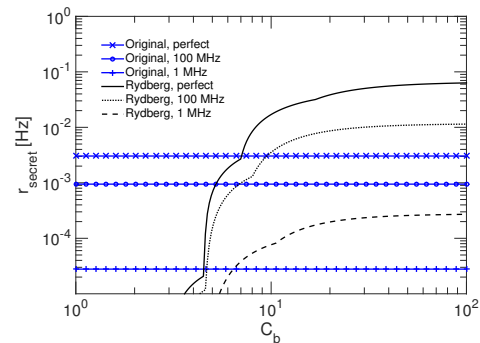


FIG. 3: Secret key rate per repeater station (r_{secret}) as a function of the blockaded cooperativity (\mathcal{C}_b) for a communication distance of 1000 km. We compare the protocol of Ref. [46] (Original) with a modified protocol where the entanglement swapping is performed with the Rydberg CP gate (Rydberg). We consider an optimistic source repetition rate of 100 MHz and a more modest one of 1 MHz, as well as a perfect single excitation state created in the atomic ensembles, e.g., using Rydberg blockade [29]. We assume an attenuation length of 22 km in the fibers and an optical signal speed of $2 \cdot 10^5\text{km/s}$. The ensemble readout efficiency and photodetector efficiency are both assumed to be 90%. The steps in the curves reflect where the fidelity of the CP gate allows additional swap levels to be employed.

plement a CP gate for photons. The gate combines the advantages of cavity defined optical modes and cavity enhanced light matter interactions with the strong Rydberg blockade obtainable in atomic ensembles. As a direct application, the proposed gate can be used to improve the communication rate of quantum repeaters, but more generally the gate may serve as a building block for photonic quantum networks.

The research leading to these results was funded by the European Union Seventh Framework Programme through SIQS (Grant No. 600645) and ERC Grant QIOS (Grant No. 306576). J.B. acknowledges funding from the Carlsberg foundation. S.D. and A.G. contributed equally to this work.

* Electronic address: sumanta@nbi.ku.dk

† Electronic address: andrey.grankin@u-psud.fr

- [1] H. J. Kimble, *Nature* **453**, 1023 (2008).
- [2] D. E. Chang, V. Vuletić and M. D. Lukin, *Nature Photonics* **8**, 685 (2014).
- [3] K. Hammerer, A. S. Sørensen, and E. S. Polzik, *Rev. Mod. Phys.* **82**, 1041 (2010).
- [4] Q. A. Turchette, C. J. Hood, W. Lange, H. Mabuchi, and H. J. Kimble, *Phys. Rev. Lett.* **75**, 4710 (1995).
- [5] S. E. Harris, and L. V. Hau, *Phys. Rev. Lett.* **82**, 4611 (1999).
- [6] B. Darquié, M. P. A. Jones, J. Dingjan, J. Beugnon, S. Bergamini, Y. Sortais, G. Messin, A. Browaeys, P. Grangier, *Science* **309**, 454 (2005).
- [7] M. K. Tey, Z. Chen, S. A. Aljunid, B. Chng, F. Huber, G. Maslennikov, and C. Kurtsiefer *Nature Phys.* **4**, 924 (2008).
- [8] W. Chen, K. M. Beck, R. Bücker, M. Gullans, M. D. Lukin, H. Tanji-Suzuki, and V. Vuletić, *Science* **341**, 768 (2013).
- [9] T. G. Tiecke, J. D. Thompson, N. de Leon, V. Vuletić, and M. D. Lukin, *Nature* **508**, 241 (2014).
- [10] A. Reiserer, N. Kalb, G. Rempe, and S. Ritter *Nature* **508**, 237

- (2014).
- [11] P. Michler, A. Kiraz, C. Becher, W. V. Schoenfeld, P. M. Petroff, Lidong Zhang, E. Hu, A. Imamoğlu, *Science* **290**, 2282 (2000).
- [12] I. Fushman, D. Englund, A. Faraon, N. Stoltz, P. Petroff, and J. Vučković, *Science* **320**, 769 (2008).
- [13] J. Hwang, M. Pototschnig, R. Lettow, G. Zumofen, A. Renn, S. Götzinger, and V. Sandoghdar *Nature* **460**, 76 (2009).
- [14] B. Casabone, K. Friebe, B. Brandstätter, K. Schüppert, R. Blatt, and T. E. Northup *Phys. Rev. Lett.* **114**, 023602 (2015).
- [15] M. H. Devoret and R. J. Schoelkopf, *Science* **339**, 1169 (2013).
- [16] P. Adhikari, M. Hafezi, and J. M. Taylor, *Phys. Rev. Lett.* **110**, 060503 (2013).
- [17] L. Neumeier, M. Leib, and M. J. Hartmann, *Phys. Rev. Lett.* **111**, 063601 (2013).
- [18] I. Friedler, D. Petrosyan, M. Fleischhauer, and G. Kurizki, *Phys. Rev. A* **72**, 043803 (2005).
- [19] A. V. Gorshkov, J. Otterbach, M. Fleischhauer, T. Pohl, and M. D. Lukin, *Phys. Rev. Lett.* **107**, 133602 (2011).
- [20] D. Petrosyan, J. Otterbach, and M. Fleischhauer, *Phys. Rev. Lett.* **107**, 213601 (2011).
- [21] J. Stanojevic, V. Parigi, E. Bimbard, A. Ourjoumtsev, and P. Grangier, *Phys. Rev. A* **88**, 053845 (2013).
- [22] J. D. Pritchard, D. Maxwell, A. Gauguet, K. J. Weatherill, M. P. A. Jones, and C. S. Adams, *Phys. Rev. Lett.* **105**, 193603 (2010).
- [23] D. Maxwell, D. J. Szwer, D. Paredes-Barato, H. Busche, J. D. Pritchard, A. Gauguet, K. J. Weatherill, M. P. A. Jones, and C. S. Adams, *Phys. Rev. Lett.* **110**, 103001 (2013).
- [24] O. Firstenberg, T. Peyronel, Q-Y. Liang, A. V. Gorshkov, M. D. Lukin and V. Vuletić *Nature* **502**, 71 (2013).
- [25] S. Baur, D. Tiarks, G. Rempe, and S. Dürr, *Phys. Rev. Lett.* **112**, 073901 (2014).
- [26] V. Parigi, E. Bimbard, J. Stanojevic, A. J. Hilliard, F. Nogrette, R. Tualle-Brouiri, A. Ourjoumtsev, and P. Grangier *Phys. Rev. Lett.* **109**, 233602 (2012).
- [27] H. Gorniaczyk, C. Tresp, J. Schmidt, H. Fedder, and S. Hofferberth *Phys. Rev. Lett.* **113**, 053601 (2014).
- [28] D. Tiarks, S. Baur, K. Schneider, S. Dürr, G. Rempe *Phys. Rev. Lett.* **113**, 053602 (2014).
- [29] Y. O. Dudin, and A. Kuzmich, *Science* **336**, 887 (2012).
- [30] A. Gaëtan, Y. Miroshnychenko, T. Wilk, A. Chotia, M. Viteau, D. Comparat, P. Pillet, A. Browaeys and P. Grangier *Nature. Phys* **5**, 115 (2009).
- [31] M. Müller, I. Lesanovsky, H. Weimer, H. P. Buchler, and P. Zoller, *Phys. Rev. Lett.* **102**, 170502 (2009).
- [32] L. Li, Y. O. Dudin, A. Kuzmich, *Nature* **498**, 466 (2013).
- [33] D. Paredes-Barato and C. S. Adams *Phys. Rev. Lett.* **112**, 040501 (2014).
- [34] M. Khazali, K. Heshami, C. Simon *Phys. Rev. A* **91**, 030301(R) (2015).
- [35] M. D. Lukin, M. Fleischhauer, R. Cote, L. M. Duan, D. Jaksch, J. I. Cirac, and P. Zoller *Phys. Rev. Lett.* **87**, 037901 (2001).
- [36] M. Saffman, T. G. Walker and K. Mølmer, *Rev. Mod. Phys.* **82**, 2313 (2010).
- [37] J. H. Shapiro, *Phys. Rev. A* **73**, 062305 (2006).
- [38] J. Gea-Banacloche, *Phys. Rev. A* **81**, 043823 (2010).
- [39] B. He and A. Scherer, *Phys. Rev. A* **85**, 033814 (2012); B. He, A.V. Sharypov, J. Sheng, C. Simon, and M. Xiao, *Phys. Rev. Lett.* **112**, 133606 (2014).
- [40] E. Bimbard, R. Boddeda, N. Vitrant, A. Grankin, V. Parigi, J. Stanojevic, A. Ourjoumtsev, and P. Grangier, *Phys. Rev. Lett.* **112**, 033601 (2014).
- [41] L. -M. Duan, H. J. Kimble, *Phys. Rev. Lett.* **92**, 127902 (2004).
- [42] A. V. Gorshkov, A. Andre, M. D. Lukin, A. S. Sørensen, *Phys. Rev. A* **76**, 033804 (2007).
- [43] See supplementary information for further details.
- [44] R. Löw, H. Weimer, J. Nipper, J. B. Balewski, B. Butscher, H. P. Büchler and T. Pfau, *J. Phys. B: At. Mol. Opt. Phys.* **45**, 113001 (2012).
- [45] J. Borregaard, P. Kómár, E. M. Kessler, M. D. Lukin, and A. S. Sørensen, *Phys. Rev. A* **92**, 012307 (2015).
- [46] N. Sangouard, C. Simon, B. Zhao, Y.-A. Chen, H. deRiedmaten, J-W. Pan, and N. Gisin, *Phys. Rev. A* **77**, 062301 (2008).

Supplementary Material

THE REFLECTION COEFFICIENT

The dynamics of the Rydberg ensemble in the cavity can be described through the no-jump Hamiltonian \mathcal{H} consisting of the free energy and decay terms \mathcal{H}_s along with the interaction part as $\mathcal{H}_I = \mathcal{H}_{L\text{-int}} + \mathcal{H}_{\text{Ryd-int}}$, where

$$\begin{aligned}\mathcal{H}_s &= \sum_l \hbar(\Delta_l - i\Gamma_{el})|e_l\rangle\langle e_l| + \hbar(\delta_l - i\Gamma_{rl})|r_l\rangle\langle r_l| - i\hbar\kappa\hat{b}\hat{b}^\dagger \\ \mathcal{H}_{L\text{-int}} &= -\sum_l \frac{\hbar\Omega_l}{2}|r_l\rangle\langle e_l| - i\sum_l \hbar\mathcal{G}_l|e_l\rangle\langle g_l|\hat{b} + \text{H.c.} \\ \mathcal{H}_{\text{Ryd-int}} &= \sum_k \hbar\mathcal{V}_{kl}|r'_k\rangle\langle r'_k| \otimes |r_l\rangle\langle r_l|,\end{aligned}\quad (\text{S9})$$

where the detunings Δ_l, δ_l , the linewidths Γ_e, Γ_r , and the coupling strengths Ω_l, \mathcal{G}_l are as defined in the main text, while 2κ is the cavity intensity decay rate. Note that all energies are measured relative to the cavity resonance, and hence the cavity term in \mathcal{H}_s only involve the loss rate κ . are as defined in the main text, while \mathcal{V}_{kl} is the van der Waals interaction among the Rydberg excitations of atoms k and l . The incoming and outgoing photons are going to be accounted for by the input-output relations. After the storage of the first pulse, the wave-function of the combined field and ensemble with the initial excitation stored in $|r'_k\rangle$ and one incoming photon is given by,

$$\begin{aligned}|\Psi\rangle &= \sum_k \int d\omega \beta_k(\omega) \hat{a}_\omega^\dagger e^{-i\omega t} |g^{N-1}, r'_k, \emptyset\rangle + \sum_k \hat{b}^\dagger C_{bk} |g^{N-1}, r'_k, \emptyset\rangle \\ &+ \sum_l \left\{ C_{ekl} |g^{N-2}, e_l, r'_k, \emptyset\rangle + C_{rkl} |g^{N-2}, r_l, r'_k, \emptyset\rangle \right\}.\end{aligned}\quad (\text{S10})$$

Here $|\emptyset\rangle$ is the vacuum state, C_{ekl} and C_{rkl} are respectively the amplitude of being in the excited state $|e\rangle$ and the Rydberg state $|r\rangle$ when there is one stored Rydberg excitation in the k^{th} atom, while C_{bk} is the amplitude of the cavity excited state. We next evaluate the Schrödinger equation for the wave-function (S10) together with the input-output relations to find the dynamical behavior of the amplitudes C_{ak}, C_{ekl}, C_{rkl}

$$\dot{C}_{bk} = \sum_l C_{ekl} \mathcal{G}_l^* - \kappa C_{bk} + \sqrt{2\kappa} \beta_k^{\text{in}}, \quad (\text{S11})$$

$$\dot{C}_{ekl} = -i(\Delta_l - i\Gamma_{el})C_{ekl} + i\frac{\Omega_l^*}{2}C_{rkl} - \mathcal{G}_l C_{bk}, \quad (\text{S12})$$

$$\dot{C}_{rkl} = -i(\delta_l - i\Gamma_{rkl})C_{rkl} + i\frac{\Omega_l}{2}C_{ekl} - iC_{rkl}\mathcal{V}_{kl}. \quad (\text{S13})$$

The outgoing field amplitude is then given by,

$$\beta_k^{\text{out}}(\omega) = \sqrt{2\kappa} C_{bk}(\omega) - \beta_k^{\text{in}}(\omega), \quad (\text{S14})$$

where C_{bk} is found by solving the set of Eqns. (S11-S13) using Fourier transformation. We thereby get,

$$\begin{aligned}C_{bk}(\omega) &= \sqrt{2\kappa} \beta_k^{\text{in}}(\omega) \mathbf{S}_k(\omega) \\ \mathbf{S}_k(\omega) &= \left(\kappa - i\omega + \sum_l \frac{|\mathcal{G}_l|^2}{(\Gamma_{el} - i\Delta_l - i\omega) + \frac{|\Omega_l/2|^2}{\Gamma_{rl} + i(\delta_l + \mathcal{V}_{kl} - \omega)}} \right)^{-1}.\end{aligned}\quad (\text{S15})$$

Substituting C_{bk} into Eq. (S14) we get,

$$\mathcal{R}_k(\omega) = 2\kappa \left(\kappa - i\omega + \sum_l \frac{|\mathcal{G}_l|^2}{(\Gamma_{el} - i\Delta_l - i\omega) + \frac{|\Omega_l/2|^2}{\Gamma_{rl} + i(\delta_l + \mathcal{V}_{kl} - \omega)}} \right)^{-1} - 1. \quad (\text{S16})$$

Assuming all fields to be resonant i.e. for $\delta_l = \Delta_l = 0$, a long lived Rydberg state ($\Gamma_{rl} = 0$), and slowly varying photon pulses ($\omega = 0$) we get,

$$\mathcal{R}_k = 2 \left(1 + \sum_l \frac{|\mathcal{G}_l|^2 / \kappa \Gamma_e}{1 - i|\Omega_l/2|^2 / \mathcal{V}_{kl} \Gamma_e} \right)^{-1} - 1. \quad (\text{S17})$$

which under the assumption of equal coupling strengths $\mathcal{G}_l = \mathcal{G}$ and Rabi frequencies $\Omega_l = \Omega$, for the defined single atom co-operativity $\mathcal{C} = |\mathcal{G}|^2/\kappa\Gamma_e$ becomes, $\mathcal{R}_k = \left[2(1 + \mathcal{C}_v^*)^{-1} - 1\right]$, where $\mathcal{C}_v^* = \sum_l \mathcal{C}/(1 - i|\Omega/2|^2/\mathcal{V}_{kl}\Gamma_e)$. To get a simple physical understanding of the scattering dynamics, we shall first assume that all atoms are identical (homogeneous). We will consider what happens for an inhomogeneous ensemble in a later section. For the van der Waals interaction potential $\mathcal{V}_{kl} = -C_6/r^6$, where r is the relative distance between the k^{th} and l^{th} atoms, we can evaluate \mathcal{C}_v^* with the sum \sum_l converted to a volume integral $\rightarrow \int ndV$. Thus we get for a homogeneous ensemble with an isotropic potential,

$$\mathcal{C}_v^* = 4\pi n\mathcal{C} \int_0^\infty dr r^2/(1 + i\zeta r^6); \quad \zeta = \frac{|\Omega|^2}{4C_6\Gamma_e}. \quad (\text{S18})$$

We can write this integral as $\mathcal{C}_v^* = \mathcal{C}_b - i\mathcal{C}'_b$ and solved it to get, $|\mathcal{C}_b| = |\mathcal{C}'_b| = \frac{2}{3}(\mathcal{C}n\pi^2/\sqrt{2\zeta})$. Above, we have solved the scattering dynamics in the case where there was already a Rydberg excitation stored. In principle, we should also solve the dynamics without the first stored excitation. In this case, however, the excitations are completely independent of each other. We can then conveniently obtain the results for this situation by simple setting $\mathcal{V}_{kl} = 0$. Then from Eq. (S17) we get $\mathcal{C}_v^* = 0$ for a long photon pulse and hence $\mathcal{R}_g = 1$.

To investigate the effect of pulses of a finite duration, we now consider the bandwidth of the scattering coefficient. To do this, we perform a Taylor series expansion of the reflection coefficient about some central frequency ω_0 ,

$$\mathcal{R}_k(\omega) = \mathcal{R}_k(\omega_0) + \partial_\omega \mathcal{R}_k|_{\omega_0}(\omega - \omega_0) + \frac{1}{2}\partial_\omega^2 \mathcal{R}_k|_{\omega_0}(\omega - \omega_0)^2. \quad (\text{S19})$$

Here we have kept upto the second order in the expansion. The above three terms in the expansion are described by,

$$\mathcal{R}_k(\omega_0) = \left(\frac{2}{1 + \mathcal{C}_v^*} - 1\right) + 2i\frac{\omega_0}{\kappa} \frac{1}{(1 + \mathcal{C}_v^*)^2}, \quad (\text{S20})$$

$$\partial_\omega \mathcal{R}_k|_{\omega_0} = \frac{-4\frac{\omega_0}{\kappa} \left(\frac{1}{\kappa} - \frac{\mathcal{C}_{\alpha v}^*}{\Gamma_e}\right)}{(1 + \mathcal{C}_v^*)^3} + \frac{2i \left(\frac{1}{\kappa} - \frac{\mathcal{C}_{\alpha v}^*}{\Gamma_e}\right)}{(1 + \mathcal{C}_v^*)^2}, \quad (\text{S21})$$

$$\begin{aligned} \partial_\omega^2 \mathcal{R}_k|_{\omega_0} = & \frac{-4 \left(\frac{1}{\kappa} - \frac{\mathcal{C}_{\alpha v}^*}{\Gamma_e}\right)^2}{(1 + \mathcal{C}_v^*)^3} + \frac{4\mathcal{C}_v^* \frac{\mathcal{C}_{\beta v}^*}{\Gamma_e} \left[(\mathcal{C}_v^*)^2 - 3\frac{\omega_0^2}{\kappa^2}\right]}{(1 + \mathcal{C}_v^*)^6} + \frac{4\frac{\omega_0}{\kappa} \frac{\mathcal{C}_{\eta v}^*}{\Gamma_e^2}}{(1 + \mathcal{C}_v^*)^4} + \frac{4\frac{\mathcal{C}_{\chi v}^*}{\Gamma_e^2}}{(1 + \mathcal{C}_v^*)^3}, \\ -4i \left\{ & \frac{3\frac{\omega_0}{\kappa} \left(\frac{1}{\kappa} - \frac{\mathcal{C}_{\alpha v}^*}{\Gamma_e}\right)^2}{(1 + \mathcal{C}_v^*)^4} - \frac{\frac{\omega_0}{\kappa} \frac{\mathcal{C}_{\beta v}^*}{\Gamma_e^2} \left[3(\mathcal{C}_v^*)^2 - \frac{\omega_0^2}{\kappa^2}\right]}{(1 + \mathcal{C}_v^*)^6} + \frac{\frac{\mathcal{C}_{\eta v}^*}{\Gamma_e^2}}{(1 + \mathcal{C}_v^*)^3} + \frac{\frac{\omega_0}{\kappa} \frac{\mathcal{C}_{\chi v}^*}{\Gamma_e^2}}{(1 + \mathcal{C}_v^*)^4} \right\}, \end{aligned} \quad (\text{S22})$$

with the parameters defined by,

$$\mathcal{C}_v^* = \sum_l \frac{\mathcal{C}}{1 - i\frac{\omega_0}{\Gamma_e} + \frac{|\Omega_l/2|^2}{i(\mathcal{V}_{kl} - \omega_0)\Gamma_e}}, \quad \mathcal{C}_{\alpha v}^* = \mathcal{C} \sum_l \frac{1 + |\Omega_l/2|^2/(\mathcal{V}_{kl} - \omega_0)^2}{\left[1 - i\frac{\omega_0}{\Gamma_e} + \frac{|\Omega_l|^2}{i(\mathcal{V}_{kl} - \omega_0)\Gamma_e}\right]^2} \quad (\text{S23})$$

$$\mathcal{C}_{\beta v}^* = \mathcal{C} \sum_l \frac{1 + |\Omega_l/2|^2/(\mathcal{V}_{kl} - \omega_0)^2}{\left[1 - i\frac{\omega_0}{\Gamma_e} + \frac{|\Omega_l/2|^2}{i(\mathcal{V}_{kl} - \omega_0)\Gamma_e}\right]^3}, \quad \mathcal{C}_{\eta v}^* = \mathcal{C} \sum_l \frac{|\Omega_l/2|^2\Gamma_e/(\mathcal{V}_{kl} - \omega_0)^3}{\left[1 - i\frac{\omega_0}{\Gamma_e} + \frac{|\Omega_l/2|^2}{i(\mathcal{V}_{kl} - \omega_0)\Gamma_e}\right]^3} \quad (\text{S24})$$

$$\mathcal{C}_{\chi v}^* = \mathcal{C} \sum_l \frac{|\Omega_l/2|^2\omega_0/(\mathcal{V}_{kl} - \omega_0)^3}{\left[1 - i\frac{\omega_0}{\Gamma_e} + \frac{|\Omega_l/2|^2}{i(\mathcal{V}_{kl} - \omega_0)\Gamma_e}\right]^3}. \quad (\text{S25})$$

Assuming the central frequency of the incoming pulse to be on resonance, we set $\omega_0 = 0$ and hence Eqs. (S20-S22) become substantially simpler and are described by,

$$\mathcal{R}_k = \left(\frac{2}{1 + \mathcal{C}_v^*} - 1\right), \quad (\text{S26})$$

$$\partial_\omega \mathcal{R}_k|_{\omega_0=0} = \frac{2i \left(\frac{1}{\kappa} - \frac{\mathcal{C}_{\alpha v}^*}{\Gamma_e}\right)}{(1 + \mathcal{C}_v^*)^2}, \quad (\text{S27})$$

$$\partial_\omega^2 \mathcal{R}_k|_{\omega_0=0} = \frac{-4 \left(\frac{1}{\kappa} - \frac{\mathcal{C}_{\alpha v}^*}{\Gamma_e}\right)^2}{(1 + \mathcal{C}_v^*)^3} + \frac{4\mathcal{C}_v^* \frac{\mathcal{C}_{\beta v}^*}{\Gamma_e} (\mathcal{C}_v^*)^2}{(1 + \mathcal{C}_v^*)^6} + \frac{4\frac{\mathcal{C}_{\chi v}^*}{\Gamma_e^2}}{(1 + \mathcal{C}_v^*)^3} - 4i \left\{ \frac{\frac{\mathcal{C}_{\eta v}^*}{\Gamma_e^2}}{(1 + \mathcal{C}_v^*)^3} \right\}. \quad (\text{S28})$$

Note that for the case of no stored photon in the ensemble, we have $\mathcal{R}_k \rightarrow \mathcal{R}_g$ and one can also get the Taylor series expansion of \mathcal{R}_g by setting $\mathcal{V}_{kl} = 0$. The expressions for such an expansion at resonance is the same as given by Eqs. (S26 - S28) but now with the set of parameters, $\mathcal{C}_v^* \rightarrow \mathcal{C}^*$, $\mathcal{C}_{\alpha_v}^* \rightarrow \mathcal{C}_\alpha^*$, $\mathcal{C}_{\beta_v}^* \rightarrow \mathcal{C}_\beta^*$, $\mathcal{C}_{\eta_v}^* \rightarrow \mathcal{C}_\eta^*$, $\mathcal{C}_{\chi_v}^* \rightarrow \mathcal{C}_\chi^*$, where the new parameters correspond to Eqs. (S23 -S25) with $\mathcal{V}_{kl} = 0$. From the set of Eqs. (S26-S28), we see that the leading order dispersive contributions are scaled down by a factor of $(\mathcal{C}_v^*)^2$ and $(\mathcal{C}_v^*)^3$ when we compare the situation with and without stored excitation in the first pulse. Hence the spectrally narrowest feature is the width of the EIT resonance without a stored excitation, and this will thus be the limiting factor for the bandwidth.

We next analyze the behaviour of the parameters listed in Eqs. (S23-S25) in different limits of operation. We can find the blockaded part by considering the limits $\mathcal{V}_{kl} \gg |\Omega_l/2|^2/\Gamma_e$, while the contribution from the remaining EIT medium is found in the limit $\mathcal{V}_{kl} \ll |\Omega_l/2|^2/\Gamma_e$. To get a feeling for the expression in Eqs. (S23-S25), we separate them into contributions coming from the blockaded atoms and that from the rest of EIT medium,

$$\mathcal{C}_v^* \approx \mathcal{C}_b + i\mathcal{C}'_b = \sum_l \frac{\mathcal{C}}{\left[1 + \frac{|\Omega/2|^4}{\mathcal{V}_{kl}^2 \Gamma_e^2}\right]} + i \sum_l \frac{\mathcal{C} \frac{|\Omega/2|^2}{\mathcal{V}_{kl} \Gamma_e}}{\left[1 + \frac{|\Omega/2|^4}{\mathcal{V}_{kl} \Gamma_e^2}\right]}; \quad (\text{S29})$$

$$\mathcal{C}_{\alpha_v}^* = \mathcal{C}_b^{*\alpha} - N_{EIT}^\alpha \mathcal{C} \frac{\Gamma_e^2}{|\Omega/2|^2}, \quad \mathcal{C}_{\beta_v}^* = \mathcal{C}_b^{*\beta}; \quad (\text{S30})$$

$$\mathcal{C}_{\eta_v}^* = \mathcal{C}_b^{*\eta} - iN_{EIT}^\eta \mathcal{C} \frac{\Gamma_e^4}{|\Omega/2|^4}, \quad \mathcal{C}_{\chi_v}^* = 0, \quad (\text{S31})$$

where we have assumed all the Rabi frequencies to be equal such that $\Omega_l = \Omega$ and $\mathcal{C}_v^{*\alpha} = \sum_l \mathcal{C}/(1 + |\Omega/2|^2/i\mathcal{V}_{kl}\Gamma_e)^2$, $\mathcal{C}_v^{*\beta} = \mathcal{C}_v^{*\eta} = \sum_l \mathcal{C}/(1 + |\Omega/2|^2/i\mathcal{V}_{kl}\Gamma_e)^3$, which scale as the number of blocked atoms \mathcal{C}_b while $N_{EIT}^\alpha, N_{EIT}^\beta$ scale as the number of remaining unblocked atoms $\sim N$. Similarly, for the case of no stored excitation, we get,

$$\mathcal{C}^* = 0, \quad \mathcal{C}_\alpha^* = -N\mathcal{C} \frac{\Gamma_e^2}{|\Omega/2|^2}, \quad \mathcal{C}_\beta^* = 0; \quad (\text{S32})$$

$$\mathcal{C}_\eta^* = -iN\mathcal{C} \frac{\Gamma_e^4}{|\Omega/2|^4}, \quad \mathcal{C}_\chi^* = 0. \quad (\text{S33})$$

Note that since in this case there is no Rydberg excitation blockade, only the EIT medium contributes and all the terms arising due to blockade are zero.

CHOI-JAMIOLKOWSKI FIDELITY

The Choi-Jamiolkowski (CJ) fidelity is a measure of how close two given quantum mechanical processes are. The idea is to apply each process to a particular entangled state and then calculate the fidelity between the two output states. Specifically, we assume that the two processes are described by the superoperators \mathcal{U} and \mathcal{V} . The superoperator \mathcal{U} represents the ideal process that we want to accomplish and is assumed to be unitary. Hence, its action on some density matrix ρ can be written as

$$\mathcal{U}(\rho) = U\rho U^\dagger, \quad (\text{S34})$$

where U is a unitary operator. The actual physical implementation is represented by the completely positive trace preserving superoperator \mathcal{V} . In general, it admits a Kraus (operator-sum) decomposition

$$\mathcal{V}(\rho) = \sum_l V_l \rho V_l^\dagger \quad (\text{S35})$$

with $\sum_l V_l^\dagger V_l = I$ (I is the identity operator). If we separate out the ‘‘no jump’’ evolution with the effective non-Hermitian Hamiltonian \mathcal{H} in Eq. (S35), we can write

$$\mathcal{V}(\rho) = V\rho V^\dagger + \sum_l K_l \rho K_l^\dagger, \quad (\text{S36})$$

where $V = \exp(-i\mathcal{H}t_f/\hbar)$ with t_f being the time it takes to accomplish the wanted operation. The operators K_l form the Kraus decomposition of the part of the evolution where at least one quantum jump occurs.

To find the CJ fidelity, we consider the superoperators $\mathcal{I} \otimes \mathcal{U}$ and $\mathcal{I} \otimes \mathcal{V}$ that are tensor products of the original ones with the identity superoperator \mathcal{I} . We pick an orthonormal basis set $\{|j\rangle\}$ for the d -dimensional Hilbert space that \mathcal{U} and \mathcal{V} act on. Now

we can define the state $|\Phi\rangle = \sum_j |j\rangle|j\rangle/\sqrt{d}$ that is an element of the original Hilbert space tensored with a copy of itself. Note that $|\Phi\rangle$ is a maximally entangled state of these two copies. We will only consider a two-qubit gate, so that $d = 4$ in the above.

After applying $\mathcal{I} \otimes \mathcal{U}$ and $\mathcal{I} \otimes \mathcal{V}$ onto the density matrix $|\Phi\rangle\langle\Phi|$, we get a pair of new states

$$\rho_{\mathcal{U}} = [\mathcal{I} \otimes \mathcal{U}]|\Phi\rangle\langle\Phi| = (I \otimes U)|\Phi\rangle\langle\Phi|(I \otimes U^\dagger), \quad (\text{S37})$$

$$\rho_{\mathcal{V}} = [\mathcal{I} \otimes \mathcal{V}]|\Phi\rangle\langle\Phi| = (I \otimes V)|\Phi\rangle\langle\Phi|(I \otimes V^\dagger) + \sum_l (I \otimes K_l)|\Phi\rangle\langle\Phi|(I \otimes K_l^\dagger). \quad (\text{S38})$$

The CJ fidelity is defined to be the fidelity of these two states. Since $\rho_{\mathcal{U}}$ is a pure state, we get

$$\begin{aligned} F_{\text{CJ}} = F(\rho_{\mathcal{U}}, \rho_{\mathcal{V}}) &= \langle\Phi|(I \otimes U^\dagger)\rho_{\mathcal{V}}(I \otimes U)|\Phi\rangle \\ &= |\langle\Phi|(I \otimes U^\dagger V)|\Phi\rangle|^2 + \sum_l |\langle\Phi|(I \otimes U^\dagger K_l)|\Phi\rangle|^2. \end{aligned} \quad (\text{S39})$$

STORAGE AND RETRIEVAL

The full physical process to implement the controlled-phase gate consists of storage of one photon, scattering of the second one, and retrieval of the first. The theory of storage and retrieval with an ensemble in a cavity is well established. In suitable regimes these results show that we have a mapping between a single mode of the atomic ensemble and a specific incoming or outgoing optical mode, and all other modes will be uncoupled [1]. Hence, the process of storage is described by a single parameter, which is the storage efficiency of a single incoming photon to create a specific spin wave

$$|S\rangle = \sum_k \alpha_k |g^{N-1}, r'_k\rangle. \quad (\text{S40})$$

After scattering of the second photon, this spin wave will get multiplied by the reflection coefficient of the second photon such that it becomes

$$|S_{\mathcal{R}}\rangle = \sum_k \alpha_k \mathcal{R}_k(\omega) |g^{N-1}, r'_k\rangle,$$

where ω is the frequency of the second photon. Note here that the scattering coefficient may depend on which atom the first photon was stored in since different atoms may experience different degrees of blockade. For the retrieval, the cavity maps the particular spin wave (S40) to a specific temporal mode. Hence, the amplitude of the retrieved photon is given by the shape of that temporal mode multiplied by the overlap

$$\langle S|S_{\mathcal{R}}\rangle = \sum_k |\alpha_k|^2 \mathcal{R}_k(\omega).$$

In general, the retrieved wavepacket will also need to be multiplied by the square root of the overall storage and retrieval efficiency, but we neglect this in our analysis.

For the fidelity calculations, one would need to calculate the overlap of the retrieved photon wavepackets corresponding to $|S\rangle$ and $|S_{\mathcal{R}}\rangle$. However, by the discussion above, the overlap of the photon wavepackets will be equal to the overlap of the spin waves $|S\rangle$ and $|S_{\mathcal{R}}\rangle$. Hence, in the calculations below, we will directly calculate the fidelities by projecting the spin waves instead of analysing the retrieval.

FIDELITY IN THE SINGLE-RAIL ENCODING

In the single-rail encoding the computational basis is

$$\begin{aligned} |00(t)\rangle &= |g^N\rangle|\emptyset\rangle, \\ |01(t)\rangle &= |g^N\rangle \int d\omega \phi(\omega) \hat{a}_\omega^\dagger e^{-i\omega t} |\emptyset\rangle, \\ |10(t)\rangle &= \sum_k \alpha_k |g^{N-1}, r'_k\rangle |\emptyset\rangle, \\ |11(t)\rangle &= \sum_k \alpha_k |g^{N-1}, r'_k\rangle \int d\omega \phi(\omega) \hat{a}_\omega^\dagger e^{-i\omega t} |\emptyset\rangle. \end{aligned} \quad (\text{S41})$$

Note that this basis is time dependent due to the free evolution phase $\exp(-i\omega t)$. Hence, we define the ideal operation \mathcal{U} such that it includes this free evolution phase. Specifically, if we denote the computational basis states at the initial time $t = 0$ by omitting the time variable, i.e. $|jj'\rangle = |jj'(t=0)\rangle$ ($j, j' \in \{0, 1\}$), then the ideal operation of the controlled-phase gate is given by

$$U|00\rangle = |00(t_f)\rangle, \quad U|01\rangle = |01(t_f)\rangle, \quad U|10\rangle = |10(t_f)\rangle, \quad U|11\rangle = -|11(t_f)\rangle. \quad (\text{S42})$$

Using the computational basis (S41) we can write

$$|\Phi\rangle = \frac{1}{2} (|00\rangle|00\rangle + |01\rangle|01\rangle + |10\rangle|10\rangle + |11\rangle|11\rangle).$$

Inserting this specific form of $|\Phi\rangle$ into (S39) we obtain

$$F_{\text{CJ}} = \frac{1}{16} \left| \langle 00|U^\dagger V|00\rangle + \langle 01|U^\dagger V|01\rangle + \langle 10|U^\dagger V|10\rangle + \langle 11|U^\dagger V|11\rangle \right|^2 + \frac{1}{16} \sum_l \left| \langle 00|U^\dagger K_l|00\rangle + \langle 01|U^\dagger K_l|01\rangle + \langle 10|U^\dagger K_l|10\rangle + \langle 11|U^\dagger K_l|11\rangle \right|^2. \quad (\text{S43})$$

For the operators K_l , we assume that $\langle jj'(t_f)|K_l|jj'\rangle = 0$, where $j, j' \in \{0, 1\}$. Physically, this assumption means that if a quantum jump (incoherent decay) occurs, the given basis will switch to another state of the physical system (possibly even one of the other basis states) but can never be driven back to the original state. I.e. if a photon is lost, it will result in a vacuum output, and thus it does not give an overlap with the original state. Under this assumption, we only need to compute the dynamics due to the non-Hermitian Hamiltonian. The detailed calculation is presented in Sec. . In essence, the result is that the dynamics of the operator V can be described by the scattering relations

$$\begin{aligned} V|00\rangle &= |g^N\rangle|\emptyset\rangle, \\ V|01\rangle &= |g^N\rangle \int d\omega \mathcal{R}_g(\omega) \phi(\omega) \hat{a}_\omega^\dagger e^{-i\omega t_f} |\emptyset\rangle, \\ V|10\rangle &= \sum_k \alpha_k |g^{N-1}, r'_k\rangle |\emptyset\rangle, \\ V|11\rangle &= \int d\omega \sum_k \alpha_k \mathcal{R}_k(\omega) \phi(\omega) \hat{a}_\omega^\dagger e^{-i\omega t_f} |g^{N-1}, r'_k\rangle |\emptyset\rangle. \end{aligned} \quad (\text{S44})$$

Gathering all the formulas in this section, the CJ fidelity becomes

$$F_{\text{CJ}} = \frac{1}{16} \left| 2 + \int d\omega |\phi(\omega)|^2 \mathcal{R}_g(\omega) - \int d\omega |\phi(\omega)|^2 \sum_k |\alpha_k|^2 \mathcal{R}_k(\omega) \right|^2. \quad (\text{S45})$$

FIDELITY IN THE DUAL-RAIL ENCODING

In this section we calculate both the CJ fidelity and the entanglement swap fidelity for the dual-rail encoding and show how they relate to each other. The circuit diagram of the entanglement swap operation is shown in Fig. S4.

The entanglement swap operation consists of evolution of the initial state (which is unitary in the ideal case) and a subsequent measurement. The evolution can be decomposed into a controlled-phase gate and Hadamard gates. If the Hadamard gates are assumed to be ideal, then the CJ fidelity of the whole evolution is equal to the CJ fidelity of the controlled-phase gate. We are going to use this fact in relating the CJ fidelity to the entanglement swap fidelity.

The abstract definition of the CJ fidelity does not make any reference to a particular basis. In this section, in addition to the computational basis, we will also use the Bell basis, since it is the natural choice for the entanglement swap operation. The Bell states are

$$\begin{aligned} |\phi^{00}\rangle &= |\phi^+\rangle = \frac{1}{\sqrt{2}} (|00\rangle + |11\rangle), \\ |\phi^{01}\rangle &= |\psi^+\rangle = \frac{1}{\sqrt{2}} (|01\rangle + |10\rangle), \\ |\phi^{10}\rangle &= |\phi^-\rangle = \frac{1}{\sqrt{2}} (|00\rangle - |11\rangle), \\ |\phi^{11}\rangle &= |\psi^-\rangle = \frac{1}{\sqrt{2}} (|01\rangle - |10\rangle). \end{aligned} \quad (\text{S46})$$

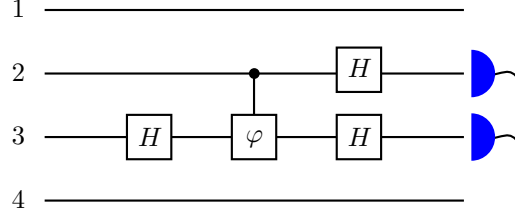


FIG. S4: (a) The circuit diagram of the entanglement swap operation. The numbers at the left edge indicate the label of the subsystem (qubit). In the circuit, the Hadamard gates are denoted by H and the controlled-phase gate is denoted by φ .

In addition to the conventional names, we also give numbers to the Bell states, which will allow us to express summations in a simple way below.

For the entanglement swap circuit of Fig. S4, the initial state is one Bell pair $|\phi^+\rangle_{12}$ between subsystems 1 and 2 and another Bell pair $|\phi^+\rangle_{34}$ between subsystems 3 and 4. Note that this initial state can be written as

$$|\phi^+\rangle_{12}|\phi^+\rangle_{34} = \frac{1}{2} \sum_{j,j'=0}^1 |\phi^{jj'}\rangle_{14}|\phi^{jj'}\rangle_{23} = |\Phi\rangle_{1423}.$$

This is exactly the state that is used as the input for the calculation of the CJ fidelity expressed in the Bell basis. After evolution of subsystems 2 and 3 as shown by the circuit and a measurement (the two detectors to the right), a Bell pair between subsystems 1 and 4 is established.

The practical implementation of the above circuit is shown in Fig. 1(c) of the main text. Whereas Fig. S4 displays the extended four-qubit Hilbert space required for the calculation of the CJ and entanglement swap fidelity, Fig. 1(c) only displays the two central subsystems (2 and 3), but each of the two subsystems are represented by the photon being in two distinct modes.

We define $\hat{a}_{0,\omega}^\dagger$ to be the creation operator for subsystem 3 in state $|0\rangle$ with frequency ω , and $\hat{a}_{1,\omega}^\dagger$ to be the creation operator for state $|1\rangle$. For notational convenience, we define the states $|0_\omega\rangle_3 = \hat{a}_{0,\omega}^\dagger|\emptyset\rangle$ and $|1_\omega\rangle_3 = \hat{a}_{1,\omega}^\dagger|\emptyset\rangle$. Then in the dual-rail encoding, the computational basis is

$$\begin{aligned} |0\rangle_2 &= \sum_k \alpha_k |g^{N-1}, r'_k\rangle_0, \\ |1\rangle_2 &= \sum_k \alpha_k |g^{N-1}, r'_k\rangle_1, \\ |0(t)\rangle_3 &= \int d\omega \phi(\omega) e^{-i\omega t} |0_\omega\rangle_3, \\ |1(t)\rangle_3 &= \int d\omega \phi(\omega) e^{-i\omega t} |1_\omega\rangle_3. \end{aligned} \tag{S47}$$

Here, $|g^{N-1}, r'_k\rangle_0$ are the states of the memory (the ensemble which does not interact with the second photon), and $|g^{N-1}, r'_k\rangle_1$ are the states of the cavity from which the second photon is scattered (see Fig. 1(c) of the main text). These two states correspond to subsystem 2 of Fig. S4. Subsystem 3 is encoded in photonic states which are not stored but only scattered. Note that all of the resulting computational basis states $|00\rangle_{23}$, $|01\rangle_{23}$, $|10\rangle_{23}$ and $|11\rangle_{23}$ physically correspond to having two excitations. Hence, it allows for simple means of error detection: if less than two excitations are present at the end of the evolution, we know that an error has occurred. In the dual-rail basis, the action of the operator V_{23} that corresponds to the physical implementation of the

controlled-phase gate can be written

$$\begin{aligned}
V_{23}|00\rangle_{23} &= \sum_k \alpha_k |g^{N-1}, r'_k\rangle_0 \int d\omega \phi(\omega) e^{-i\omega t_f} |0_\omega\rangle_3, \\
V_{23}|01\rangle_{23} &= \sum_k \alpha_k |g^{N-1}, r'_k\rangle_0 \int d\omega \mathcal{R}_g(\omega) \phi(\omega) e^{-i\omega t_f} |1_\omega\rangle_3, \\
V_{23}|10\rangle_{23} &= \sum_k \alpha_k |g^{N-1}, r'_k\rangle_1 \int d\omega \phi(\omega) e^{-i\omega t_f} |0_\omega\rangle_3, \\
V_{23}|11\rangle_{23} &= \int d\omega \sum_k \alpha_k \mathcal{R}_k(\omega) \phi(\omega) e^{-i\omega t_f} |g^{N-1}, r'_k\rangle_1 |1_\omega\rangle_3.
\end{aligned} \tag{S48}$$

For the operators corresponding to the full evolution of the circuit of Fig. S4, we also need to describe the Hadamard operators. In the dual-rail encoding, the Hadamard operations are obtained by impinging the photons on beamsplitters which work on all frequency components separately. This is important for subsystem 3 (the scattered photon), since the frequency components will be multiplied with, in general, different reflection coefficients $\mathcal{R}_g(\omega)$ and $\mathcal{R}_k(\omega)$ depending on the input state. Hence the definition of the Hadamard operator here needs to be per frequency component, i.e. $H_3|0_\omega\rangle_3 = (|0_\omega\rangle_3 + |1_\omega\rangle_3)/\sqrt{2}$ and $H_3|1_\omega\rangle_3 = (|0_\omega\rangle_3 - |1_\omega\rangle_3)/\sqrt{2}$. For subsystem 2, the single mode retrieval precludes any such difference in the mode shape for photons that are incident on the beamsplitters. Hence we can define the Hadamard operators to act on the spin wave states directly, $H_2|0\rangle_2 = (|0\rangle_2 + |1\rangle_2)/\sqrt{2}$ and $H_2|1\rangle_2 = (|0\rangle_2 - |1\rangle_2)/\sqrt{2}$.

In analogy with Eqs. (S34) and (S36), we define the superoperators \tilde{U} and \tilde{V} for the ideal and the real version of the circuit of Fig. S4. They can be written as

$$\tilde{U}_{23}(\rho) = \tilde{U}_{23} \rho \tilde{U}_{23}^\dagger,$$

and

$$\tilde{V}_{23}(\rho) = \tilde{V}_{23} \rho \tilde{V}_{23}^\dagger + \sum_l \tilde{K}_{l,23} \rho \tilde{K}_{l,23}^\dagger,$$

where

$$\begin{aligned}
\tilde{U}_{23} &= (H_2 \otimes H_3) U_{23} (I_2 \otimes H_3), \\
\tilde{V}_{23} &= (H_2 \otimes H_3) V_{23} (I_2 \otimes H_3), \\
\tilde{K}_{l,23} &= (H_2 \otimes H_3) K_{l,23} (I_2 \otimes H_3).
\end{aligned} \tag{S49}$$

Note that with the definitions (S42), (S46) and (S49), it holds that $\tilde{U}_{23}|\phi^{jj'}\rangle = |jj'(t_f)\rangle$.

In this setting, not only the input states used for the entanglement swapping match the ones used for the CJ fidelity, also the actual operation itself has the same form: an identity operation acting on subsystems 1 and 4, while subsystems 2 and 3 are evolved according to either \tilde{U} or \tilde{V} . The two output states are then

$$\begin{aligned}
\rho_{\tilde{U}} &= [\mathcal{I}_{14} \otimes \tilde{U}_{23}] (|\Phi\rangle\langle\Phi|) = (I_{14} \otimes \tilde{U}_{23}) |\Phi\rangle\langle\Phi| (I_{14} \otimes \tilde{U}_{23}^\dagger), \\
\rho_{\tilde{V}} &= [\mathcal{I}_{14} \otimes \tilde{V}_{23}] (|\Phi\rangle\langle\Phi|) = (I_{14} \otimes \tilde{V}_{23}) |\Phi\rangle\langle\Phi| (I_{14} \otimes \tilde{V}_{23}^\dagger) + \sum_l (I_{14} \otimes \tilde{K}_{l,23}) |\Phi\rangle\langle\Phi| (I_{14} \otimes \tilde{K}_{l,23}^\dagger).
\end{aligned}$$

Now we want to use the error detection property of the dual-rail encoding. We define the projection operators

$$\hat{P}_{jj'} = I_{14} \otimes |j\rangle\langle j|_2 \otimes \left(\int d\omega |j'_\omega\rangle\langle j'_\omega|_3 \right) \tag{S50}$$

where $j, j' \in \{0, 1\}$, and we also define their sum

$$\hat{P} = \sum_{j,j'=0}^1 \hat{P}_{jj'}. \tag{S51}$$

The projection operators of Eq. (S50) correspond to measuring the states $|jj'\rangle_{23}$ on the detectors of circuit of Fig. S4. Note that for subsystem 3, we project onto the entire subspace that is spanned by the states $|j'_\omega\rangle$ instead of choosing a particular mode. This is equivalent to the assumption that all frequency components contribute to the probability of a ‘‘click’’ on the detector. On the

other hand, the operator of Eq. (S51) has a less clear physical interpretation. Formally, it projects a given state onto the subspace with two excitations. The motivation for defining such an operator is to be able to relate the CJ fidelity to the entanglement swap fidelity as we will see below. Since the entanglement swap fidelity can only be understood as a conditional fidelity (conditioned on the measurement outcomes corresponding to the operators of Eq. (S50)), the CJ fidelity also needs to be conditional.

Let us begin with the calculation of the entanglement swap fidelity. Using the states after the measurement has taken place

$$\rho_{jj'} = \frac{\hat{P}_{jj'} \rho_{\tilde{V}} \hat{P}_{jj'}^\dagger}{\text{tr}(\hat{P}_{jj'} \rho_{\tilde{V}} \hat{P}_{jj'}^\dagger)},$$

we can define the conditional fidelities for the entanglement swap

$$F_{jj'} = \langle \phi^{jj'} | \text{tr}_{23}(\rho_{jj'}) | \phi^{jj'} \rangle_{14}. \quad (\text{S52})$$

Here, we take the trace over subsystems 2 and 3, since the relevant question is how close subsystems 1 and 4 are to a particular Bell pair. The trace can be written as

$$\text{tr}_{23}(\rho_{jj'}) = \sum_{n,n'=0}^1 \int d\omega \langle n | {}_2 \langle n'_\omega | {}_3 \rho_{jj'} | n'_\omega \rangle_3 | n \rangle_2 = \frac{1}{\text{tr}(\hat{P}_{jj'} \rho_{\tilde{V}} \hat{P}_{jj'}^\dagger)} \int d\omega \langle j | {}_2 \langle j'_\omega | {}_3 \rho_{\tilde{V}} | j'_\omega \rangle_3 | j \rangle_2.$$

Projecting $\rho_{\tilde{V}}$ onto $|\phi^{jj'}\rangle_{14}$ we obtain

$$\langle \phi^{jj'} | \rho_{\tilde{V}} | \phi^{jj'} \rangle_{14} = \frac{1}{4} \tilde{V}_{23} |\phi^{jj'}\rangle_{23} \langle \phi^{jj'} | {}_{23} \tilde{V}_{23}^\dagger + \frac{1}{4} \sum_l \tilde{K}_{l,23} |\phi^{jj'}\rangle_{23} \langle \phi^{jj'} | {}_{23} \tilde{K}_{l,23}^\dagger.$$

For the dual-rail encoding, we have a stronger assumption about the operators K_l than for the single-rail encoding. We are going to assume that $\langle n | {}_2 \langle n'_\omega | {}_3 K_l | j j' \rangle = 0$, where $n, n', j, j' \in \{0, 1\}$. Physically, this assumption means that the decay processes take the state out of the computational basis entirely, since any such decay will reduce the number of the total excitations to less than two. Then the expression for the fidelity (S52) becomes

$$F_{jj'} = \frac{1}{4 \text{tr}(\hat{P}_{jj'} \rho_{\tilde{V}} \hat{P}_{jj'}^\dagger)} \int d\omega \left| \langle j | {}_2 \langle j'_\omega | {}_3 (H_2 \otimes H_3) V_{23} (I_2 \otimes H_3) | \phi^{jj'} \rangle_{23} \right|^2.$$

with the trace in the denominator given by

$$\text{tr}(\hat{P}_{jj'} \rho_{\tilde{V}} \hat{P}_{jj'}^\dagger) = \frac{1}{4} \sum_{n,n'=0}^1 \int d\omega \left| \langle n | {}_2 \langle n'_\omega | {}_3 (H_2 \otimes H_3) V_{23} (I_2 \otimes H_3) | \phi^{jj'} \rangle_{23} \right|^2.$$

For all j and j' we get

$$\text{tr}(\hat{P}_{jj'} \rho_{\tilde{V}} \hat{P}_{jj'}^\dagger) = \frac{1}{16} \int d\omega |\phi(\omega)|^2 \left(2 + |\mathcal{R}_g(\omega)|^2 + \left| \sum_k |\alpha_k|^2 \mathcal{R}_k(\omega) \right|^2 \right)$$

and

$$F_{\text{swap}} = F_{jj'} = \frac{1}{16 P_{\text{suc}}} \int d\omega |\phi(\omega)|^2 \left| 2 + \mathcal{R}_g(\omega) - \sum_k |\alpha_k|^2 \mathcal{R}_k(\omega) \right|^2, \quad (\text{S53})$$

where we have defined the success probability $P_{\text{suc}} = \sum_{j,j'=0}^1 \text{tr}(\hat{P}_{jj'} \rho_{\tilde{V}} \hat{P}_{jj'}^\dagger)$, i.e.

$$P_{\text{suc}} = \frac{1}{4} \int d\omega |\phi(\omega)|^2 \left(2 + |\mathcal{R}_g(\omega)|^2 + \left| \sum_k |\alpha_k|^2 \mathcal{R}_k(\omega) \right|^2 \right). \quad (\text{S54})$$

Now we look at the conditional CJ fidelity. Using the state

$$\rho'_{\tilde{V}} = \frac{\hat{P} \rho_{\tilde{V}} \hat{P}^\dagger}{\text{tr}(\hat{P} \rho_{\tilde{V}} \hat{P}^\dagger)} \quad (\text{S55})$$

we can define the conditional CJ fidelity as $F'_{\text{CJ}} = F(\rho_{\bar{U}}, \rho'_{\bar{V}})$. By the cyclicity and linearity of the trace, we have

$$\text{tr}(\hat{P}\rho_{\bar{V}}\hat{P}^\dagger) = \sum_{j,j'=0}^1 \text{tr}(\hat{P}_{jj'}\rho_{\bar{V}}\hat{P}_{jj'}^\dagger) = P_{\text{succ}}.$$

The projection operator \hat{P} has no effect on the states $|\Phi\rangle$, hence $F(\rho_{\bar{U}}, \hat{P}\rho_{\bar{V}}\hat{P}^\dagger) = F(\rho_{\bar{U}}, \rho_{\bar{V}})$, and the analysis reduces to finding the unconditional CJ fidelity and dividing by the success probability P_{succ} . The final result is

$$F'_{\text{CJ}} = \frac{1}{16P_{\text{succ}}} \left| 2 + \int d\omega |\phi(\omega)|^2 \mathcal{R}_g(\omega) - \int d\omega |\phi(\omega)|^2 \sum_k |\alpha_k|^2 \mathcal{R}_k(\omega) \right|^2. \quad (\text{S56})$$

Comparing Eqs. (S53) and (S56) we see that the only difference is the order of integration and taking the absolute value. Thus in general, we have $F'_{\text{CJ}} \leq F_{\text{swap}}$. If the bandwidth of the second photon is narrow compared to the the frequency variations of \mathcal{R}_g and \mathcal{R}_k , then the two fidelity measures become equal. The reason for this similarity is that the two measures consider the same input, but they do not consider exactly the same output. For the CJ fidelity the question we ask is what is the output with a particular mode, which we for simplicity take to be the same as the input mode. Possibly the CJ fidelity can therefore be increased by considering a more appropriate output mode. For the swapping fidelity we on the other hand consider everything which is incident on the photodetectors regardless of the temporal mode and hence this fidelity is higher.

THE GATE FIDELITIES FOR THE RYDBERG CONTROLLED-PHASE GATE

In the single-rail case, we evaluate the CJ fidelity (S45). To evaluate the quantity inside the modulus square we expand it and use Eq. (S19) and the corresponding expansion for \mathcal{R}_g to get,

$$\Delta\mathcal{R} = \mathcal{R}_g - \sum_k |\alpha_k|^2 \mathcal{R}_k = \frac{2\mathcal{C}_b + 2i\mathcal{C}'_b}{(1 + \mathcal{C}_b) + i\mathcal{C}'_b} \quad (\text{S57})$$

$$\Delta\mathcal{R}' = \left[\mathcal{R}'_g - \sum_k |\alpha_k|^2 \mathcal{R}'_k \right] = 2i \left(\frac{1}{\kappa} + \frac{N\mathcal{C}\Gamma_e}{|\Omega/2|^2} \right) - 2i \left(\frac{1}{\kappa} + \frac{N_{\text{EIT}}^\alpha \mathcal{C}\Gamma_e}{|\Omega/2|^2} \right) \frac{1}{(1 + \mathcal{C}_b)^2} + \frac{2i\mathcal{C}_b^{*\alpha}}{\Gamma_e} \quad (\text{S58})$$

$$\begin{aligned} \Delta\mathcal{R}'' &= \left[\mathcal{R}''_g - \sum_k |\alpha_k|^2 \mathcal{R}''_k \right] = -4 \left(\frac{1}{\kappa} + \frac{N\mathcal{C}\Gamma_e}{|\Omega/2|^2} \right)^2 + 4 \left(\frac{1}{\kappa} + \frac{N_{\text{EIT}}^\alpha \mathcal{C}\Gamma_e}{|\Omega/2|^2} \right)^2 \frac{1}{(1 + \mathcal{C}_b)^3} \\ &+ 4 \frac{(\frac{\mathcal{C}_b^{*\alpha}}{\Gamma_e})^2}{(1 + \mathcal{C}_b)^3} - 4 \frac{N\Gamma_e^2 \mathcal{C}}{|\Omega/2|^4} + 4 \frac{N_{\text{EIT}}^\eta \Gamma_e^2 \mathcal{C}}{|\Omega/2|^4} \frac{1}{(1 + \mathcal{C}_b)^3} - 4 \frac{\mathcal{C}_b^{*\beta}}{\mathcal{C}_b^3} + 4i \frac{\mathcal{C}_b^{*\eta}}{\Gamma_e^2 (1 + \mathcal{C}_b)^3} \end{aligned} \quad (\text{S59})$$

In deriving the above expressions, we have assumed that the ensemble is homogeneous and that the potential is isotropic. Hence we have dropped the index k from \mathcal{V}_{kl} . We can then do the sum over k and given that α_k are normalized, we have $\sum_k |\alpha_k|^2 = 1$ in the above expressions.

A closer look at Eq. (S45) suggests a further simplification which gives us,

$$F_{\text{CJ}} = \frac{1}{16} \left(4 + |\Delta\mathcal{R}|^2 + 4\mathbf{Re}[\Delta\mathcal{R}] + 2\mathbf{Re}[\Delta\mathcal{R}''](\Delta\omega)^2 + \mathbf{Re}[\Delta\mathcal{R}\Delta\mathcal{R}''^*](\Delta\omega)^2 \right) \quad (\text{S60})$$

where we have assumed narrow bandwidth of the pulse and defined the variance of the incoming pulse as $(\Delta\omega)^2 = \int d\omega |\phi(\omega)|^2 (\omega - \omega_0)^2$. Substituting Eqs. (S57 - S59) in Eq. (S60) and assuming that $\mathcal{C}_b, \mathcal{C}'_b \gg 1$ and $\mathcal{C}_b^{*\beta}, \mathcal{C}_b^{*\alpha} < \mathcal{C}_b^2$, we get,

$$\begin{aligned} F_{\text{CJ}} &\simeq \left[1 - \frac{(1 + \mathcal{C}_b)}{(1 + \mathcal{C}_b)^2 + \mathcal{C}_b'^2} \right] + \frac{1}{4[(1 + \mathcal{C}_b)^2 + \mathcal{C}_b'^2]} - \frac{N\mathcal{C}\Gamma_e^2}{2|\Omega/2|^4} (\Delta\omega)^2 \left(1 + \frac{\mathcal{C}_b(1 + \mathcal{C}_b) + \mathcal{C}_b'^2}{(1 + \mathcal{C}_b)^2 + \mathcal{C}_b'^2} \right) \\ &- \frac{1}{2} \left(\frac{1}{\kappa} + \frac{N\mathcal{C}\Gamma_e}{|\Omega/2|^2} \right)^2 \left(1 + \frac{\mathcal{C}_b(1 + \mathcal{C}_b) + \mathcal{C}_b'^2}{(1 + \mathcal{C}_b)^2 + \mathcal{C}_b'^2} \right) (\Delta\omega)^2 \end{aligned} \quad (\text{S61})$$

Considering only the leading order contribution to the fidelity, we get,

$$F_{\text{CJ}} = 1 - \frac{(1 + C_b)}{(1 + C_b)^2 + C_b'^2} - \frac{N\mathcal{C}\Gamma_e^2}{|\Omega/2|^4}(\Delta\omega)^2 - \left(\frac{1}{\kappa} + \frac{N\mathcal{C}\Gamma_e}{|\Omega/2|^2}\right)^2 (\Delta\omega)^2 \quad (\text{S62})$$

For the dual-rail case, we calculate a conditional swap fidelity (S53) and the success probability (S54). We can write (S53) as

$$F_{\text{swap}} = \frac{1}{16P_{\text{suc}}} \left(4 + |\Delta\mathcal{R}|^2 + 4\mathbf{Re}[\Delta\mathcal{R}] + |\Delta\mathcal{R}'|^2(\Delta\omega)^2 + 2\mathbf{Re}[\Delta\mathcal{R}''](\Delta\omega)^2 + \mathbf{Re}[\Delta\mathcal{R}\Delta\mathcal{R}''^*](\Delta\omega)^2 \right) \quad (\text{S63})$$

which under the assumption that $C_b, C_b' \gg 1$ and $C_b^{*\beta}, C_b^{*\alpha} < C_b^2$, becomes,

$$\begin{aligned} &= \frac{1}{16P_{\text{suc}}} \left(16 \left[1 - \frac{(1 + C_b)}{(1 + C_b)^2 + C_b'^2} \right] + \frac{4}{(1 + C_b)^2 + C_b'^2} - \frac{8N\mathcal{C}\Gamma_e^2}{|\Omega/2|^4}(\Delta\omega)^2 \left(1 + \frac{C_b(1 + C_b) + C_b'^2}{(1 + C_b)^2 + C_b'^2} \right) \right. \\ &- 8 \left(\frac{1}{\kappa} + \frac{N\mathcal{C}\Gamma_e}{|\Omega/2|^2} \right)^2 \left(1 + \frac{C_b(1 + C_b) + C_b'^2}{(1 + C_b)^2 + C_b'^2} \right) (\Delta\omega)^2 + 4 \left(\frac{1}{\kappa} + \frac{N\mathcal{C}\Gamma_e}{|\Omega/2|^2} \right)^2 (\Delta\omega)^2 \\ &\left. - 8 \left(\frac{1}{\kappa} + \frac{N\mathcal{C}\Gamma_e}{|\Omega/2|^2} \right) \left(\frac{1}{\kappa} + \frac{N_{\text{EIT}}^\alpha \mathcal{C}\Gamma_e}{|\Omega/2|^2} \right) \frac{1}{(1 + C_b)^2} (\Delta\omega)^2 \right) \quad (\text{S64}) \end{aligned}$$

The success probability (S54) is then

$$P_{\text{suc}} = \frac{1}{4} \left(2 + |\mathcal{R}_g|^2 + |\mathcal{R}_g'|^2(\Delta\omega)^2 + \mathbf{Re}[\mathcal{R}_g\mathcal{R}_g''^*](\Delta\omega)^2 + |\mathcal{R}_k|^2 + |\mathcal{R}_k'|^2(\Delta\omega)^2 + \mathbf{Re}[\mathcal{R}_k\mathcal{R}_k''^*](\Delta\omega)^2 \right), \quad (\text{S65})$$

which under the assumption that $C_b, C_b' \gg 1$ and $C_b^{*\beta}, C_b^{*\alpha} < C_b^2$, becomes,

$$P_{\text{suc}} = 1 - \frac{C_b}{(1 + C_b)^2 + C_b'^2} - \frac{N\mathcal{C}\Gamma_e^2}{|\Omega/2|^4}(\Delta\omega)^2 \quad (\text{S66})$$

Substituting Eq. (S66) and (S61) into Eq. (S53), we get the expression for the conditional swap fidelity,

$$F_{\text{swap}} \simeq 1 - \frac{3}{4[C_b^2 + C_b'^2 + 2C_b]} - \frac{C_b^2}{[C_b^2 + C_b'^2 + 2C_b]^2} - \frac{3}{4} \left[\frac{1}{\kappa} + \frac{N\mathcal{C}\Gamma_e}{|\Omega/2|^2} \right]^2 \left[1 + \frac{C_b}{C_b^2 + C_b'^2 + 2C_b} \right] (\Delta\omega)^2 \quad (\text{S67})$$

Finally, keeping only the dominant contribution to the gate operation, we get the conditional swap fidelity,

$$F_{\text{swap}} = 1 - \frac{1}{[C_b^2 + C_b'^2]} - \frac{3C_b^2 - C_b'^2}{4[C_b^2 + C_b'^2]^2} - \frac{3}{4} \left[\frac{1}{\kappa} + \frac{N\mathcal{C}\Gamma_e}{|\Omega/2|^2} \right]^2 (\Delta\omega)^2 \quad (\text{S68})$$

INHOMOGENEOUS ENSEMBLE

So far, we have considered only a homogeneous ensemble without decay of the Rydberg level. In this section we discuss the case for an inhomogeneous ensemble. For simplicity, we only consider $\Delta\omega = 0$. Here the scattering dynamics depends on where the excitation was stored in the ensemble. From the fidelity expressions Eq. (S45) and Eq. (S53) we see that the essential parameter is $\sum_k |\alpha_k|^2 \mathcal{R}_k$ which for $\delta_l = \Delta_l = 0$ is given by

$$\sum_k |\alpha_k|^2 \mathcal{R}_k = \sum_k |\alpha_k|^2 \left[\frac{2}{1 + \sum_l \frac{|\mathcal{G}_l|^2 / \kappa \Gamma_{el}}{1 + |\Omega_l/2|^2 / (\Gamma_{rl} \Gamma_{el} + i\nu_{kl} \Gamma_{el})}} - 1 \right]. \quad (\text{S69})$$

When the ensemble was homogeneous, we defined the blockaded co-operativity C_b and C_b' such that $\mathcal{R}_k = \frac{1}{1 + C_b + iC_b'}$. Analogous to this for an inhomogeneous ensemble, we can define the blockaded co-operativity through $\sum_k |\alpha_k|^2 \mathcal{R}_k = 1 / (1 + C_b^{\text{inh}} + iC_b'^{\text{inh}})$

where,

$$\begin{aligned} \mathcal{C}_b^{\text{inh}} &= \text{Re} \left[\frac{1}{\sum_k |\alpha_k|^2 \left(1 + \sum_{l \neq k} \frac{\mathcal{C}_l}{1 + |\Omega/2|^2 / (\Gamma_{rl} \Gamma_{el} + i \mathcal{V}_{kl} \Gamma_{el})} \right)^{-1}} \right] - 1, \\ \mathcal{C}'_b{}^{\text{inh}} &= \text{Im} \left[\frac{1}{\sum_k |\alpha_k|^2 \left(1 + \sum_{l \neq k} \frac{\mathcal{C}_l}{1 + |\Omega/2|^2 / (\Gamma_{rl} \Gamma_{el} + i \mathcal{V}_{kl} \Gamma_{el})} \right)^{-1}} \right] \end{aligned} \quad (\text{S70})$$

Note that contrary to the homogeneous case the above defined effective co-operativity for inhomogeneous ensemble also includes the effect of Rydberg decoherence on the scattering process. Thus, to study the Fidelity of the phase gate for an inhomogeneous ensemble and in presence of decoherence, the results in Eqs. (S62) and (S68) can be utilized but now with \mathcal{C}_b replaced by $\mathcal{C}_b^{\text{inh}}$ and \mathcal{C}'_b by $\mathcal{C}'_b{}^{\text{inh}}$.

* Electronic address: sumanta@nbi.ku.dk

† Electronic address: andrey.grankin@u-psud.fr

[1] Alexey V. Gorshkov, Axel André, Mikhail D. Lukin, Anders S. Sørensen, Phys. Rev. A **76**, 033804 (2007)

Bibliography

- A. Abrikosov, L. Gorkov, and I. Dzyaloshinski. *Methods of Quantum Field Theory in Statistical Physics*. Dover Books on Physics Series. Dover Publications, 1975. ISBN 9780486632285.
- C. Ates, J. P. Garrahan, and I. Lesanovsky. Thermalization of a strongly interacting closed spin system: From coherent many-body dynamics to a fokker-planck equation. *Phys. Rev. Lett.*, 108:110603, Mar 2012.
- S. Baur, D. Tiarks, G. Rempe, and S. Dürr. Single-photon switch based on rydberg blockade. *Phys. Rev. Lett.*, 112:073901, Feb 2014.
- P. Bienias and H. P. Büchler. Quantum theory of kerr nonlinearity with rydberg slow light polaritons. *arXiv preprint arXiv:1604.05125*, 2016.
- P. Bienias, S. Choi, O. Firstenberg, M. F. Maghrebi, M. Gullans, M. D. Lukin, A. V. Gorshkov, and H. P. Büchler. Scattering resonances and bound states for strongly interacting rydberg polaritons. *Phys. Rev. A*, 90:053804, Nov 2014.
- K. M. Birnbaum, A. Boca, R. Miller, A. D. Boozer, T. E. Northup, and H. J. Kimble. Photon blockade in an optical cavity with one trapped atom. *Nature*, 436(7047): 87–90, 2005.
- R. Boddeda, I. Usmani, E. Bimbard, A. Grankin, A. Ourjoumtsev, E. Brion, and P. Grangier. Rydberg-induced optical nonlinearities from a cold atomic ensemble trapped inside a cavity. *Journal of Physics B: Atomic, Molecular and Optical Physics*, 49(8):084005, 2016.
- K.-J. Boller, A. Imamoglu, and S. E. Harris. Observation of electromagnetically induced transparency. *Phys. Rev. Lett.*, 66:2593–2596, May 1991.
- R. W. Boyd. *Nonlinear optics*. Academic press, 2003.
- R. J. Brecha, L. A. Orozco, M. G. Raizen, M. Xiao, and H. J. Kimble. Observation of oscillatory energy exchange in a coupled-atom-cavity system. *J. Opt. Soc. Am. B*, 12(12):2329–2339, Dec 1995.

BIBLIOGRAPHY

- H.-P. Breuer and F. Petruccione. *The theory of open quantum systems*. Oxford University Press on Demand, 2002.
- E. Brion, K. Mølmer, and M. Saffman. Quantum computing with collective ensembles of multilevel systems. *Phys. Rev. Lett.*, 99:260501, Dec 2007a.
- E. Brion, L. H. Pedersen, and K. Mølmer. Adiabatic elimination in a lambda system. *Journal of Physics A: Mathematical and Theoretical*, 40(5):1033, 2007b.
- E. Brion, L. H. Pedersen, and K. Mølmer. Implementing a neutral atom rydberg gate without populating the rydberg state. *Journal of Physics B: Atomic, Molecular and Optical Physics*, 40(9):S159, 2007c.
- E. Brion, L. H. Pedersen, M. Saffman, and K. Mølmer. Error correction in ensemble registers for quantum repeaters and quantum computers. *Phys. Rev. Lett.*, 100:110506, Mar 2008.
- E. Brion, F. Carrier, V. M. Akulin, and K. Mølmer. Quantum repeater with rydberg-blocked atomic ensembles in fiber-coupled cavities. *Phys. Rev. A*, 85:042324, Apr 2012.
- M. Brune, F. Schmidt-Kaler, A. Maali, J. Dreyer, E. Hagley, J. M. Raimond, and S. Haroche. Quantum rabi oscillation: A direct test of field quantization in a cavity. *Phys. Rev. Lett.*, 76:1800–1803, Mar 1996.
- D. Budker, D. F. Kimball, S. M. Rochester, and V. V. Yashchuk. Nonlinear magneto-optics and reduced group velocity of light in atomic vapor with slow ground state relaxation. *Phys. Rev. Lett.*, 83:1767–1770, Aug 1999.
- I. Carusotto and C. Ciuti. Quantum fluids of light. *Rev. Mod. Phys.*, 85:299–366, Feb 2013.
- M.-D. Choi. Completely positive linear maps on complex matrices. *Linear algebra and its applications*, 10(3):285–290, 1975.
- S. Das, A. Grankin, I. Iakoupov, E. Brion, J. Borregaard, R. Boddeda, I. Usmani, A. Ourjoumteev, P. Grangier, and A. S. Sørensen. Photonic controlled-phase gates through rydberg blockade in optical cavities. *arXiv preprint arXiv:1506.04300*, 2015.
- S. Das, A. Grankin, I. Iakoupov, E. Brion, J. Borregaard, R. Boddeda, I. Usmani, A. Ourjoumteev, P. Grangier, and A. S. Sørensen. Photonic controlled-phase gates through rydberg blockade in optical cavities. *Phys. Rev. A*, 93:040303, Apr 2016.
- Y. Dudin and A. Kuzmich. Strongly interacting rydberg excitations of a cold atomic gas. *Science*, 336(6083):887–889, 2012.

-
- L. Faddeev. Scattering theory for a three particle system. *Sov. Phys. JETP*, 12(5):1014, 1961.
- O. Firstenberg, T. Peyronel, Q.-Y. Liang, A. V. Gorshkov, M. D. Lukin, and V. Vuletić. Attractive photons in a quantum nonlinear medium. *Nature*, 502(7469):71–75, 2013.
- M. Fleischhauer and M. D. Lukin. Dark-state polaritons in electromagnetically induced transparency. *Phys. Rev. Lett.*, 84:5094–5097, May 2000.
- M. Fleischhauer and S. F. Yelin. Radiative atom-atom interactions in optically dense media: Quantum corrections to the lorentz-lorenz formula. *Phys. Rev. A*, 59:2427–2441, Mar 1999.
- I. Friedler, D. Petrosyan, M. Fleischhauer, and G. Kurizki. Long-range interactions and entanglement of slow single-photon pulses. *Phys. Rev. A*, 72:043803, Oct 2005.
- A. Gaëtan, Y. Miroshnychenko, T. Wilk, A. Chotia, M. Viteau, D. Comparat, P. Pillet, A. Browaeys, P. Grangier, et al. Observation of collective excitation of two individual atoms in the rydberg blockade regime. *Nature Physics*, 5(2):115–118, 2009.
- T. F. Gallagher. *Rydberg atoms*, volume 3. Cambridge University Press, 2005.
- T. Giamarchi, T. Giamarchi, and T. Giamarchi. *Quantum physics in one dimension*. Clarendon Oxford, 2004.
- H. Gorniaczyk, C. Tresp, J. Schmidt, H. Fedder, and S. Hofferberth. Single-photon transistor mediated by interstate rydberg interactions. *Phys. Rev. Lett.*, 113:053601, Jul 2014.
- A. V. Gorshkov, A. André, M. D. Lukin, and A. S. Sørensen. Photon storage in Λ -type optically dense atomic media. i. cavity model. *Phys. Rev. A*, 76:033804, Sep 2007.
- A. V. Gorshkov, J. Otterbach, M. Fleischhauer, T. Pohl, and M. D. Lukin. Photon-photon interactions via rydberg blockade. *Phys. Rev. Lett.*, 107:133602, Sep 2011.
- A. V. Gorshkov, R. Nath, and T. Pohl. Dissipative many-body quantum optics in rydberg media. *Phys. Rev. Lett.*, 110:153601, Apr 2013.
- P. Grangier, G. Roger, and A. Aspect. Experimental evidence for a photon anticorrelation effect on a beam splitter: a new light on single-photon interferences. *EPL (Europhysics Letters)*, 1(4):173, 1986.
- A. Grankin, E. Brion, E. Bimbard, R. Boddeda, I. Usmani, A. Ourjoumtsev, and P. Grangier. Quantum statistics of light transmitted through an intracavity rydberg medium. *New Journal of Physics*, 16(4):043020, 2014.

BIBLIOGRAPHY

- A. Grankin, E. Brion, E. Bimbard, R. Boddeda, I. Usmani, A. Ourjoumtsev, and P. Grangier. Quantum-optical nonlinearities induced by rydberg-rydberg interactions: A perturbative approach. *Phys. Rev. A*, 92:043841, Oct 2015.
- A. Grankin, E. Brion, R. Boddeda, S. Ćuk, I. Usmani, A. Ourjoumtsev, and P. Grangier. Inelastic photon scattering via the intracavity rydberg blockade. *arXiv preprint arXiv:1604.06385*, 2016.
- C. Guerlin, E. Brion, T. Esslinger, and K. Mølmer. Cavity quantum electrodynamics with a rydberg-blocked atomic ensemble. *Phys. Rev. A*, 82:053832, Nov 2010.
- S. Haroche and J. M. Raimond. *Exploring the quantum*. Oxford Univ. Press, 2006.
- S. E. Harris, J. E. Field, and A. Imamoglu. Nonlinear optical processes using electromagnetically induced transparency. *Phys. Rev. Lett.*, 64:1107–1110, Mar 1990.
- L. V. Hau, S. E. Harris, Z. Dutton, and C. H. Behroozi. Light speed reduction to 17 metres per second in an ultracold atomic gas. *Nature*, 397(6720):594–598, 1999.
- T. Holstein and H. Primakoff. Field dependence of the intrinsic domain magnetization of a ferromagnet. *Phys. Rev.*, 58:1098–1113, Dec 1940.
- L. Isenhower, E. Urban, X. L. Zhang, A. T. Gill, T. Henage, T. A. Johnson, T. G. Walker, and M. Saffman. Demonstration of a neutral atom controlled-not quantum gate. *Phys. Rev. Lett.*, 104:010503, Jan 2010.
- K. Jachymski, P. Bienias, and H. P. Büchler. Three-body interaction of rydberg slow light polaritons. *arXiv preprint arXiv:1604.03743*, 2016.
- D. Jaksch, J. I. Cirac, P. Zoller, S. L. Rolston, R. Côté, and M. D. Lukin. Fast quantum gates for neutral atoms. *Phys. Rev. Lett.*, 85:2208–2211, Sep 2000.
- A. Jamiołkowski. Linear transformations which preserve trace and positive semidefiniteness of operators. *Reports on Mathematical Physics*, 3(4):275–278, 1972.
- A. Kamenev. *Field theory of non-equilibrium systems*. Cambridge University Press, 2011.
- H. Labuhn, D. Barredo, S. Ravets, S. de Léséleuc, T. Macrì, T. Lahaye, and A. Browaeys. A highly-tunable quantum simulator of spin systems using two-dimensional arrays of single rydberg atoms. *arXiv preprint arXiv:1509.04543*, 2015.
- I. Lesanovsky, B. Olmos, and J. P. Garrahan. Thermalization in a coherently driven ensemble of two-level systems. *Phys. Rev. Lett.*, 105:100603, Sep 2010.
- W. Li and I. Lesanovsky. Coherence in a cold-atom photon switch. *Phys. Rev. A*, 92:043828, Oct 2015.

- R. Loudon. *The quantum theory of light*. OUP Oxford, 2000.
- R. Löw, H. Weimer, U. Krohn, R. Heidemann, V. Bendkowsky, B. Butscher, H. P. Büchler, and T. Pfau. Universal scaling in a strongly interacting rydberg gas. *Phys. Rev. A*, 80:033422, Sep 2009.
- M. D. Lukin, M. Fleischhauer, R. Cote, L. M. Duan, D. Jaksch, J. I. Cirac, and P. Zoller. Dipole blockade and quantum information processing in mesoscopic atomic ensembles. *Phys. Rev. Lett.*, 87:037901, Jun 2001.
- A. Lvovsky. Squeezed light. *Photonics: Scientific Foundations Technology and Applications*, 1, 2014.
- M. F. Maghrebi, M. J. Gullans, P. Bienias, S. Choi, I. Martin, O. Firstenberg, M. D. Lukin, H. P. Büchler, and A. V. Gorshkov. Coulomb bound states of strongly interacting photons. *Phys. Rev. Lett.*, 115:123601, Sep 2015.
- M. Moos, M. Höning, R. Unanyan, and M. Fleischhauer. Many-body physics of rydberg dark-state polaritons in the strongly interacting regime. *Phys. Rev. A*, 92:053846, Nov 2015.
- I. Mourachko, D. Comparat, F. de Tomasi, A. Fioretti, P. Nosbaum, V. M. Akulin, and P. Pillet. Many-body effects in a frozen rydberg gas. *Phys. Rev. Lett.*, 80:253–256, Jan 1998.
- J. W. Negele and H. Orland. *Quantum many-particle systems*, volume 200. Addison-Wesley New York, 1988.
- J. Otterbach, M. Moos, D. Muth, and M. Fleischhauer. Wigner crystallization of single photons in cold rydberg ensembles. *Phys. Rev. Lett.*, 111:113001, Sep 2013.
- A. Ourjoumtsev, A. Kubanek, M. Koch, C. Sames, P. W. Pinkse, G. Rempe, and K. Murr. Observation of squeezed light from one atom excited with two photons. *Nature*, 474(7353):623–626, 2011.
- D. Paredes-Barato and C. S. Adams. All-optical quantum information processing using rydberg gates. *Phys. Rev. Lett.*, 112:040501, Jan 2014.
- V. Parigi, E. Bimbard, J. Stanojevic, A. J. Hilliard, F. Nogrette, R. Tualle-Brouri, A. Ourjoumtsev, and P. Grangier. Observation and measurement of interaction-induced dispersive optical nonlinearities in an ensemble of cold rydberg atoms. *Phys. Rev. Lett.*, 109:233602, Dec 2012.
- T. Peyronel, O. Firstenberg, Q.-Y. Liang, S. Hofferberth, A. V. Gorshkov, T. Pohl, M. D. Lukin, and V. Vuletić. Quantum nonlinear optics with single photons enabled by strongly interacting atoms. *Nature*, 488(7409):57–60, 2012.

BIBLIOGRAPHY

- J. D. Pritchard, D. Maxwell, A. Gauguet, K. J. Weatherill, M. P. A. Jones, and C. S. Adams. Cooperative atom-light interaction in a blockaded rydberg ensemble. *Phys. Rev. Lett.*, 105:193603, Nov 2010.
- J. D. Pritchard, K. J. Weatherill, and C. S. Adams. Nonlinear optics using cold rydberg atoms. *Annual Review of Cold Atoms and Molecules, Volume 1. Edited by Madison Kirk et al. Published by World Scientific Publishing Co. Pte. Ltd., 2013. ISBN# 9789814440400, pp. 301-350, 1:301–350, 2013.*
- I. E. Protsenko, G. Reymond, N. Schlosser, and P. Grangier. Operation of a quantum phase gate using neutral atoms in microscopic dipole traps. *Phys. Rev. A*, 65:052301, Apr 2002.
- J. Rammer. *Quantum field theory of non-equilibrium states*. Cambridge University Press, 2007.
- F. Robicheaux and J. Hernández. Many-body wave function in a dipole blockade configuration. *Physical Review A*, 72(6):063403, 2005.
- M. Saffman, T. G. Walker, and K. Mølmer. Quantum information with rydberg atoms. *Rev. Mod. Phys.*, 82:2313–2363, Aug 2010.
- P. Schauß, M. Cheneau, M. Endres, T. Fukuhara, S. Hild, A. Omran, T. Pohl, C. Gross, S. Kuhr, and I. Bloch. Observation of spatially ordered structures in a two-dimensional rydberg gas. *Nature*, 491(7422):87–91, 2012.
- I. Schuster, A. Kubanek, A. Fuhrmanek, T. Puppe, P. W. Pinkse, K. Murr, and G. Rempe. Nonlinear spectroscopy of photons bound to one atom. *Nature Physics*, 4(5):382–385, 2008.
- M. O. Scully and M. S. Zubairy. *Quantum optics*. Cambridge university press, 1997.
- S. Sevinçli, N. Henkel, C. Ates, and T. Pohl. Nonlocal nonlinear optics in cold rydberg gases. *Phys. Rev. Lett.*, 107:153001, Oct 2011.
- A. Sommer, H. P. Büchler, and J. Simon. Quantum crystals and laughlin droplets of cavity rydberg polaritons. *arXiv preprint arXiv:1506.00341*, 2015.
- J. Stanojevic and R. Côté. Many-body rabi oscillations of rydberg excitation in small mesoscopic samples. *Physical Review A*, 80(3):033418, 2009.
- J. Stanojevic, V. Parigi, E. Bimbard, A. Ourjoumtsev, and P. Grangier. Dispersive optical nonlinearities in a rydberg electromagnetically-induced-transparency medium. *Phys. Rev. A*, 88:053845, Nov 2013.

- G. Stefanucci and R. van Leeuwen. *Nonequilibrium Many-Body Theory of Quantum Systems: A Modern Introduction*. Cambridge University Press, 2013.
- M. Tavis and F. W. Cummings. Exact solution for an n -molecule—radiation-field hamiltonian. *Phys. Rev.*, 170:379–384, Jun 1968.
- D. Tiarks, S. Baur, K. Schneider, S. Dürr, and G. Rempe. Single-photon transistor using a förster resonance. *Phys. Rev. Lett.*, 113:053602, Jul 2014.
- E. Urban, T. A. Johnson, T. Henage, L. Isenhower, D. Yavuz, T. Walker, and M. Saffman. Observation of rydberg blockade between two atoms. *Nature Physics*, 5(2):110–114, 2009.
- T. Vogt, M. Viteau, J. Zhao, A. Chotia, D. Comparat, and P. Pillet. Dipole blockade at förster resonances in high resolution laser excitation of rydberg states of cesium atoms. *Phys. Rev. Lett.*, 97:083003, Aug 2006.
- V. Vuletic. When superatoms talk photons. *Nature Physics News & Views*, 2:801, 2006.
- D. F. Walls and G. J. Milburn. *Quantum optics*. Springer Science & Business Media, 2007.
- H. Weimer, R. Löw, T. Pfau, and H. P. Büchler. Quantum critical behavior in strongly interacting rydberg gases. *Phys. Rev. Lett.*, 101:250601, Dec 2008.
- H. Weimer, M. Müller, I. Lesanovsky, P. Zoller, and H. P. Büchler. A rydberg quantum simulator. *Nature Physics*, 6(5):382–388, 2010.
- T. Wilk, A. Gaëtan, C. Evellin, J. Wolters, Y. Miroshnychenko, P. Grangier, and A. Browaeys. Entanglement of two individual neutral atoms using rydberg blockade. *Phys. Rev. Lett.*, 104:010502, Jan 2010.
- B. Zhao, M. Müller, K. Hammerer, and P. Zoller. Efficient quantum repeater based on deterministic rydberg gates. *Phys. Rev. A*, 81:052329, May 2010.
- X. T. Zou and L. Mandel. Photon-antibunching and sub-poissonian photon statistics. *Phys. Rev. A*, 41:475–476, Jan 1990.

Titre : Etudes théoriques d'effets optiques non-linéaires dans un gaz ultrafroid d'atomes de Rydberg

Mots clés : atomes de Rydberg, optique quantique, corrélations photoniques

Résumé: La propagation de lumière en milieu non-linéaire permet d'engendrer des interactions photon-photon effectives, nécessaires à la réalisation de portes logiques optiques à deux qubits. Le présent mémoire est consacré à l'étude des effets optiques quantiques non-linéaires induits au sein d'un ensemble atomique en cavité par le phénomène de transparence électromagnétiquement induite combiné au blocage d'excitation dû aux fortes interactions dipôle-dipôle entre atomes de Rydberg. Après avoir présenté le système d'étude (Chap. 1), nous traitons le régime dispersif (Chap. 2), i.e. lorsque les atomes peuvent être restreints à deux niveaux, dans l'approximation des bulles Rydberg, et montrons que la lumière transmise peut être "groupée" ou "dégroupée", selon les paramètres de la cavité. Nous présentons ensuite un traitement alternatif du système (Chap. 3), fondé sur la factorisation des moyennes de produits d'opérateurs, qui nous permet d'étudier le régime résonant à l'ordre le plus bas de la théorie de perturbation et révèle de nouvelles caractéristiques de la fonction de corrélation de la lumière transmise et réfléchiée par la cavité. Le formalisme de Schwinger-Keldysh nous permet de pousser plus loin le développement perturbatif par rapport au Hamiltonien d'alimentation (Chap. 4) : nous obtenons notamment l'expression analytique des composantes élastique et inélastique du spectre en transmission de la cavité et identifions une nouvelle structure de résonance polaritonique. Enfin, nous décrivons un protocole de porte photonique de phase de haute fidélité fondé sur le blocage Rydberg dans un ensemble atomique placé dans une cavité optique (Chap. 5).

Title : Theoretical studies of optical non-linear effects in ultracold Rydberg gases

Keywords : Rydberg atoms, quantum optics, photonic correlations

Abstract : Light propagation in non-linear media generates effective photon-photon interactions, which are necessary to the implementation of two-qubit optical logic gates. This work is devoted to the study of quantum optical non-linear effects induced in an atomic ensemble in a cavity by the electromagnetically induced transparency phenomenon combined with the excitation blockade due to the strong dipole-dipole interactions between Rydberg atoms. After presenting the system of interest (Chap. 1), we tackle the dispersive regime (Chap. 2), i.e. atoms can be effectively considered two-level, in the Rydberg bubble approximation, and show that the transmitted light can be either "bunched" or "antibunched", according to the cavity parameters. Then we present an alternative treatment of the system (Chap. 3), based on the factorization of operator product averages, which allows us to study the resonant regime at the lowest non-vanishing perturbative order and reveals new features of the transmitted and reflected light correlation function. The Schwinger-Keldysh formalism allows us to push further the perturbative expansion with respect to the cavity feeding Hamiltonian (Chap. 4) : we obtain, in particular, the analytic expression of the elastic and inelastic components of the cavity transmission spectrum and identify a new polaritonic resonance structure. Finally, we describe a new high fidelity photonic phase gate protocol based on the Rydberg blockade in an atomic ensemble placed in an optical cavity (Chap. 5).

